REQ. NO. 1-9001

CONTRACT REPORT NO. OSQ81-00086

DESIGN OF A HIGH TEMPERATURE EROSION TEST FACILITY
PHASE I - DESIGN

Final Report
by
Montreal Engineering Company, Limited

Work on this project was conducted under the auspices of the Canada Centre for Mineral and Energy Technology, Energy, Mines and Resources, Canada.

DSS FILE NUMBER	:	14SQ.23440-1-9001
DSS CONTRACT SERIAL NUMBER	:	OSQ81-00086
CANMET PROJECT NUMBER	:	430902
CANMET SCIENTIFIC AUTHORITY	:	Mr. Alex Lui

257 pp
2 charts.

TABLE OF CONTENTS

PAGE

Table of Contents (i)

1. SUMMARY

2. INTRODUCTION

3. TECHNICAL DISCUSSION

4. CONCLUSIONS

APPENDICES

A. Statement of Work (Prepared by CANMET)
B. Specification
C. MECo Letter of 22 December 1981
D. Foster Wheeler Limited Quotation dated 25 March 1982
E. Foster Wheeler Drawings
  - C825-282, Rev. 1 - High Temperature Erosion Test Facility
  - C825-283 - High Temperature Erosion Test Facility - Details
F. List of Purchased Equipment Suppliers (April 21, 1982)
G. Visit Reports
  - General Electric Co., Schenectady
  - University of Delaware
  - National Bureau of Standards
  - Battelle - Columbus Laboratories
  - University of Cincinatti
  - Electric Power Research Institute
  - Lawrence Berkeley Laboratories, University of California
H. Reference Papers

PART 1

SUMMARY

1.0 SUMMARY

After discussions with the operators of most of the high temperature erosion test facilities in the U.S.A. a specification was prepared containing the range of parameters defined by the Physical Metallurgy Research Laboratory of CANMET.

The detailed design was carried out by Foster Wheeler Limited. Their cost quotation for this design was almost double their original estimate prepared at the proposal stage in the early summer of 1981.

The reasons for this increase in price are reviewed in Part 3 - Technical Discussion and a possible route to follow to reduce the price is covered in Part 4 - Conclusions.

The Appendices contain details of the equipment layout, the seven visit reports to U.S. test facilities and a collection of eight of the principal reference papers.

2.0 INTRODUCTION

The overall objective of this project is to design, construct and test a transportable High Temperature Erosion Test Facility. The project was divided into three phases, the first phase being concerned with the design of the facility. It is this phase which is the subject of this report.

There is no similar facility anywhere in Canada.

There are a number of erosion-testing facilities in the U.S.A. and other parts of the world. Some of these facilities are very simple and only designed to operate at room temperatures; others are quite elaborate and are primarily designed to test materials under temperature, pressure and aerodynamic conditions relevant to the inlet blade conditions in a modern gas turbine. The size and cost of the facilities thus covers a wide range.

Visits were made to seven sites in the U.S.A. covering the whole range of uses. However, none of the test rigs inspected had the operational flexibility to cover the range of parameters laid down in the Statement of Work (Appendix A).

The draft specification (Appendix B) was reviewed with Foster Wheeler and CANMET and agreed modifications issued to Foster Wheeler (Appendix C).

PART 3

TECHNICAL DISCUSSION

3. TECHNICAL DISCUSSION

The price quoted by Foster Wheeler Limited, in their proposal dated 25 March, 1982, was $153,415 excluding the cost of commissioning and testing and subject to a monthly escalation factor charge. Including these costs would bring the total cost to $185,000 - $190,000.

In addition the overall height of the complete facility exceeded that specified by over 40 percent. Subsequent discussion with Foster Wheeler established that the height could be reduced, without adversely affecting the operation of the facility, by 0.80 metres as shown on Revision 1 of Drawing No. C 825-282. The final height would thus be less that 10 percent greater than that specified. The space requirement of 8 feet high given in Section 2.02.1 of the Specification was given for guidance only and not as an absolute limit.

The difference between the quoted price and that originally estimated by Foster Wheeler in the proposal stage of $90,000 can be considered under the two broad headings of design and manufacturing.

3.1 Design Factors

The broad objective of the design phase was to review existing U.S. high temperature erosion test facilities and come up with a composite design that incorporated the best features from all of them. The resulting specification included many features that were superior to those on the U.S. rigs. However, all these improvements would represent added cost compared to the U.S. rigs and compared to the little that was known of detail design features at the proposal stage.

These features were:-

(a) Overcoming the problem of bringing the particles temperature up to the gas temperature and maintaining it steady until impact on the test specimen. This was achieved, in the Foster Wheeler design, by incorporating a one metre long acceleration tunnel or tube ahead of the specimen furnace. This tube, for its entire length, passes through a refractory lined electric resistance furnace. Apart from the added cost that this represents, this feature also adds significantly to the height, amounting to nearly 40 percent of the revised total height of the test facility.

(b) Size of coupons and number of specimens that can be mounted on the specimen holder determines the minimum diameter of the specimen furnace, which is a key element in the overall design. The original specified coupon size of 2 x 3 cm was modified, by agreement, to 1-1/2 x 2 cm with the capability of mounting 12 specimens on the holder. In the U.S. rigs the normal specimen size was about 0.5 cm square. Even with the modified requirements the final specimen furnace diameter was double that of the University of Delaware specimen furnace.

(c) None of the U.S. rigs were capable of operating over the range of particle size, particle velocity and particle loading rates specified. The expected parameter ranges in the Foster Wheeler design (Appendix D, page 4) are appreciably better than on any of the U.S. designs even though falling short of the specified minimum velocity and maximum particle size.

3.2 Manufacturing Factors

At the time of submitting the original proposal no visits had been made to the test facilities in the U.S.A. and no detailed specification was available. Foster Wheeler envisioned a simple rig comparable to the early rigs of the National Bureau of Standards. The visits to the test rigs at Battelle and the University of Delaware represented more sophisticated rigs, which even then did not have the range desired by CANMET and also had operational problems which could be overcome by modifying the design. The final specification called for a more elaborate piece of laboratory apparatus that would meet, as nearly as possible, the upgraded requirements.

In their letter dated 19 April, 1982, Foster Wheeler commented on their proposed price to build the test facility in the following terms:

> "The Foster Wheeler facility in St. Catharines is not the ideal place to construct this test apparatus. The plant carries an overhead cost to support equipment, engineering skills and a sales and management force more suited to heavy equipment. A better cost would be obtained by going to a small shop."

This question is addressed further in Part 4 - Conclusions.

PART 4

CONCLUSIONS

4. CONCLUSIONS

The specified range of parameters for the proposed high temperature erosion test facility represents a considerable advance on those attainable on existing test rigs in the U.S.A. The design prepared by Foster Wheeler covers most of the specified range. However, the cost of such a facility, manufactured and assembled by a heavy equipment maker of the caliber of Foster Wheelers, would be approximately double the amount budgeted. In order to obtain a test facility at an acceptable price two steps should be taken.

First, a careful review by the user of the range of parameters over which the facility is required to operate. The narrower the range the less elaborate the facility need be. In addition, consideration should be given to the size of coupon and number of specimens to be mounted on the holder because of the influence these factors have on the specimen furnace diameter.

Second, alternative sources of supply should be considered. Although small machine shops, operating at low overhead relative to Foster Wheeler, could manufacture and assemble the facility as designed they would not have the capability to modify the design or to test and adjust it in operation. A preferred source of supply would be a Canadian research laboratory with metallurgical laboratory experience and an interest in erosion testing. Possible suitable laboratories would be those of the Ontario Research Foundation, Ontario Hydro Research Division, Atomic Energy of Canada Limited and universities with metallurgical programs. This report could be used as a basis, together with any modifications to the design parameters proposed by the user, to obtain quotations from selected laboratories.

APPENDIX A

STATEMENT OF WORK (Prepared by CANMET)

TITLE

Design, Construction and Testing of a High Temperature Erosion Test Facility.

BACKGROUND

When coal is used for power generation the products of combustion or gasification contain solid particles, the presence of which cause erosion of metallic materials. In fluidized bed combustion systems, the wear occurs under high temperature dense-phase erosion/corrosion conditions involving fluidized solids. In the hot gas transfer lines and cyclone, wear occurs under high temperature dilute phase erosion/corrosion involving high temperature high velocity particulate laden gas streams. In the high temperature high pressure gasification process, the raw gas prior to quenching carries particulate matter (char, ash, dolomite, etc.). Materials loss and resulting deterioration of structures also stems from high temperature erosion/corrosion.

At present, a facility for the characterization of materials for use in these high temperature erosive environments does not exist in Canada. However, such a facility is a prerequisite for reliable materials selection. A test facility for such work should be versatile, easy to use, as automated as possible and incorporate all of the best features of apparatus which exists elsewhere. Therefore, quality, experienced engineering design and construction is required. The purpose of this contract is to call upon private sector expertise to design and build a high temperature erosion testing apparatus for use in the laboratory which meets the above design criteria.

REQUIREMENTS

The Contractor will carry out the following task in 3 phases:

PHASE I - Design of a High Temperature Erosion Test Facility.

The unit should be compact enough for use in a laboratory, transportable and fully automatic in operation (particle preheating, injection, mixing, etc.), control (test temperature, particle velocity, particle loading rate, etc.) and data acquisition (with micro-processor). The following parameters should be incorporated in the design:

Temperature: ambient to 1000°C

Pressure: one atmosphere

Environment: combustion gases (containing 0.5% SO_2 max.)

Particle Velocity: 2 to 40 m/sec

Particle Size: 40-2000 micron diameter (.04 to 2.0 mm)

Particle Loading Rate: 100 g/m^3 max.

Sample Shape/Size: coupons/at least 2x3 cm.

Angle of Impingement: 0° to 90°C (sample holder should be rotatable)

Particle Materials: coal, ash, dolomite and sand

Sample Materials: various alloy steels

The Contractor is expected to become familiar with existing facilities in the U.S.A. and to incorporate the best features of each in the design. Consideration should also be given to materials of construction, maintainability and power and water requirements consistent with laboratory use. Alternate design options with cost estimates may be submitted to the scientific authority for consideration.

APPENDIX B

DSS File No. 14SQ 23440-1-9001
Serial No. 0SQ81-00086

SPECIFICATION
FOR
DESIGN, CONSTRUCTION AND TESTING OF A HIGH TEMPERATURE EROSION TEST FACILITY

W.O. EMR 7887-1

NOVEMBER 1981

Prepared by: Dr. M. Natarajan

Approved by: A Wyatt

Montreal Engineering Company, Limited
P.O. Box 1540
St. Catharines, Ontario
Canada
L2J 3S2

SPECIFICATION

HIGH TEMPERATURE EROSION TEST FACILITY

PART I - GENERAL

1.01 DESCRIPTION

A. Definition

The high temperature erosion test facility shall be a versatile, transportable testing apparatus which can be used for the characterization of materials for use in high-temperature erosive environments.

B. Work Included

Phase I - Design of a high-temperature erosion test facility.

C. Work Not Included

.1 Phase II - Construction of the apparatus according to the design agreed upon.

.2 Phase III - Testing of the apparatus and carrying out minor modifications, as required.

1.02 REFERENCES

.1 DSS File No. 14SQ.23440-1-9001.
Serial No.: 0SQ81-00086.
Statement of Work.

.2 MECo visit report on the existing high temperature erosion test facilities.

.3 Sheldon M. Wiederhorn and D. Ellis Roberts, Institute of Materials Research, National Bureau of Standards, Washington, D.C., "A technique to investigate high temperature erosion of refractories". (1976)

.4 Padraic A. Doyle, Alan V. Levy, Lawrence Berkeley Laboratory, University of California, "The elevated temperature erosion of 1100-0 aluminum by a gas-particle stream". (1978)

.5 J.A. Maasberg and A.V. Levy, Lawrence Berkeley Laboratory, University of California, "Erosion of elevated temperature corrosion scales on metals". (1981)

.6 David McFadden, University of California, "Erosion of ductile metals by solid particles".

.7 W. Tabakoff, A. Hamed, J. Ramachandran, Department of Aerospace Engineering, University of Cincinnati, "Study of metals erosion in high temperature coal streams". (1980)

1.02 REFERENCES (Cont'd)

.8 W. Tabakoff and T. Wakeman, University of Cincinnati. "Test facility for materials erosion at high temperature". (1979)

.9 (Material in mail from EPRI) - not yet received.

1.03 SUBMITTALS

.1 Detailed design drawings (minimum of two, showing a plan and an elevation) of the proposed equipment.

.2 Details of the specimen holder.

.3 List of components with appropriate performance characteristics.

.4 Description of the apparatus.

.5 Cost estimates for the construction and testing.

PART 2 - PRODUCTS

2.01 GENERAL

The high temperature erosion test facility is intended for use in the Physical Metallurgical Research Laboratories, Corrosion Science Centre of the Canada Centre for Minerals & Energy Technology (CANMET). The laboratory is located at 555 Booth Street, Ottawa. The facility is to be used for characterization of materials under high temperature erosive environments.

CANMET authorized MECo through Contract Ser. No. OSQ81-00086 to become familiar with existing high temperature erosion test facilities in the U.S.A. and to incorporate their best features in the design of the Canadian high temperature erosion test facility.

MECo visited six U.S. laboratories where high temperature erosion test facilities have been constructed and experimental work carried out since 1975. Further, an overview of the "state-of-the-art" in erosion testing and erosion/corrosion testing at elevated temperature as gathered from the Electric Power Research Institute is as follows:

Erosion can be a serious problem in any industrial process in which solid particles are conveyed in gas streams. Currently there is a great deal of interest in coal utilization. From conventional coal-fired steam power plant experience and from pilot plant results and experience on advanced

2.01 REFERENCES (Cont'd)

coal utilization systems, control of erosion problems appears to be an important factor in the development of successful processes. An understanding of the basic mechanisms by which erosion occurs already exist to predict material behaviour when used in the new processes. The behavior of materials under elevated temperatures coupled with erosion of metals has been studied seriously in the last decade. Erosion studies related to the quality of erodent and erosion/corrosion problems are also under investigation.

Based on the assessment of the U.S. test rigs visited it is clear that it would be difficult and expensive to design and construct a portable universal high temperature erosion test rig that would be suitable for the study of different materials, different erodents and the investigation of the aerodynamic characteristics of the erodent flow dealing with particle rebound correlations, effect of angle of attack and particle velocity. It is also recognized that the erosion/corrosion characteristics can only be inferred from the test results and from detailed analysis to be carried out on specimens after testing.

Based on the discussions held with CANMET on the potential use of the Canadian high temperature test facility and the details gathered during the visit of MECo, the rig at the University of Delaware, Materials Durability Division, College of Engineering would appear to be closest to the one envisioned by CANMET for their laboratory requirements.

The test rig at the University of Delaware is built from standard laboratory equipment, and appears to work well. Certain design modifications to the test rig, e.g. the carrier gas heater sizing, insulation of accelerator nozzle region, specimen holder arrangement, etc., should, however, be considered in the design of the Canadian test rig.

2.02 DESIGN SUMMARY

.1 Interface

Consideration should be given to materials of construction, maintainability, power and water requirements consistent with laboratory use.

The Physical Metallurgy Research Laboratories Corrosion Science Section, CANMET has the required space to install the high temperature erosion test rig. A space requirement of 8' wide x 8' high x 3' deep is considered as adequate to locate the test facility and the associated accessories.

Electric power supply of 480 volts, 3 phase and 120 volts, single phase is available, cooling water supply, if required, is available from the domestic water supply line in the building.

2.02 DESIGN SUMMARY (Cont'd)

.1 Interface (Cont'd)

The laboratory has the required facility to prepare test specimens and to perform metallurgical test analysis on specimens, as required.

.2 Principal Characteristics

.1 Temperature range for erosion testing: ambient to 1000°C.

.2 Pressure: one atmosphere.

.3 Environment: combustion gases (containing 0.5% SO_2 max.).

.4 Particle velocity m/sec: 2 to 65.

.5 Particle size microns: 10 to 2000 (emphasis to be given up to particle size of up to 200 microns).

.6 Particle loading rate g/m3: 100 max.

.7 Specimen shape: coupons at least 2 x 3 cm.

.8 Angle of tilt capability of test specimen on specimen holder: 0 - 90°.

2.03 DESIGN REQUIREMENTS

.1 Design Criteria

It is recognized that Foster Wheeler has one high-temperature erosion test rig of their own in their Foster Wheeler Energy Application Group, Livingston, New Jersey facility. Foster Wheeler "in house" experience and the knowledge gained from high temperature erosion test facilities in the U.S.A. should be utilized in the design of the specified Canadian test facility.

CANMET interest in the erosion study of different materials is very general and it is intended to study the effects of temperature on the behaviour of metals under erosion by particulate matter using this high-temperature erosion facility. CANMET are not only looking at erosion study of materials affected by coal ash particles, nor are they only aiming at a program for hot corrosion erosion materials testing for application to advanced coal utilization systems (e.g. fluidized bed coal combustion, gasification, gas turbine blade velocity range, etc.), although the idea for the high-temperature erosion testing facility stemmed from their interest in these areas.

2.03 DESIGN REQUIREMENTS (Cont'd)

.2 Basic Materials and Methods

A schematic diagram of the erosion test equipment is given in Figure 1.

The basic operation of the test shall be simple and effective.

By varying the gaseous supply from the gas supply rack, the desired gas composition could be achieved. The gas pressure reducing valve, flow element, gas sampling device shall be included as part of the gas supply system.

The gas shall be preheated to the desired temperature up to 1000°C in the multiple stage electric heaters. The thermoelements and the insitu controllers shall be included as part of the heating system. The materials selected for the high temperature carrier gas shall be of appropriate material with long range high temperature withstanding characteristics.

The particulate feed hopper, regulator shall be of SYLVESTER AND CO. or equivalent supply. (Refer to MECo visit report of University of Delaware for contact address.) A uniform flow of particles shall be obtained. Particles injected into the carrier gas stream shall be accelerated in the carrier gas stream, which in turn shall be further accelerated in an accelerator nozzle. The accelerator nozzle shall have a replaceable spray tip, since this may have to be replaced frequently during the experiments. The flow element, flow transmitter for flow recording purposes shall be included as part of the particulate injection system.

While selecting the particulate feeder and the erodent jet, the following shall be given consideration.

Density of particles in the gas stream of 0.2 to 2.0 g/m^3 (depending on gas velocity) may be selected for general experimentation, so that individual particles impingement on test specimen without much interaction at the erosion surface can be achieved. This thin density is, however, considerably less than the specified 100 g/m^3 (max.).

To determine the particle velocity, a rotating disc device shall be employed. This equipment shall be based on the design of RUFF and IVES and as shown in Fig. 4, of the MECo visit report to Berkeley Test rig at the University of California, or as referred in this Specification Section 1.02.3. The strong points of the rotating discs are that they are less expensive to build and operate, have proven to give accurate results, and the time required for calibration is short.

The specimen chamber shall be heated by electric heaters. The temperature of the specimen chamber shall be monitored with the help of thermoelements peaned on to the spray jet. Thermoelements and insitu temperature

2.03 DESIGN REQUIREMENTS (Cont'd)

.2 Basic Materials and Methods (Cont'd)

controllers shall be included as part of the heating system. The specimen furnace shall be designed generally as supplied by Allied Test Systems Inc. to the test rig at the Univeristy of Delaware. The test specimen (prepared and cleaned for testing) shall be held directly below the exit of the erodent spray jet. The specimen holder discs shall be capable of being adjusted with reference to the spray tip location. The specimen holder disc shall be rotated through a speed adjustable drive and capable of being rotated at speeds up to 100 rpm.

All heated sections of the rig shall be designed to be cold wall.

The drive spindle shall be provided with a cooling system to obviate overheating.

The spent gas-erodent stream shall be vented to atmosphere, through a dust collection system.

The entire high temperature test rig shall be designed as an integral equipment which can be dismantled in sections for ease of transport, if required. Each section should be assembled on a rigid bed plate.

.3 Alternatives

Alternatives to the above will be considered if they are either clearly superior or achieve the same goals at lower cost.

APPENDIX C

MONTREAL ENGINEERING COMPANY, LIMITED

ONE ST. PAUL STREET, ST. CATHARINES, ONTARIO
CORRESPONDENCE:
P.O. Box 1540, St. Catharines, Ontario L2R 7J9
Tel: (416) 688-9263
Telex: 061-5219
Cables: "Monenco"

22 December 1981

Foster Wheeler Limited
P.O. Box 3007
St. Catharines, Ontario
L2R 7B7

Attention: Mr. R. Hall,
Special Projects Division

Dear Sir:

Re: Design of a High Temperature
Erosion Test Facility - Phase I
DSS File No: 14SQ.23440-1-9001

This letter is to confirm the discussions, held in this office on December 15, 1981, with yourselves and Mr. Alex Lui of CANMET, reference our specification for the Design of a High Temperature Erosion Test Facility.

1) S.I. Units to be used.
2) Specimen shape: coupons 1½ x 2 cm. max.
3) Specimen holder to be designed to hold maximum of 12 - 25 specimens.
4) Two specimen holder/twin disc assemblies to be supplied (one as spare).
5) A hand-held tachometer (in client supply) will be used to measure specimen shaft speed.
6) Reference Clause 2.03.2 of the Specification and Figure 1 - Schematic Diagram the gas pressure reducing valve and flow element are both Foster Wheeler supply. The gas sampling system is client supply.
7) Two one-hour tests will be required in the test-phase. Foster Wheeler to define in their proposal the test conditions for each test so as to cover as wide a combination of maximum, minimum or normal operating conditions as possible.
8) As an option Foster Wheeler will define the cost of making the indexing of the specimen holder infinitely variable as opposed to only being able to centre each specimen under the erodent jet.

. 2

HALIFAX • FREDERICTON • MONTREAL • OTTAWA • TORONTO • ST. CATHARINES • CALGARY • EDMONTON • VANCOUVER

9) Flow indicator recorders for the gas flow, particulate feed and for the specimen chamber temperature shall be of stripchart type, twin speed, one with one inch per hour and the other with six inches per hour.

10) Test temperature, particle feed rate, gas flow rate will be processed with micro processor into a data acquisition system. The data logger will also print out the corresponding particulate velocity maintained during testing. Details of how the particle jet velocity determining device will be introduced into the microprocessor unit will have to be investigated after the system design has been finalized. The microprocessor will be supplied by others.

11) A revised Schematic Diagram, labelled Figure 1, is attached.

12) The submittals listed in Section 1.03 of the Specification are required by 15 February, 1982. The cost quotation for your supply of equipment and testing, per the specification, should be valid for sixty (60) days from 15 February, 1982.

If you have any queries please feel free to contact myself or Dr. Natarajan.

Yours very truly,

A. Wyatt
Head, Advanced Technology

AW/cr
cc: Mr. S. Detre
Mr. A. Lui - CANMET
Dr. M. Natarajan

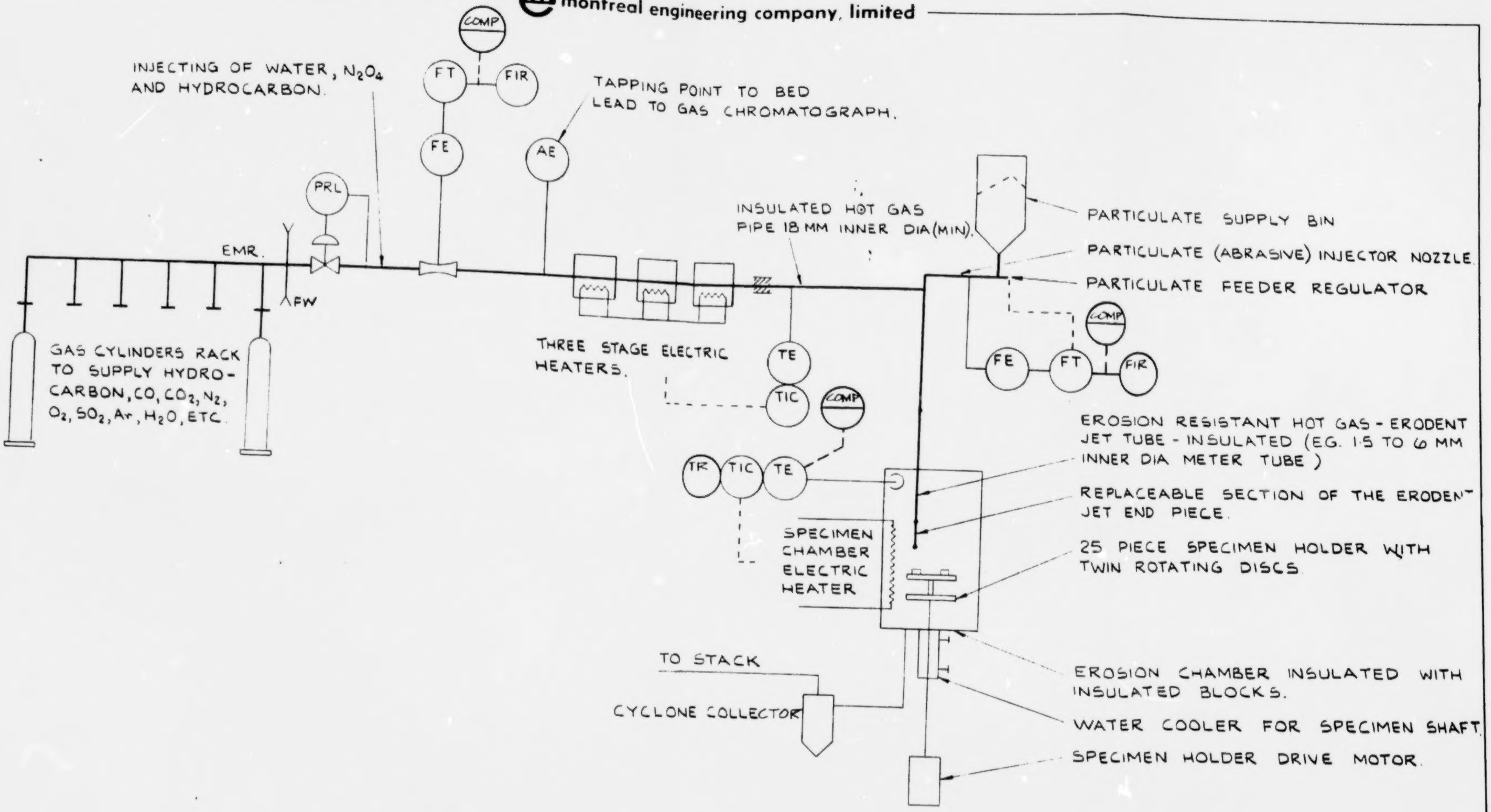
INJECTING OF WATER, N2O4 AND HYDROCARBON.
COMP
FT
FIR
FE
AE
PRL
TAPPING POINT TO BED LEAD TO GAS CHROMATOGRAPH.
EMR.
FW
INSULATED HOT GAS PIPE 18 MM INNER DIA (MIN).
PARTICULATE SUPPLY BIN
PARTICULATE (ABRASIVE) INJECTOR NOZZLE.
PARTICULATE FEEDER REGULATOR
GAS CYLINDERS RACK TO SUPPLY HYDROCARBON, CO, CO2, N2, O2, SO2, Ar, H2O, ETC.
THREE STAGE ELECTRIC HEATERS.
TE
TIC
COMP
FE
FT
COMP
FIR
TR
TIC
TE
EROSION RESISTANT HOT GAS - ERODENT JET TUBE - INSULATED (EG. 1.5 TO 6 MM INNER DIA METER TUBE)
REPLACEABLE SECTION OF THE ERODENT JET END PIECE.
25 PIECE SPECIMEN HOLDER WITH TWIN ROTATING DISCS.
SPECIMEN CHAMBER ELECTRIC HEATER
TO STACK
CYCLONE COLLECTOR
EROSION CHAMBER INSULATED WITH INSULATED BLOCKS.
WATER COOLER FOR SPECIMEN SHAFT.
SPECIMEN HOLDER DRIVE MOTOR.

FIGURE 1
SCHEMATIC DIAGRAM
HIGH TEMPERATURE EROSION TEST FACILITY
W.O. EMR 7887-1

APPENDIX D

FOSTER WHEELER LIMITED
DESIGNERS - MANUFACTURERS - CONSTRUCTORS
ST. CATHARINES, ONTARIO L2R 7B7

TELEPHONE 688-4434
TELEX - 061-5134
CABLE - REWOP
PO BOX 3007

MONTREAL
TORONTO
CALGARY
VANCOUVER

QUOTATION

YOUR REF DSS File No. 14SQ.23440-1-9001 OUR REF 8-51-2751/882-005 DATE March 25, 1982

Montreal Engineering Company Limited
Corbloc
80 King Street
ST. CATHARINES, Ontario.

(ATTENTION: Mr. A. Wyatt)

FOR

Department of Energy, Mines and Resources
CANMET
Physical Metallurgy Research Laboratories
552 Booth Street
OTTAWA, Ontario.
K1A 0G1

(ATTENTION: Mr. Alex W. Lui)

Gentlemen:

This quotation covers the fabrication of one High Temperature Erosion Test Facility as fully described herein.

Any acceptance of the offer to sell contained herein is limited to acceptance of the express terms of such offer contained on the face and back hereof.

GENERAL CONDITIONS OF SALE

1. ACCEPTANCE: Foster Wheeler reserves the right to amend pricing on any quotation not accepted within 30 days from the date of the price quotation or to withdraw this quotation at any time. Upon acceptance by Purchaser, postponement or cancellation will be accepted only upon provision that Foster Wheeler shall be reimbursed for all costs incurred, plus those resulting from postponement or cancellation such as Vendor charges or shop disruption, plus a reasonable profit thereon.

2. TERMS: Unless stated otherwise on the face of this Quotation, all prices quoted are in Canadian funds f.o.b. the manufacturer's plant, exclusive of all taxes, payable net 30 days from date of shipment or offer to ship, should shipment be delayed at request of Purchaser. Prices are subject to adjustment to cover for changes in cost to Foster Wheeler in freight, exchange, duties, taxes, or other imposts between the date of quotation and completion date unless specified to the contrary. If normal supplies or production are upset by Canada's participation in war or international police action the conditions of this quotation are subject to adjustment. Foster Wheeler shall retain title to all equipment regardless of its mode of attachment, until paid for in full. Purchaser shall reimburse Foster Wheeler for storage and maintenance costs when shipment is delayed at his request. Interest is charged on overdue accounts.

3. SHIPMENT: Foster Wheeler's stated shipment refers to that from plant of manufacture and is based on prompt release of information or data required from Purchaser and approval of Foster Wheeler's drawings. Shipment is subject to delay caused by fires, floods, strikes, riots, accidents, acts of sub-suppliers, inability to obtain material, labour, components, fuel or transportation, or other causes beyond Foster Wheeler's control. Stated shipment times are best expected but not guaranteed, and shall be extended for causes beyond Foster Wheeler's control.

4. CONSTRUCTION: Whenever this quotation covers work on the site of the Purchaser it is intended that this form cover only such work on a cost plus basis in accordance with Foster Wheeler's Standard formula. Should, in the event of expendiency, this quotation cover field work in its price, such pricing shall be subject to Foster Wheeler's standard general conditions for field work (copy available upon request).

5. INSURANCE: Foster Wheeler shall maintain Workmen's Compensation coverage for its own employees, comprehensive general liability insurance in a minimum amount of $100,000.00 inclusive per accident. The Purchaser shall maintain insurance or himself assume risks for direct damage to the equipment on which the work is taking place. Purchaser shall, in his Use and Occupancy insurance (including boiler insurance and business interruption) and his direct damage insurance policies covering the overall facility on which work is to be performed, provide for waivers of subrogation in favour of Foster Wheeler. The Purchaser shall indemnify and hold harmless Foster Wheeler for failure to effect such waivers or from any claims of loss or damage to Purchaser's property, outside the scope of or in excess of aforementioned general liability coverage.

6. WARRANTY: Foster Wheeler agrees to repair at its shop or replace FOB its shop, any equipment or part of its manufacture proven defective (corrosion, erosion, wear and tear excepted) due to faulty material or workmanship provided Purchaser so notifies Foster Wheeler promptly upon discovery, but not later than one (1) year after shipment. Replacements or repairs made by the Purchaser or others shall not be reimbursable unless Foster Wheeler has issued prior written approval for same pursuant to such notification. Any equipment not of Foster Wheeler's manufacture is guaranteed only insofar as guaranteed by the maker. THE FOREGOING WARRANTIES ARE EXCLUSIVE AND IN LIEU OF ALL OTHER WARRANTIES, EXCEPT THAT OF TITLE, WHETHER WRITTEN, ORAL, OR IMPLIED, IN FACT OR IN LAW (INCLUDING ANY WARRANTY OF MERCHANTABILITY OR FITNESS FOR PURPOSE). Correction of non conformities in the manner provided above, shall constitute the entire liability of Foster Wheeler with respect to such equipment, whether in contract, in tort, strict liability or otherwise, unless otherwise expressly provided in this Quotation.

7. PATENTS: Foster Wheeler will defend any action resulting from alleged patent infringement of apparatus patents, provided it receives notification of such claim promptly. If equipment is held to constitute infringement Foster Wheeler will pay all damages and costs awarded, and either procure the right for Purchaser to continue its use; or replace same with non-infringing equipment; or modify equipment to make it non-infringing; or accept return of equipment and refund purchase price. Patent protection offered is restricted to patents of Canada unless otherwise agreed in writing and does not extend to process patents due to incorporation of equipment into a process by Purchaser or others. Foster Wheeler assumes no patent responsibility when working to drawings or sketches provided by Purchaser.

8. LIMITATION OF LIABILITY: In no event shall Foster Wheeler or its sub-contractors or vendors be liable, in contract, tort, strict liability, warranty or otherwise, for any special, indirect, incidental or consequential damages, such as, but not limited to, loss of anticipated profits or revenue, loss of use, non-operation or increased expense of operation of other equipment, cost of capital, cost of purchased or replacement power and/or facilities, damage to environment, or claims of customers of Purchaser for damages.

The remedies of the Purchaser set forth herein are exclusive.

The liability of Foster Wheeler or its sub-contractors or vendors with respect to any contract, or anything done in connection therewith, or from the manufacture, sale, delivery, resale, installation or technical direction of installation, repair, replacement or use of any equipment covered or furnished under this proposal whether in contract, in tort, under any warranty, strict liability or otherwise, shall not, except as otherwise stated, exceed the purchase price paid to Foster Wheeler by the Purchaser.

9. LIABILITY TO OWNER: Where the Purchaser is other than the Owner or ultimate User, the Purchaser shall obtain from the Owner, in favour of Foster Wheeler, an agreement that Owner shall be bound by the remedies extended herein, or Purchaser in lieu thereof, will indemnify Foster Wheeler from liability, damages, costs, losses or expenses, in excess of those provided for herein. Purchaser shall obtain from the Owner, in favour of Foster Wheeler, or its subcontractors or vendors a release from consequential damages to the extent stated under the "Limitation of Liability" clause herein, or in lieu thereof, the Purchaser will indemnify and hold harmless Foster Wheeler from and against liability, damages, costs, losses and expenses resulting from Owner's consequential losses of any nature.

10. DRAWINGS, MANUALS: Unless otherwise provided on the face hereof, Foster Wheeler shall provide to the Purchaser drawings or manuals only in the case of complete items of equipment as provided hereunder and in such event restricted to 3 prints of general arrangement drawings and 3 operating manuals.

11. RULES, REGULATIONS ETC.: Unless provided specifically on the face of the Quotation, the equipment offered is not represented to comply with any pollution, ecological or environmental requirements or other Governmental rules, regulations or codes in effect now or to come into effect in the future. Purchaser shall arrange all permits, licenses or compliance with other requirements for installation of equipment at site.

12. NUCLEAR EXCEPTION: Equipment offered hereunder is conventional and not intended for any nuclear activity unless so recognized on the face of this Quotation including special terms regarding indemnification, insurance and decontamination. If such equipment is used in or with a nuclear installation or activity, or used in connection with radioactive materials, without notification to Foster Wheeler and its consent thereto, Foster Wheeler disclaims all responsibility or every kind including negligence, and, in addition, the Purchaser shall indemnify and hold Foster Wheeler harmless for any liability or damage whatsoever arising out of use of such equipment in such a manner.

DESCRIPTION OF APPARATUS

The main gas mixture flow will be controlled by a pressure reducing valve and will be measured/recorded by an orifice pipe, pressure and differential pressure transmitter and stripchart recorder system (Customer supply). The main gas mixture flow will pass through an 8.9 cm (3.5 inch) I.D. ceramic retort which will be heated by a 12.7 cm (5 inch) I.D. tube type, refractory lined, electric resistance furnace. The retort will be packed with high temperature wire filaments which will provide additional heat transfer area to aid in heating the gas mixture to the required temperatures. A control cabinet will be supplied.

A room temperature carrier gas (e.g. argon) containing a measured amount of particulate will be injected into the heated gas mixture. The particulate/gas stream will then be accelerated in a 1 m (40 inch), 6.3 mm (0.25 inch) acceleration tube and will impinge on the rotating test speciments. After impinging on the test specimens the gas/particle stream will pass through a settiing chamber where the larger particles will be removed. The gas stream will be connected via a flexible steel pipe to the customer's laboratory exhaust system.

The acceleration tunnel's entire length will pass through a 9.5 cm (3.75 inch) I.D. tube type, refractory lined, electric resistance furnace. This furnace will maintain the gas temperature. In tests where most of the gas flow consists of the room temperature carrier gas (particulate injection) the furnace will heat the gas mixture. Testing will determine how much heat can be transferred to the gas stream. The specimen holder/twin rotating disk assembly will be contained within a 30.8 cm (12.125 inch) I.D. split type, refractory lined, electric resistance furnace. This furnace and the acceleration tube furnace will be controlled by a two-zone control system including two (2) SCR power controllers with power adjusting potentiometer and ammeter, providing independent control for each zone (furnace). The specimen furnace could be operated as the master zone with the acceleration tube furnace operated as a slave zone. That is, the heat rate of the acceleration tube furnace could be set as a percentage of the heat rate of the specimen furnace. The temperature of the specimen furnace will be recorded on a multi-speed strip-chart recorder. A control cabinet housing the control systems for both furnaces and the strip-chart recorder will be supplied.

The specimen holder/twin rotating disk assembly will be driven by a variable speed DC motor coupled with a gear reducer. A tachogenerator and rpm meter will be supplied with the motor since a hand-held tachometer cannot be used. The specimen holder shaft will be cooled/supported by a water jacket incorporating two high temperature graphite-type bushings. The specimen holders will be 2.54 cm (1 inch) round bar stock cut at different angles and machined to accept 2 cm by 1.5 cm test coupons. The test coupons will be held in place with stainless steel bolts, nuts and washers. Twelve (12) "dummy" specimen holders will also be supplied. The specimen holders will be held in the upper disk by set screws. The height of the specimen holders above the disk will be adjustable in order to offset the thermal expansion (change in length) of the acceleration tube. A slit will be cut in the upper disk and a replaceable layer of soft material will be placed on the bottom disk for particle velocity determination. The area, on the upper disk, between the specimen holders will be overlaid with a hard, erosion resistant material.

The particle feeder will be supplied with standard size 4 pitch and 10 pitch feed screws for particles up to 250 microns. Specially ground 4 pitch and 10 pitch feed screws will be supplied for feeding particles up to 600 microns. The use of 4 pitch and 10 pitch feed screws will extend the range of particle feed rates. The manufacturer also offers 6 pitch and 8 pitch feed screws which the customer could purchase if they were considered desirable. The particle feeder will also be supplied with a Caster Equipped Base Unit, Remote Control Circuitry with Cord, inlet and outlet hoses and a stainless steel liner for the carburetor mixer. Please note that when the particles exit the particle feeder they are carried by a carrier gas. As such the particle flow cannot be measured and recorded. However, the particle feeder includes a feed screw rpm indicator. The volumetric feed rate of the particles is directly related to the rpm of the feed screw.

Please refer to Drawing Numbers C-825-282 and C-825-283. The performance characteristics of the components are given in Appendix A.

EXPECTED PARAMETER RANGES

1. Temperature: ambient to 1000°C.
2. Pressure: one atmosphere.
3. Environment: simulated combustion gases (0.5% SO_2 max.).
4. Particle Velocity: 65 m/sec. max.
   3.5 m/sec. min. for 70°F gas.
   15 m/sec. min. for 1800°F gas.
5. Particle Size: 10 to 600 microns.
6. Particle Loading Rate: to be determined during commissioning phase.
7. Specimen Shape: twelve (12) 1.5 cm x 2 cm coupons.
8. Angle of Tilt: 0° - 90° in 5° increments.
9. Specimen Shaft Speed: 4 to 117 rpm.

FACILITY REQUIREMENTS

Main Gas Mixture:	The main gas mixture to be supplied at 100 psig max. and at room temperature.
Carrier Gas Supply:	Argon to be supplied at room temperature. Supply pressure shall be variable from 0 to 25 psig.
Power Supply for Particle Feeder:	115 volts, 1 phase, 60 Hertz A.C., 120 watts.
Power Supply for Main Gas Heater:	240 volts, 1 phase, 60 Hertz A.C., 8000 watts.
Power Supply for Acceleration Tube Furnace:	240 volts, 1 phase, 60 Hertz A.C., 7700 watts.
Power Supply for Specimen Furnace:	240 volts, 1 phase, 60 Hertz A.C., 8400 watts.
Power Supply for Furnace Strip Chart Recorder:	115 volts, 1 phase, 60 Hertz A.C.
Power Supply for Specimen Holder Drive:	115 volts, 1 phase, 60 Hertz A.C., 15 amps.
Power Supply for Flow Sensing/Recording Equipment:	115 volts, 1 phase, 60 Hertz A.C., 3.3 amps.
Domestic Water Supply:	Domestic water is required for the specimen shaft water cooler and the water cooled pull rods of the ceramic retort in the main gas heater.

GENERAL NOTES

1. Foster Wheeler Limited would prefer not to supply the Flow Element - Strip Chart Recorder System for the main gas flow. We have obtained a quotation for the above system and all pertinent information is included in Appendix "B".

2. Under certain conditions ,carbon monoxide in the presence of nickel can produce Nickel Carbonyl which can be extremely dangerous (poisonous and explosive). The customer should satisfy himself that conditions for its formation will not be present and that the user will not be in any danger.

3. Foster Wheeler Limited would prefer not to test the proposed equipment on its own premises. We therefore suggest that commissioning (setup and debugging) and final customer witnessed testing be done at the customer's facilities, with FWL consultation and advice. Please see Page 74 for applicable rates for this service. Foster Wheeler Limited estimates that two people for one month would be required for this service.

4. During the commissioning phase Foster Wheeler Limited would aid in establishing the operating limits of the as-built system, prior to customer witnessed testing.

5. Equipment proposed is prototype in nature so that the only warranty extended hereunder is regarding material and workmanship.

F.W. Tender 882-005
March 25, 1982

APPENDIX "A"

PERFORMANCE CHARACTERISTICS OF COMPONENTS

F.W. Tender 882-005
March 25, 1982

MAIN GAS HEATER

We have not yet received detailed specifications for the main gas heater. We will forward detailed specifications as soon as we receive them. We have the following general information:

Retort

Material:	Ceramic with 304 stainless steel flanges and end connections with water-cooled pull rods.
I.D:	3-1/2 inches.
O.D:	4 inches.
Overall Length:	52 inches.

Furnace

Type:	Series 3110 Tube Type Furnace.
I.D:	5 inches.
O.D.	16 inches.
Heated Length:	36 inches.
Overall Length:	40 inches.
Zones:	One zone construction.
Temperature:	1100°C.
Power:	33 amps/zone, 8000 watts total @ 240 VAC, 1 phase, 60 Hertz.
Mounting Bracket:	Horizontal mounting supplied.

Control Cabinet

8" W x 12" D x 10" H.

1 Series 3210 Split Type Furnace, ref. bulletin 3210. @

-Dimensions: 12 1/8" I.D. x 22" O.D. x 16" long.

-Elements: Kanthal Al for 2200° F. service, embedded windings.

-Furnace Temperature Rating: 1100° C is normal operating temperature.

-Zones: 1-zone construction
12" heated length.

-Connections: With opposing quarter sections connected in parallel.

-Power: 36.5 amps/zone, 8400 watts total @ 240 VAC, 1 phase, 60 Hz.

-End Bore: Bottom has two 2" diameter holes. One at the center line of the furnace and the other at 90° from the split on a 4" radius from the center line of the furnace.

Top: has 3 3/4" diameter hole at 90° from the split and on a 4" radius from the center line of the furnace.

-End caps: not required.

-Thermocouple Port: 1/4" dia., located at midlength of heat zone.

Accessory Equipment:

-Thermocouple: Type K, with ceramic insulators. @

-Thermocouple connector with mounting bracket. Type K. @

-Split furnace mounting bracket with 1 3/16 in. I.D. collar and position locking. 15" center to center on 22" O.D. furnace. @

2) 1 Series 3110 Tube Type Furnace, ref. bulletin 3110. @

-Dimensions: 3 3/4" I.D. x 12" O.D. x 34" long.
-Elements: Kanthal Al for 2200° F. service, embedded windings.
-Furnace Temperature Rating: 1100° C. is normal operating temperature.
-Zones: Single zone construction
30" heated length.
-Connections: With opposing half sections connected in parallel.
-Power: 32 amps/zone, 7700 watts total @ 240 VAC, 1 phase, 60 Hz.
-End Bore: Top 1/2" dia. bottom 3 3/4" dia.
-End Caps: Not Required
-Thermocouple Port: 1/4" dia., located 3" from bottom of furnace O.D.

Accessory Equipment:

-Thermocouple: Type K, with ceramic insulators.
-Thermocouple connector with mounting bracket, Type K.
-Furnace mounting bracket with 1 3/16 in. I.D. collar and position locking feature.
-Furnace bar, 1 3/16 in. dia. Length: 48"
-Engineering charge

3) 1 Series 2935 Two-zone furnace temperature control system, furnished with digital setpoint controller, 3-mode, with deviation indicator and on-off switch. Including two (2) SCR power controllers with power adjusting potentiometer and ammeter, providing independent control for each zone. With circuit breaker, indicating lamp, 6 ft. interconnecting cable and connector with power and thermocouple leads.

Temperature range: 0-1200° C, Type K.

No. 238-13/2, SCR/40 amps/zone.

4) 1 Model 300D Eurotherm Recorder. Ref. Bulletin 300.

-1-channel strip chart recorder, panel mounted, installed and wired complete.
-Disposable ink cartridge.
-Chart: 4 in. (100 mm.) W x 47 ft. (15 m.) L.

4)	Continued	-Standard chart: 50 Grid, RH zero. -Chart speed: 1 cm. in 5, 10, 30 or 60 minutes -Accuracy: DC input ± 0.50%; thermocouple input ± 0.70% full span. -Input: 0-10 VDC	
		Optional Equipment: -Thermocouple input, range : customer must specify temperature range he will be using.	@
	1	Control cabinet, including installation of power leads, connector and 19 in. rack mount panel(s). Finish: Medium blue textured enamel, with light blue control panel. -Bench top cabinet 22" W x 17" D x 19 1/4" H,	@
5)	1	Engineering charge	@
	1	Instruction Manual	

This equipment is in compliance with ONTARIO HYDRO electrical specifications.

Enclosures: Lab Furnace Catalog
LFE Bulletin, Eurotherm Bulletin

FOSTER WHEELER LIMITED

ST. CATHARINES, ONTARIO

MATERIAL AND LABOUR PRICE ADJUSTMENT CLAUSES

The price(s) quoted in this proposal are based on the Contractor's costs as of the escalation dateline identified below under (e) (i), which shall be referred to as the base and are subject to increases or decreases as defined by the adjustment clauses (a), (b), (c), where applicable as follows:

(a) MATERIAL PRICE ADJUSTMENT CLAUSE

(i) For the purpose of adjustment, the proportion of the contract price representing material is accepted as the factor identified as (e) (ii) below.

(ii) Such adjustments will be based upon the Industry Selling Price indexes — Iron and Stell Mills (Primary Metal Industries) SIC 12-2910 as published monthly in "Prices and Price Indexes" by Statistics Canada, Ottawa. An average of such index numbers for the period during which the material and equipment is being delivered to the Contractor will be computed and the percentage increase or decrease will be obtained by a comparison with index number for the base. The adjustments for changes in material prices will be obtained by applying such percentage of increase or decrease to the amount representing material as stated in (a) (i).

(b) PRODUCTION LABOUR ADJUSTMENT CLAUSE

(i) For the purpose of adjustment, the proportion of the contract price representing production labour is accepted as the factor identified as (e) (iii) below.

(ii) Such adjustments will be based upon the "Average Hourly Earnings, Metal Fabrication Industries" (SIC 300-309) for the Province of Ontario as shown in "Employment Earnings and Hours" published monthly by Statistics Canada, Ottawa. An average of such monthly hourly earnings for the period during which the equipment is being fabricated will be computed and the percentage increase or decrease will be obtained by a comparison with such hourly earnings for the base. The adjustment for changes in production labour rates will be obtained by applying such percentage of increase or decrease to the amount representing labour as stated in (b) (i).

c) FIELD CONSTRUCTION ADJUSTMENT CLAUSE

(i) For the purpose of adjustment, the proportion of the contract price representing field construction is accepted as the factor identified as (e) (iv) below.

(ii) Such adjustment will be based upon the "Average Hourly Earnings, Special Trade Contractors Construction" (SIC 421) for the region or province identified as (e) (v) below as Construction Zone as shown in "Employment Earnings and Hours" published monthly by the Statistics Canada, Ottawa, for the field construction of equipment described in this proposal. An average of such published monthly hourly earnings for the period during which the equipment is being constructed in the field will be computed and the percentage increase or decrease will be obtained by a comparison with such hourly earnings for the base. The adjustment of the change in field construction rates will be obtained by applying such percentage of increase or decrease to the amount representing field construction as stated in (c) (i).

(iii) Where provision is made herein for the Contractor to furnish Construction Superintendents and/or Service Engineers at a per diem rate, (whether current rate is stated or not) rates in effect at the time the work is done shall apply.

(d) APPLICATION

(i) Should any of the Statistic Canada Indexes referred to herein become unavailable, or the base year change or a significant change in weighting or content for such indexes be made by Statistics Canada contract price adjustments shall be made by using an acceptable Statistics Canada Index.

(ii) Any change in the price by reason of any of the above mentioned price adjustment clauses will be billed or credited to the Purchaser as soon as practicable after shipment and/or the Contractor may issue progress or partial billings or credits as the case may be.

(iii) Settlement of all such price adjustments shall be due upon receipt of the invoice or credit, as the case may be.

(iv) Any increase or decrease of price applicable under the terms of these price adjustment clauses shall conform to Government Regulations.

(e) APPLICABLE DATA

(i) Base — Average for months of December, 1981, Jan/Feb. 1982
(ii) Material Factor 56 % of) Total Selling Price.
(iii) Labour Factor 34 % of)
(iv) Construction Factor — % of
(v) Construction Zone —

FOSTER WHEELER LIMITED

ST. CATHARINES, ONTARIO

BASIS FOR SUPERVISORY SERVICES

To serve the best interests of the Purchaser and to facilitate installation or start-up in accordance with Manufacturer's recommendation for warranty purposes. Purchasers are urged to use available field supervisory services:

1. Upon receipt of order 30 days in advance of the date required, Foster Wheeler will furnish Construction Superintendent(s) to assist the Purchaser in the installation of equipment. Fourteen days written notice confirming starting date is required. The superintendent will act as a consultant or an advisor in the interpretation of drawings and specifications, will make recommendations, when requested, on methods of installation of the equipment. He will not be responsible for the procurement and direction of labour or quality of mechanical work performed by others.

2. Upon similar notice, Foster Wheeler will furnish Service Engineer(s) to advise and consult with the Purchaser or his representatives in the boiling out, starting up or operation of the equipment. Representatives of Foster Wheeler shall not be deemed licensed to operate the equipment, and shall not be expected to take the place of operators.

3. The Construction Superintendent or Service Engineer shall not be called upon to supervise the installation of brickwork, refractory setting or specialty equipment, but if required by similar notice in writing, Foster Wheeler shall provide the services and such Superintendent(s) who shall act as a consultant and advisor in the installation of same.

4. For the services of each Superintendent and/or Engineer as defined above, the Purchaser will pay to Foster Wheeler a per diem rate per working day and hourly rates for overtime in effect when service is rendered.

Personnel of Vendors shall be charged at actual Vendor's billing to Foster Wheeler plus a 10% handling fee.

The Purchaser shall also pay for all time consumed in travel from and to home office at a straight time hourly rate (ie daily rate divided by regular work hours per day as defined herein). Where travel and working time occur on the same day, overtime charges shall apply only where working time is beyond the normal working day. In addition to these rates, the Purchaser shall pay to Foster Wheeler all living and travelling expenses incurred by such personnel from the time of departure until return to home office, including all long distance communications. Such travel expenses shall include periodic return trips to Representative's home as permitted by prevailing policies. The working days and hours of above personnel shall be regular hours, and days per week in accordance with Foster Wheeler's current Field Union contract. No overtime shall be worked without written authority from the Purchaser, in which event overtime shall be paid for by the Purchaser at the hourly overtime rate shown herein. All rates are exclusive of sales, use or other tax on such services.

For guidance current rates are	**Per Diem** (per working day)	**Overtime** (per hour)
(a) Foster Wheeler	$450.	$85.
(b)		
(c)		
(d)		

5. The Purchaser is requested, when placing orders for services, to indicate to Foster Wheeler any special tools he may require Foster Wheeler to supply on a rental basis for the erection of the equipment. The rental for such tools will include the following:

(a) All crating and shipping (including insurance where not covered by carrier) charges to and from the Purchaser's site.

(b) Prevailing rental rate based on replacement value of all Foster Wheeler tools.

(c) Total cost of any tools not returned in a usable condition.

(d) Rental charges paid by Foster Wheeler on any local equipment plus 10%.

(e) Any taxes or duties applicable to such rentals.

6. Foster Wheeler shall not be responsible for injury to persons or damage to property during the installation and/or operation of equipment and the Purchaser shall indemnify and save harmless Foster Wheeler against any loss, personal injury (including death) or damage resulting from the installation or operation of equipment. Foster Wheeler shall provide Workmen's Compensation Insurance and Public Liability and Property Damage Insurance with limits of $1,000,000.00 inclusive on his own employees only and such coverage shall be the extent of Foster Wheeler's liability hereunder, whether such liability is based on contract, negligence or otherwise.

In no event shall Foster Wheeler or its subcontractors be liable for any special, indirect, incidental or consequential damages, such as, but not limited to, loss of anticipated profits or revenue, loss of use of power system, non-operation or increased expense of operation of other equipment, cost of capital, cost of purchased or replacement power, or claims of customers of Purchaser for service interruptions, or for any expense not specifically enumerated in this contract, whether or not such damages or expenses are alleged to be due, in whole or in part, to negligence attributable to Foster Wheeler or its subcontractors.

If the Purchaser is not the Owner, Purchaser shall obtain Owner's agreement in favour of Foster Wheeler re such limits of remedies and liabilities or in lieu thereof indemnify Foster Wheeler for any claims in excess of such limits.

The remedies of the Purchaser set forth in this contract are exclusive.

7. Payment shall be made on presentation of invoices. Minimum charge shall be for one day's service.

Form 455 (Rev. B)

PRICE: $153,415. (ONE HUNDRED AND FIFTY-THREE THOUSAND, FOUR HUNDRED AND FIFTEEN DOLLARS).

FREIGHT: $862. (EIGHT HUNDRED AND SIXTY-TWO DOLLARS).

VALIDITY: Valid for acceptance on or before May 31, 1982.

DELIVERY: Ex Works one year from date of order. Prices are fully escalatable according to Page 73. Federal and Provincial Taxes are extra.

TERMS OF PAYMENT:

10% within 60 days of order award.

25% 4 months after order award.

25% 8 months after order award.

40% on shipment.

We trust that the above fully satisfies your requirements. However, should you have further questions please contact us.

Yours very truly,

FOSTER WHEELER LIMITED

R.H. Renshaw,
Vice-President,
Nuclear and Special Products.

RHR:cmu

APPENDIX E

FOSTER WHEELER DRAWINGS:

C 825-282, Rev. 1 - High Temperature Erosion Test Facility

C 825-283, - High Temperature Erosion Test Facility - Details

APPENDIX F

PURCHASED EQUIPMENT SUPPLIERS

1. Fisher 620 Regulator – Lakeside Controls Limited (519-472-6771).

2. Particle Feeder – Sylvestor & Company (216-831-0880).

3. Acceleration Tube Furnace, Main Gas Heater Furnace, Ceramic Retort and Controls – Applied Test Systems, Inc. (412-265-1546).

   Canadian Agent for above – Intertechnology Limited (416-445-5500).

4. Specimen Holder Drive Components: – Canadian Bearings (416-688-4380)

   Boston Control VEL100
   Boston Motor V9100B
   Boston Reducer F321-15-G
   Boston Base 56588
   Boston Tach Generator TG-2 63327
   Meter for Tach Generator
   Dodge Rigid Coupling R-25
   Dodge Bushing 2517

April 21, 1982

APPENDIX G

VISIT REPORTS

General Electric Co., Schenectady
University of Delaware
National Bureau of Standards
Battelle - Columbus Laboratories
University of Cincinatti
Electric Power Research Institute
Lawrence Berkeley Laboratories,
University of California

VISIT REPORT

To:
General Electric Company
55 North Avenue
Schenectady, NY 12345

Person Contacted:
Adrian M. Beltran
Manager, High Temperature Materials Processing
(518) 385-5416

Date:
20 October 1981

Principal work carried out on the G.E. test rig is the investigation of high-temperature gas turbine alloys and of materials in a PFBC environment. They also do erosion work on blade coatings.

The present rig has been in use since 1979 under a two-year contract from EPRI, which G.E. expect to see extended for another two years shortly. The present rig replaced an earlier rig built in the 1950's.

The rig operates at one atmosphere, with maximum temperature of 875°C and maximum gas entry velocity of 300 m/sec. Mass flow rate 0.4 kg/sec. Aim is to simulate the conditions that the first stage of a gas turbine would see with impulse stage velocities of 270 m/sec. and reaction stage velocities of 420 m/sec. They have been using flyash smaller than 10 microns (only 2% above 10 microns, most in the range 3-5 microns). The Coal Utilisation Research Laboratory (CURL) on the same site as the Central Electricity Generating Board (CEGB) Laboratory at Leatherhead in the U.K. and EXXON in New Jersey both have similar purpose test rigs.

In the G.E. rig natural gas is burnt to get the required temperature and velocity. The flyash used in their tests is supplied in drums by CURL and EXXON, the material is very hygroscopic and is liable to cake unless kept dry.

The complete rig cost about US$250,000.

Corrosion problem decreased rapidly with lower temperatures. At high temperatures there are high alkali levels in the vapour phase.

Caution about ceramic lined walls in the test rig is that the ceramic may flake off. The rig was insulated with loose glass-wool insulation - untidy, inefficient, the dust is a health hazard - definitely to be avoided.

A. Wyatt
....
A. Wyatt

AW/djp

2 November 1981

VISIT REPORT

To:
University of Delaware
Materials Durability Division
College of Engineering
University of Delaware, Newark, DE 19711

Person Contacted: Dr. Abdul Latif (302) 738-2411

Date: 21 October 1981

Dr. Latif is a post-doctoral student of Dr. Jeff Edington. Egyptian-born, he is a Canadian citizen and completed his Ph.D. at the University of Waterloo and is planning to return to Canada on completion of his current contract.

The University has two test rigs - a room temperature one and a new high-temperature rig only recently completed and debugged. The high-temperature rig is much closer to that envisioned for Canadian use, and is readily portable. Argon is used as the carrier gas and is electrically heated. Although the argon gas can easily be heated to 1000°C, it rapidly cools and drops to 800°C at the specimen. A supplementary electric heater is used just ahead of the specimen furnace to control the temperature to within a few degrees Celsius. The rig operates over a velocity range of 25-200 m/sec., up to eight specimens can be mounted on the circular specimen holder. Care is required in mounting the specimen furnace to the supporting frame to allow for expansion but with low heat conduction losses. The inside dimensions of the specimen furnace were approximately 20 cm. diameter x 30 cm. high. All equipment is cold wall.

Equipment was supplied by:-

Gas Heater - Astro Industries
606 Olive Street
Santa Barbara, CA 93101 (805) 963-3461

Specimen Furnace - Applied Test Systems Inc. (Ed Abel - Sales Manager)
Saxonburg Boulevard
Saxonburg, PA 16056 (412) 265-3300

Powder Feeder - Sylvester and Co
24700 Highpoint Road
Beechwood, OH 44122 (216) 831-0880

... /2

Pressure Differential Transducers - Sensotec Inc.
1200 Chesapeake Avenue
Columbus, OH 43212 (1-800-848-6564)

Alumina Particles - Diamonite Products Mfg. Inc.
453 West McConkey Street
Shreve, OH 44676 (216) 567-2145

....
A. Wyatt

AW/djp

2 November 1981

VISIT REPORT

To: National Bureau of Standards
U.S. Department of Commerce
Gaithersburg, MD

Person Contacted: Dr. A. W. (Bill) Ruff
Materials Building, Room B114
(301) 921-2811 Ext. 2966

Date: 21 October 1981

NBS have two test rigs - both for operation at high temperature. The construction details of the rigs are very simple. Oxygen and propane are used to give temperatures up to 1400°C. Most of their testing was done at about 975°C with particle velocities of 15 to 70 m/sec. Abrasive particles are loaded into a shaker and entrained with compressed air into the hot gas stream.

Only one specimen can be tested at a time. Particle velocity is measured with a standard two-disc device. The rig was built in 1975 and has not been used for the past couple of years. The burners and cones were supplied by Jacob Knapp & Son of Newark, N.J.

A. Wyatt
....
A. Wyatt

AW/djp

2 November 1981

VISIT REPORT

To: Battelle
Columbus Laboratories
505 King Avenue
Columbus, Ohio 43201

Person Contacted: Dr. Ian G. Wright
Associate Manager, Corrosion Section (614) 424-4377

Date: 10 November 1981

Battelle Metal Science Group has done a lot of work in corrosion design for high temperature applications, particularly in the field of erosion/corrosion testing.

Initially the problem orientation was to study for high temperature erosion characteristics in coal utilization projects. Tests carried out assisted, however, in understanding factors involved in erosion/corrosion, identification of alloys, formation of oxide scales, material degradation by erosion, oxidation resistance, regimes in which erosion dominates or contributes to degradation, the quality of erodant and how it modifies oxidation patterns, etc.

Battelle's high temperature test rig operates up to 1450°F and with velocities up to 60 m/sec.

Gas mixed to standard flue gas composition, heated in an electric furnace filled with silicon carbide chips, is used as carrier gas. The heated gas passes through 304 stainless steel gauze. The erodant jet (carrier gas and the erodant) is accelerated from the low velocity chamber through the accelerator nozzle. The length of the accelerator nozzle was selected to suit the velocity range (higher the velocity, longer the piece).

Alumina and silica balls of 15 to 75 microns and fly ash of 10-20 microns have been used as erodant. A SYLCO powder feeder (Mark IX, Serial 561), which cost US $2,700, is used. This is the same type of feeder as used in the test rigs of Pratt & Whitney (Connecticut) and of the University of Delaware.

Battelle stated that the test rig at the University of Delaware is an improved version of their own with reference to the particle feed control and specimen heating system.

. . . 2

Velocity of the erodant jet is determined by measuring the differential pressure in the accelerator nozzle pipe. Control of velocity is by precalibrating the differential. The temperature sensor of the erodant flow is protected by a cold argon flush.

The specimen furnace is quartz lamp heated. Thermocouples in the furnace are shielded stagnant type. The slip ring type thermocouple used to measure the specimen temperature did not result in accurate temperature measurement.

A 20 specimen holder can be used in this test rig. The specimen holder is water cooled at the bottom to cool the rotating mechanism.

The test rig cost was US $18,000 in 1975 without the powder feeder and instrumentation. The complete test rig takes up a space about 9 ft. high X 6 ft. wide X 3 ft. deep.

In their work they have found that at higher velocities the protective oxide scale is destroyed and the corrosion rate accelerated, with a linear relationship between velocity and corrosion rate. At lower velocities there is a parabolic relationship. There is some question about where this change point occurs, but it is in the region of 20-25 m/sec.

....

A. Wyatt

AW/lc

18 November 1981

VISIT REPORT

To:

Department of Aerospace Engineering
& Applied Mechanics
University of Cincinatti
Cincinatti, Ohio 45221

Person Contacted: Dr. Widen Tabakoff (513) 475-8000

Date: 10 November 1981

The Cincinatti rig is very different from those at Delaware, National Bureau of Standards and Battelle. In the design of this rig considerable attention was given to aerodynamic considerations, more exact control of variables such as gas velocity, particle velocity, particle size and particle flow rate. The rig can be operated at temperatures up to 1100°C, and in the particle velocity range of 60 to 450 m/s. Its principal purpose is to test jet engine materials. In order to get the particles up to gas stream velocity and temperature they pass down a vertical steam-cooled duct approximately 4 m long. There is also provision for high speed photography of the gas stream impacting on the specimen.

Tabakoff drew attention to the problems of wear at the end of the gas nozzle on the other rigs, which would affect the angle of the issuing gas jet and thus the area of imprringement on the specimen and the true velocity of impact. To reduce this problem the nozzle could be made of hardened materials and the final 10 cm. or so made to be easily replaceable.

....
A. Wyatt

AW/lc

18 November 1981

VISIT REPORT

To:
Electric Power Research Institute
3412 Hillview Avenue
P. O. Box 10412,
Palo Alto, Calif. 94303

Person Contacted:
Dr. John Stringer
Program Manager, High Temperature Corrosion-Materials Support (415) 855-2472

Date:
11 November 1981

Dr. Stringer gave an overview of the "state-of-the-art" in erosion and erosion/corrosion with reference to high temperature erosion testing. The method of getting the particles into the gas stream is important-Stringer considered the Battelle and Delaware test rigs as "semi universal" erosion test rigs. The method of heating the gas is also important from point of view of maintaining a uniform temperature at the test specimen and being able to accurately control the temperature. He considered that the best maximum velocity would be in the region of 50-60 m/sec. and maximum particle size of about 50 microns. The higher the temperature that the rig is designed for, the more difficult it is to make the rig portable.

He emphasized the difference in the erosion mode of brittle and ductile materials. Experiments show that for large particles (above about 50 microns) that the ratio of grams of material removed to grams of erodant material is virtually constant regardless of how large the particles are above that size.

EPRI are interested in corrosion/erosion problems in a number of different areas:

1. Erosion Damage in I.D. Fans

   This can be reduced by:
   -redesign of fan for lower velocities
   -build the fan of more erosion resistant materials
   -"armour" specific areas so that they can be replaced easily when they wear.

2. Erosion in Economiser (Much less of a problem in superheaters and reheaters since their surfaces are largely protected by slag).
   This can be reduced by:
   -reduce velocities over economiser surface

. . . 2

- re-direct the flue gas so as to avoid concentrating particles in particular area
- "armouring" (as in 1 above)
- careful positioning of sootblowers

Problems can be increased with changes in coal supply and conversion from oil to coal.

3. Let-down valves in coal liquefaction plants

4. Burner nozzles in gasifiers, also gas coolers where there are entrained particles. There are no particular erosion problems downstream of desulphurisation equipment.

5. Corrosion in atmospheric fluidized bed coal combustion

6. Hot corrosion/erosion materials for application to pressurized fluidized bed boilers and gas turbine systems.

A. Wyatt
....
A. Wyatt

AW/lc

18 November 1981

VISIT REPORT

To:
Lawrence Berkeley Laboratories
Building 62, Room 351
University of California
Berkeley, Calif. 94720

Person Contacted: Dr. Alan V. Levy (415) 486-5822

Date: 12 November 1981

Berkeley has both a high-temperature and a room-temperature rig. A brief description of the high temperature test rig is attached. Also attached are Fig. 3, 4 and 5 showing the arrangement of the room temperature erosion test rig. Levy emphasized the importance of heating the whole system since the heat content of the gas is so low that very rapid cooling will occur in any unheated portions of the rig. He did not consider it too important that the particles were not at exactly the same temperature as the gas stream or the specimen.

The Berkeley rig has not operated too well to-date but is undergoing modification and is expected to run satisfactorily in future.

A. Wyatt
....
A. Wyatt

AW/lc
Encl.
18 November 1981

BERKELEY TEST RIG

UNIVERSITY OF CALIFORNIA

DESCRIPTION OF THE HIGH TEMPERATURE EROSION-CORROSION TEST DEVICE

The erosion-corrosion test device has been designed to simulate a wide range of conditions. Fig. 1 shows the tester. Fig. 2 is a schematic of it with the principal components designated. Nitrogen was used as the carrier gas for the particles. Test temperatures can range from room temperature to 1000°C. Achievable velocities range from $<$ 100 feet per second to the supersonic range. Particle loadings range from 0.05 to 30 lb/100 SCF of carrier gas. Gas composition can be varied in future testing as needed to simulate part or all of the reactive gases in a coal gasifier with the composition monitored by a gas chromatograph system. Solid materials can then be subjected to test conditions to determine material behavior in the hostile environment of a coal gasifier, simulating all conditions but the elevated pressures. The angle of impingement of the gas-particle stream is varied by proper placement of the test specimen relative to the eroding-corroding stream.

The function of the device is to mix particles at a known feed rate with a gas and bring the resulting gas-particle stream to a desired temperature and particle velocity. This gas-particle stream then impinges on the test specimen. The test specimen is also to be at the desired temperature before testing is started and is to stay at that temperature during testing.

Refer to Fig. 2 for the following description of system operation. Particles are introduced into the device by means of a pressurized hopper that ensures an adequate supply of abrasive material during testing up to several hours duration at solid loadings simulating those that occur in coal gasifiers. An auger, powered by a motor and motor controller that can be set for various speeds, uniformly feeds particles into the mixing chamber. The particles are preheated by the particle radiant heater before entering the mixing chamber. The gas or gas mixture also enters the mixing chamber after being pre-heated by heating tapes and the gas radiant heater. The velocity of the incoming gas, the tumbling action of the auger, the relative small size of the abrasive particles and the small exit size (3/16 inch I.D.) compared to the size of the mixing chamber (1.5 inches I.D.) ensure a thorough mixing of the particles and the gas stream. The exiting gas-particle stream is then further heated by the nozzle radiant heater. Uniform stream characteristics are imparted to the gas-particle stream as it moves from the mixing chamber, through the nozzle, to the nozzle exit approximately 7/8 of an inch above the specimen. Gas velocities, and thus particle velocities, are achieved by releasing pressurized gas through the device to the near atmospheric pressures encountered in the test chamber. The test chamber is attached to a settling chamber which collects the particles from the exiting gas. The gas is vented to the atmosphere after passing through air filter bags which collect the particles not deposited in the settling chamber.

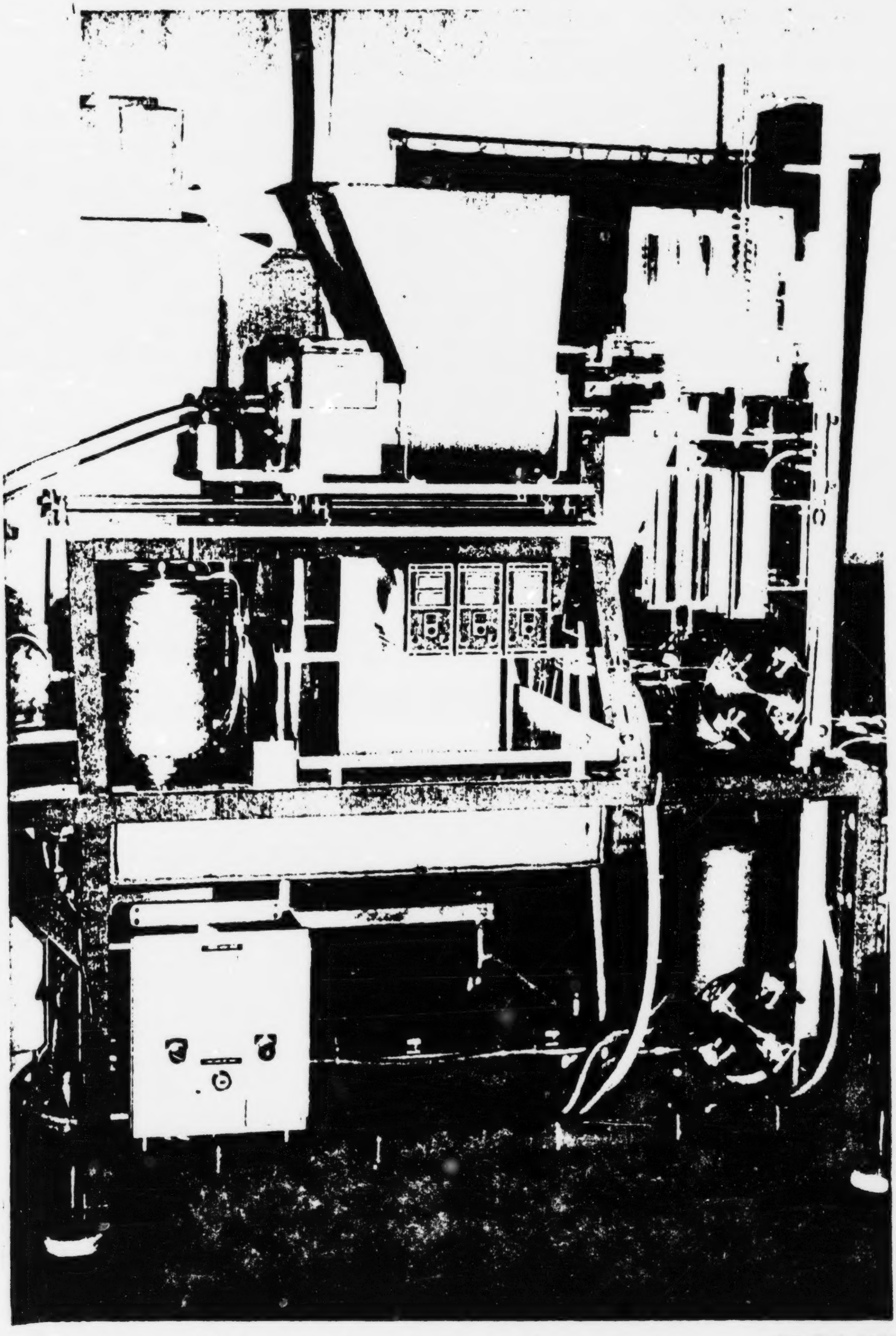

FIG. 1 High Temperature Erosion-Corrosion Test Device CBB 763-2071

Fig. 2. EROSION/COROSION TESTER GAS SYSTEM

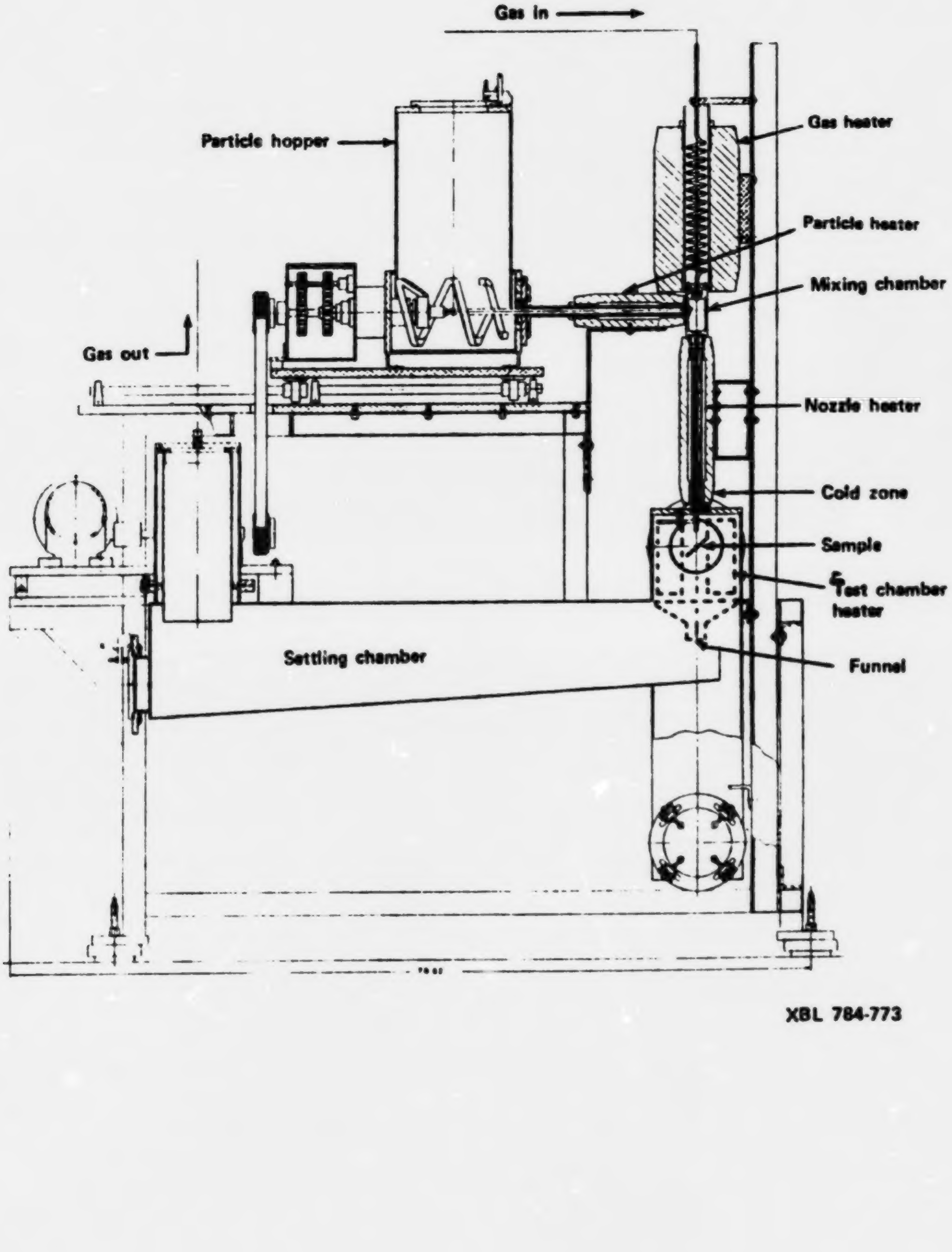
Gas in
Particle hopper
Gas heater
Particle heater
Mixing chamber
Gas out
Nozzle heater
Cold zone
Sample
Test chamber heater
Settling chamber
Funnel

XBL 784-773

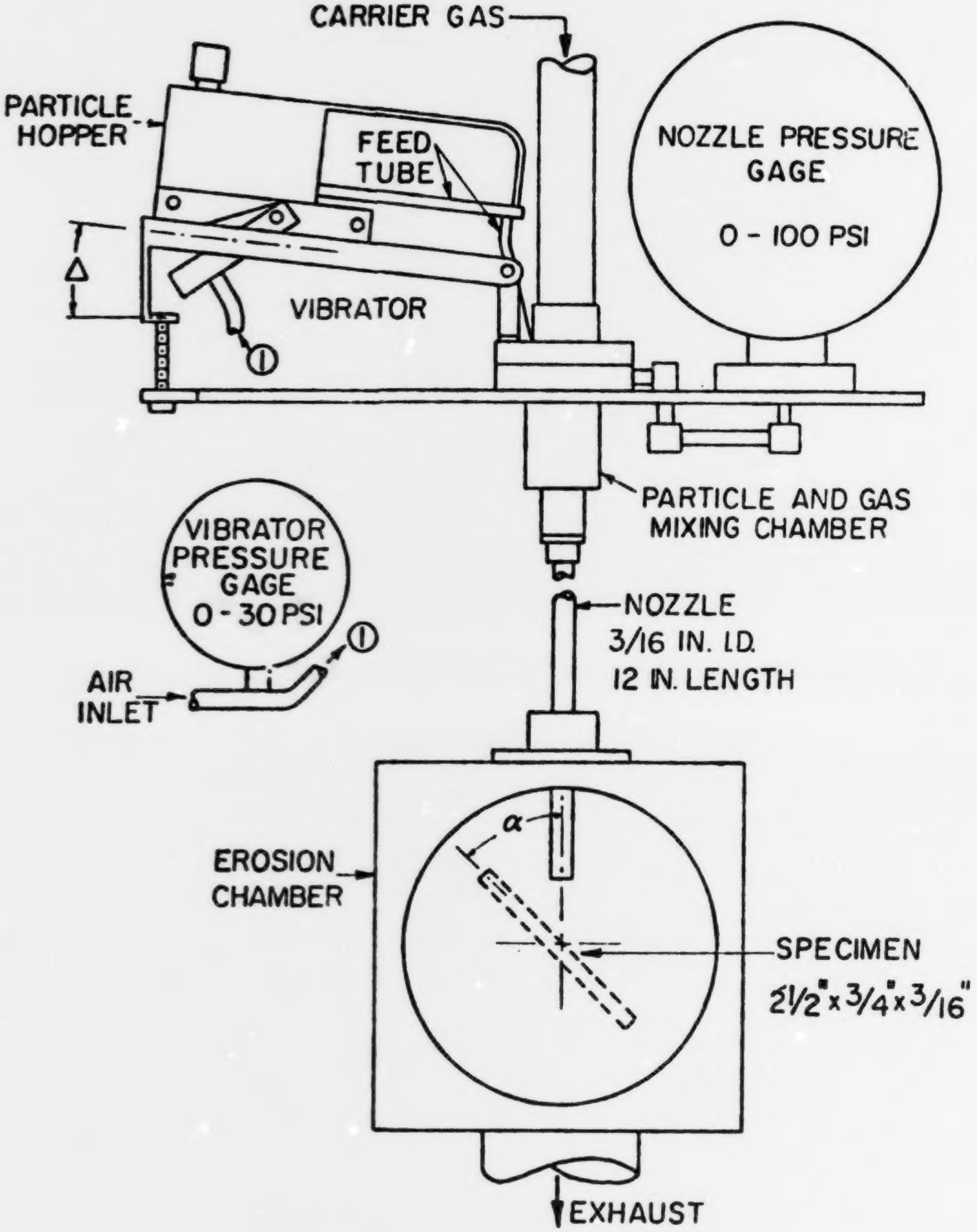
CARRIER GAS
PARTICLE HOPPER
FEED TUBE
NOZZLE PRESSURE GAGE
0 - 100 PSI
Δ
VIBRATOR
①
PARTICLE AND GAS MIXING CHAMBER
VIBRATOR PRESSURE GAGE
0 - 30 PSI
AIR INLET
①
NOZZLE
3/16 IN. I.D.
12 IN. LENGTH
α
EROSION CHAMBER
SPECIMEN
2 1/2" x 3/4" x 3/16"
EXHAUST

Fig. 3

XBL775-5525

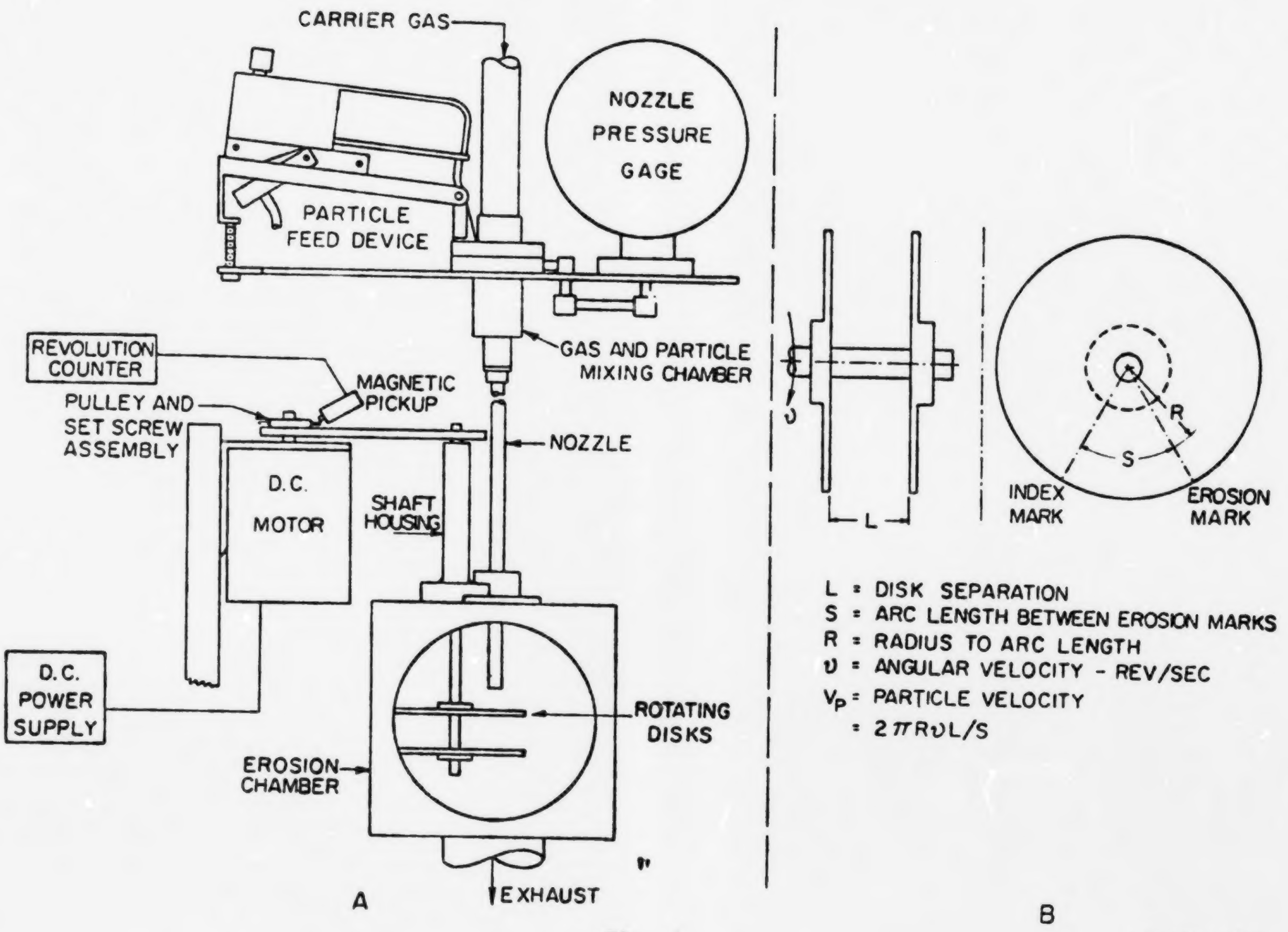
CARRIER GAS
NOZZLE PRESSURE GAGE
PARTICLE FEED DEVICE
GAS AND PARTICLE MIXING CHAMBER
REVOLUTION COUNTER
MAGNETIC PICKUP
PULLEY AND SET SCREW ASSEMBLY
NOZZLE
D.C. MOTOR
SHAFT HOUSING
D.C. POWER SUPPLY
ROTATING DISKS
EROSION CHAMBER
EXHAUST
A
υ
L
S
R
INDEX MARK
EROSION MARK
B

L = DISK SEPARATION
S = ARC LENGTH BETWEEN EROSION MARKS
R = RADIUS TO ARC LENGTH
υ = ANGULAR VELOCITY - REV/SEC
V_P = PARTICLE VELOCITY
$= 2\pi R\upsilon L/S$

Fig. 4

XBL 775-5524

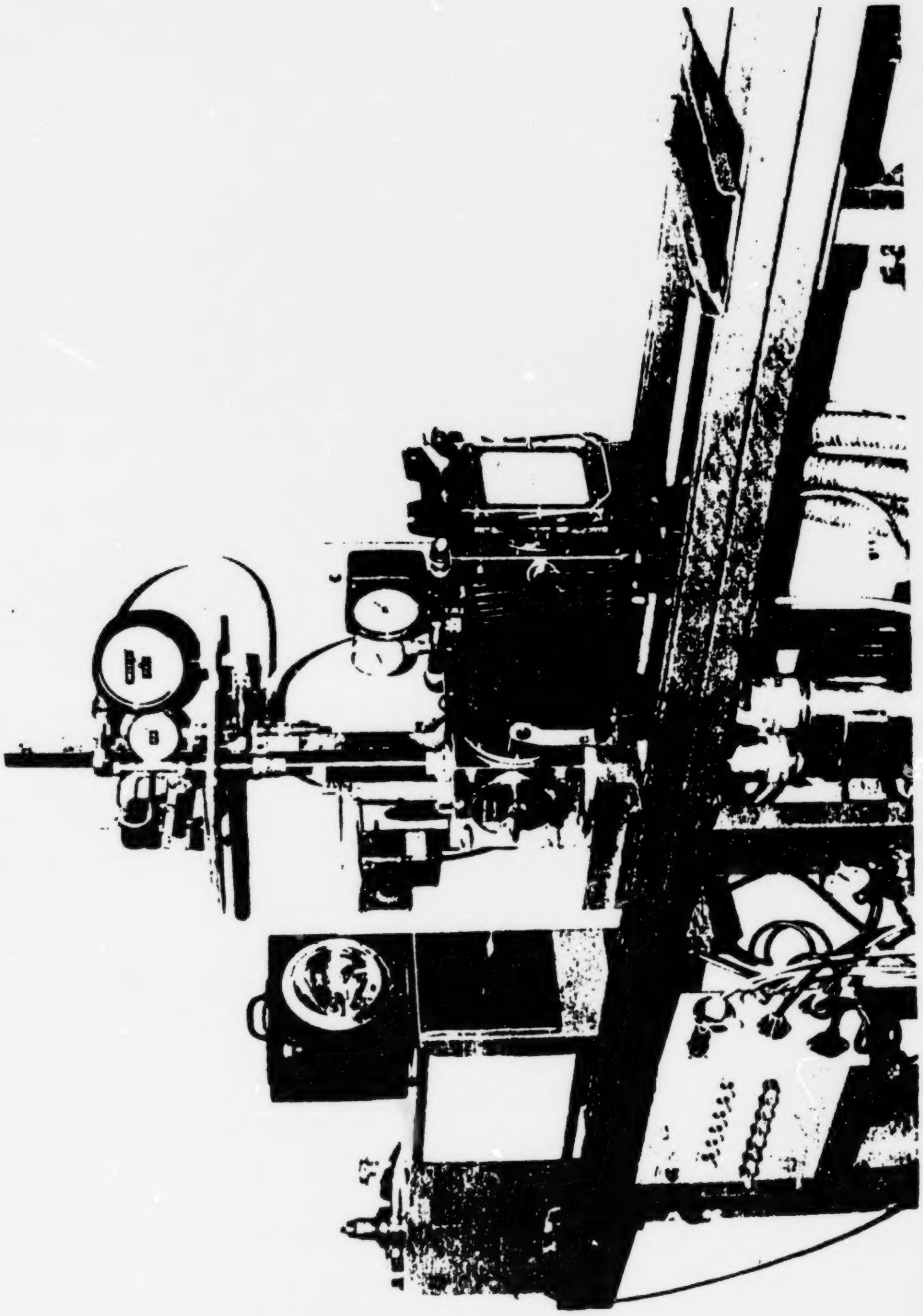

Fig. 5

APPENDIX H

REFERENCE PAPERS

APPENDIX H

REFERENCE PAPERS

Erosion Behavior in a Simulated Jet Engine Environment

- T. Wakeman and W. Tabakoff

A New Approach for Erosion Prediction due to Fly Ash

- R. Kotwal and W. Tabakoff

A Technique to Investigate High Temperature Erosion of Refractories

- Sheldon M. Wiederhorn and D. Ellis Roberts

The Elevated Temperature Erosion of 1100-0 Aluminum by a Gas-Particle Stream

- Padraic A. Doyle and Alan V. Levy

Erosion of Elevated Temperature Corrosion Scales on Metals

- J.A. Maasberg and A.V. Levy

Erosion of Ductile Metals by Solid Particles

- David McFadden

Study of Metals Erosion in High Temperature Coal Gas Streams

- W. Tabakoff, A. Hamed and J. Ramachandran

Test Facility for Material Erosion at High Temperature

- W. Tabakoff and T. Wakeman

ARTICLE NO. 79-0041R

Erosion Behavior in a Simulated Jet Engine Environment

T. Wakeman* and W. Tabakoff†
University of Cincinnati, Cincinnati, Ohio

This paper presents erosion data relevant to gas turbine engines. Data were obtained in a material erosion facility for Ti 6-4 and INCO 718 alloys, for temperatures between ambient and 1300°F, particle velocities between 200 and 900 ft/s, and particle impingement angles between 20 and 90 deg. These data indicate that the erosion rate as a function of temperature is relatively constant for each material up to a temperature which is unique to the material, beyond which it increases rapidly. Further, the angle dependence of erosion rate remains relatively constant with increasing material temperature.

Introduction

IN many industrial and military applications, the erosive action of high-speed particles results in serious problems. Erosion has been pointed out as a problem in such diverse areas as gas turbines, rocket nozzles, coal-fired boiler systems, etc. Recent interest into this old problem coincides with increased usage of gas turbines in dusty terrains. The cost of maintaining such engines in dusty environments is great. Air filtration has alleviated the problem somewhat, but filtration reduces both payload and engine performance. If erosion can be incorporated as an engine design parameter, perhaps an erosion-tolerant engine can be produced.

Two problems are involved in erosion prediction. First, the velocity, direction, and number of particles striking the surface must be determined. These are naturally affected by the general and local flow conditions. The second part involves the calculation of the surface material removed using the information obtained from the first part. The problem of predicting erosion in rotating machinery is particularly complicated by multiple impacts.[1]

Present State of the Art

The theoretical studies concerning erosion are predominantly empirical. They involve basic assumptions as to the process governing material removal. Finnie[2] and Smeltzer et al.[3] have conducted theoretical analyses of the erosion of ductile materials. In more recent investigations,[1,4,5] further insight into the actual mechanism of erosion has been obtained by examining the target surface at high magnification using metallographic techniques and electron microscopy. A detailed description of these test facilities at the University of Cincinnati's Propulsion Laboratory can be found in Refs. 1 and 6.

In many turbomachinery applications, erosion takes place at elevated temperatures near the strength limiting temperatures of the materials used. For example, even in the case of turbojet engine compressors, titanium used in the early stages and the INCO 718 used in the aft stages are operated at metal temperatures in excess of 316 and 593°C (600 and 1100°F), respectively. In both cases, these temperatures are very close to the maximum operating temperatures used for these materials. The erosion characteristics can significantly change under elevated temperatures, as evidenced in the data presented by Tabakoff and Hamed.[6] These data were obtained with the sample heated to temperatures up to 204°C (400°F). Although this temperature falls far short of those experienced in turbine engines, it still indicates the significant effect of temperature on erosion and probably on the rebound characteristics.

High-Temperature Erosion Rig

An erosion test facility was designed to provide erosion and rebound data in the range of operating temperatures experienced in compressors and turbines. For that purpose, this facility has been designated to operate at a test section temperature in the range of ambient to 1093°C (2000°F). In addition to high temperatures, the facility properly simulates all erosion parameters which were found to be important from previous testing at ambient temperatures. These parameters include particle velocity, angle of impact, particle size, particle concentration, and sample size. Close attention was given to aerodynamic effects to insure that important parameters, such as angle of attack, are not masked or altered.

General Description of the Erosion Rig

The schematic of the test apparatus, is shown in Fig. 1, consists of the following components: particle feeder (A), main air supply pipe (B), combustor (C), particle preheater (D), particle injector (E), acceleration tunnel (F), test section (G), and exhaust tank (H).

The equipment functions as follows: A measured amount of abrasive grit of a given constituency is placed into the particle feeder (A). The particles are fed into a secondary air source and blown up to the particle preheater (D), and then to the injector (E) where it mixes with the main air supply (B), which is heated by the combustor (C). The particles are accelerated by the high-velocity air in a constant area duct (F), which is steam cooled before impacting the specimen in the test section (G). Past the test section, the particulate flow is mixed with the coolant and dumped in the exhaust tank.

The important individual components of the high-temperature erosion facility will be described. Each component was designed with cost, maintainability, availability, and functionality as prime considerations.

Particle Feeder Assembly (A)

The particles from the feeder are blown up to the particle injector area. The feeder is designed as a pressure vessel to operate at high air pressures. However, this pressure is equalized above and below the plunger by a bypass line. This

---

Received Dec. 4, 1978; presented as Paper 79-0041 at the AIAA 17th Aerospace Sciences Meeting, New Orleans, La., Jan. 15-17, 1979; revision received May 21, 1979. Copyright © American Institute of Aeronautics and Astronautics, Inc., 1978. All rights reserved. Reprints of this article may be ordered from AIAA Special Publications, 1290 Avenue of the Americas, New York, N.Y. 10019. Order by Article No. at top of page. Member price $2.00, nonmember, $3.00 each. **Remittance must accompany order.**

Index categories: Structural Stability; Thermal Stresses.

*Graduate Research Assistant, Dept. of Aerospace Engineering and Applied Mechanics.

†Professor, Dept. of Aerospace Engineering and Applied Mechanics. Associate Fellow AIAA.

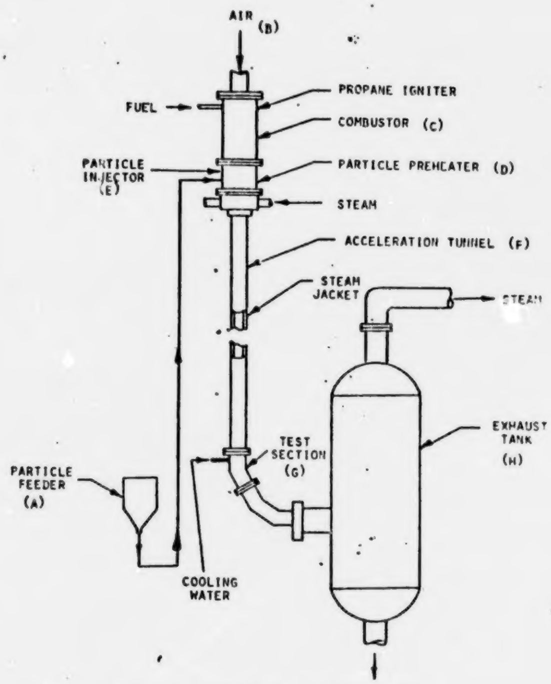

Fig. 1 Schematic of erosion test facility.

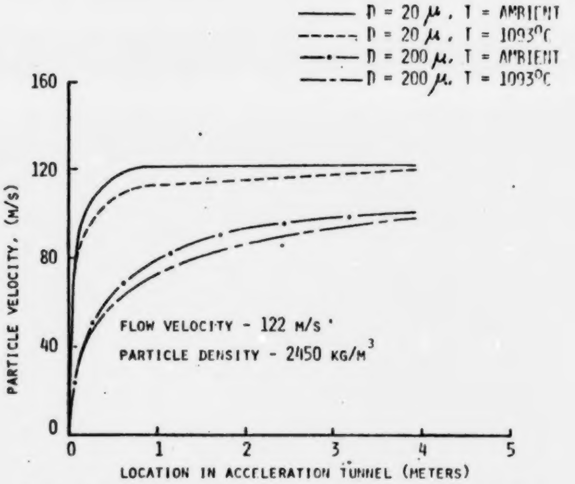

Fig. 2 Particle dynamics in a constant area acceleration tube.

Table 1 Composition of sample materials and heat treat conditions of INCO 718

Ti 6-4[a]		INCO 718[b]	
Al	6.2%	Cr	19.0%
V	3.95%	Cb + Ta	5.1%
Fe	0.12%	Mo	2.95%
O	0.11%	Ti	1.0%
N	0.025%	Al	0.5%
Others	0.40% max.	Ni	52.5%
Ti	Balance	Cu	0.5%
		Si	0.3%
		C	0.1% max.
		Fe	Balance

[a] No heat treat (as received from mill). [b] Heat treat 1700°F-1 h air cool; at 1325°F-8 h furnace cool at 100°F/h to 1150°F-8 h air cool.

allows the system to be calibrated under gravity feed conditions.

Combustor (C)

High-temperature combustion products are supplied by a modified General Electric J93 can combustor.

Particle Preheater (D) and Injector (E)

The preheater consists of a coil contained in a 203.2 mm (8 in.) i.d. pipe section with a distributor/injector to provide a well-distributed preheated particle supply. The particles are blown up to the accelerating section of the tunnel by secondary air, which flows from the particle feeder and passes through the preheater coils. The particles are distributed in the main airstream through their impingements on a specially contoured ball. It was observed that the particles impinging on this ball did not fragment. The particle gas mixture is accelerating through an elliptical nozzle to the acceleration section.

Acceleration Section (F)

The acceleration tunnel has a rectangular cross section of 89 × 25.4 mm (3½ × 1 in.) which is 3.66 m (12 ft) long. This section is steam cooled to minimize the heat losses. With this type of cooling, the 316 stainless-steel liner operates at a maximum of 760°C (1400°F). This results in a drop in the gas stream temperature of about 93°C (200°F). The use of water as a coolant would have resulted in at least three time the heat loss and an unacceptable gas stream temperature drop in this section.

The particle velocities attained in this acceleration section were predicted analytically and verified by experimental methods. Pressure measurements at the inlet, midsection, and exhaust were used to account for the tunnel friction when calculating the fluid velocity variation in this section. These velocities were used in calculating the particle velocities due to their acceleration by the gas stream. The calculated particle velocities are shown in Fig. 2 in the case of low fluid velocity of 122 m/s (400 ft/s) at 1093°C (2000°F) and at ambient temperature. From this figure it can be seen that the particle velocity is an exponential function of tunnel length. The law of diminishing returns would dictate that a tunnel length of 0.6-0.92 m (2-3 ft) would be sufficient for both relatively large and small particles (200 and 20 μ). A tunnel length of 3.66 m (12 ft) was chosen, however, for several theoretical and practical reasons.

Test Section (G)

The test section is designed such that the particle-laden air is channeled over the specimen and the aerodynamics of the fluid surrounding the test sample are preserved. The test specimen can be oriented at different angles to the gas stream by rotating the specimen holder. The test section is water cooled. The coolant water is discharged into the particulate gas stream at the downstream end of the test section.

Test Model

The previously described erosion test facility was used to obtain basic erosion data for two sample materials—Ti 6-4 and INCO 718. Detailed analysis of these two materials, as well as the heat treat conditions, are given in Table 1.

The material erosion was determined from the weight of the 19.0 × 25.4 mm specimen and after testing. The abrasive particles used consisted of quartz sand (SiO_2) obtained from commercial suppliers. The sand was sifted to obtain a particle size range of 150-180 μ. The experimental measurements were obtained for sand-particle velocities varying from 200 to 900 ft/s and target temperature varying from ambient to 1300°F, approximately 10% of the test points were repeated and the test facility was calibrated at approximately 100 test point intervals to assure uniformity of data. Several test points were accumulated with no particle injection resulting in no significant change in sample weight. Significant oxidation and corrosion of the samples were not expected, due to the short duration (5 min at test temperature).

It is well known from previous testing that particle velocity, particle impingement angle, aerodynamic effects, and the material sample temperature strongly influence the erosion rate. These parameters were varied in the present test program. Parameters of second importance, such as particle size, sample size, particle concentration, and sample heat treat conditions, were held constant in this investigation.

Particle velocity was controlled by varying the tunnel airflow. The particle impingement angle was set by rotating the sample relative to the flow stream direction. Sample temperature was varied by heating the flow stream which heated the material sample to the desired temperature. Aerodynamic effects are preserved by the test section tunnel design. Flow conditions in the tunnel provide the aerodynamics around the blades sample.

Test data were accumulated by setting the particle impingement angle at 20, 25, 45 and 90 deg; the sample temperature and the particle velocity. The experimental data were then plotted primarily vs velocity with angle of attack and temperature. Cross plates were made to show the effect of the angle of attack and the material sample temperature on the erosion rate,

Experimental Results and Discussion

Effect of Particle Velocity

Particle velocity was found to have a powerful effect on erosion rates. In all cases investigated, the erosion rate was shown to be proportional to the particle velocity taken to a constant power. This is similar to the results found by earlier investigators. Erosion rate vs particle velocity data for Ti 6-4 is displayed in Figs. 3-6. On each figure, the volumetric erosion rate is plotted vs particle density for different sample temperatures. Each figure represents a different particle impingement angle. For Ti 6-4, the erosion rate is shown to be proportional to the particle velocity to the *n* power, when *n* represents the slope of the straight lines on these figures. The range of *n* is dependent on the angle of attack and the sample temperature.

Erosion rate data for INCO 718 are similarly plotted on Figs. 7-10. Similar to Ti 6-4, the erosion rate was found to be proportional to particle velocity, taken to a power with the exponent a function of both sample temperature and impingement angle.

Both materials tested exhibited similar characteristics with the velocity exponent tending to increase with increasing impingement angle and decrease with increasing sample temperatrure. It is interesting to note the wide range of the exponent values for any one material. This variation has been shown to be related to the particle velocity restitution ratio in Ref. 1. Apparently, both increases in impingement angle and sample temperature affects the erosion rate.

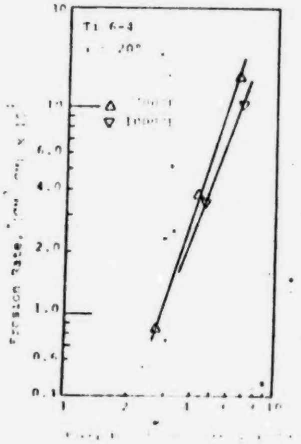

Fig. 3 Ti 6-4 erosion rate vs particle velocity for different sample temperatures, α = 20 deg.

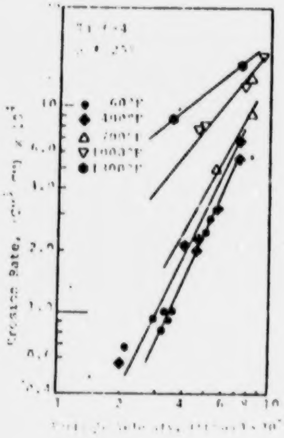

Fig. 4 Ti 6-4 erosion rate vs particle velocity for different sample temperatures, α = 25 deg.

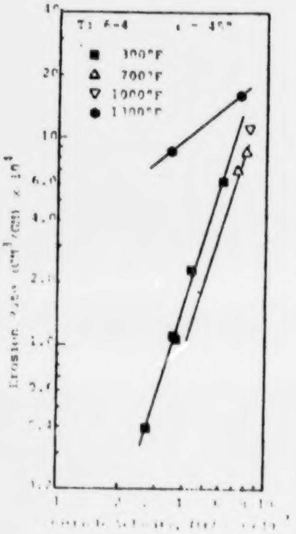

Fig. 5 Ti 6-4 erosion rate vs particle velocity for different sample temperatures, α = 45 deg.

Effect of Sample Temperature

The erosion rate vs the sample temperature is presented in Figs. 11 and 12 for the two other materials being considered. The results in these figures are for a particle velocity of 500 ft/s, and are cross plotted from the erosion rate vs particle velocity curves presented earlier. Erosion rate vs sample temperature showns a slightly different trend for Ti 6-4, as shown in Fig. 11. The erosion rate increases slowly as the sample temperature is increased from room temperature to 800°F for 25 and 45 deg particle impingement angles. As the sample temperature is increased above 800°F, the erosion rate increases rapidly. The erosion rate shows a much slower rate of increase for Ti 6-4 at an impingement angle of 90 deg as sample temperature is increased. Inspection of Fig. 12 shows that the erosion rate for INCO 718 increases slowly or stays constant up to a sample temperature around 900°F, then increases abruptly as the sample temperature increases. This trend is independent of the impingement angle for INCO 718.

Effect of Particle Impingement Angle

It is well known that erosion rate is a function of particle impingement angle. For ductile materials, erosion rate in-

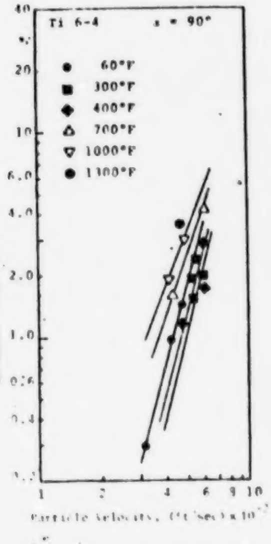

Fig. 6 Ti 6-4 erosion rate vs particle velocity for different sample temperatures, $\alpha = 90$ deg.

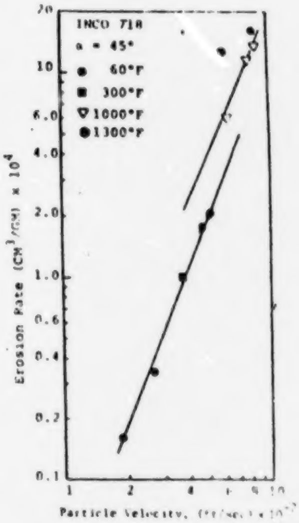

Fig. 9 INCO 718 erosion rate vs particle velocity for different sample temperatures, $\alpha = 45$ deg.

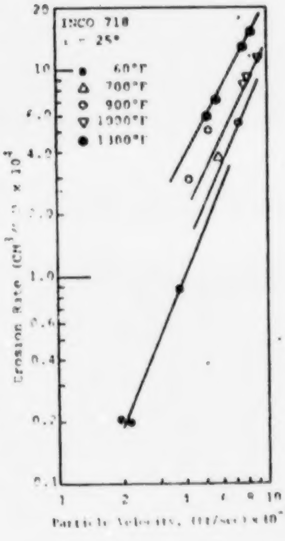

Fig. 7 INCO 718 erosion rate vs particle velocity for different sample temperatures, $\alpha = 25$ deg.

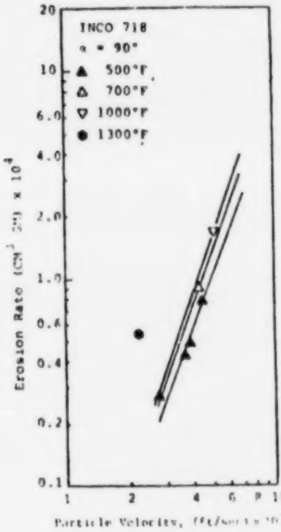

Fig. 10 INCO 718 erosion rate vs particle velocity for different sample temperatures, $\alpha = 90$ deg.

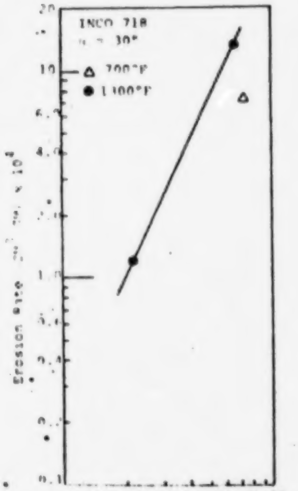

Fig. 8 INCO 718 erosion rate vs particle velocity for different sample temperatures, $\alpha = 30$ deg.

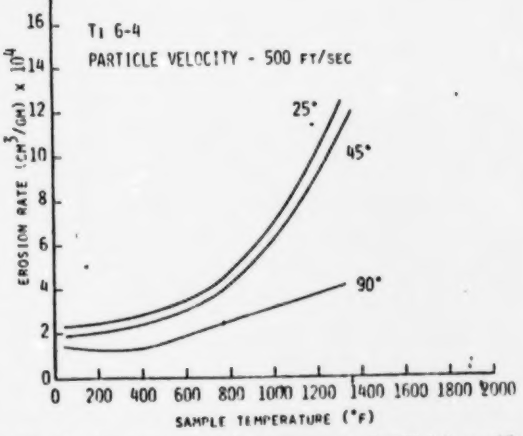

Fig. 11 Erosion rate vs sample temperature, for Ti 6-4, $\alpha = 25$, 45, and 90 deg.

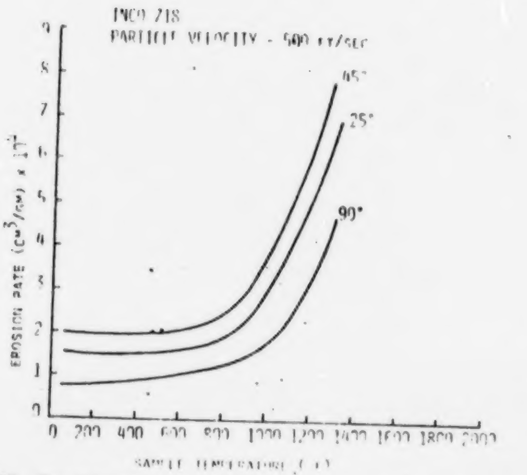

Fig. 12 Erosion rate vs sample temperature, for INCO 718, $\alpha = 25$, 45, and 90 deg.

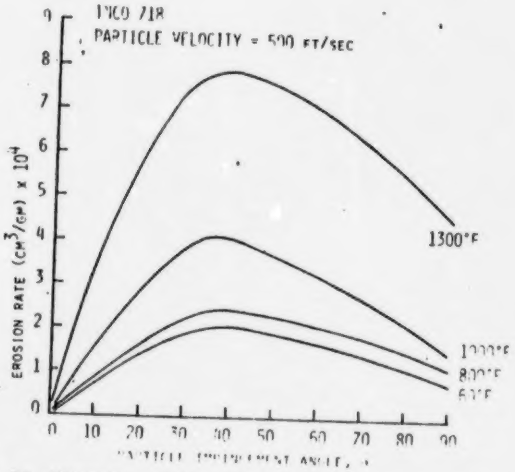

Fig. 14 INCO 718 erosion rate vs particle impingement angle for different temperatures.

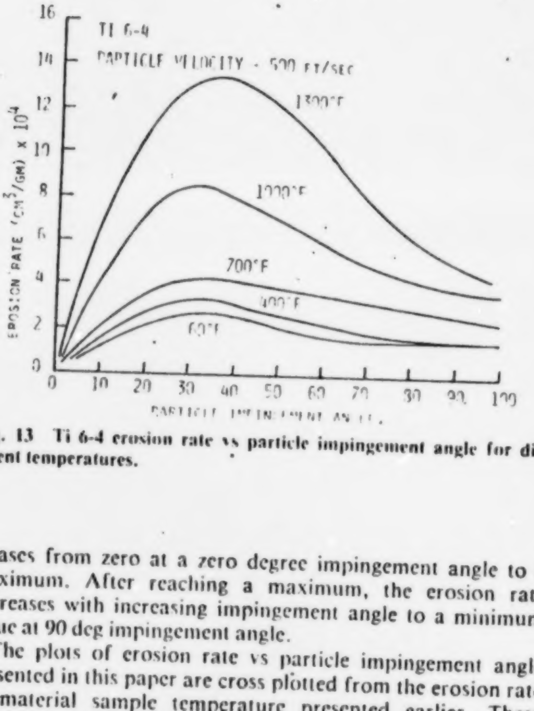

Fig. 13 Ti 6-4 erosion rate vs particle impingement angle for different temperatures.

creases from zero at a zero degree impingement angle to a maximum. After reaching a maximum, the erosion rate decreases with increasing impingement angle to a minimum value at 90 deg impingement angle.

The plots of erosion rate vs particle impingement angle presented in this paper are cross plotted from the erosion rate vs material sample temperature presented earlier. These impingement angle curves are for a particle velocity of 500 ft/s in all cases. Also, each plot of erosion rate vs impingement angle is for a constant sample temperature. The erosion rates vs the particle impingement angles for different sample temperatures are presented in Figs. 13 and 14 for Ti 6-4 and INCO 718, correspondingly. The erosion rate is a maximum for Ti 6-4 at an impingement angle of 30 deg and for the INCO 718 at 35 deg.

Effect of Sample Material

The erosion rate results presented previously show significantly different levels for the two different materials considered. An attempt was made to determine a parameter that would account for the different material properties. The erosion rate vs the sample temperature for a particle velocity of 500 ft/s and impingement angle of 25 deg is presented for the two materials in Fig. 15. From this figure, it becomes apparent that the erosion rate behaves in a similar fashion for each material. The level of erosion and the temperature where the erosion rate increases rapidly is different for each material.

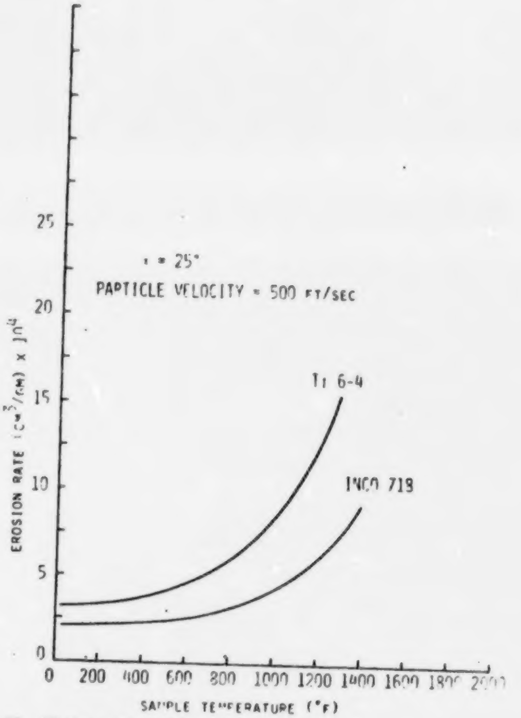

Fig. 15 Ti 6-4 and INCO 718 erosion rate vs sample temperature, $\alpha = 25$ deg.

In order to improve the correlation of erosion rate with the sample temperature and remove the material effect, the erosion rate was plotted vs the normalized sample temperature. In Fig. 16, the sample temperature is normalized using sample melting temperature (2920°F for Ti 6-4 and 2300°F for INCO 718). This plot does not seem a significant improvement compared with sample temperature (Fig. 15). In addition, the sample material annealed temperature (650°F for Ti 6-4 and 1750°F for INCO 718) was used as the normalizing temperature and is shown in Fig. 17. This normalization of the data gives the best correlation of the data for both materials.

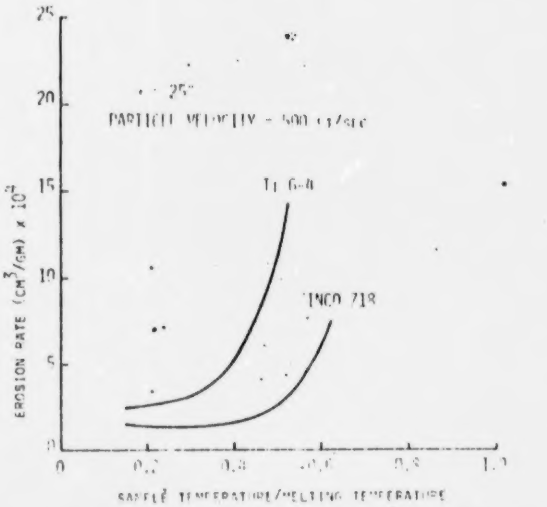

Fig. 16 Ti 6-4 and INCO 718 erosion rate vs sample temperature/melting temperature, $\alpha = 25$ deg.

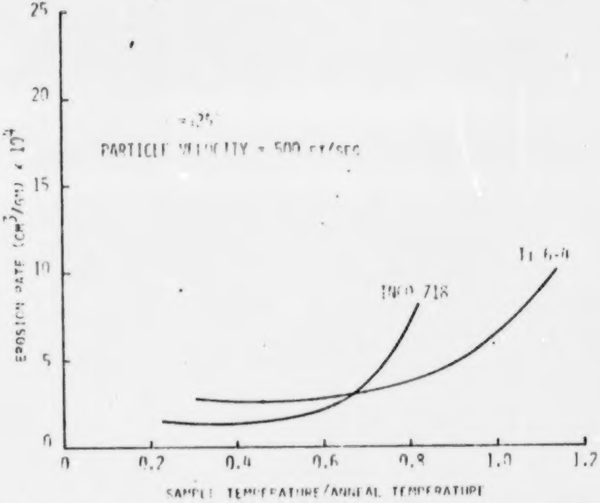

Fig. 17 Ti 6-4 and INCO 718 erosion rate vs sample temperature/anneal temperature, $\alpha = 25$ deg.

The material erosion rate has been related to material yield strength, as in Ref. 8. The annealed temperature indicates a reduction in yield strength to a low level. Figure 17 shows that the material erosion rate may be related to the annealed temperature, and that the erosion rate increases abruptly as the material sample temperature approaches the annealed temperature. This could indicate that the material erosion rate increases rapidly as the yield strength decreases rapidly near the annealed temperature. This would support the contention that material erosion rate is related to material yield strength.

Presently, we are investigating other alloys which will be used in future gas turbines. After the experimental work is completed, the data obtained will be used in developing empirical equations for predicting the erosion rates of ductile alloys at different temperatures. The empirical equations, which were developed by Grant and Tabakoff,[1] are applicable only at ambient temperatures. These relations will be used as a base for modifications to include the measured effects of higher temperatures on erosion. These modifications will incorporate the dependency of the erosion rate on the target temperature, as well as the thermal properties of the target material itself.

Conclusion

Two significant conclusions can be drawn from the data presented. Erosion rate remains relatively constant for INCO 718 and Ti 6-4 from room temperature up to a temperature unique for each material, then increases rapidly with material temperature. Also, the impingement angle at which maximum erosion occurs for each material is independent of the material sample temperature. Additionally, the velocity exponent varies considerably with changes in both the impingement angle and the material sample temperature. Ultimately, the data presented herein will be used to predict the erosion in jet engine compressors. Use of only room temperature data could yield erroneous results due to the changes in the material erosion rate with increasing material temperature.

Acknowledgment

This work was sponsored by the U.S. Army Research Office—Durham, under Contract No. DAAG-29-76-G-0229.

References

[1] Grant, G. and Tabakoff, W., "Erosion Prediction in Turbomachinery Resulting from Environmental Solid Particles," *Journal of Aircraft*, Vol. 12, May 1975, pp. 471-478.

[2] Finnie, I., Wolak, J., and Kabil, Y., "Erosion of Metals by Solid Particles," *Journal of Materials*, Vol. 2, Sept. 1967, pp. 682-700.

[3] Smeltzer, C.E., Gulden, M.E., McElmury, S.S., and Compton, W.A., "Mechanisms of Sand Dust Erosion in Gas Turbine Engines," USAAVLABS Tech. Rept., Aug. 1970.

[4] Frass, A.P., "Survey of Turbine Bucket Erosion Deposits, and Corrosion," ASME Paper 75-GT-125, presented at the Gas Turbine Conference, Houston, Texas, March 2-6, 1975.

[5] Finnie, I., "An Experimental Study on Erosion," *Proceedings of the Society for Experimental Stress Analysis*, Vol. 17, No. 2, pp. 65-70.

[6] Tabakoff, W. and Hamed, A., "Aerodynamic Effects on Erosion in Turbomachinery," JSME and ASME Paper 70, 1977 Joint Gas Turbine Congress, Tokyo, Japan, May 22-27, 1977.

[7] Tabakoff, W. and Wakeman, T., "Test Facility for Material Erosion at High Temperatures," ASTM Publication, "Erosion: Prevention and Useful Applications," STP 664, 1978.

[8] Bitter, J.G.A., "A Study of Erosion Phenomena," *Journal of Wear*, Vol. 6, 1963, Pt. I, pp. 5-21, and Pt. II, pp. 169-190.

R. Kotwal
Graduate Research Assistant.
Mem. ASME

W. Tabakoff
Professor
Mem. ASME

Department of Aerospace Engineering
and Applied Mechanics,
University of Cincinnati,
Cincinnati, Ohio

A New Approach for Erosion Prediction Due To Fly Ash

With increasing interest in the burning of coal in industrial gas turbines, there is also concern for the precise determination of the erosive effects on the turbine components. Series of experiments were conducted to determine the effects of fly ash constituents, particle size, particle velocity, angle of attack and target temperature on the erosion of iron and nickel base alloys. Based on the experimental results, a semi-empirical equation has been obtained for the prediction of the erosion losses. This equation provides a new technique for predicting the metal erosion due to the fly ash produced by the conventional burning of coal.

Introduction

The major problem confronting earlier developers of coal-burning turbines is the serious erosion of turbine blades and other components caused by the fly ash contained in the combustion gases. It is possible to remove approximately 85 percent by weight of the ash in these gases using cyclones. However, small particles ranging in size between 1 and 20 μm still pass through the cyclones and enter the turbine. The severity of this problem can be judged from the fact that a gas turbine operating on pulverized coal combustion is considered to have a short life. Typical ash concentrations for such a turbine are about 7.8 mgm/ft^3 [1]. The damage is caused principally by erosion of the blade trailing and leading edges. Several changes in the blade design to reduce the erosion problem have been made. These include changing the blade configurations to direct the ash towards the turbine casing instead to the rotor hub, and providing large annular space between the first stage stator and rotor blades through which the ash can centrifuge to the casing. Some designs have introduced wear strips at the base of the rotor and stator blades to minimize the erosion at these points. Nabors, et al. [1] estimated that the maximum life of the stator blades would be 5000 hr and that of the rotor blades 10,000 hr. This is far below the minimum life expectancy of a commercial power plant. A thorough knowledge of the various parameters which influence the extent of erosion damage is required to improve the life and the aerodynamic performance of turbomachinery operating in an ambient with fly ash particles. The future of advanced turbomachinery for use in the coal industry, gasification, mining, pipelines' gas transport, powder coal burning, coal-oil gas refinery, and many others is dependent upon this understanding.

Previous mathematical models [2-4] used to predict erosion rates consider only the influence of parameters such as particle velocity and angle of attack. The effects of composition and particle size should also be considered in order to predict the erosion rates of heterogeneous abrasives such as fly ash. This paper takes into consideration these additional parameters in the development of a semiempirical equation which can be used to predict metal erosion due to fly ash produced during the conventional burning of coal.

Preliminary studies were carried out with the following purposes. First, to find out the variation in the amount of erosion caused by fly ash particles acquired from different sources; and second, to understand the nature of the constituents in the fly ash.

Experimental Erosion Study of 301 Stainless Steel. Experiments were conducted on erosion test rigs developed by Grant, et al. [5] and Tabakoff, et al. [6]. Four types of fly ash acquired from different sources with different compositions and particle sizes were used. The four types of fly ash were: (1) Cincinnati Gas and Electric Company (CG&E), (2) Kingston I, (3) Kingston II, and (4) Exxon. Kingston II fly ash was obtained by the removal of large coarse particles, by using sieves, from Kingston I ash. A series of erosion tests were carried out using these fly ashes. The chemical analyses of three types of fly ash are given in Table 1, and the particle size distributions

Table 1 Chemical analysis of fly-ash

Substance	Amount Present (%)		
	Kingston Fly-Ash	CG&E Fly-Ash	Exxon Fly-Ash
Si	54.39	48.08	15.40
Al	28.58	21.16	25.40
Fe	10.08	20.05	5.53
Ca	1.28	--	7.20
Ti	0.47	--	--
Mg	1.04	0.93	3.84
Na	0.20	0.64	0.59
K	2.09	--	1.16
S	1.03	1.20	0.05
P_2O_5	0.06	--	--
SO_4	--	--	22.4
Cl	--	--	0.14
PO_4	--	--	0.25
C	--	--	1.2
F	--	--	0.02
Undetermined	0.78	7.94	16.82
Total	100.00	100.00	100.00

Contributed by the Gas Turbine Division of The American Society of Mechanical Engineers and presented at the Gas Turbine Conference and Products Show, New Orleans, La., March 10-13, 1980. Manuscript received at ASME Headquarters December 19, 1979. Paper No. 80-GT-96.

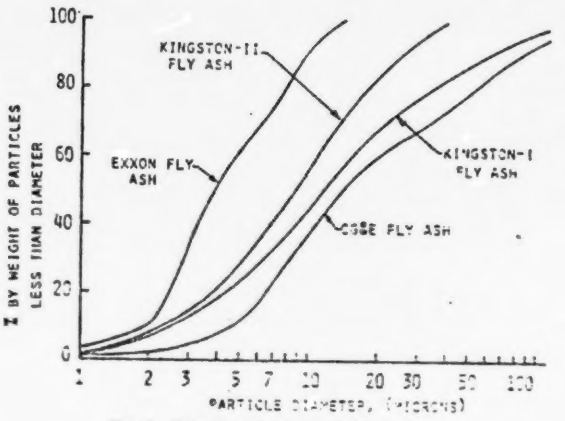

Fig. 1 Fly ash particle size distributions

are shown in Fig. 1. The mean particle sizes of CG&E, Kingston I, Kingston II and Exxon fly ash were 3[illegible]4μ, 28μ, 15μ and 3.9μ respectively.

Figure 2 shows the measured erosion on 304 stainless steel subject to various angles of attack by the fly ash particles. The tests were carried out at room temperature and for a particle velocity of 450 ft/s. It can be seen in this figure that the erosion loss reduces significantly when the coarse particles from the Kingston I fly ash were removed. The erosiveness of CG&E fly ash is observed to be smaller than that of Kingston I fly ash. The results presented in this figure also show that Exxon fly ash is least erosive among the four samples of fly ash tested.

Kingston and CG&E fly ash were produced during the conventional combustion of coal. From Table 1, it can be seen that the compounds of aluminum, silicon and iron are the major constituents of these samples of fly ash. The composition of Exxon fly ash is quite different and contains $CaSO_4$ as one of the major constituents. This is because Exxon fly ash was generated during the fluidized-bed combustion of coal using dolomite as the sorbent for capturing sulfur dioxide.

Fly Ash Composition. The constituents of fly ash from a given furnace are related to many factors, such as coal composition and size, initial state of raw coal, fuel burning rate, combustion efficiency and methods of fly ash collection. The principal ash-forming minerals in coal are as follows: aluminosilicates [Kaolinite $Al_4Si_4O_{10}(OH)_8$, Illite $KAL_2(AlSi_3O_{10})(OH)_2$, and mixed layer clay minerals]; sulfides (primarily pyrite FeS_2); carbonates (calcite $CaCO_3$), siderite $FeCO_3$ and ankerite $CaCO_3 \cdot FECO_3 \cdot MgCO_3$); and quartz ($SiO_2$).

The character of the fly ash is related to the thermal changes which the mineral matter undergoes during the combustion of coal. Ash composition is generally reported in terms of percent weight of metal oxides in their highest oxidation state. Chemical analyses of a large number of U.S. fly ash [7] produced during the conventional combustion of coal show ranges in composition given in Fig. 3. These representative data show that there is a large variation in the amounts of various substances that are present in fly ash. For example, the percent by weight of aluminum compound in a fly ash may be as low as 10 and as high as 60. The fly ash contains compounds of silicon, aluminum and iron and smaller amounts of compounds containing titanium, calcium, magnesium, sodium, potassium and sulfur. These compounds occur in fly ash primarily as silicates, oxides and sulfates, along with lesser amounts of phosphates and carbonates.

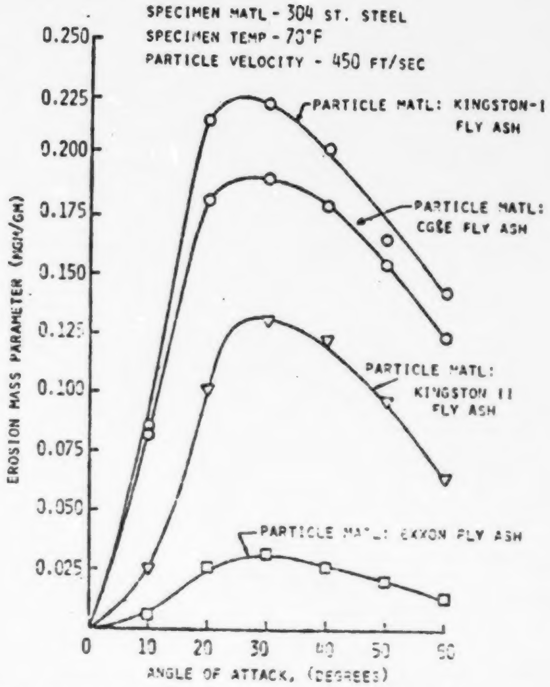

Fig. 2 Erosion caused by various types of fly ash particles (experimental results)

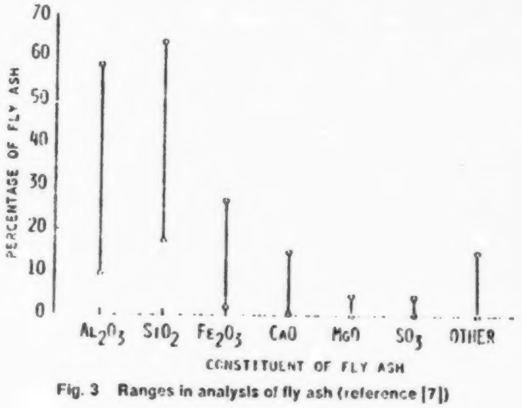

Fig. 3 Ranges in analysis of fly ash (reference [7])

Erosion Prediction Equation. It is evident that the prediction of erosion caused by fly ash particles is complicated because of the varying properties of fly ash. It is desirable to determine which constituents in fly ash affect metal erosion. The usual method of doing this is to control all other constituents and change only the constituent being considered. This approach cannot be taken in the case of fly ash because its constituents are inseparable. Hence, it was decided to develop a semi-empirical equation which relates the erosive characteristics of a fly ash to that of the commercial abrasives. The effects of chemical composition and particle size distribution in the fly ash

Nomenclature

D = particle diameter
m = total number of different substances in the fly ash
n = a number to account for the particle size effect in the erosion prediction equation
V = particle velocity
W_i = percent by weight of commercial abrasive particles corresponding to ith substance in the fly ash
ω_j = percent by weight of commercial abrasive particles having diameter D_j
ϵ = erosion mass parameter, expressed as milligrams of material eroded per gram of abrasive impacted on the specimen surface
ψ = erosion constant
μ = microns
α = impingement angle

will be included in this equation. It will be shown that the equation is general in nature and can be extended to erosion wear situations involving different materials, particle velocities, impingement angles and target temperatures. The amount of material removed by a unit mass of fly ash particles ϵ, can be expressed as follows:

$$\epsilon = \psi \sum_{i=1}^{m} \sum_{j=1}^{n} W_i[\epsilon_{ij}\omega_j] \tag{1}$$

where ψ = erosion constant, the value of this constant depends on the properties of the fractional components of the fly ash and the properties of the abrasives available commercially. W_i = percent by weight of commercial abrasive particles corresponding to ith substance in the fly ash, e.g., the commercial abrasives silica (SiO_2), alumina (Al_2O_3) and iron oxide (Fe_2O_3) correspond to silicon, aluminum and iron compounds respectively in the fly ash. ϵ_{ij} = erosion due to unit mass of commercial abrasive particles having diameter D_j and corresponding to ith substance in the fly ash. ω_j = percent by weight of commercial abrasive particles having diameter D_j, and corresponding to particle size distribution in the fly ash. m = total number of different substances in the fly ash. n = a number which can be selected depending on the erosion versus particle size relationship (for higher values of n, the accuracy of the present analysis improves).

Equation (1) can be simplified by the following considerations. From the results presented in Fig. 3, the percent by weights of all the substances (constituents) in the fly ash except those of aluminum, silicon and iron compounds are negligible, i.e.,

$$W_i \ll W_1, W_2, W_3 \quad \text{for} \quad i > 3. \tag{2}$$

Equation (2) suggests a value of 3 for the variable m in equation (1). Therefore equation (1) can be written in the following form.

$$\underset{\substack{\text{erosion due}\\ \text{to fly ash}}}{\underset{\downarrow}{\epsilon}} = \psi \left[\underbrace{\sum_{j=1}^{n} W_1\epsilon_{1j}\omega_j}_{\substack{\text{erosion due}\\ \text{to alumina}}} + \underbrace{\sum_{j=1}^{n} W_2\epsilon_{2j}\omega_j}_{\substack{\text{erosion due}\\ \text{to silica}}} + \underbrace{\sum_{j=1}^{n} W_3\epsilon_{3j}\omega_j}_{\substack{\text{erosion due}\\ \text{to iron oxide}}} \right] \tag{3}$$

The equation above can be further simplified by examining the experimental results presented in Fig. 4. This figure shows the results of the tests in which 304 stainless steel alloy was eroded by 25 microns alumina, silica and iron oxide particles. The tests were conducted at room temperature with particle velocities of 450 ft/s. It can be seen that the magnitudes of erosion due to alumina and silica particles are comparable but the magnitudes of erosion due to alumina and iron oxide differ markedly. For example, at an impingement angle of 30 deg (keeping in mind that the average particle size is the same), the erosiveness of the silica and iron oxide are, respectively, about 65 and 1 percent based on 100 percent for alumina. Tests at elevated temperature (900°F) also revealed similar results. Terefore it can be assumed that the erosion due to iron oxide may be neglected and equation (3) can be rewritten as follows.

$$\epsilon = \psi \left[\sum_{j=1}^{n} W_1\epsilon_{1j}\omega_j + \sum_{j=1}^{n} W_2\epsilon_{2j}\omega_j \right] \tag{4}$$

The values of W_1 and W_2 can be obtained from the chemical analysis of the fly ash. The particle size analysis of the fly ash provides the values for ω_j. For a given target material, the values of ϵ_{1j} and ϵ_{2j} can be obtained from erosion versus particle size characteristics of alumina and silica particles respectively (as will be shown later). The appropriate value of ψ is not easily estimated, because the shape, hardness and strength of the particles in the fly ash are so different from those in conventional form. In view of the present uncertain nature of the particles in fly ash, it is preferable to establish this quantity by erosion experiments involving the abrasives and target material of interest. The effects of angle of attack, particle velocity and target temperature can be included by substituting the appropriate values for the variables ϵ_{1j} and ϵ_{2j} on the right hand side of equation (4).

Application of Erosion Prediction Equation. In the following discussion, equation (4) will be used to predict the erosion caused by different types of fly ash particles on three target materials, namely 304 stainless steel, Rene 41 and INCO 718. These alloys are widely used in turbomachinery applications. Data on fly ash erosion for such materials is not available in the literature. Therefore before using this equation, it is necessary to obtain data on the amount of erosion caused by alumina and silica particles of various sizes and the value of the erosion constant ψ.

Figure 5 shows the test data for the variation in erosion wear of 304 stainless steel as a function of particle size. The tests were carried out at room temperature. The results are presented for two angles of attack (30 and 60 deg) and two particle velocities (260 and 450 ft/s).

Figure 6 shows the erosion versus particle size plots for three target materials; namely, 304 stainless steel, Rene 41 and INCO 718. The

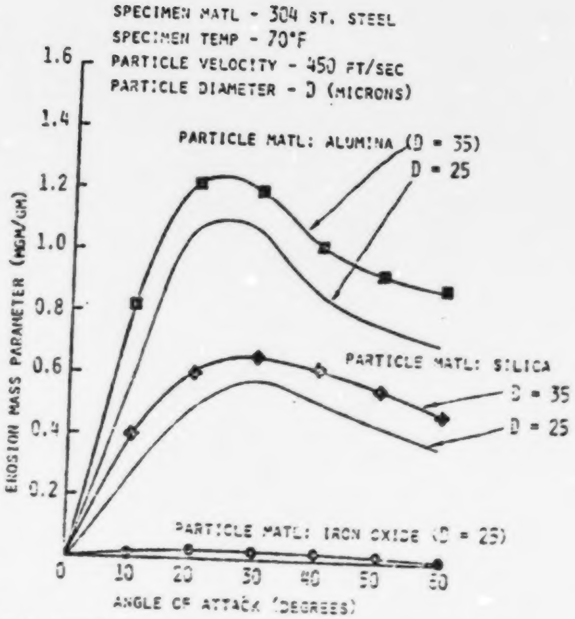

Fig. 4 Erosion versus angle of attack for different commercial abrasives (experimental results)

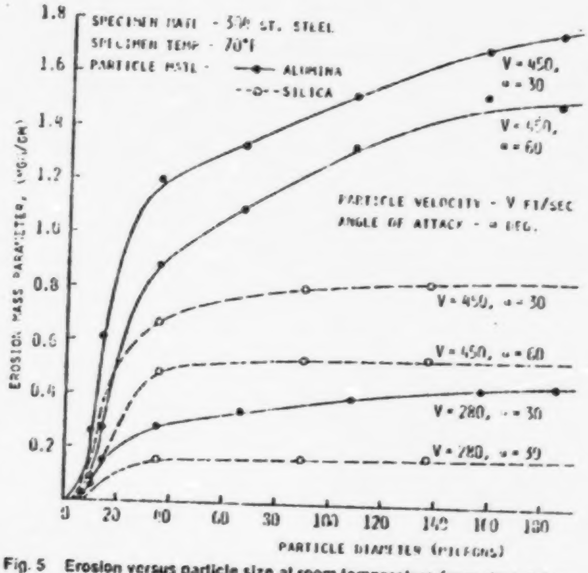

Fig. 5 Erosion versus particle size at room temperature (experimental results)

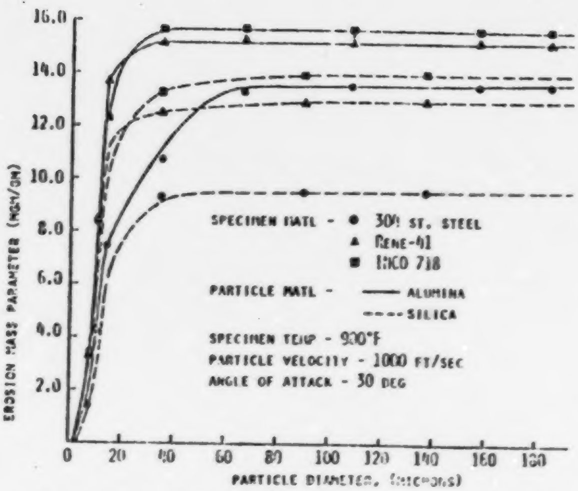

Fig. 6 Erosion versus particle size at 900°F (experimental results)

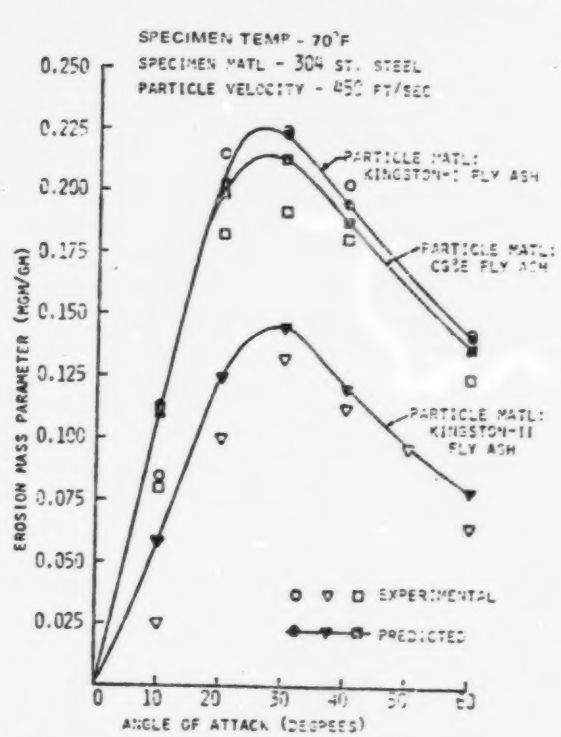

Fig. 7 Erosion versus angle of attack (experimental and predicted results)

Table 2 Value of erosion constant in equation (4)

Target Material	Target Temperature (°F)	Particle Velocity (ft/sec)	Angle of Attack (degree)	Erosion Constant ψ
304 St. Steel	70	200-500	0-90	0.65
304 St. Steel	900	500-1000	30	0.425
Rene 41	900	500-1000	30	0.480
INCO 718	900	500-1000	30	0.525

test results are shown for a target temperature of 900°F and a particle velocity of 1000 ft/s. Only one impingement angle was employed (30 deg) which was close to the angle of maximum erosion for all three target materials.

For a given target temperature, one erosion test was conducted for each target material using CG&E fly ash particles. The results of these tests and the results presented in Figs. 5 and 6 were used in equation (4) to evaluate the value of the erosion constant ψ. Table 2 lists the values of the erosion constant ψ for the three target materials. The value of ψ was found to be between 0.425 and 0.65. The variation in the value of this constant tends to confirm the complexity of the material property parameters and abrasive property parameters which are controlling the erosion.

Using the appropriate values for ψ and other quantities in equation (4), the erosion mass parameter values for other fly ash particles were obtained. Figure 7 shows the experimental and predicted erosion mass parameter values for 304 stainless steel and three different fly ash particle types. The predicted and experimental erosion values of 304 stainless steel, Rene 41 and INCO 718 by using CG&E fly ash for specimen temperature of 900°F and angle of attack of 30 deg, are shown in Fig. 8. There is good agreement between the predicted and experimental erosion results, thus verifying the usefulness of equation (4) to predict the erosion resistance of a material under attack by fly ash particles. Additional experimental data using fly ash may be found in reference [8].

To facilitate the use of equation (4), a simple computer program was developed. This program was used to study the effects of fly ash composition and particle size distribution on the erosion of a material. For a given target material of interest, the appropriate value of the erosion constant ψ and the erosion values for different sizes of alumina and silica particles (such as shown in Figs. 5 and 6), were provided as input to this program.

The procedure outlined above was used to estimate the erosion on the three target materials (304 stainless steel, Rene 41 and INCO 718) caused by various types of fly ash having assumed compositions and particle size distributions. Table 3 shows 12 different fly ash compositions which were investigated in this study. These compositions were chosen on the basis of ranges in fly ash composition that occurs in

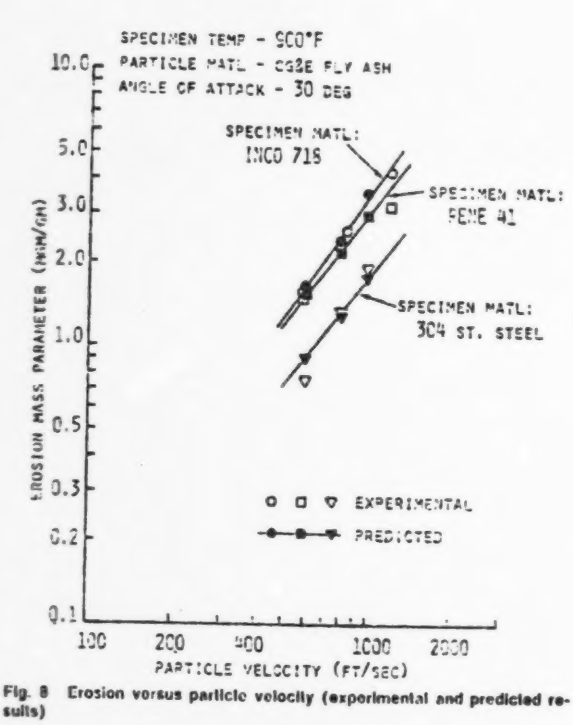

Fig. 8 Erosion versus particle velocity (experimental and predicted results)

practice. Figure 9 shows the 15 different particle size distribution numbers, N, considered (from $N = 1$ to $N = 15$) plotted versus the particle diameters (1 to 200 μm). The fly ash compositions are identified by capital letters (A, B, C, . . . L) as shown in Table 3. A particular fly ash is therefore identified by a combination of a letter and a number. Among the fly ash compositions studied, composition A (with 30 percent Al compound and 60 percent Si compound) and composition L (with 30 percent Al compound and 40 percent Si compound) gave maximum and minimum erosion values, respectively, and composition G (with 30 percent Al compound and 50 percent Si compound) gave an intermediate erosion value, for a given particle size distribution. Therefore, computed erosion results will be presented for these three fly ash compositions only.

Figure 10 shows the estimated relative erosion caused by different types of fly ash particles on 304 stainless steel specimens at room temperature. The results are presented for two angles of attack (30 and 60 deg) and two particle velocities (280 and 450 ft/s). The spread in the erosion data shown by the three symbols for a given particle size distribution indicates the effect of fly ash composition. The effect of fly ash content is significant when the larger particles (greater than 30μ) are present in the fly ash. For a given fly ash composition, particle size distributions $N = 5$ (with particles 1–10μ) and particle size distribution $N = 6$ (with particles 80–100μ) were found to be the least and most erosive, respectively.

The predicted dependence of the erosion mass parameter on the fly ash compositions and particle size distributions is shown in Figs. 11–13. The results are presented for the three target materials (304 stainless steel, Rene 41 and INCO 718). These results were obtained from the computer program for a target temperature of 900°F, a particle velocity of 1000 ft/s and an angle of attack of 30 deg. At these conditions the computed results show that 304 stainless steel has a higher erosion resistance compared to Rene 41 and INCO 718. It is seen that the earlier observations (Fig. 10) regarding the effects of composition and particle distribution in the fly ash on the room temperature erosion are true for the elevated temperature erosion also. The computed results also show that the effect of fly ash composition on erosion is more significant in the case of high velocity particles impinging a target material at elevated temperatures.

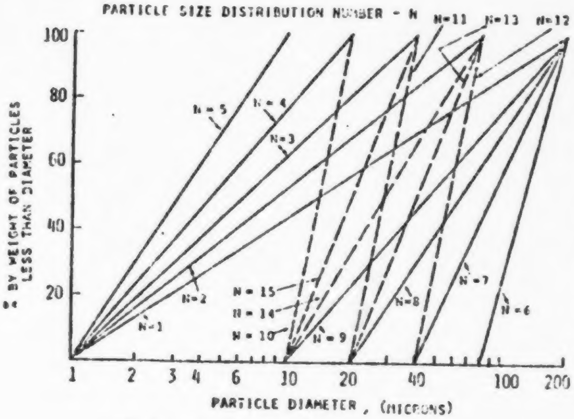

Fig. 9 Assumed particle size distributions

Table 3 Assumed fly ash compositions

Composition Name	Fly Ash Composition			
	Si Compound	Al Compound	Fe Compound	Other
A	60.00	30.00	5.00	5.00
B	60.00	25.00	10.00	5.00
C	60.00	20.00	15.00	5.00
D	55.00	30.00	10.00	5.00
E	55.00	25.00	15.00	5.00
F	55.00	20.00	20.00	5.00
G	50.00	30.00	15.00	5.00
H	50.00	25.00	20.00	5.00
I	50.00	20.00	25.00	5.00
J	45.00	30.00	20.00	5.00
K	45.00	25.00	25.00	5.00
L	40.00	30.00	25.00	5.00

Summary and Conclusions

The most important findings of the present study were concerned with the amount and the nature of the erosion caused by different types of fly ash on three different materials (304 stainless steel, Rene 41 and INCO 718). A model to predict erosion (in the form of a semi-empirical equation), was developed which takes into account the effects of composition, particle size and complicated structure of the fly ash particles. It was shown that the technique is general in nature and can be extended to erosion wear situations involving different materials, particle velocities, impingement angles and target temperatures. This equation relates the erosive characteristics of a fly ash to that of the commercial abrasives. The equation was simplified by assuming that, for the fly ash, the percent by weight of all the substances (constituents) excluding that of aluminum, silicon and iron compounds are negligible. This assumption is true only for fly ash produced during the conventional combustion of coal. There was good agreement between the predicted erosion values and the test results, as shown in Figs. 7 and 8.

The study of a variety of fly ashes shows that their erosiveness is

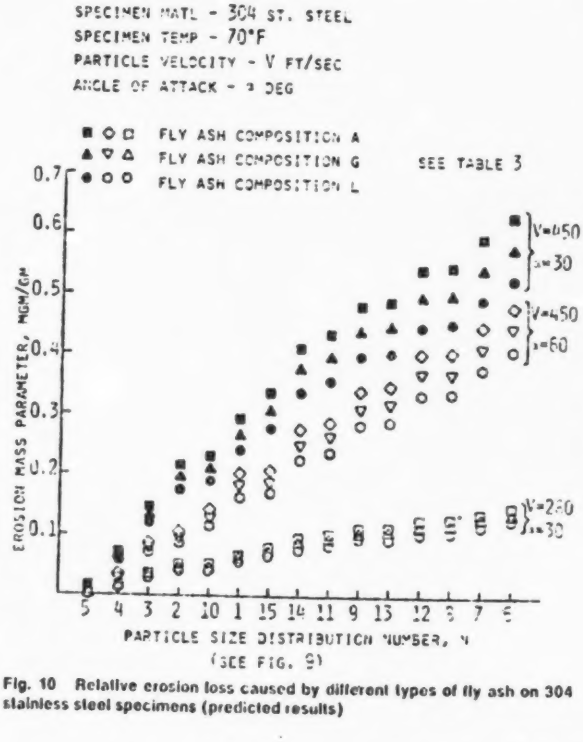

Fig. 10 Relative erosion loss caused by different types of fly ash on 304 stainless steel specimens (predicted results)

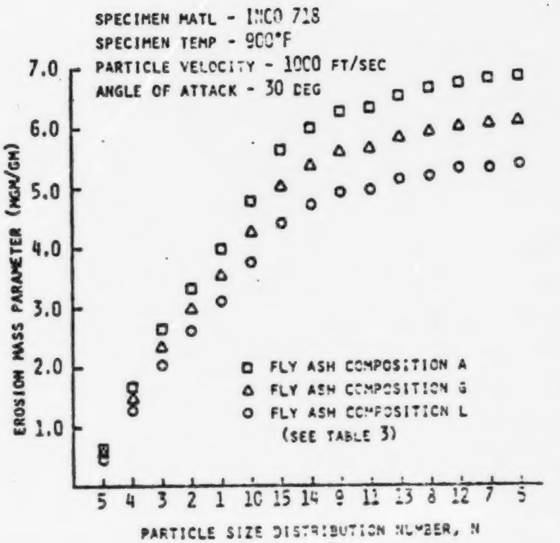

Fig. 11 Relative erosion loss caused by different types of fly ash particles on INCO-718 specimens (predicted results)

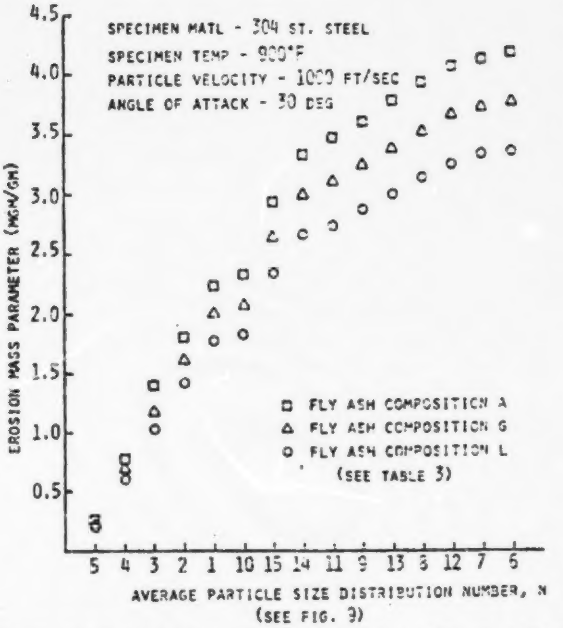

Fig. 12 Relative erosion loss caused by different types of fly ash particles on 304 stainless steel specimens (predicted results)

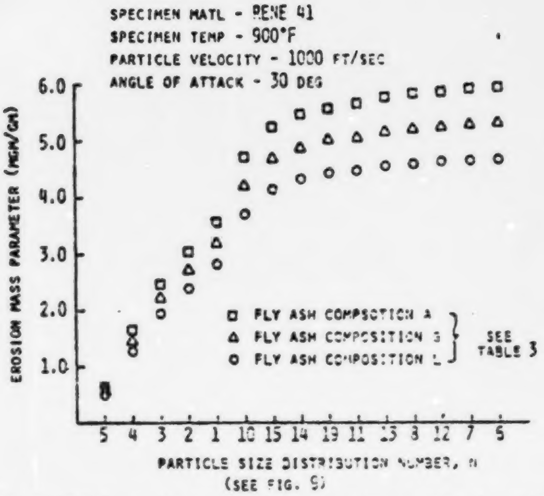

Fig. 13 Relative erosion loss caused by different types of fly ash particles on Rene 41 specimens (predicted results)

directly proportional to the percentage of the aluminum and the silicon compounds. The effect of fly ash content on erosion is significant when larger particles (greater than 30μ) are present. The computed results also show that the effect of fly ash composition on erosion is more significant in the case of high velocity particles impinging a target material at elevated temperatures. The predicted and test results show that the erosion mass parameter increases at a rapid rate with increasing particles diameter up to about 40 μm and at a slower rate with further increase in particles diameter.

Acknowledgments

This research was sponsored by ERDA Contract No. E(49-18)-2465. The authors wish to express their appreciation for the useful discussions provided by Dr. J. Moteff.

References

1 Nabors, W. M., Strimbeck, D. C., Cargill, R. W. and Smith, J., "Bureau of Mines Progress in Developing the Coal Burning Gas Turbine Power Plant," ASME *Journal of Engineering for Power*, April 1965, pp. 215–222.

2 Finnie, I., "The Mechanism of Erosion of Ductile Metals," *Proceedings of 3rd National Congress of Applied Mechanics, Trans. ASME*, 1958, pp. 527–532.

3 Bitter, J. G. A., "A Study of Erosion Phenomena, Part I and Part II," *Wear*, Vol. 6, 1963, pp. 5–21 and pp. 169–190.

4 Neilson, J. H., and Gilchrist, A., "Erosion by a Stream of Solid Particles," *Wear*, Vol. 2, 1968, pp. 111–122.

5 Grant, G. and Tabakoff, W., "Erosion Prediction in Turbomachinery Resulting from Environmental Solid Particles," *Journal of Aircraft*, Vol. 12, No. 5, May 1975, pp. 471–478.

6 Tabakoff, W. and Wakeman, T., "Test Facility for Material Erosion at High Temperature," ASTM Special Technical Publication, No. 664, 1979.

7 White, H. J., "Effect of Fly Ash Characteristics on Collector Performance," *JAPCA*, Vol. 15, May 1955, pp. 37–50, 62.

8 Tabakoff, W., Kotwal, R. and Hamed, A., "Erosion Study of Different Materials Affected by Coal Ash Particles," *Wear*, Vol. 52, 1979, pp. 161–173.

A Technique to Investigate High Temperature Erosion of Refractories

SHELDON M. WIEDERHORN* and D. ELLIS ROBERTS

Institute for Materials Research, National Bureau of Standards,
Washington, D.C.

A description is given of equipment used to study erosion of refractories under controlled environments at temperatures as high as 1500°C. Erosive wear of a high alumina castable refractory currently used in coal gasification pilot plants is investigated. Erosion occurs preferentially in the cement matrix of the refractory. At 25°C erosion occurs by brittle fracture of the matrix, while at 1000°C, erosion occurs by fracture and shear deformation of the matrix phase. Data are discussed with reference to current theories of erosion.

Erosion can be a serious problem in industrial processes in which solids are conveyed in slurries or flowing gas streams. In the petrochemical industry, for example, erosion was encountered as a serious problem when fluidized catalyst cracking units were first used for the production of gasoline. Fluidized beds required the circulation of catalyst particles between different parts of the refinery which resulted in severe problems of erosion in valves, hot transfer lines and cyclone separators, where velocities were high and changes occurred in the direction of flow.[1-4] Because of improved engineering practices and development of new erosion resistant materials, erosion problems have been minimized in the petrochemical industry. However, severe erosion problems are expected in the coal gasification industry[5] because of high operating temperatures and pressures and the use of superheated steam.

To assure the availability of erosion resistant refractories that can withstand the severe environmental conditions expected in gasification processes, data on high temperature erosion of refractories are needed. In this paper a description is given of equipment that can be used to collect such data. The equipment is capable of environmental control at one atmosphere total pressure and can be operated to temperatures as high as 1500°C. Use of this equipment is illustrated in a study of the erosion behavior of an Al_2O_3 castable refractory currently used in coal gasification pilot plants. Data from this study are compared with other erosion data and are discussed with reference to current theories of erosion.

Equipment

A schematic diagram of the erosion equipment is given in Fig. 1. Abrasive particles are fed by gravity from a hopper into a flowing gas stream (air or some other gas) which carries the particles through the nozzle and into the combustion environment of the test apparatus. A uniform flow of particles is obtained by use of a vibrator located in the hopper. Particles are accelerated to impact velocity as they pass through a 2-in. long stainless steel nozzle which has either a 1/16-in. or 1/8-in. ID. The nozzle is replaced frequently during the experiment to limit the effect of nozzle wear on particle velocity.

High temperatures are obtained by burning a mixture of propane and oxygen in a four-nozzle burner and feeding hot combustion gases into the top of the combustion tube where they mix with the particle-gas mixture coming through the nozzle. A uniform beam of particles, 3/4 in. in diameter, exits from the bottom of the combustion tube. Specimens (1/4-in. cubes) are held below the exit of the combustion tube on a 3/8-in. Al_2O_3 rod. The temperature of the specimen surface is monitored with an optical pyrometer.

Typical erosion conditions for this apparatus are given in Table I. Although abrasive particles for this study were 150 μm SiC particles, the equipment is not limited to this particle size, and other particles (Al_2O_3, pulverized coal slag) have been used. Silicon carbide particles were selected for the experiment to accelerate the rate of erosion, so tests could be conducted in a reasonable time. The velocity range indicated in Table I was selected to overlap the range occurring in coal gasification applications. The lower portion of this range, 10 m/s, is typical of gas velocity in hot transfer lines. Density of particles in the gas stream (0.2 to 2.0 g/m^3 depending on gas velocity) was selected so individual particles would impinge on the test specimen without interaction at the erosion surface. This load-

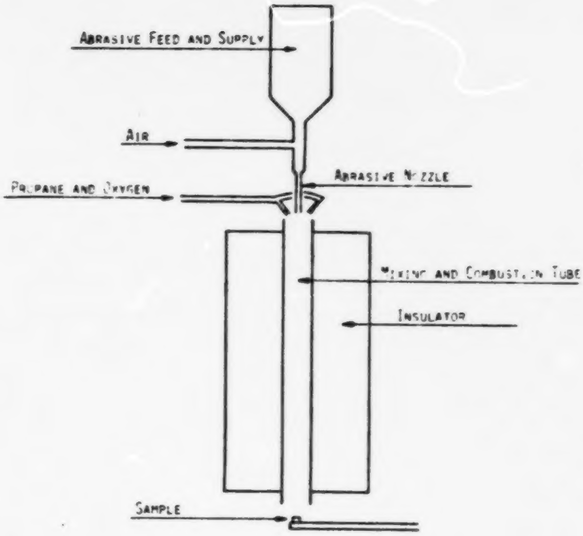

Fig. 1. Schematic diagram of erosion equipment.

Table I. Typical Erosion Conditions

Abrasive	Velocity	Loading	Environments (vol%)			
			Reducing		Oxidizing	
150 μm SiC	10–100 m/s	0.2–2.0 g/m^3	N_2	49	N_2	75
			CO	17	CO_2	8
			H_2	18	O_2	8
			CO_2	5	H_2O	9
			Hydrocarbons	3		
			H_2O	8		

---

*Member, the American Ceramic Society.

Presented at the Fall Meeting of the Refractories Division of the American Ceramic Society, Bedford, Pa., October 4, 1975 (13-R-75F).
Received January 10, 1976.

BULLETIN OF AM. CERAMIC SOC.

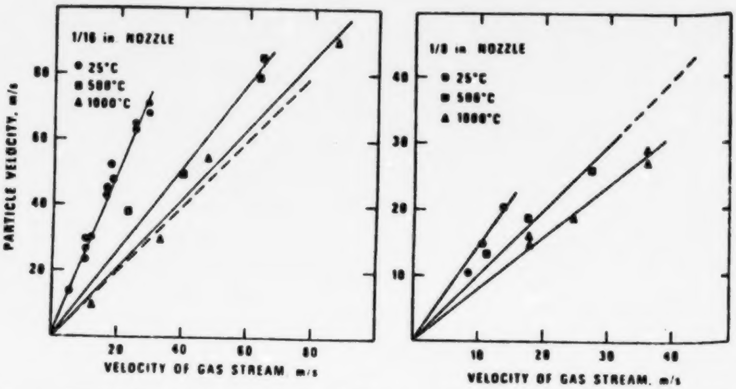

Fig. 4. Comparison of gas stream velocity and particle velocity at point of impact with specimen surface.

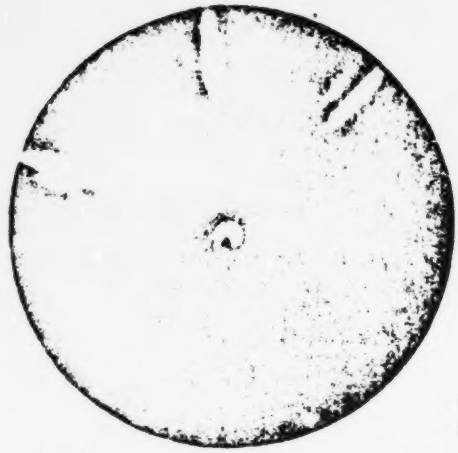

Fig. 2. Photograph of a disk with erosion marks from three different particle velocity determinations. Heavy marks made with disks stationary; light marks made with disks rotating. Space between marks was used to determine particle velocity (after A. W. Ruff and L. K. Ives, Ref. 7).

ing density is considerably < the 300 g/m^3 expected in coal gasification applications.[6]

Gas compositions can be controlled by varying concentrations of gases passing through the nozzle and burner. To obtain a reducing environment, an excess of propane is fed through the system. The reducing environment shown in Table I is typical of that obtained in the Morgantown low Btu gasifier. The oxidizing environment shown in Table I was obtained by feeding excess oxygen through the equipment so that complete combustion was obtained. If the equipment is operated in air, nitrogen from the air is sucked through the apparatus as the gases pass from the nozzle into the mixing tube and is found in the effluent gas stream. Nitrogen can be eliminated by enclosing the apparatus so that air is not admitted to the system. An enclosure has the further advantage that H_2S or other noxious gases can be added to the gas streams.

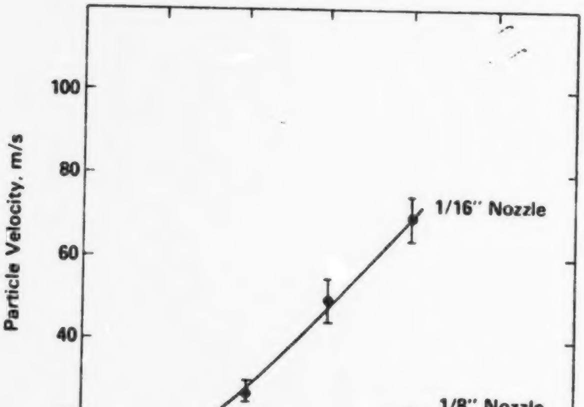

Fig. 3. Typical velocity calibration; data collected at 25°C.

Particle Velocity Calibration

The method used to calibrate the particle velocity was developed by Ruff and Ives.[7] Two disks are used, one solid and one containing a slit, both rotating on a common axis. The disk with the slit is closest to the exit port of the combustion tube. Particles passing through this disk impinge upon the second disk, leaving an erosion mark from which velocity can be determined. Since the disks are rotating, the mark on the second disk does not occur directly beneath the slit, but suffers an angular displacement (Fig. 2) that depends on particle velocity, spacing of the disks and angular velocity.

The average particle velocity is given by $v = 2\pi r \nu L/s$ where s is the linear displacement of the abrasion marks at a radius, r, from the center of the disk; L is the separation of the two disks; ν is the rotational frequency of the disks. A typical velocity calibration using this technique is shown in Fig. 3 for tests conducted at 25°C. Calibration curves were also obtained at specimen temperatures of 500° to 1000°C. The particle velocity depends on the diameter of the nozzle used to accelerate the particles; for a given gas flow rate, higher velocities are obtained through the smaller diameter nozzle.

Particle and gas velocities at the end of the combustion tube are compared in Fig. 4 for the two nozzles used in this study. For the 1/16-in. nozzle, the particle velocity exceeds the gas velocity at 25°C; at 1000°C the particle and gas velocities are nearly equal; at 500°C the data lie intermediate between the 25° and 1000° data. Thus, the particle and gas velocities are not the same at the end of the combustion chamber. This conclusion is confirmed for the ⅛-in. nozzle. However, the particle velocity is equal to the gas stream velocity at 500°C, while at 25°C, the particle velocity is faster than the gas stream velocity, and at 1000°C, particle velocity is less than the gas stream velocity. These results indicate the importance of experimentally determining the particle velocity. A significant error can result if it is assumed that particle and gas stream velocities are the same at the exit port of the erosion equipment.

Erosion Measurements

Surface Topology

The refractory tested in the erosion equipment was a 95% Al_2O_3 castable refractory bonded with calcium aluminate cement. This type refractory is used as an internal liner in many major components of coal gasification pilot plants where erosion is expected to be severe. Microscopic examination of the refractory reveals a coarse irregularly shaped Al_2O_3 aggregate embedded in a matrix of calcium aluminate. This matrix is filled with fine interconnecting pores that weaken it, resulting in a friable structure that is easily damaged during impact. Because of this structure, erosion occurs primarily within the matrix.

Surface structure of the castable refractory is shown in Figs. 5 and 6 for erosion studies conducted at 25° and 1000°C, respectively. Sequences shown in these figures were for a range of particle velocities using 100 g SiC. For both high and low temperature erosion, wear occurs primarily in the weak calcium aluminate

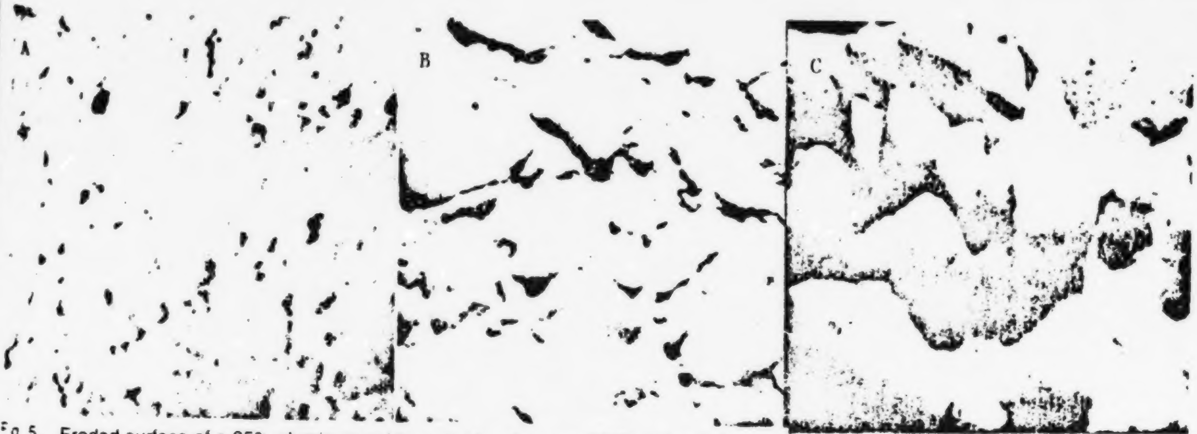

Fig. 5. Eroded surface of a 95% aluminum oxide castable refractory: 25°C, 100 g SiC, 150 μm particles: (A) 12 m/s particle velocity, (B) 25 m/s, (C) 46 m/s and (D) 66 m/s. Each photograph shows full specimen dimension (0.25 in.).

matrix. The matrix is eroded first, followed by the fine grains of Al_2O_3. In the most severe erosion conditions, large Al_2O_3 particles are left protruding high above the underlying matrix, with residual calcium aluminate cement at points of contact between the Al_2O_3 grains as their only support. Once the remaining cement is removed, these particles should also fall from the surface of the refractory. Slight rounding of the protruding Al_2O_3 particles indicates that those too are eroded by the SiC particles, but at a much slower rate than the calcium aluminate.

A major difference between the high and low temperature erosion studies is the occurrence of plasticity at high temperatures. The conclusion that the refractory is plastic is based on the fact that at 1000°C, small pieces of SiC are found embedded in the surface of both the aggregate and cement portions of the refractory. This behavior is typical for metals in which hard particles become embedded in the soft metal matrix.[5-8] Occurrence of plastic deformation in the specimen surface suggests a change in erosion mechanism at high temperatures, a suggestion that is supported by wear measurements made at both low and high temperatures.

Wear Rates

Wear measurements made on the castable refractory are shown in Figs. 7 and 8. Figure 7 illustrates the dependence of erosion rate on temperature and particle velocity for a 90° angle of impingement, while Figs. 8(A) and (B) illustrate the dependence of erosion rate on angle of impingement at 25° and 1000°C, respectively. Erosion rate

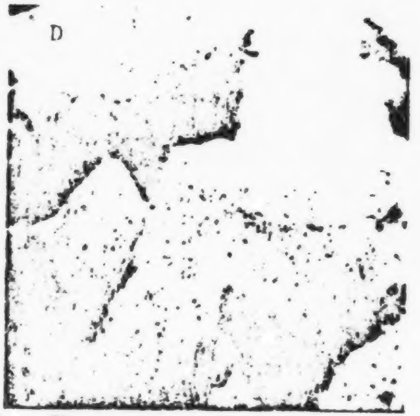

Fig. 6. Eroded surface of a 95% aluminum oxide castable refractory: 1000°C, 100 g of SiC, 150 μm particles: (A) 12 m/s particle velocity, (B) 30 m/s, (C) 70 m/s and (D) 90 m/s. Each photograph shows full specimen dimension (0.25 in).

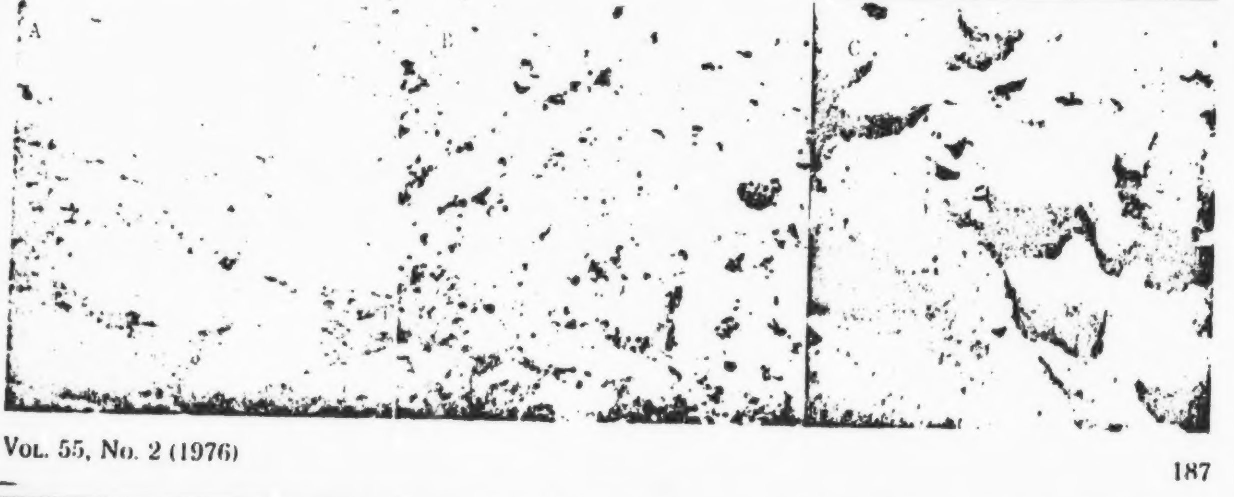

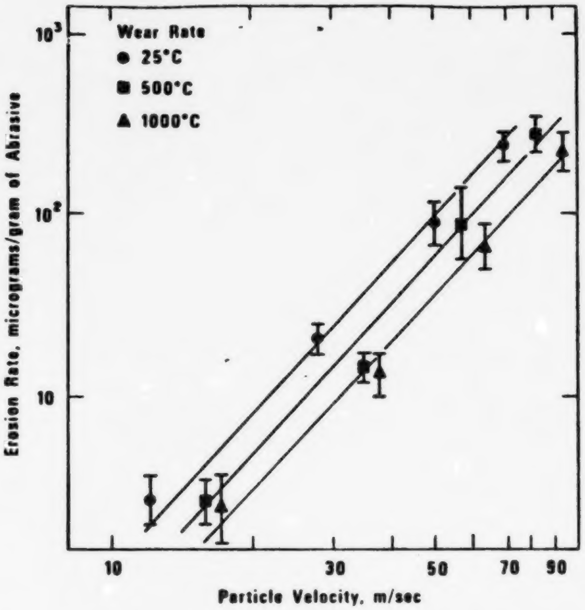

Fig. 7. Dependence of erosion rate on particle velocity and temperature. Error bars represent one standard deviation from the mean.

is defined as the weight loss per unit weight of abrasive impinging upon the refractory surface. Velocity, temperature and impingement angle were chosen as parameters for this study because of their importance in evaluating mechanisms of erosion.

For all temperatures the erosion rate, w, increases as the particle velocity is increased. The data in Fig. 7 can be expressed as a power function of the particle velocity, v: $w \propto v^b$, where the velocity exponent, b, has a value of ≈2.8. This value is consistent with others reported in the literature, and can be justified in terms of the erosion theory developed by Oh et al.[10] They assume erosion occurs by the gradual loss of material as the result of localized fracture at the points of particle impact, and predict values of the velocity exponent should fall between 2.6 and 3 for brittle materials. The value of b obtained in the present experiment falls within this range which suggests the erosion of the castable refractory occurs primarily by a fracture mechanism.

The fracture mechanism of erosion described by Oh et al. would also be consistent with the temperature dependence of the erosion rate depicted in Fig. 7. As the temperature is increased, fracture becomes more difficult because the castable refractory exhibits some ductility at high temperatures. Therefore, at 90° impingement, the force of impacting particles is partially absorbed by plastic flow and as a result less material is removed during each impact; consequently, the erosion rate decreases. Thus, both the particle velocity and temperature dependence of the erosion rate can be explained by the fracture mechanism suggested by Oh et al.[10]

Data shown in Figs. 8(A) and (B) illustrate the dependence of erosion rate on impingement angle.* At 25°C (Fig. 8(A)), the erosion rate is a maximum at a 90° impingement angle, decreasing slightly as the angle decreases from 90° to 30°. A more significant decrease in the erosion rate occurs at 15°, where the rate has dropped by ≈50%. This behavior is almost identical to that reported for porcelain,[11] another brittle material, and is similar to that reported for glass,[11] although in the case of glass the erosion rate is observed to decrease more rapidly as the angle of impingement is decreased. Thus, the erosion behavior of the castable refractory is typical of brittle materials that exhibit little if any plastic deformation.

At 1000°C (Fig. 8(B)) erosion behavior of the castable refractory is typical of ductile materials, such as metals, that exhibit high rates of erosion at low angles of impingement. To explain this behavior, it must be assumed that material is removed from the castable refractory surface by a shear mechanism such as one of those used to explain the erosion of metals.[11-13] These mechanisms are based on the assumption that particles hitting the surface at low angles of impingement apply a considerable shear stress to the surface which removes material by plastic flow. This type mechanism is used to explain a maximum in the erosion rate for ductile metals at ≈15°-20° impingement and a relatively low rate of erosion at 90° impingement.

The erosion behavior of most materials results from a combination of two erosion mechanisms, one being shear erosion to account for wear at low angles of impingement.[12,13] For castable refractories at high temperature, the two mechanisms most likely are erosion by

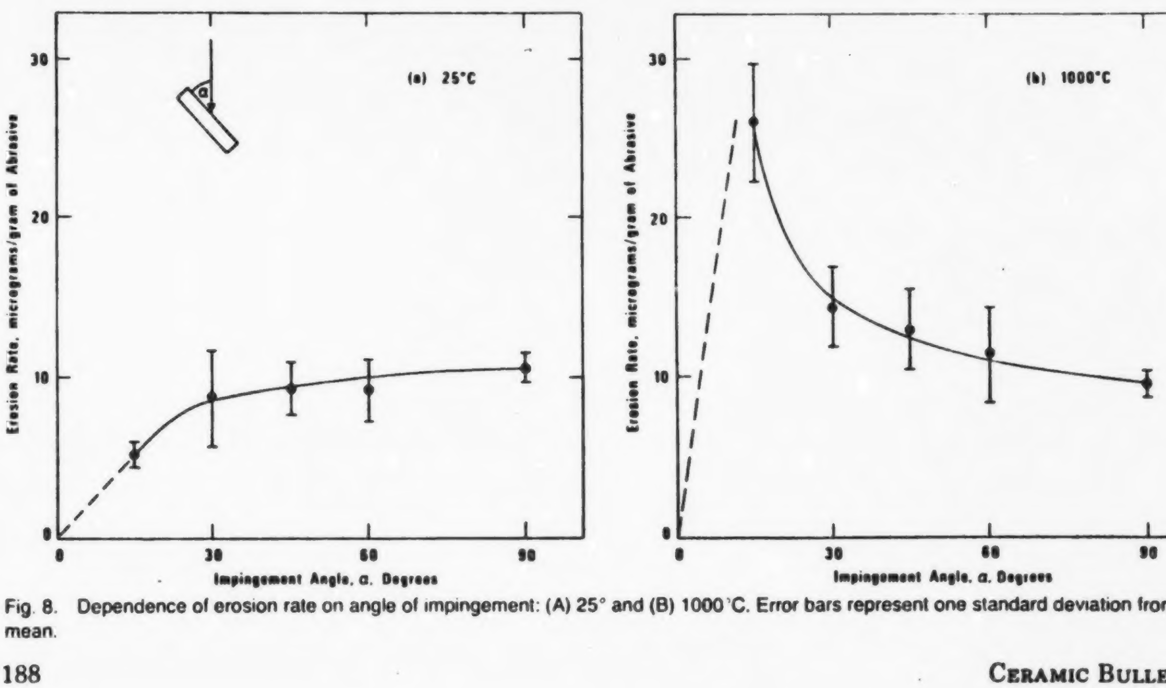

Fig. 8. Dependence of erosion rate on angle of impingement: (A) 25° and (B) 1000°C. Error bars represent one standard deviation from the mean.

---

*These data were collected using relatively low velocity particles (28 and 39 m/s) for temperatures of 25° and 1000°C, respectively, and small quantities of abrasive (100 g) so that the results given in Fig. 9 are not influenced by shadowing of the calcium aluminate cement by the aluminum oxide particles.

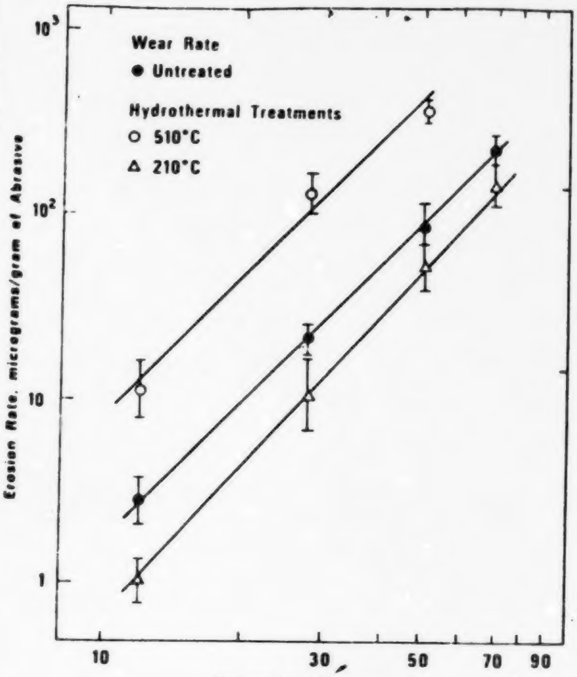

Fig. 9. Effect of hydrothermal environments on erosion rate. All measurements at 25 C. Error bars represent one standard deviation from the mean

fracture at high angles of impingement and erosion by shear deformation at low angles of impingement. The simultaneous occurrence of these two erosion mechanisms offers a qualitative explanation for the erosion data shown in Fig. 8(B).

Comparison with Earlier Work

The results of this paper are generally consistent with those obtained by earlier authors.[1-3] The observation that the weaker matrix is removed first during erosion has been noted in several earlier papers.[1,3] This observation suggests that the erosion resistance of castable refractories is determined in large part by the cement phase strength. By increasing the strength of this phase, the erosion resistance of the castable refractory can be increased. Conversely, chemical reactions that tend to reduce the strength of the cement phase will be detrimental to the erosion properties of the castable refractory.

A room temperature experiment illustrating the influence of chemical reactions on erosion resistance is shown in Fig. 9. The castable used in the study was the same as that discussed earlier, but now specimens were given hydrothermal treatments at 210° and 510°C before they were eroded at room temperatures.[14] The 210°C treatment enhanced the strength of the refractory by a factor of 2 while the 510°C treatment decreased the strength by a factor of ≈10. These observed changes in strength were attributed to chemical changes in cement phase of the refractory. The erosion resistance of these refractories (Fig. 9) parallels the strength behavior. The 510°C treatment results in a decrease by a factor of ≈7 in erosion resistance while the 210° treatment results in an increase by a factor of ≈2. Thus, reactions that occur when a refractory is used can drastically affect the erosion resistance.

To characterize fully the effect of environment, erosion studies should be made at temperatures and in the environment expected in coal gasifiers. The erosion equipment described in this paper provides a first step toward this type of measurement, since the temperature and environment can be controlled at one atmosphere of total pressure. Additional design features will be necessary to attain the high pressures expected in coal gasification applications.

Sheldon M. Wiederhorn is chief of the Physical Properties Section at the National Bureau of Standards, Washington, D.C. His photograph and biographical sketch appeared on page 580 of the June 1975 issue of *Ceramic Bulletin*.

D. Ellis Roberts has been with NBS since 1953. He received A.B. and B.S. degrees in physics from Oregon State College in 1951. He is studying deformation, fracture, wear and abrasion characteristics of ceramic materials.

D Ellis Roberts

Summary

A high temperature apparatus has been designed to study the erosive wear of ceramic materials. The equipment has a temperature capability of ≈1500°C and can accelerate particles over the velocity range 10 to 100 m/s. The importance of particle velocity measurement was illustrated by showing the particle velocity depended on the temperature and nozzle design, and could be either greater or less than gas stream velocity. A main feature of the erosion equipment is a combustion chamber that enables uniform temperatures and particle densities to be attained at the sample location.

The equipment was used to study the erosion behavior of a high purity Al_2O_3 castable refractory. Erosion occurred primarily by wear of the cement phase of the refractory. For 90° impingement, the erosion rate was a power function of the particle velocity. The velocity exponent agreed with those reported in the literature. At 25°C, erosion occurred primarily by a fracture mechanism, since the erosion rate was a maximum at 90° impingement and decreased as the impingement angle decreased. At 1000°C, however, the erosion behavior was partially influenced by plastic flow, since erosion particles were found embedded in the refractory, and erosion rate increased rapidly as the impingement angle decreased. As a consequence of this behavior, the erosion rate at 1000°C was greater than at 25°C for low angles of impingement.

Acknowledgement

The authors gratefully acknowledge the support of the Energy Research and Development Administration, Fossil Energy Research Program.

References

[1] M. S. Crowley, "Influence of Particle Size on Erosion Resistance of Refractory Concretes," *Am. Ceram. Soc. Bull.*, **48** [7] 707-10 (1969).

[2] C. R. Venable, Jr., "Erosion Resistance of Ceramic Materials for Petroleum Refinery Applications," *ibid.*, **38** [7] 363-68 (1959).

[3] J. F. Wygant and W. L. Bulkley, "Refractory Concrete for Refinery Vessel Linings," *ibid.*, **33** [8] 233-39 (1954).

[4] A. J. van Riemsdijk and H. W. van der Hoeven, "How to Test Cement for Erosion Resistance," *Petroleum Processing*, **8** [10] 1514-18 (1953).

[5] Workshop on Materials Problems and Research Opportunities in Coal Conversion, Vol. 1, Conclusions and Recommendations, Columbus, Ohio, April 16-18, 1974.

[6] A. Mac Nab and H. E. Frankel, "Erosion Problems in Coal Conversion Processes," ASM, AIME Materials Science Symposium, November 11-13, 1975, Cincinnati, Ohio.

[7] A. W. Ruff and L. K. Ives, "Measurement of Solid Particle Velocity in Erosive Wear," *Wear*, **35**, 195-99 (1975).

[8] G. L. Sheldon and A. Kanhere, "Impingement Erosion Using Single Particles," *ibid.*, **21** [1] 195-209 (1972).

[9] G. P. Tilly, "Erosion Caused by Airborne Particles," *ibid.*, **14**, 63-79 (1969).

[10] H. L. Oh, K. P. L. Oh, S. Vaidyanathan and I. Finnie, pp. 119-32 in Science of Ceramic Machining and Surface Finishing. Edited by S. J. Schneider, Jr. and R. W. Rice. *Nat. Bur. Stand. (U.S.), Spec. Publ.* **348**, Washington, D.C., 1972.

[11] I. Finnie, "Erosion by Solid Particles in a Fluid Stream," ASTM spec. tech. publ. No. 307, American Society for Testing and Materials, Philadelphia, Pa., 1962.

[12] J. G. A. Bitter, "A Study of Erosion Phenomena: II," *Wear*, **6**, 169-90 (1963).

[13] J. H. Neilson and A. Gilchrist, "Erosion by a Stream of Solid Particles," *ibid.*, **11**, 111-22 (1968).

[14] E. R. Fuller, "Effect of Hydrothermal Environments on the Strength of Castable Refractories," to be published. □

To be submitted for Publication

LBL-7327
Preprint

THE ELEVATED TEMPERATURE EROSION OF 1100- 0 ALUMINUM BY A GAS - PARTICLE STREAM

Padraic A. Doyle
Alan V. Levy

May 1978

Prepared for the U.S. Department of Energy
under Contract W-7405-ENG-48

LAWRENCE BERKELEY LABORATORY
UNIVERSITY OF CALIFORNIA
BERKELEY

LBL-7327

LEGAL NOTICE

This report was prepared as an account of work sponsored by the United States Government. Neither the United States nor the Department of Energy, nor any of their employees, nor any of their contractors, subcontractors, or their employees, makes any warranty, express or implied, or assumes any legal liability or responsibility for the accuracy, completeness or usefulness of any information, apparatus, product or process disclosed, or represents that its use would not infringe privately owned rights.

LBL-7327

THE ELEVATED TEMPERATURE EROSION OF 1100-0 ALUMINUM BY A GAS - PARTICLE STREAM

By

Padraic A. Doyle
and
Alan V. Levy

May, 1978

Materials and Molecular Research Division
Lawrence Berkeley Laboratory
Berkeley, California 94720

ACKNOWLEDGMENT

This work was supported by the Division of Materials Sciences, Office of Basic Energy Sciences, U. S. Department of Energy.

ABSTRACT

Erosion rates of a face centered cubic (FCC) metal, 1100-0 aluminum, by SiC particles in a nitrogen gas stream as a function of homologous temperature, angle of impingement and particle velocity are presented. Refinements of the experimental device for these experiments are described. The effect of elevated temperatures to 0.8 homologous temperature (HT) was found to no more than double the room temperature erosion rates in spite of the fact that the tensile strength has decreased seven-fold. At a particle velocity of 100 fps, the erosion rate decreased with increasing temperature to 0.6 HT. Other anomalies occurred that indicate a need to modify models for the room temperature erosion of ductile metals to account for the observed elevated temperature behavior.

TABLE OF CONTENTS

I. Introduction 1

II. Description of the High Temperature Erosion-Corrosion Device 3

III. Development of the Erosion-Corrosion Device

- Temperature Profile of Gas-Particle and Test Specimen 7
- Particle Feed Rate 12
- Particle Velocity Determination 15

IV. Elevated Temperature Erosion of 1100-0 Aluminum 18

V. Discussion of Results 20

VI. Conclusions 49

References 51

Tables 52

Figure Captions 57

I. INTRODUCTION

With the advent of the energy crisis, attention has turned to the increased use of coal as a source of energy. A potential use of large quantities of coal is to gasify it into a low or high BTU synthetic natural gas. The gasification process can subject component materials to high erosion and corrosion deterioration. As a necessary approach to the development and selection of materials for these plants, the basic deteriorating mechanisms of erosion, corrosion and combined erosion-corrosion must be understood. Studying erosion and corrosion processes separately will provide clearer understanding when the combined mechanism is investigated.

This investigation concerns the erosion of a representative face centered cubic (FCC) metal, 1100-0 aluminum. It has the same microstructure as the types of alloys which are currently candidate material for coal gasifier internals. Since it could be tested at lower absolute temperatures than 300 series stainless steels, its selection permitted more precise control of the test environment at the initial operational stage of the test machine.

While much is understood about erosion under ambient conditions,[1-6] little elevated temperature work has been conducted. A device to run controlled erosion-corrosion experiments in the simulated environments of coal gasifiers is being developed at the Lawrence Berkeley Laboratory. Much development effort has been expended in the refinement of the erosion-corrosion tester to provide well-controlled, well-monitored and duplicatable experimental test conditions. The equipment development and

The present operating characteristics of the device are presented.

1100-0 aluminum was tested in the erosion-corrosion test device in this research program. The material was eroded by a non-reacting gas-particle stream of SiC (250 μm to 300 μm) particles and nitrogen gas. Particle velocities were 100 fps and 200 fps. The angle of impingement of the particles on the sample, α, was varied from 10° to 90°. The gas, particle and target material test temperatures were set at various homologous temperatures of the target material (the fraction of the absolute temperature to the absolute melting point temperature) from 0.32 to 0.8.

This work was done with support from the U.S.Department of Energy.

II. DESCRIPTION OF THE HIGH TEMPERATURE EROSION-CORROSION TEST DEVICE

Test Device

The erosion-corrosion test device has been designed to simulate a wide range of conditions. Fig. 1 shows the tester. Fig. 2 is a schematic of it with the principal components designated. Nitrogen was used as the carrier gas for the particles. Test temperatures can range from room temperature to 1000°C. Achievable velocities range from $<$ 100 feet per second to the supersonic range. Particle loadings range from 0.05 to 30 lb/100 SCF of carrier gas. Gas composition can be varied in future testing as needed to simulate part or all of the reactive gases in a coal gasifier with the composition monitored by a gas chromatograph system. Solid materials can then be subjected to test conditions to determine material behavior in the hostile environment of a coal gasifier, simulating all conditions but the elevated pressures. The angle of impingement of the gas-particle stream is varied by proper placement of the test specimen relative to the eroding-corroding stream.

The function of the device is to mix particles at a known feed rate with a gas and bring the resulting gas-particle stream to a desired temperature and particle velocity. This gas-particle stream then impinges on the test specimen. The test specimen is also to be at the desired temperature before testing is started and is to stay at that temperature during testing.

Refer to Fig. 2 for the following description of system operation. Particles are introduced into the device by means of a pressurized hopper that ensures an adequate supply of abrasive material during testing up to several hours duration at solid loadings simulating those that occur in coal gasifiers. An auger, powered by a motor and motor controller that can be set for various speeds, uniformly feeds particles into the mixing chamber. The particles are preheated by the particle radiant heater before entering the mixing chamber. The gas or gas mixture also enters the mixing chamber after being pre-heated by heating tapes and the gas radiant heater. The velocity of the incoming gas, the tumbling action of the auger, the relative small size of the abrasive particles and the small exit size (3/16 inch I.D.) compared to the size of the mixing chamber (1.5 inches I.D.) ensure a thorough mixing of the particles and the gas stream. The exiting gas-particle stream is then further heated by the nozzle radiant heater. Uniform stream characteristics are imparted to the gas-particle stream as it moves from the mixing chamber, through the nozzle, to the nozzle exit approximately 7/8 of an inch above the specimen. Gas velocities, and thus particle velocities, are achieved by releasing pressurized gas through the device to the near atmospheric pressures encountered in the test chamber. The test chamber is attached to a settling chamber which collects the particles from the exiting gas. The gas is vented to the atmosphere after passing through air filter bags which collect the particles not deposited in the settling chamber.

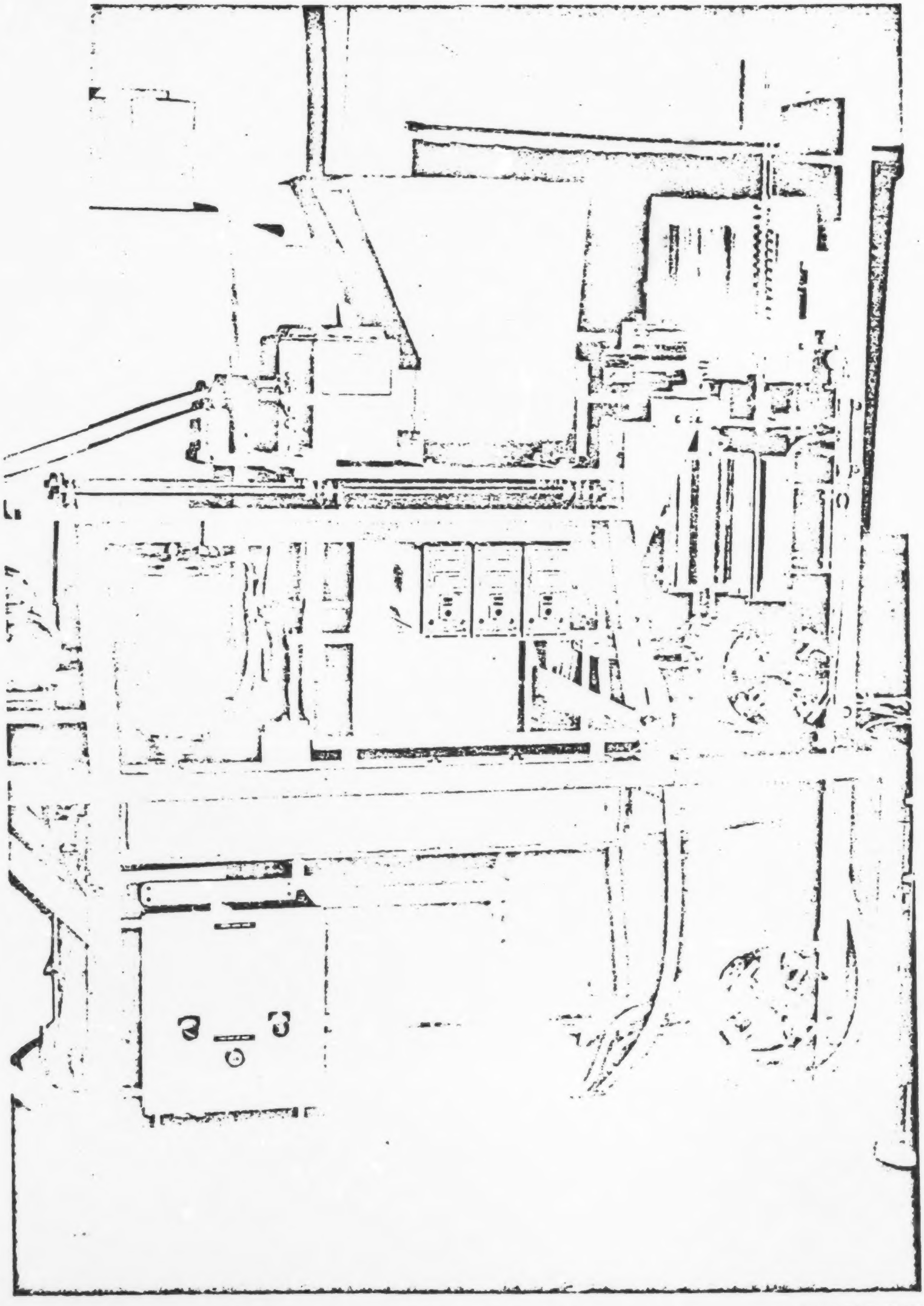

FIG. 1 High Temperature Erosion-Corrosion Test Device CBB 763-2071

EROSION/COROSION TESTER GAS SYSTEM

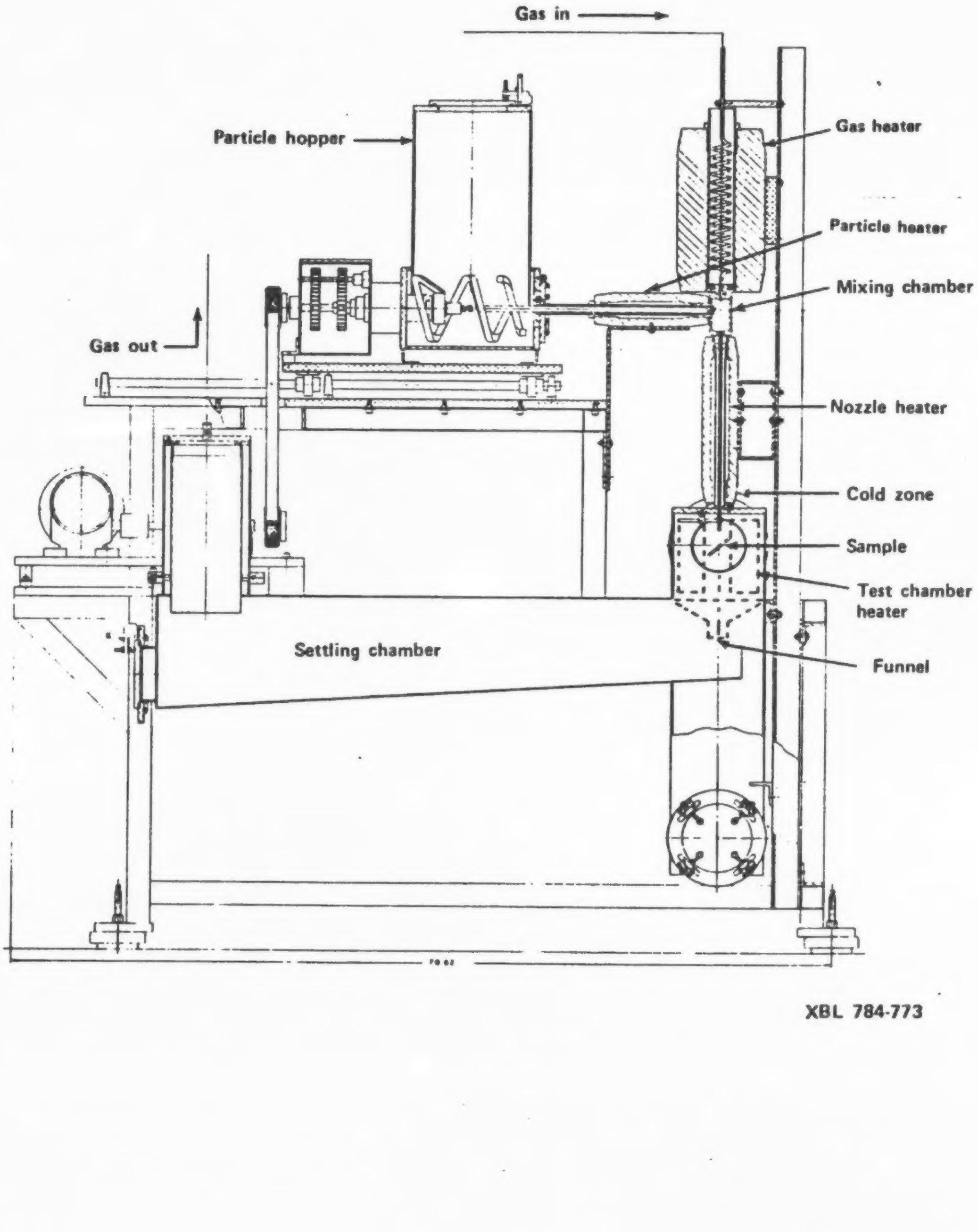
Gas in
Particle hopper
Gas heater
Particle heater
Mixing chamber
Gas out
Nozzle heater
Cold zone
Sample
Test chamber heater
Funnel
Settling chamber

XBL 784-773

III. DEVELOPMENT OF THE EROSION-CORROSION TEST DEVICE

Temperature Profile of Gas-Particle Stream and Test Specimen

Initial operation of the device revealed that problems existed in the gas-particle stream and test specimen temperature determination and control. As originally conceived it was felt that the heat imparted to the gas-particle stream by the radiant heaters and the use of a specimen back heater would achieve the required temperatures. The temperatures were met a certain points but the overall temperature profile was not uniform.

The erosion-corrosion device uses the radiant heaters to heat sections of the system: the gas heat exchanger, most of the pipe enclosing the particle auger and most of the nozzle. The radiant heaters, with their electronic controllers, provide a very responsive and reliable heat source. A uniform heat zone is provided through 80% of the heater's length. The other 20% accounts for the ends of the heater where there is no heat source. In fact, due to the cooling design of the heaters, the ends are water-cooled to below room temperature when no power is applied. Radiation heat sinks are thus presented to the heated gas, particle or gas-particle streams as they pass from the heater to the next section of the erosion-corrosion tester.

A uniform temperature is of particular importance in the nozzle region where final temperature and stream characteristics are imparted to the gas-particle stream. The nozzle extends from the mixing chamber, through the nozzle heater and into the test chamber. A thermocouple inserted inside the nozzle at various lengths from the nozzle exit indicated a distinct temperature profile. See Table I. Desired stream temperatures (~1000°C) were achieved in the nozzle heat zone. In the position corresponding to the cooled end of the heater, 4 inches from the nozzle exit, at least 100°C had been lost from the gas particle stream. Further down the nozzle, 2 inches from the nozzle exit, more heat was lost to a water-cooled plate that makes up the top of the test chamber. At the nozzle exit the temperature had dropped even further. About 250°C was lost from the nozzle heater heat zone to the nozzle exit. Heat was also lost in the 7/8 inch from the exit to the position corresponding to the top of the test specimen, See Table 2. Once inside the test chamber radiation to the unheated walls of the test chamber caused the further heat loss.

Thus when a test specimen back heater was used the back of the specimen had to be heated higher than desired to achieve a given specimen surface temperature in order to compensate for the cooling effect of the impinging gas. Neither the specimen surface temperature nor the particle temperature could be directly determined without interference from the cooler gas. As a result the boundary conditions governing the test specimen surface and the eroding particles impinging on that surface were indeterminable directly. Indications pointed to a quite undesirable, nonuniform temperature profile for the gas-particle stream and the test specimen.

The following actions alleviated most of the temperature profile difficulties. Cooling water to the radiant heaters was cut back to the minimum design limit after the installation of a flow meter. Cooling water to the 1/2 inch plate at the top of the test chamber was eliminated. In the present configuration, when heat is applied, this plate bends inward about 3/8 of an inch. The test specimen back heater was removed and a wire coil resistance heater was installed within the periphery of the test chamber. This resistance heater heats the inside of the test chamber from the top of the chamber to a position below the test specimen. The two halves of the heater are split and are positioned close to the walls of the test chamber to facilitate the insertion of a velocity tester. The test chamber heater heats the test specimen and prevents radiative heat loss from the exiting gas-particle stream to the inside walls of the test chamber.

Initial runs with the test chamber heater inserted included the placement of thermocouples at the nozzle exit and in a hole drilled about 1/4 inch into the side of the test specimen just below the test surface. See the photographs of the test specimens for thermocouple placement. Before the release of the gas and particles, the pre-heated test chamber indicated the desired uniform temperatures at the two locations. With the start of the erosion process the temperature of the specimen was seen to drop approximately 100°C to 150°C. This was caused by the exiting gas-particle stream passing around the test specimen with sufficient momentum to stir up the cooler ambient air below the specimen. A funnel inserted below the specimen and the test chamber heater allowed the passage of the exiting gas and particles but prevented the entrance of the cooler ambient gas into the test chamber region. During a test the temperatures at the nozzle and the test specimen can be within 2°C or 3°C of each other.

Much temperature data was acquired during the course of these experiments. Temperatures were recorded for each velocity run, each particle catch run, and each test specimen erosion experiment. The thermocouple placement is a follows (refer to Fig. 2):

--heating tapes (on gas in line)
--gas radiant heater
--particle radiant heater
--particle heater cold zone
--mixing chamber outside
--mixing chamber inside
--nozzle radiant heater
--nozzle heater cold zone
--tip of nozzle
--test specimen
--outside of test chamber
--velocity tester (if used).

The data thus recorded should prove useful in guiding further development of the erosion-corrosion test device.

It is to be noted that all stream thermocouples are on the outside of the walls containing the gas, particle or gas-particle streams. The exception to this rule is the thermocouple that is open to the inside of the mixing chamber. It enters from the outside, is slightly beyond the mixing region of the chamber and is not in contact with particles. The mixing chamber inside temperature is indicative of the actual gas temperature. Actual particle temperature was not obtained but is assumed to be that of the gas in the test chamber. The temperature of the mixing chamber inside is continually lower than the outside. See Table III for sample recorded temperatures for the erosion-corrosion test device.

The cold zones at the ends of the radiant heaters, with their attendant variations in temperature profile, are still present in the device. The present work used nitrogen gas and silicon carbide particles. The chemical properties of these materials are relatively insensitive to temperature variations and it was felt that the drop and subsequent rise in the temperature of the gas-particle stream as it passed by the cooler zones at the test velocities of 100 and 200 feet per second for the particles would be of a minor consequence in the erosion process as the temperatures at the nozzle exit and in the test specimen were very close to each other and to the desired level. The cold zones will have to be reconsidered in subsequent work involving reactive gases.

A source of trouble in reaching temperatures of 1000°C is the mixing chamber. At present this section of the device is insulated only. A test heater placed around the mixing chamber demonstrated the achievement of high temperatures in this region. The outside of the chamber was red hot. Most of the material in this region and in the other heat zones is stainless steel. A single heating device, with no cold zones from the mixing chamber to below the test specimen is recommended for reactive gas work to ensure uniform temperature profiles and adequate heating.

Particle Feed Rate

It is necessary that the particle feed rate be constant during the course of an experiment. An accurate determination of the particle feed rate is required for the evaluation of the erosion rates. Feed rates were found for the various conditions under which the erosion-corrosion test device operated by catching particles in a container and weighing them. The particle catcher container was attached to the end of the nozzle, the device was run for three minutes and the weight of the particles caught divided by the time yielded the particle feed rate.

Operation of the device indicated inconsistencies in the feed rate determination. The reasons for this were readily defined but a relatively sophisticated solution was required for the resolution of the problem.

The hopper is open, through the auger, to the mixing chamber. The addition of particles will retard but not stop the passage of gas between the hopper and the mixing chamber if a differential pressure exists. It is necessary to ensure that the gas entering the mixing chamber does not pass through the auger and particles and into the hopper. This is achieved by pressurizing the hopper.

Previous testing had demonstrated that a slightly greater pressure in the hopper than in the mixing chamber provides very uniform feed rates. These tests were performed at comparatively high pressures (3-6 psi) corresponding to velocities of several hundred feed per second. Under these conditions the maintenance of a slightly higher pressure on the hopper was readily accomplished by manually operating valves. To achieve a velocity of 100 feet per second, pressures on the order of 1 psi are required. The manually operated valves could not maintain the required differential pressure. Often the mixing chamber pressure would be higher than that of the hopper resulting in gas release into the hopper. The hopper pressure could just as easily exceed, by 2 or 3 times, that of the mixing chamber. This caused gross movement of particles past the auger into the mixing chamber, resulting in an uncontrolled gas-particle stream.

The use of gauges that had barely lifted off the 0 psi peg at one psi compounded the diffculties. In addition, shutting down the device required the near as possible simultaneous operation of several switches and valves. The gas supply to the device is an electrically controlled solenoid valve. The auger controller requires another switch. The hopper gas supply valve must be closed, while the hopper vent valve should be opened to prevent the continuted flow of particles past the auger. All of these difficulties contributed to a poorly controlled particle feed system at the low pressures required to achieve 100 fps particle velocity.

The Calibration Lab at Lawrence Livermore Laboratory helped to provide a system that virtually eliminated the stated problems. The key element is a pressure transducer that measures the differential pressure between the mixing chamber and the hopper. The transducer is sensitive to ± 1 psi and produces an electric signal that is transmitted to an associated indicator and is used as an input of a pressure differential controller built at LLL. Based on settings dialed into the controller, two electrically operated solenoid valves are set which provide the gas supplies to the erosion-corrosion device and the hopper. In addition, an electrically operated vent valve was installed on the hopper. The hopper vent valve and the erosion-corrosion device and hopper gas supply valves are now operated with the same switch. Shut down now only requires the movement of a switch that secures the device gas supply valve and opens the hopper vent valve. The auger motor controller also needs to be turned off in a separate operation. Pressure gauges that read from 0-5 psi were obtained and installed to permit precise settings of 1 psi.

Referring to the recorded SiC feed rates on the 100 fps curves of erosion rate vs. impingment angle, Fig. 3-10, it is noted that the feed rates are often within a gram or two of each other for the different impingement angle tests. This would not be possible without the transducer system. The 200 fps feed rates show a slightly greater variation. There are several reasons for this. The electrically operated hopper vent valve is of a small diameter (3/8 inch). To protect the transducer element during shutdown the manual hopper vent valve is operated. The 200 fps runs required pressures up to 5 and 6 psi and, upon shutdown, the nozzle would immediately vent leaving several pounds of pressure on the hopper side of the transducer. The delay and variation in the timing of operation of the manual hopper vent valve for the 200 fps tests would allow extra particles to be pushed from the auger into the particle catcher.

Another problem occurred because the particle catcher container was operating near its capacity for the 200 fps runs. The diameter of the particle catcher has to fit through the hole in the funnel beneath the test area of the chamber and is thereby limited in its volume. At the end of the 200 fps particle catch runs, a build-up in back pressure was observed. It is felt that these variations did not greatly affect the 200 fps test results.

Particle Velocity Determination

The erosion-corrosion device uses a velocity measurement device based on a design developed by the Metallurgy Division of the National Bureau of Standards[7]. An air-cooled design was developed to permit velocity determinations up to 500°C. It is shown in Fig. 3. It is mounted on the test chamber door. The method involves two circular discs mounted on a common shaft whose planes are inserted perpendicular to the gas-particle stream exiting from the nozzle. The discs are a known distance apart, less than 3/4 of an inch. The disc closest to the nozzle exit has a slit cut in the radial direction, from its outer edge towards, but not to, its center for the passage of particles through the top disc to impinge on the lower disc. The insertion of these discs, rotating at a constant rate, into the gas-particle stream results in an eroded pattern on the lower disc of a replaceable soft, polished aluminum to make the eroded pattern more easily observed. This pattern is shifted from a radial line that corresponds to the position directly below the slit of the upper disc. This measured shift, the radial distance of the pattern, the disc rotation rate and the distance between the discs are then used to calculate the particle velocity using the following equation:

$$V = \frac{2\pi R \nu L}{S}$$

where V = particle velocity

R = radius from center of disc to center of erosion pattern

ν = angular velocity of disc

L = distance between plates

S = arc length between reference point and erosion pattern

The National Bureau of Standards suggested the use of the gas-particle stream without rotation of the discs to erode a mark on the bottom disc to set the slit or zero mark reference. Use of this method of defining the location of the slit resulted in an error of up to 25% in the zero mark determination. This was due to problems of inserting the upper disc slit directly below the nozzle exit. One zero mark pattern was shifted a full pattern width from where it should have been. The patterns are approximately 0.2 inches wide and are themselves a source of error, since a visual determination of the center of the pattern is required. A typical shift between the zero mark and the rotating patterns is on the order of 0.275 inches. The use of a zeroing pin between the two discs with zero marks machined on the bottom disc greatly enhanced the consistency of the results. Such an approach is recommended.

The National Bureau of Standards article discusses a not fully investigated possible source of measurement error. The rotating discs will cause a disturbance of the gas-particle stream. Indeed, a reduction of about 1/2 psi with the velocity tester, out of 5 or 6 psi without the velocity tester, was noted in the mixing chamber pressure. The velocity measurements were made without changing the test device controls from the previous run and the return to previous operating values was observed when the device was again operating without the velocity tester.

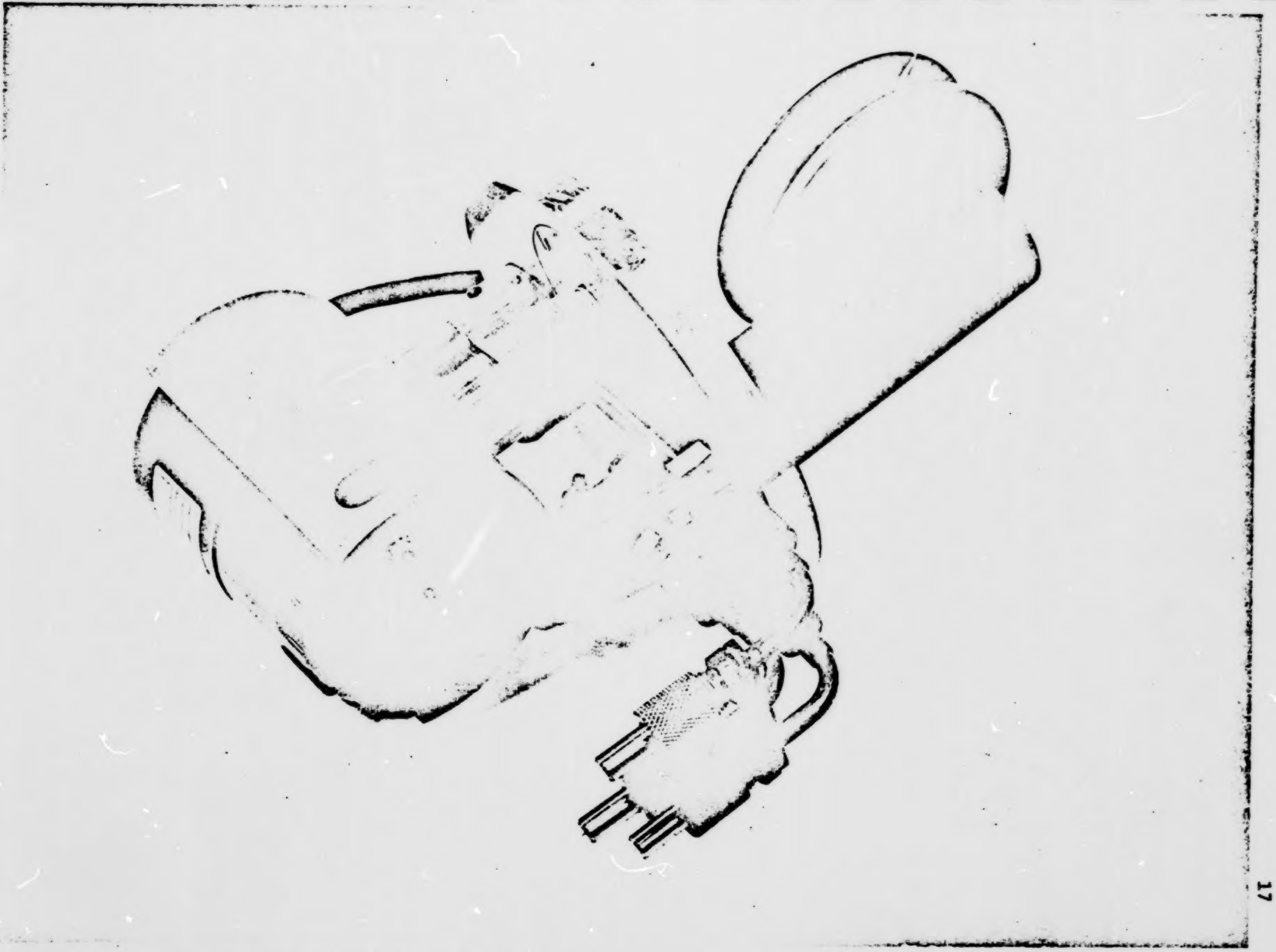

FIG. 3 Particle Velocity Measurement Device

XBB 784-4135

IV. HIGH TEMPERATURE EROSION OF 1100-0 ALUMINUM

Much work has been done in the study of room temperature erosion. Comparatively little study of erosion at elevated temperatures has been conducted. Tilly[8] has reported some elevated temperature data. Smeltzer, et al[9] have also done some elevated temperature work. Petit, et al[10-11] and Wright and Herchenroeder[12] are involved in ongoing studies of erosion-corrosion processes at elevated temperatures.

The present study is part of a larger erosion-corrosion investigation at the Lawrence Berkeley Laboratory. The aim of the total program is to study the erosion and the corrosion processes separately, thus leading to a clearer understanding of the operative mechanisms when combined erosion-corrosion tests are conducted. The focus of this work is an investigation of erosion rates and their variation with temperature.

The choice of test temperatures is based on the concept of the homologous temperature. The homologous temperature (HT) is defined as:

$$\text{homologous temperature} = \frac{\text{absolute temperature}}{\text{absolute melting point temperature}}$$

The tests were run at 0.32, 0.4, 0.6, and 0.8 HT. Normally, metals are not used in structural applications above ~ 0.5 HT. The material tested was 1100-0 aluminum, an example of a face-centered cubic material. Silicon carbide was the eroding material; its size ranged from 250 μm to 300 μm. It was felt that silicon carbide is an idealized abrasive. Tests using char, fly-ash and other abrasives will be done in the future. Nitrogen was the carrier gas utilized. The chemical composition of silicon carbide, nitrogen and aluminum are fairly stable over the temperature range of interest. Therefore, little or no corrosion took place and the erosion process was performed without interference from corrosion mechanisms. The angular dependence of erosion rates at room temperature is well known. This project's tests also showed similar angular variations of erosion rate at each of the homologous temperatures tested. A complete set of experiments were run at each of two velocities, 100 fps and 200 fps.

The erosion experiments were run using the following variables:

--material tested: 1100-0 aluminum (2.5"X0.75"X0.25")

--abrasive: Silicon carbide 250 μm - 300 μm

--carrier gas: nitrogen

--homologous temperature: 0.32 (room temperature),
0.4 (99°C), 0.6(285°C),
0.8(471°C)

--angle of impingement: $\alpha = 10°, 15°, 30°, 60°, 90°$

--particle velocity: 100 fps, 200 fps

--time of experiment: 30 min. for 100 fps tests
10 min. for 200 fps tests

Erosion rates are measured and reported in terms of:

$$\text{Erosion Rate} = \frac{\text{gm Al lost}}{\text{gm SiC}}$$

It is important to note that particle feed rate tests and particle velocity tests were run before and after each experiment. Recorded values of particle feed rates, particle velocities, specimen temperatures and specimen weight losses are to be found in Tables IV and V.

V DISCUSSION OF RESULTS

The results of the experiments were plotted in two ways: erosion rate (gm/gm) Vs. angle of impingement, α, for each homologous temperature and velocity tested; and erosion rate (gm/gm) Vs. homologous temperature for each angle of impingement and velocity tested.

A. Erosion rate Vs. angle of impingement

1. 100 fps velocity

At all homologous temperatures tested (0.32,0.4, 0.6, 0.8) the familiar effect of impingement angle on rate of erosion was observed (Fig. 4). The peak erosion rate occurred near α = 15° for all temperatures. At 100 fps particle velocity, the rate of erosion decreased with increasing temperature for all temperatures tested except for 0.8 HT. This indicates that the direct relationship between erosion resistance and hardness or strength does not hold at elevated temperatures for the particle velocity in this test series. The tensile strength of 1100-0 aluminum decreases from 13,000 psi at RT to 8500 psi at 0.6 HT. The slopes of the curves for the 0.32, 0.4, and 0.6 HT tests are approximately the same for angles up to α = 45° indicating that the cutting type mechanism of low impingement angle erosion was the same at the lower temperatures. The erosion rate at all three of the lower temperatures was approximately the same for the α = 90° tests.

The 0.8 HT curve slope is approximately 1/2 that of the lower temperatures, indicating a different mechanism is probably occurring. The difference in the erosion rate between peak

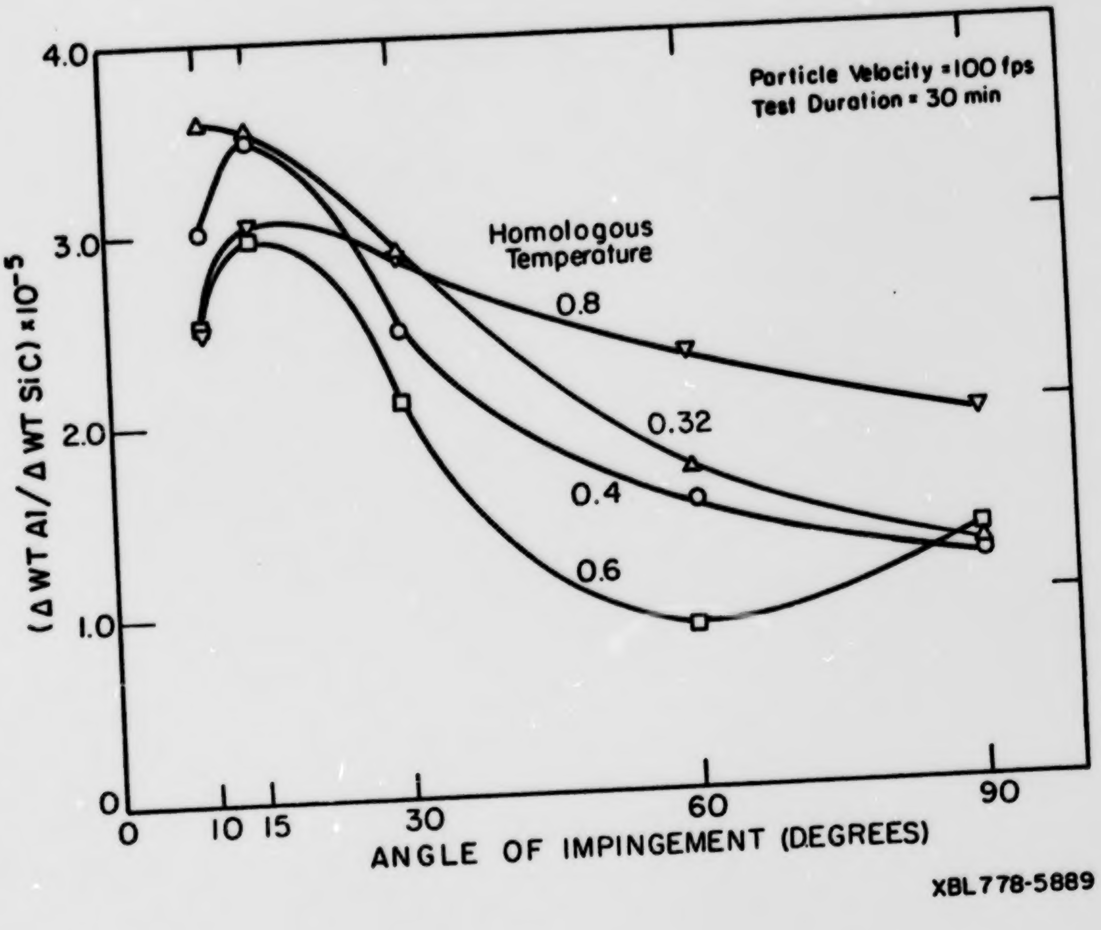
Particle Velocity = 100 fps
Test Duration = 30 min
Homologous Temperature
0.8
0.32
0.4
0.6
4.0
3.0
2.0
1.0
0
(Δ WT Al / Δ WT SiC) × 10^{-5}
0
10
15
30
60
90
ANGLE OF IMPINGEMENT (DEGREES)
XBL778-5889

FIG. 4

rate at $\alpha = 15°$ and the $\alpha = 90°$ rate for the 0.8 HT tests is approximately 1/2 of that of the lower temperature curves. This indicates that the effect of impingement angle on erosion rate is markedly decreased at 0.8 HT. At $\alpha = 90°$ the erosion rate of the 0.8 HT test was approximately 50% higher than the rates observed at the three lower temperatures.

The patterns of erosion shown in Figs. 5, 6, 7 and 8 indicate a consistent pattern of surface ripples for the 10°, 15°, and 30° impingement angles and a bump or mogul* type pattern for the 60° and 90° angles. The patterns intensify in depth and the width of each ripple increases with increasing temperature. Since the rate of erosion is decreasing with increasing temperatures for the lower three temperatures, it is possible that an increasing amount of plastic flow without corresponding increased metal removal is occurring to consume the kinetic energy of the impacting particles. The depth of the erosion and severity of the patterns formed at the higher temperatures indicate a modification of the actual impingement angle with time.

---

*a term used in snow skiing wherein alternating depressions and mounds occur on a ski slope due to skier use.

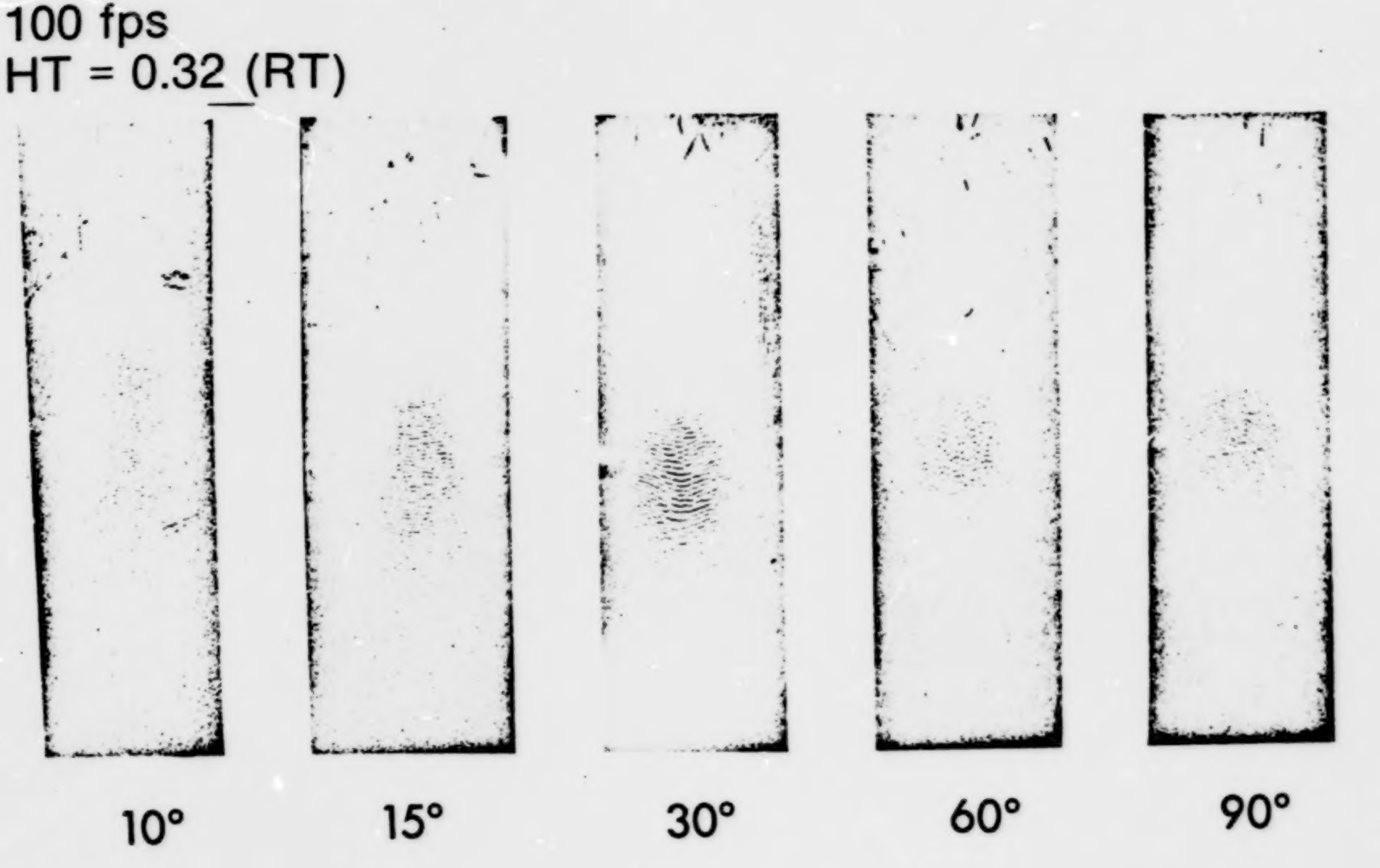
100 fps
HT = 0.32 (RT)
10°
15°
30°
60°
90°
1 cm

FIG. 5.

XBB 784-4444

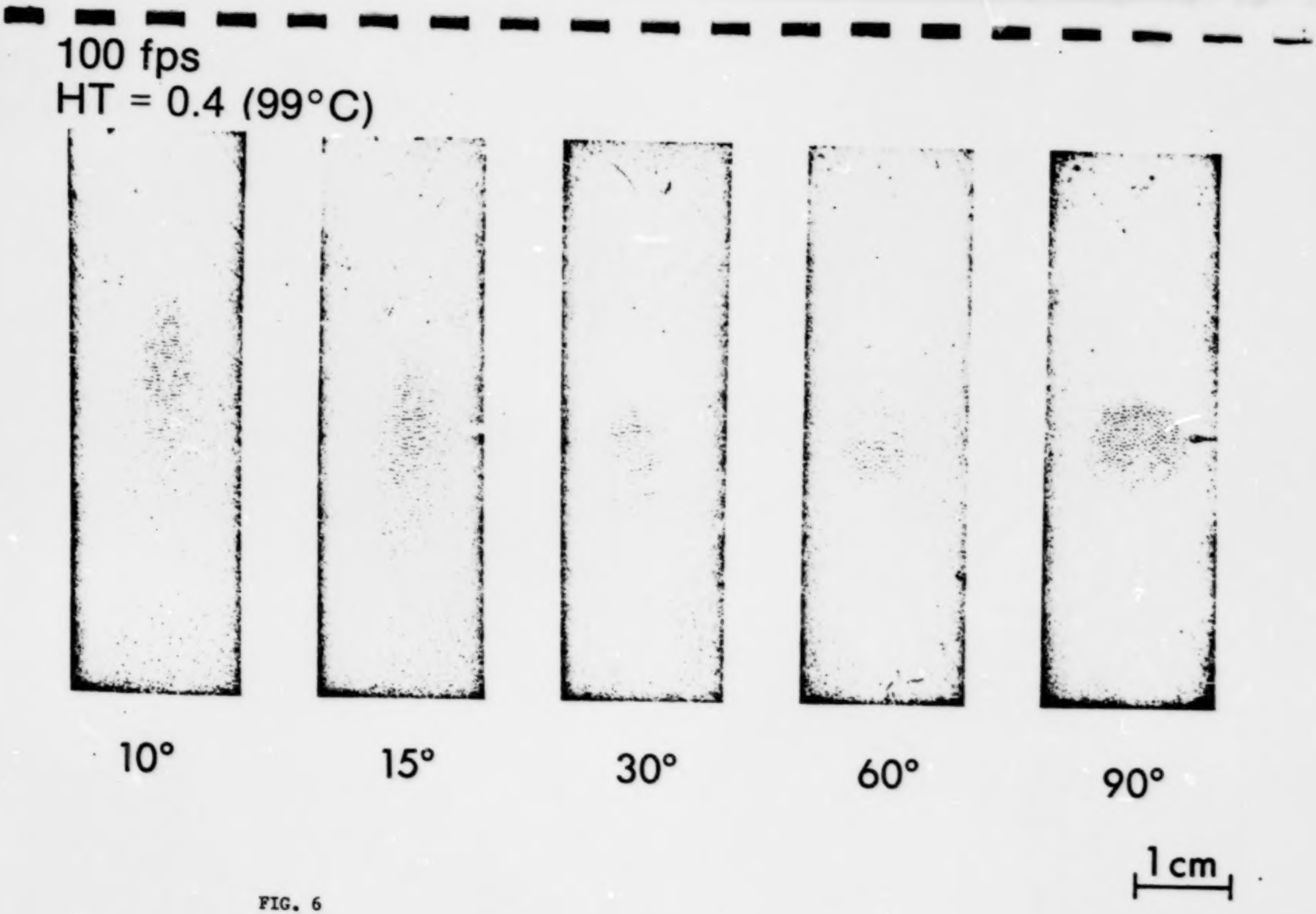
100 fps
HT = 0.4 (99°C)
10°
15°
30°
60°
90°
1 cm

FIG. 6

XBB 784-4454

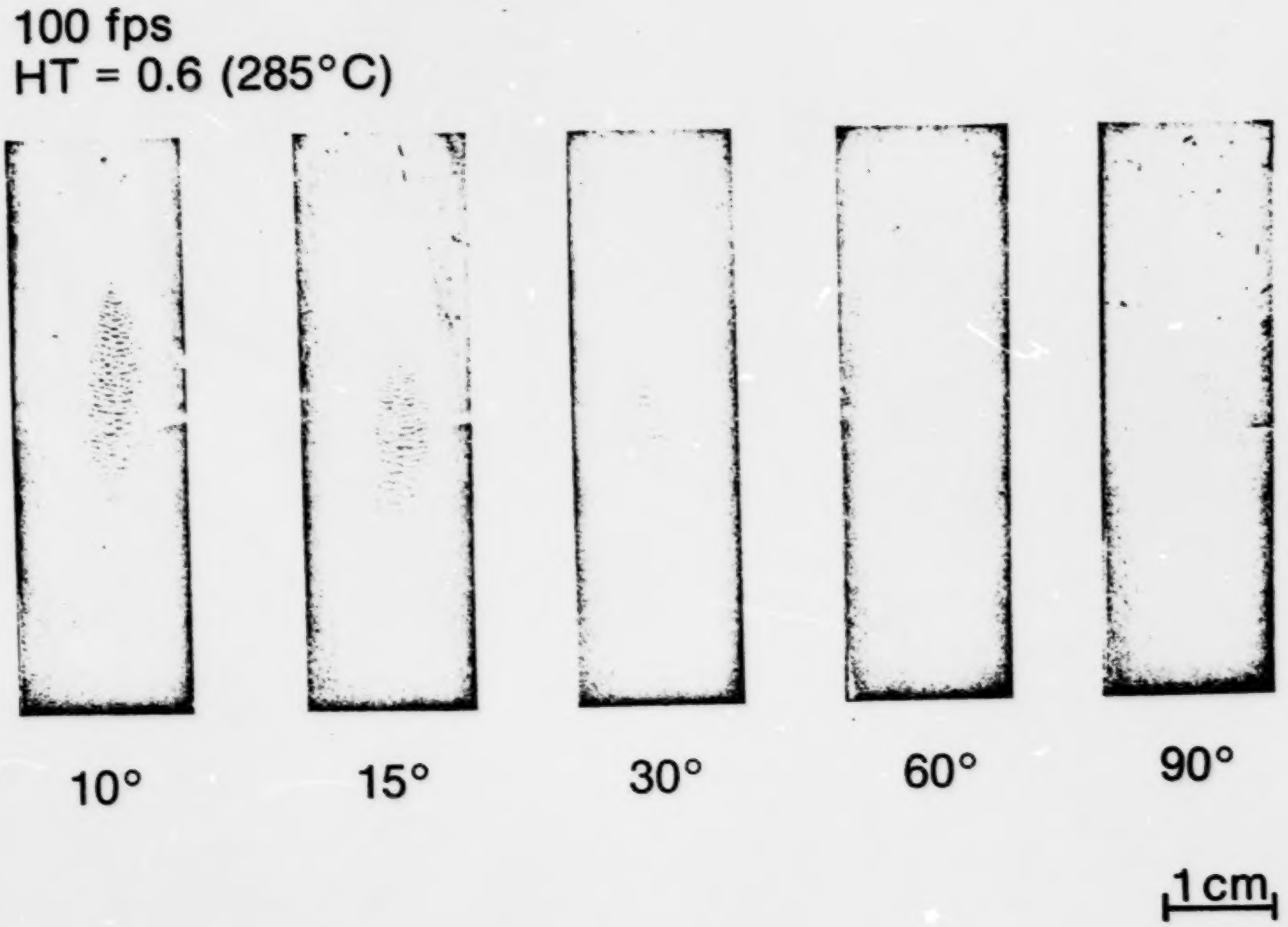
100 fps
HT = 0.6 (285°C)
10°
15°
30°
60°
90°
1 cm

FIG. 7

XBB 785-5204

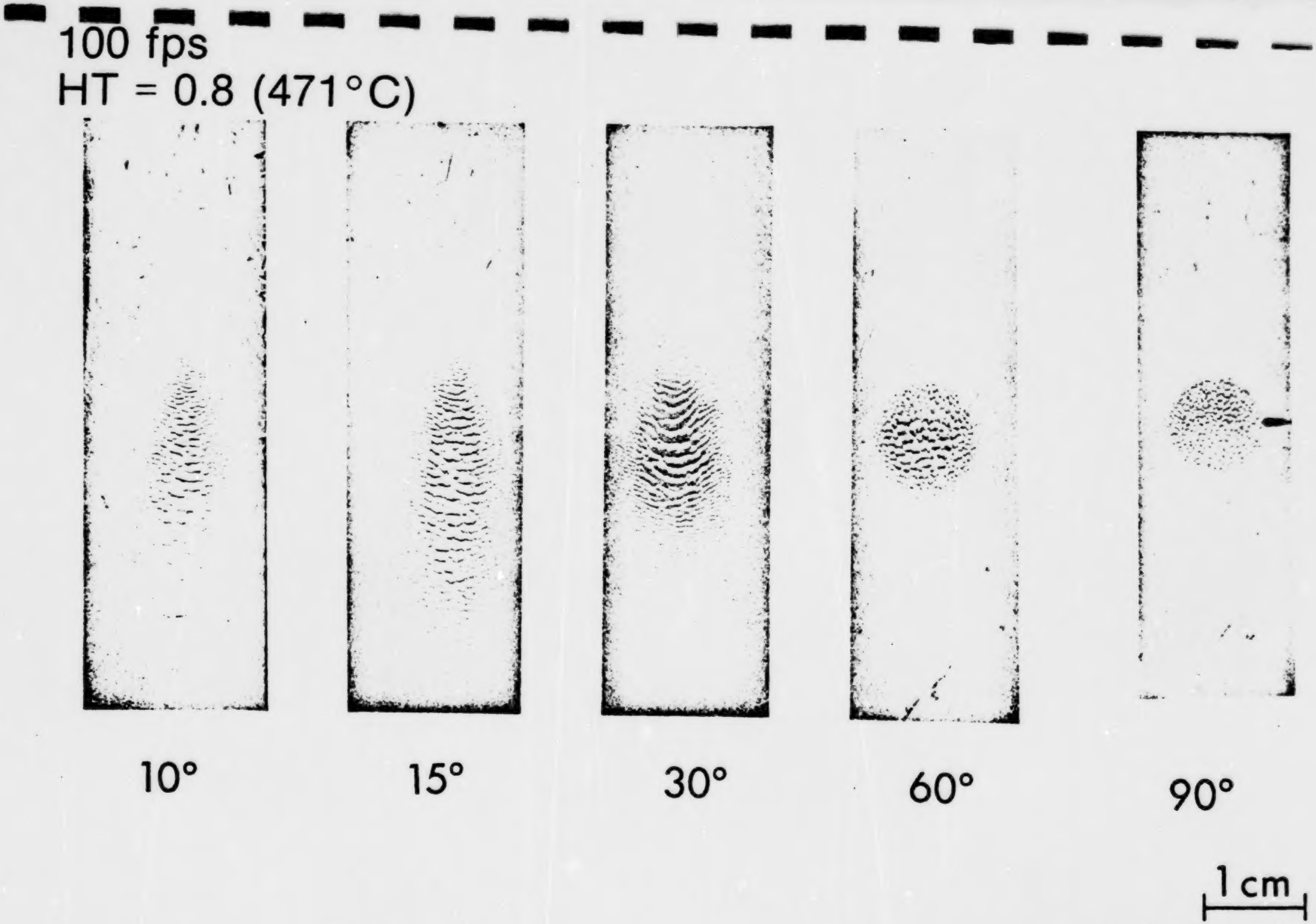
100 fps
HT = 0.8 (471°C)
10°
15°
30°
60°
90°
1 cm

FIG. 8

XBB 784-4445

2. 200 fps velocity

At the higher velocity, the effect of impingement angle on erosion rate is decreased (Fig. 9). While the curves have the same general shape, the difference between peak rate and $\alpha = 90°$ rate is less, particularly for the 0.8 HT tests where the difference is only 15%. Note that the rate of erosion has increased by approximately 1 order of magnitude between 100 and 200 fps. Also, the rate for 0.8 HT is now 100% higher than for 0.32 and 0.4 HT and 40% higher than for 0.6 HT at $\alpha = 90°$.

In the higher velocity tests, the peak angle is still near $\alpha = 15°$. The actual peak may be somewhat higher as no tests were performed between 15° and 30° (this may also be true for 100 fps). Unlike the 100 fps tests, the rate of erosion increases with temperature, a more expected occurrence, considering the decrease in hardness and strength with increasing temperature. The slope of the curves at the three lower temperatures are approximately the same for angles up to approximately 45° as they were at 100 fps but the slope of the 0.8 HT curve is now less than 1/2 of that at the other temperatures, again indicating that a different mechanism of material loss may be occurring at 0.8 HT.

The same patterns of erosion occur at 200 fps as at 100 fps (Figs. 10-13) except they are more intense for each temperature tested. Ripples occur at 10°, 15°, and 30° and moguls at 60° and 90°. The 60° sample at 0,32 HT shows a transition from the ripple to the mogul pattern.

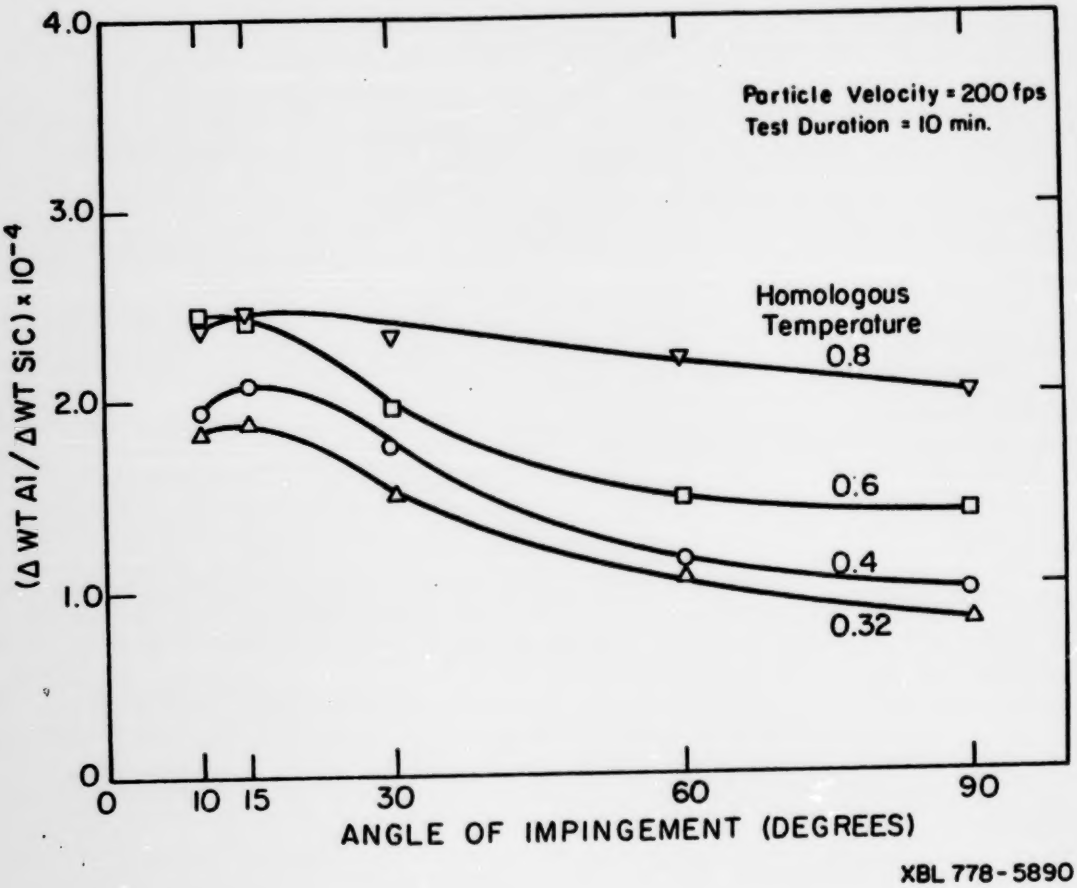
4.0
3.0
2.0
1.0
0
0
10
15
30
60
90
(Δ WT Al / Δ WT SiC) x 10⁻⁴
ANGLE OF IMPINGEMENT (DEGREES)
Particle Velocity = 200 fps
Test Duration = 10 min.
Homologous Temperature
0.8
0.6
0.4
0.32
XBL 778-5890

FIG. 9

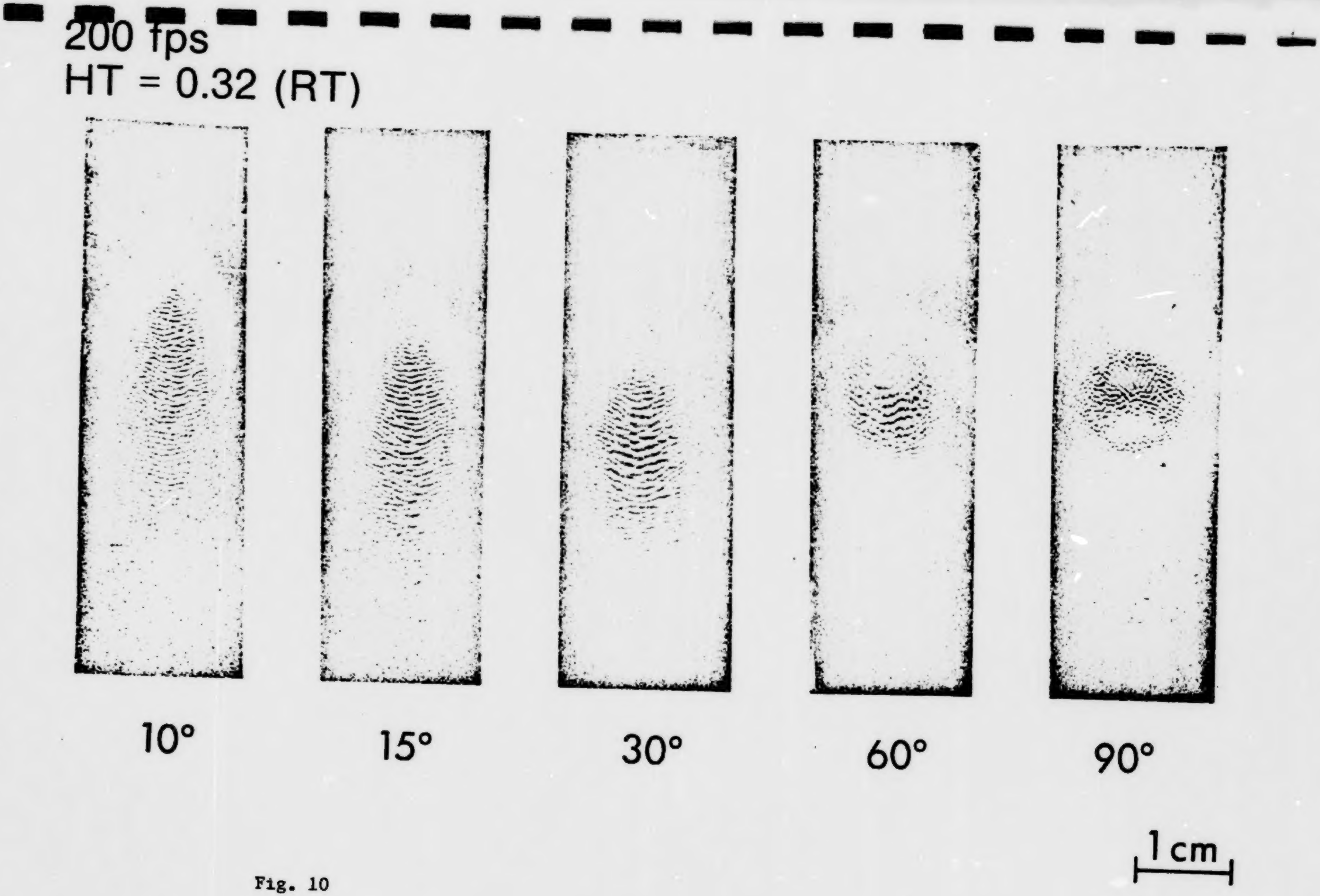
200 fps
HT = 0.32 (RT)
10°
15°
30°
60°
90°
1 cm

Fig. 10

XBB 784-4446

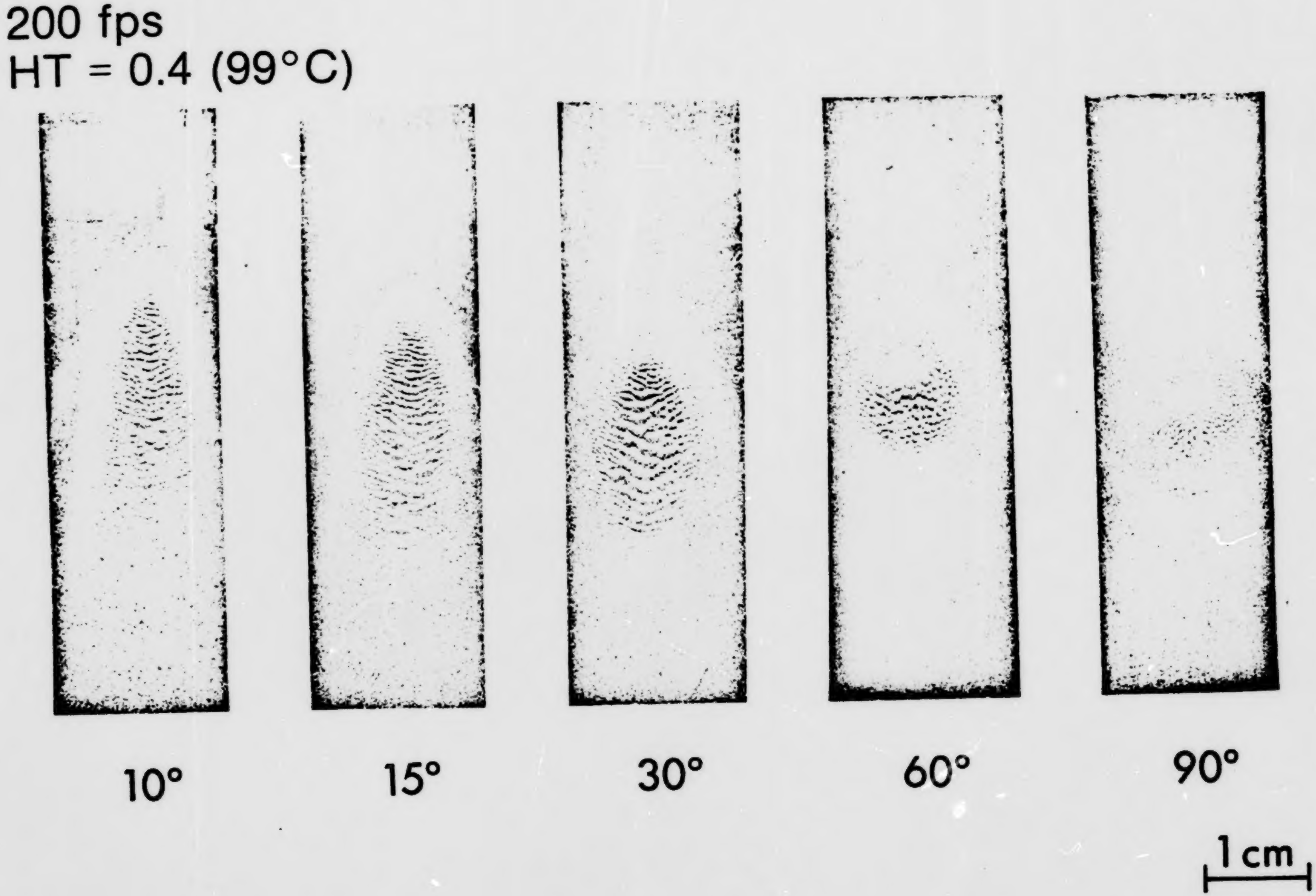
200 fps
HT = 0.4 (99°C)
10°
15°
30°
60°
90°
1 cm

FIG 11

XBB 784-4447

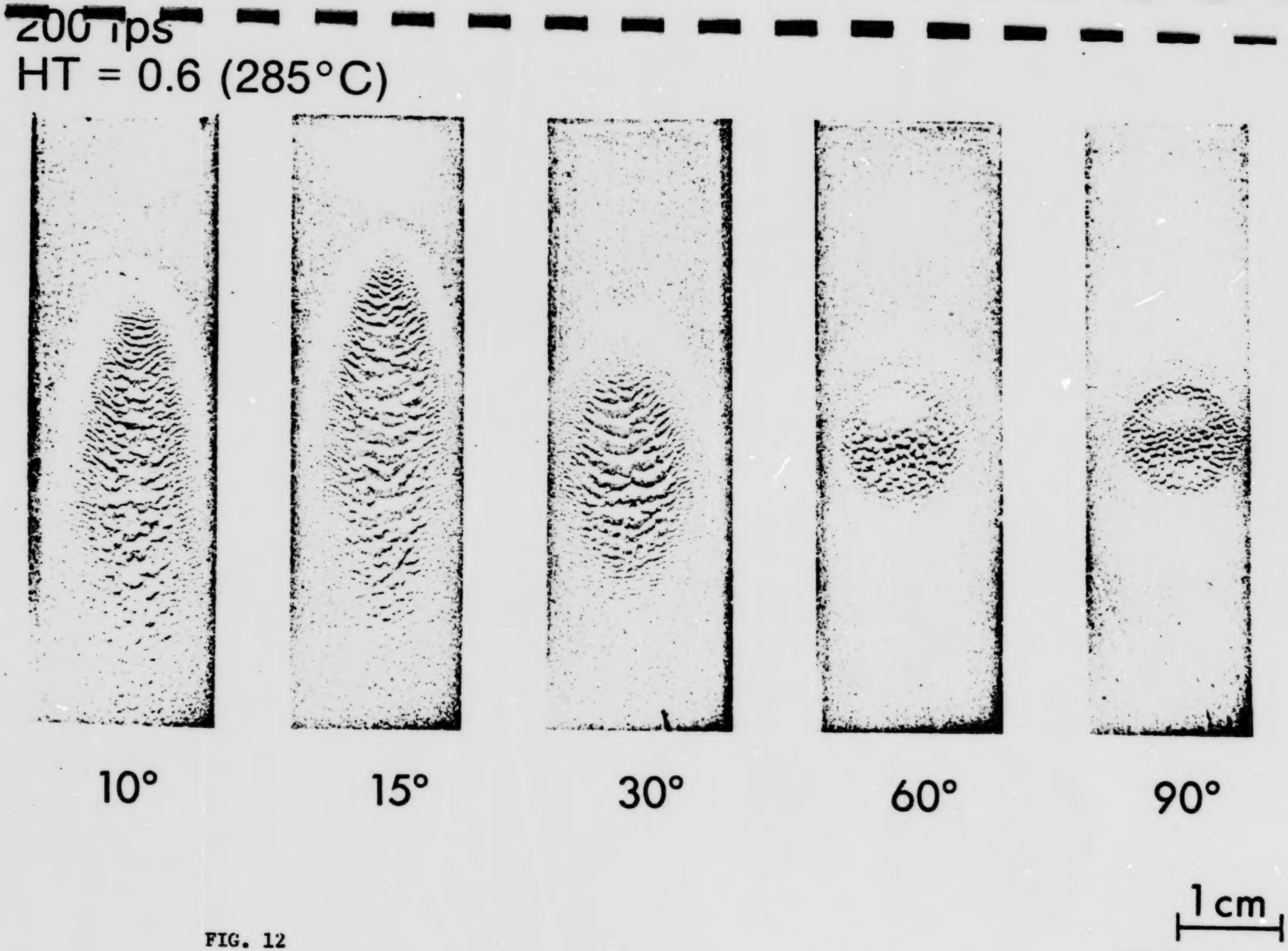
200 ips
HT = 0.6 (285°C)
10°
15°
30°
60°
90°
1 cm

XBB 784-4452

FIG. 12

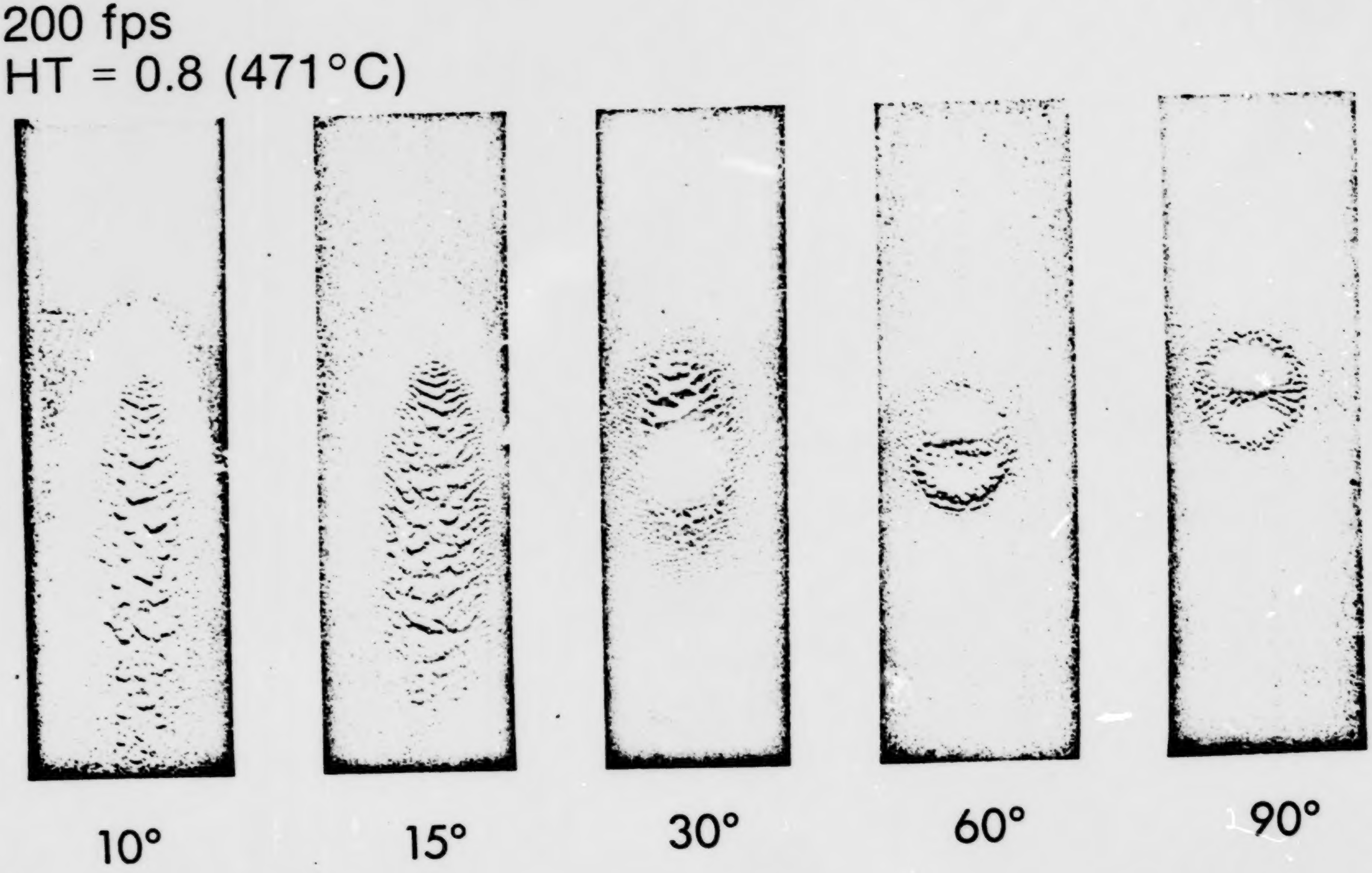
200 fps
HT = 0.8 (471°C)
10°
15°
30°
60°
90°

XBB 784-4451

FIG. 13

B. Erosion rate Vs. homologous temperature

1. 100 fps velocity

The effect of increasing temperature on the erosion rate is shown in Fig. 14. It can be seen that at the lower impingement angles where micro-machining is the predominant mechanism of material removal and surface ripples occur (Fig. 15), the effect of increasing temperature to 0.8 HT has a relatively small effect on erosion rate. While the tensile strength of the material has decreased from 13,000 psi to 4000 psi from 0.32 to 0.8 HT with a similar reduction in hardness, the erosion rate has decreased at α = 10° and 15° and remained the same at α = 30°. Thus the flow stress of the material which relates directly with strength and hardness and is known to have an inverse relationship to erosion rate at room temperature does not maintain this effect at elevated temperatures for shallow impingement angles. The difference between the lowest and highest erosion rates at the steep impingement angles of 60° and 90°, where mogul patterns develop (Fig. 16), is 120% and 71% respectively. This difference is still far less than the flow stress changes, indicating that the flow stress term in the micro-machining erosion model[1] should be reassessed for elevated temperature erosion.

An orderly transition in the shape of the curves occurs as the impingement angle changes, from a decrease in the erosion rate at low angles, to having a minimum at 30° and 60°, to an increase for 90°. There is no break in the shape of the

EROSION RATE VS HOMOLOGOUS TEMPERATURE

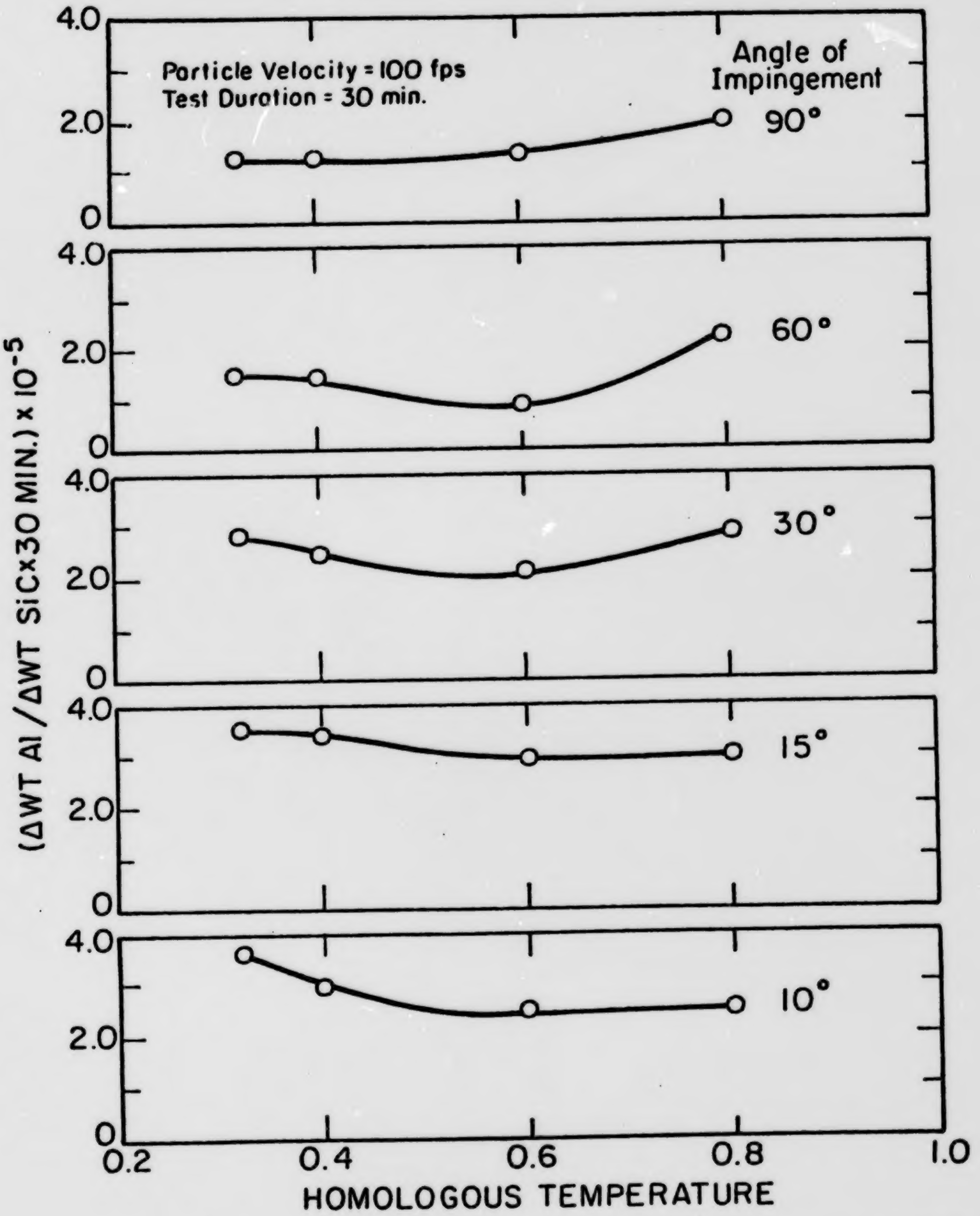

FIG. 14

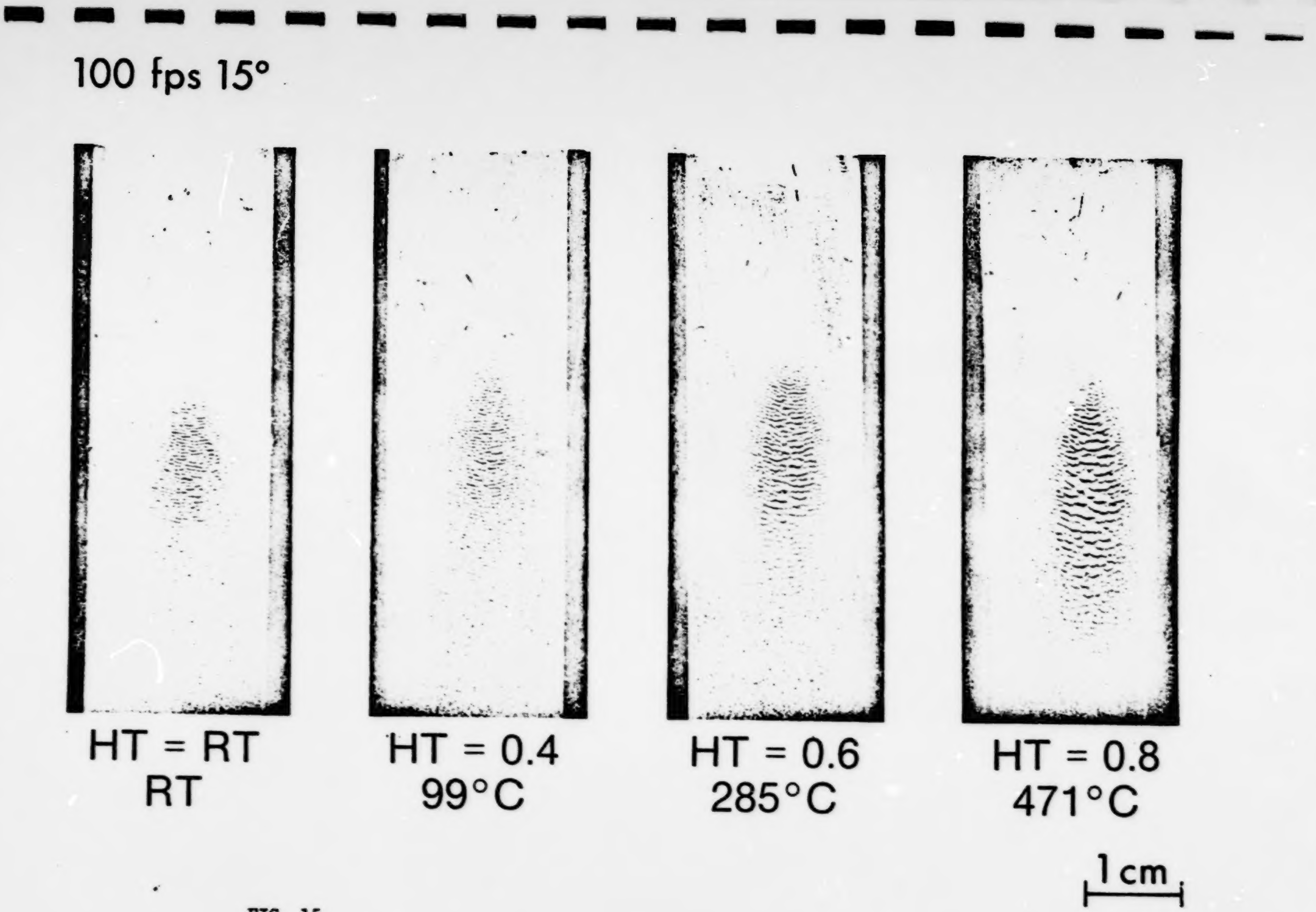
100 fps 15°
HT = RT
RT
HT = 0.4
99°C
HT = 0.6
285°C
HT = 0.8
471°C
1 cm

FIG. 15

XBB-784-4450

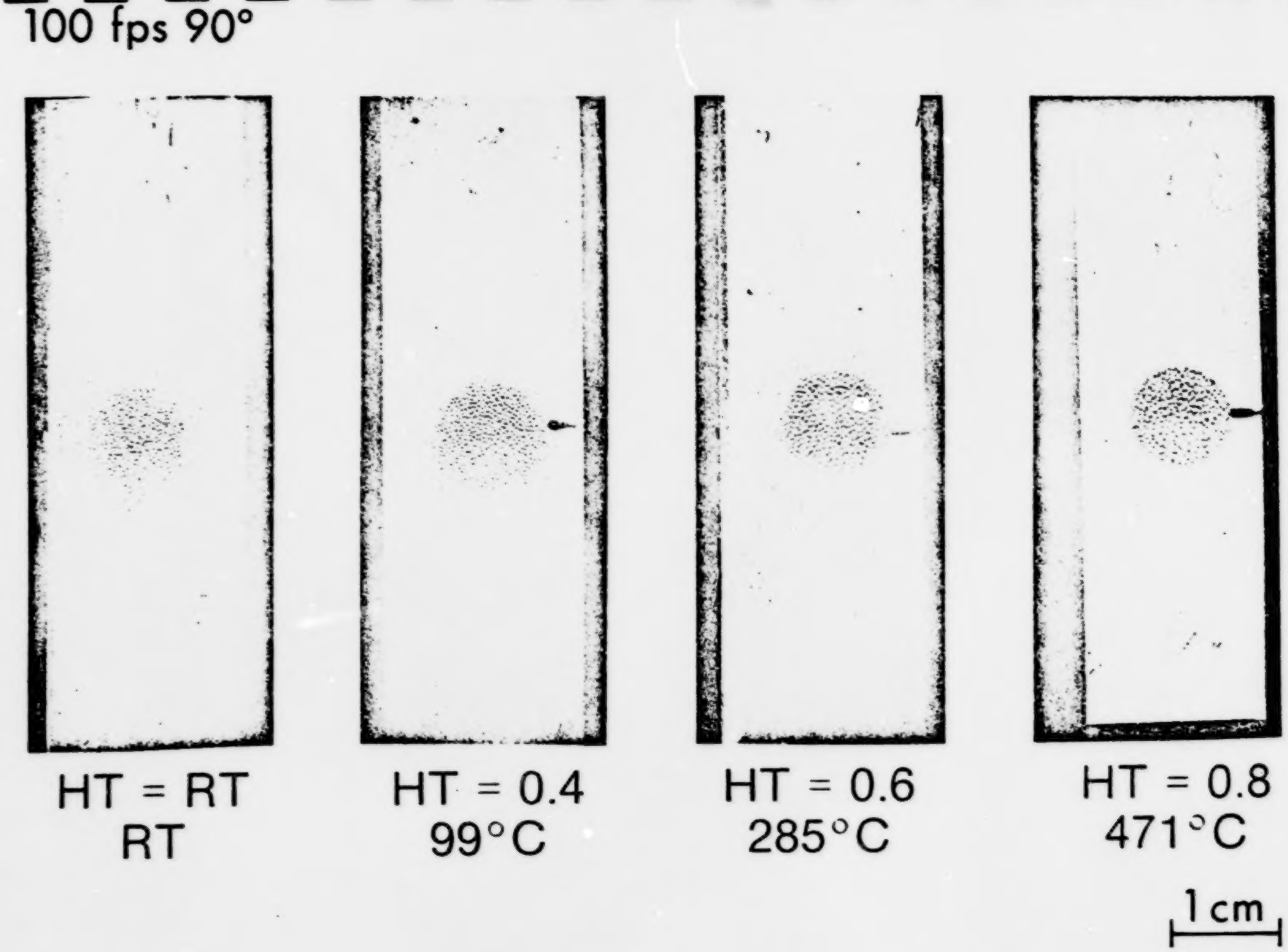
100 fps 90°
HT = RT
RT
HT = 0.4
99°C
HT = 0.6
285°C
HT = 0.8
471°C
1 cm

XBB 784-4449

FIG. 16

EROSION RATE VS HOMOLOGOUS TEMPERATURE

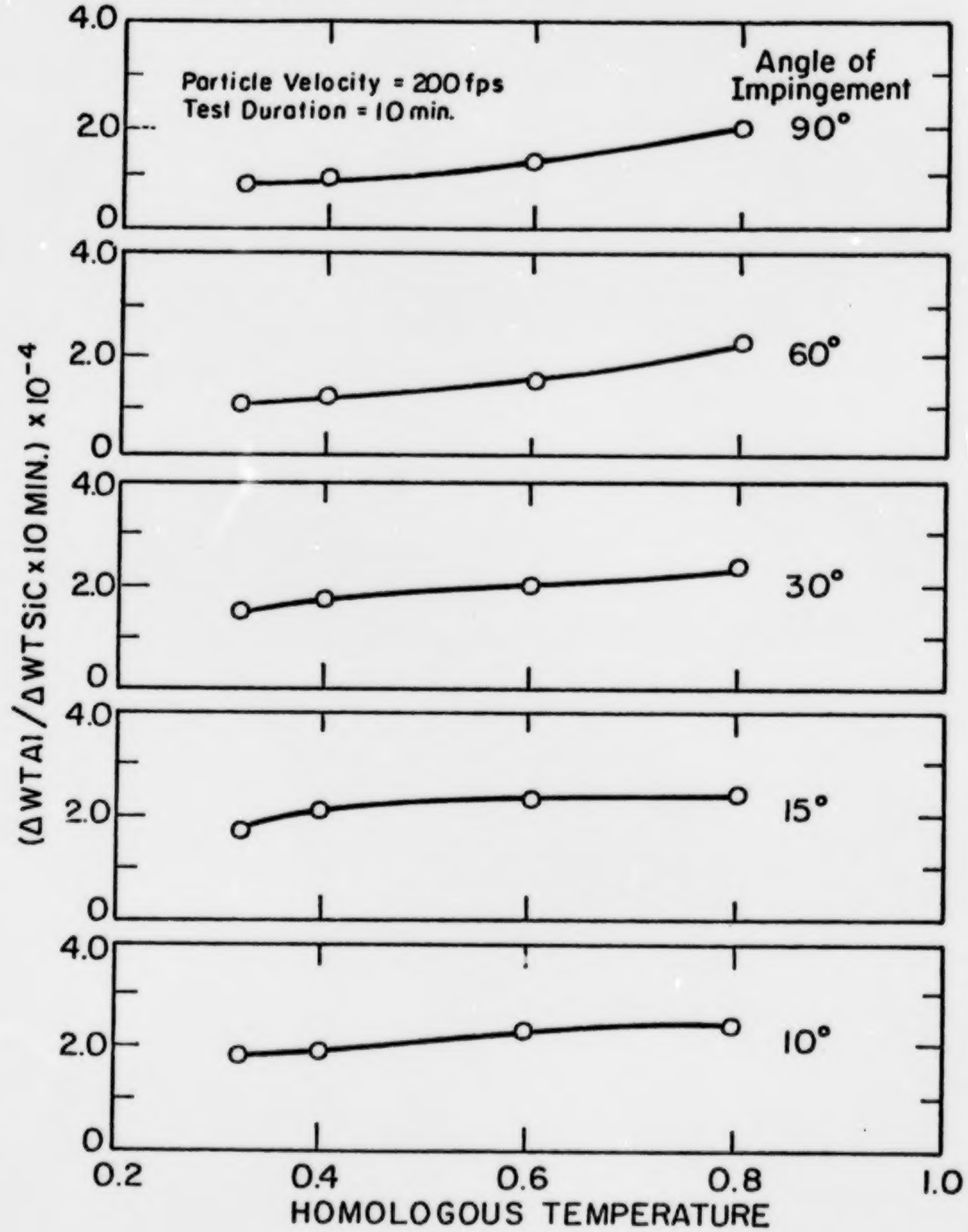

XBL 778-5892

Fig. 17

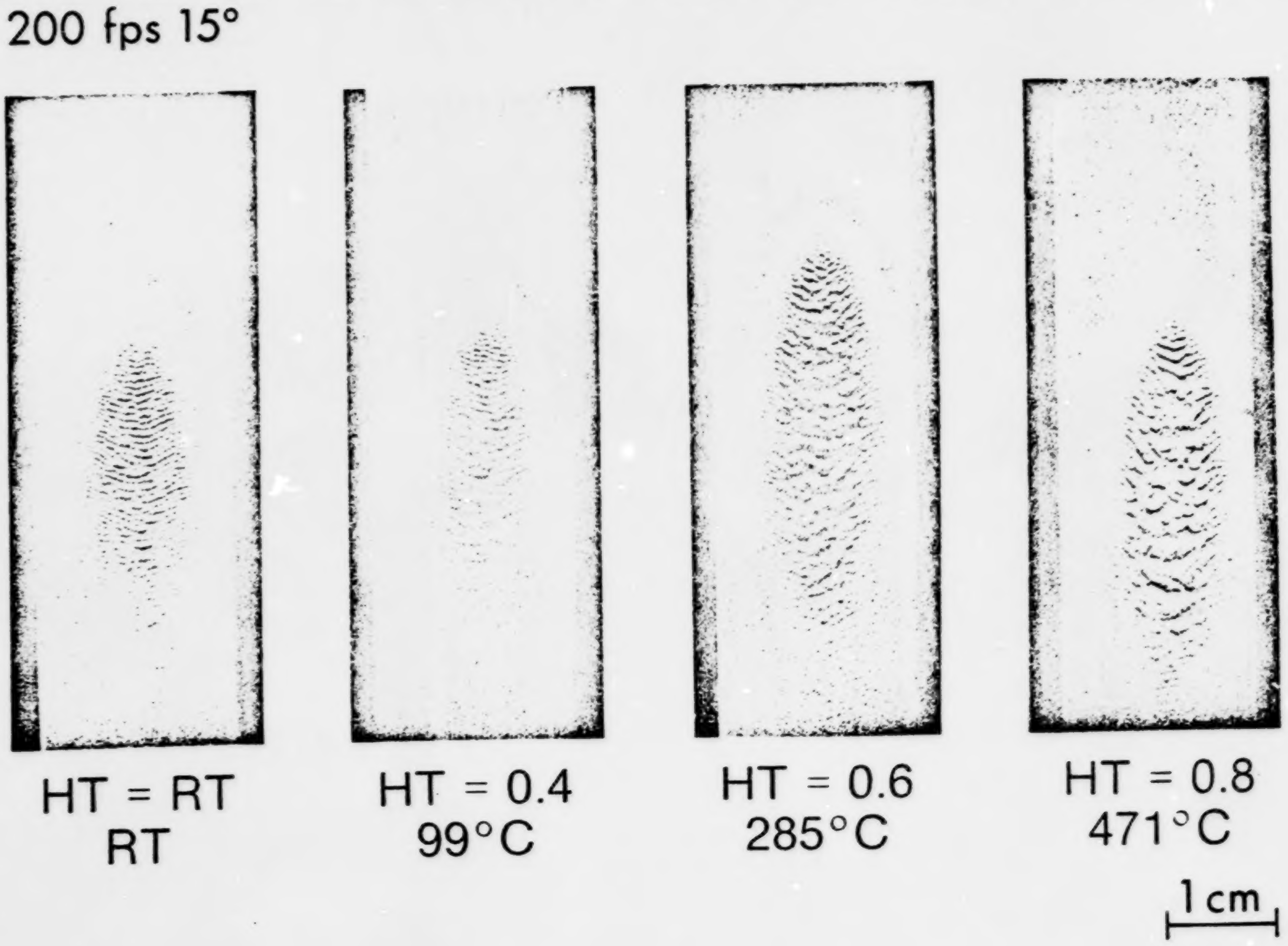
200 fps 15°
HT = RT
RT
HT = 0.4
99°C
HT = 0.6
285°C
HT = 0.8
471°C
1 cm

XBB-784-4448

FIG. 18

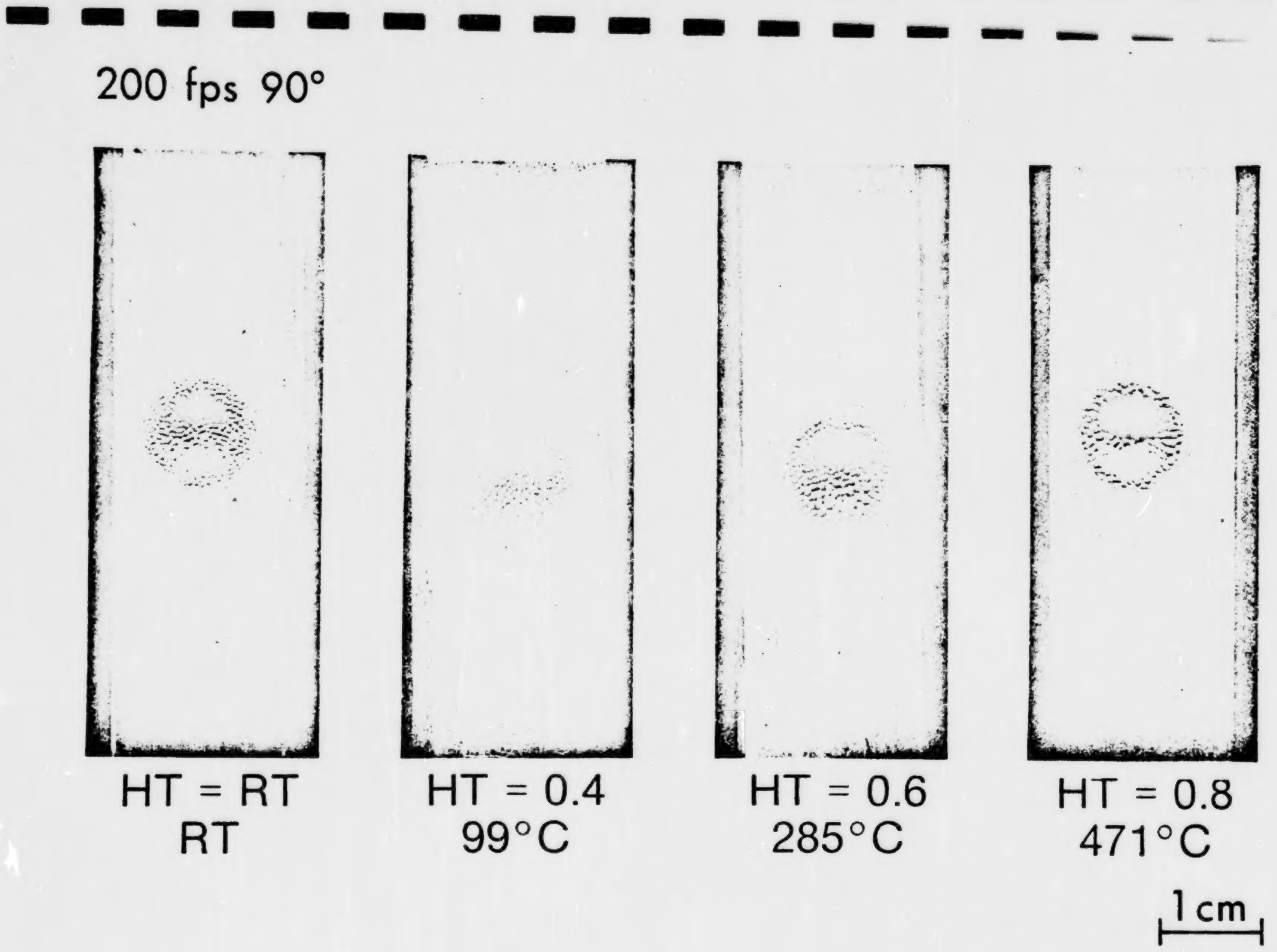
200 fps 90°
HT = RT
RT
HT = 0.4
99°C
HT = 0.6
285°C
HT = 0.8
471°C
1 cm

FIG. 19

XBB 784-4453

C. Microstructures of eroded specimens

Cross sections of eroded specimens tested at 0.6 homologous temperature (285°C) show the type of deformation that occurs in the surface layers. Figs. 20-22 show the condition of the surface at 30°, 60° and 90° impingement angles for the 100 fps test series. The general behavior of the alloy was the same for both velocities. In Fig. 20 it can be seen that at 30°, the ripples are formed by material that has been raised over the original metal surface by multiple impacts leaving porous, cracked areas on the downstream side. The darker areas near the surface are pieces of SiC that have broken off the eroding particles and become embedded in the severely deformed metal. The dark particles beneath the eroded area are particles of polishing compound that were taken up in the soft aluminum.

At an impingement angle of 60° (Fig 21) the structure is an extension of the 30° angle test mechanism but moguls instead of ripples have formed. The downstream side of each raised area appears to have entrapped more pieces of SiC than in the 30° tests and the cracked area indicates somewhat greater porosity. At 90° (Fig. 22) the same characteristic entrappment of SiC particles has occurred and the surface is more generally porous, indicating severe deformation to have occurred during erosion. At 90° there is no evidence of the downstream cracks extending in under the raised areas as occurred at the shallower angles.

Scanning electron microscope photos of the surface of the eroded material at shallow impingement angles where ripples form and steep impingement angles where moguls form are shown in Figs. 23 and 24, respectively. The occurrence of multitudinous individual particle impact craters over the eroded surfaces can be seen. No particular mechanism indicating micro-structure effects at these and higher magnifications were observed.

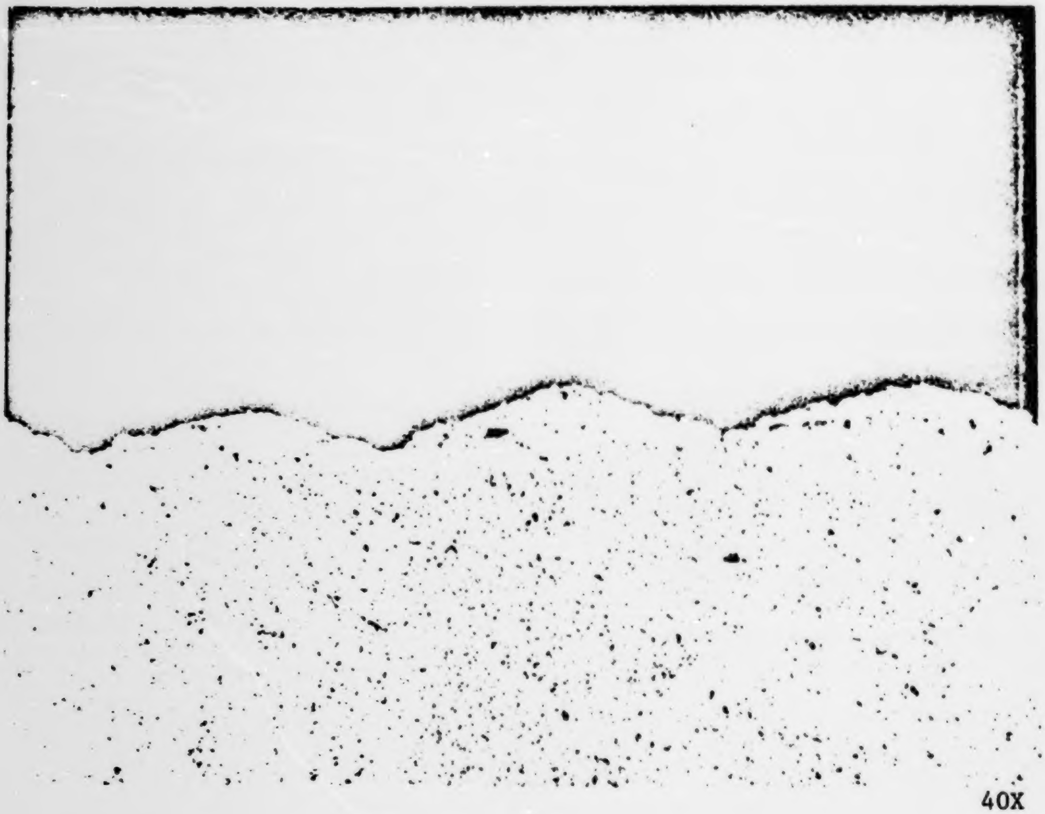

FIG. 20 0.6 HT (285°C) 100 fps, 30°

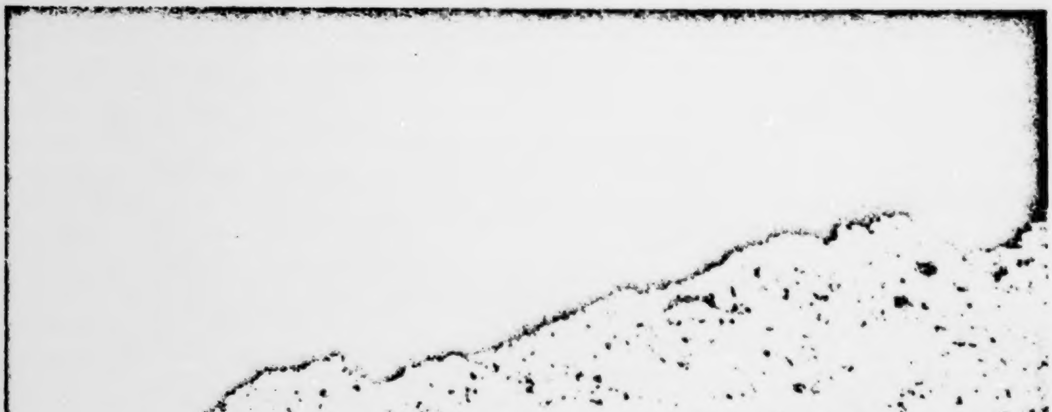

XBB 784 4581

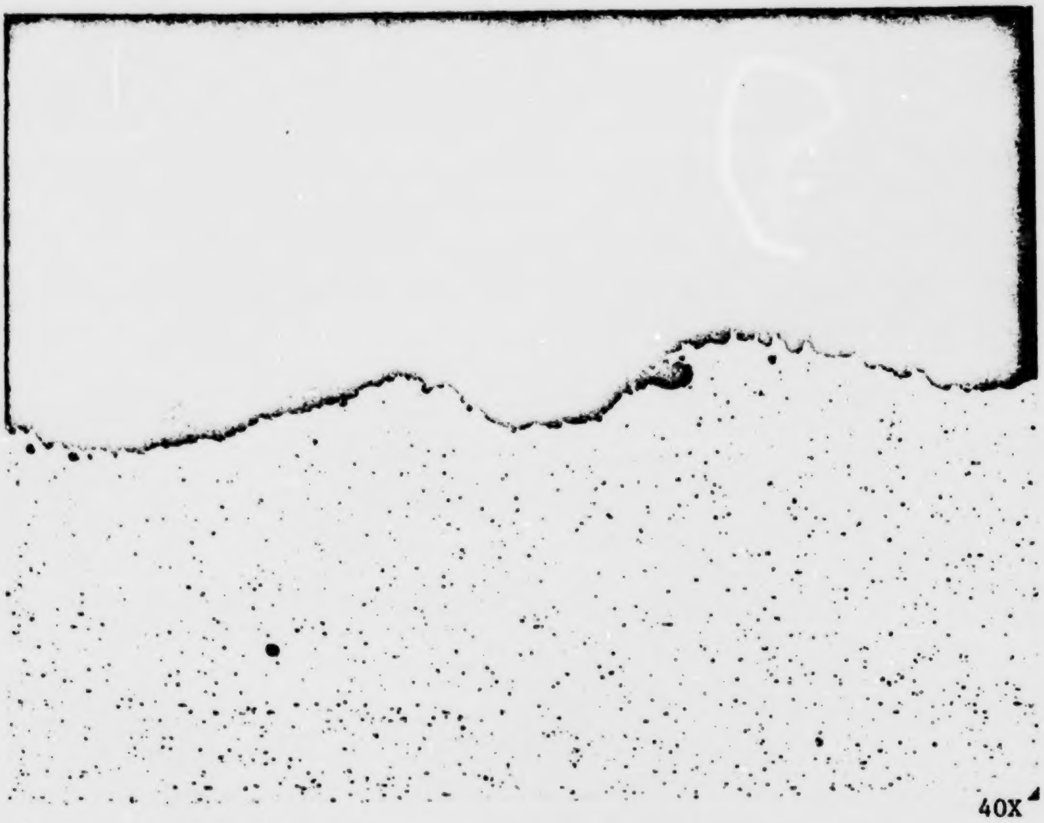

FIG. 21. 0.6 HT (285°C) 100 fps. 60°

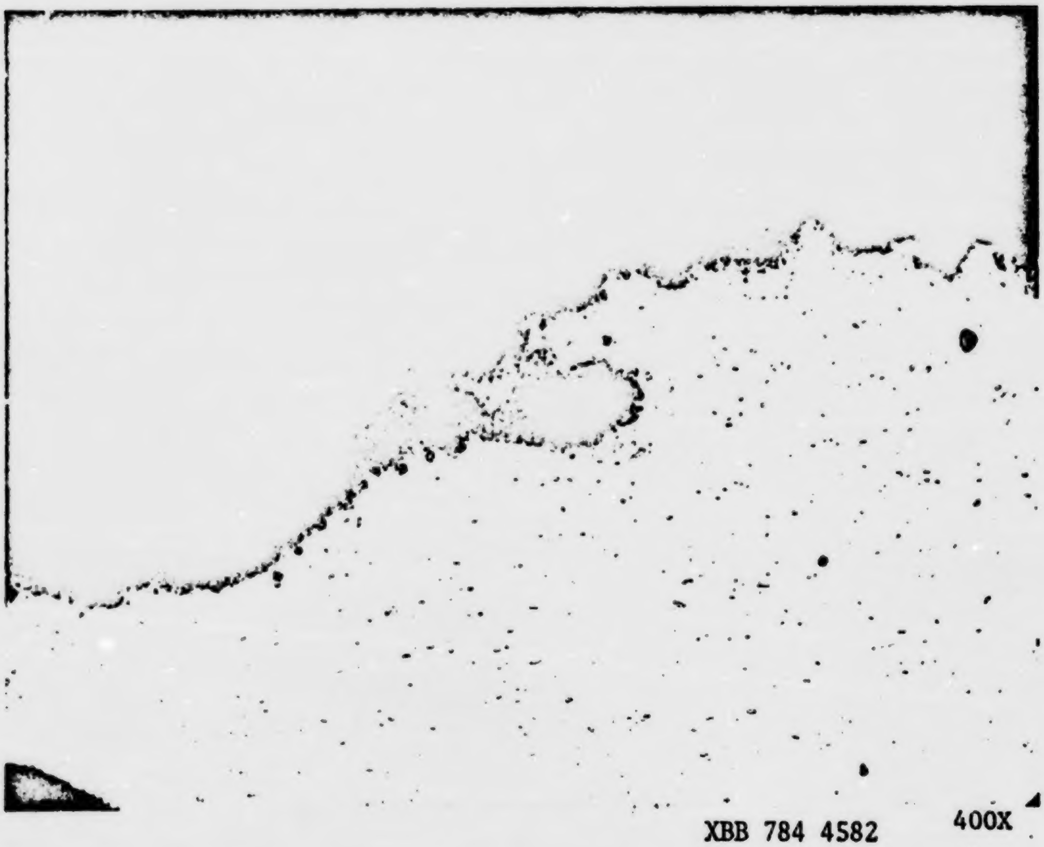

XBB 784 4582

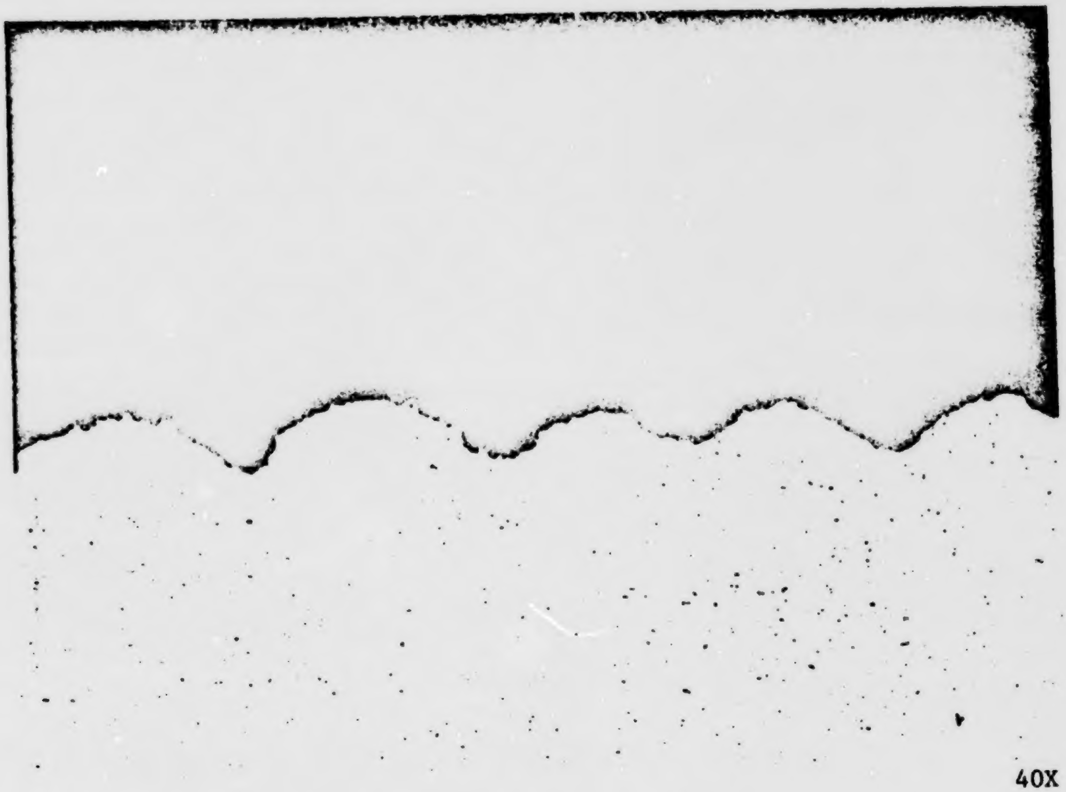

40X

FIG. 22. 0.6 HT (285°C) 100 fps, 90°

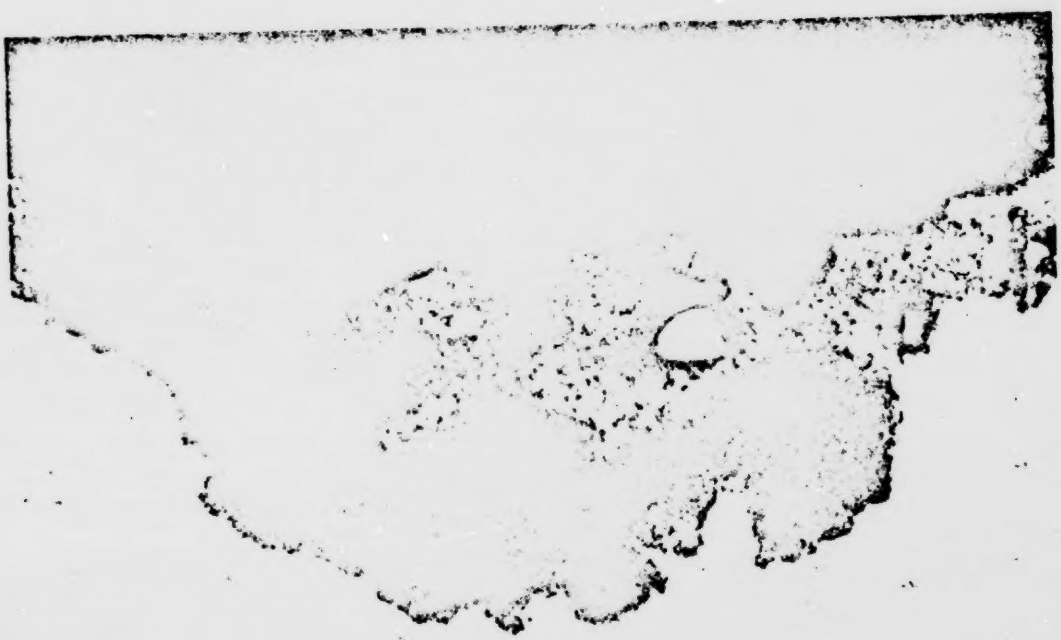

XBB 784-4580

400X

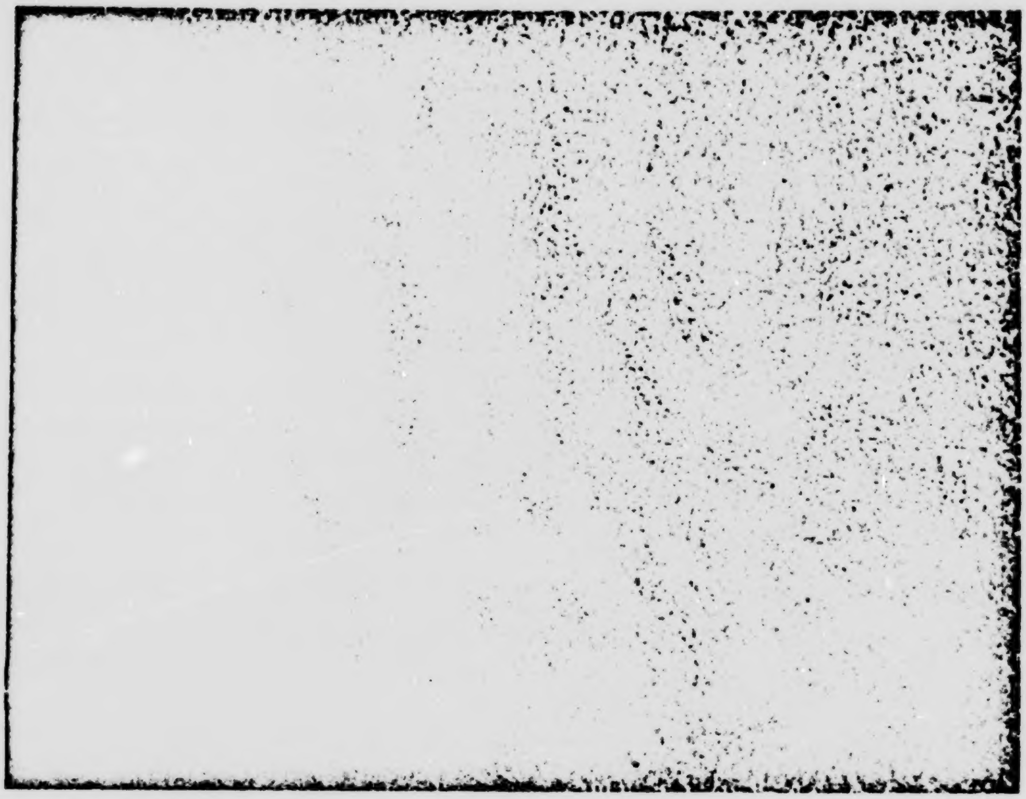

12.3X

FIG. 23. SEM, 100 fps, Room Temperature, 30°

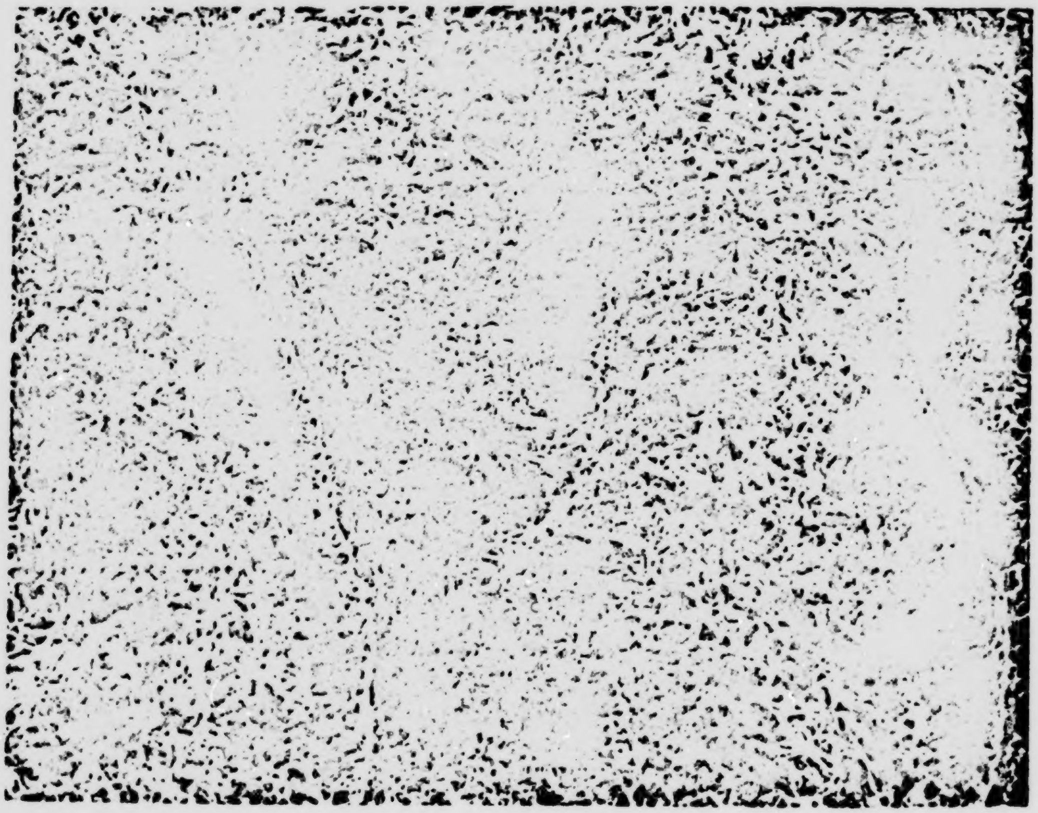

XBB 784-4579

50X

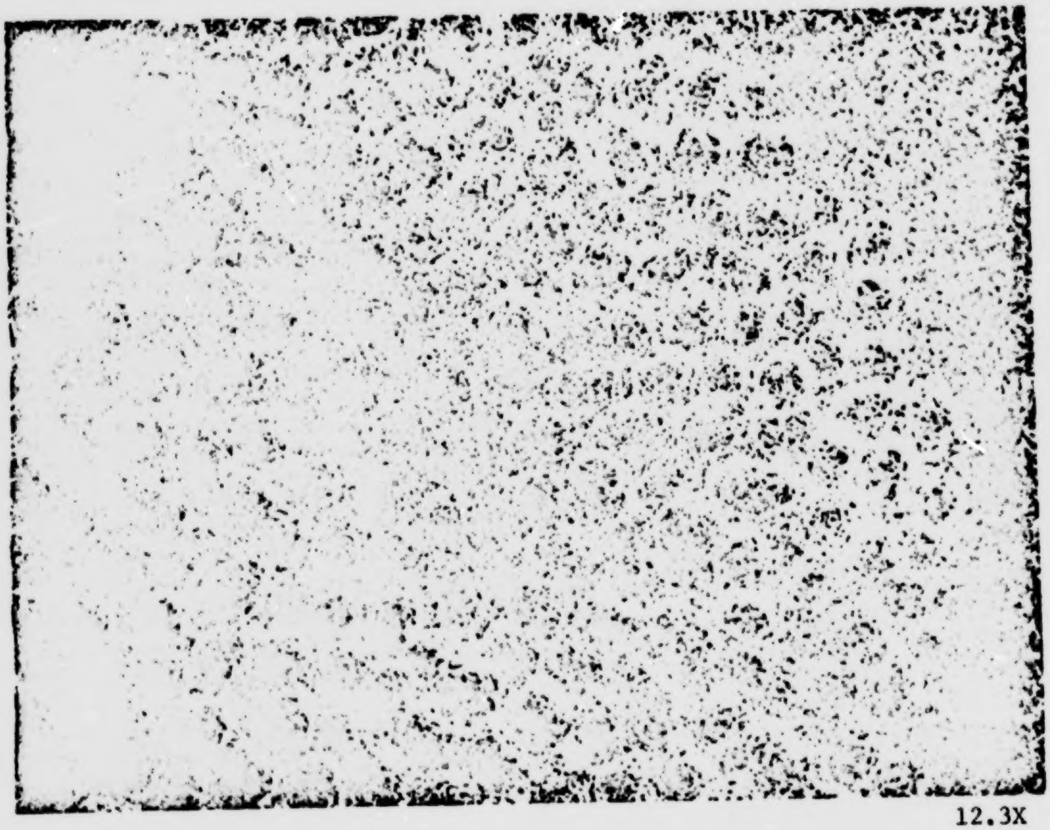

12.3X

FIG. 24. SEM, 100 fps 285°C, 90°

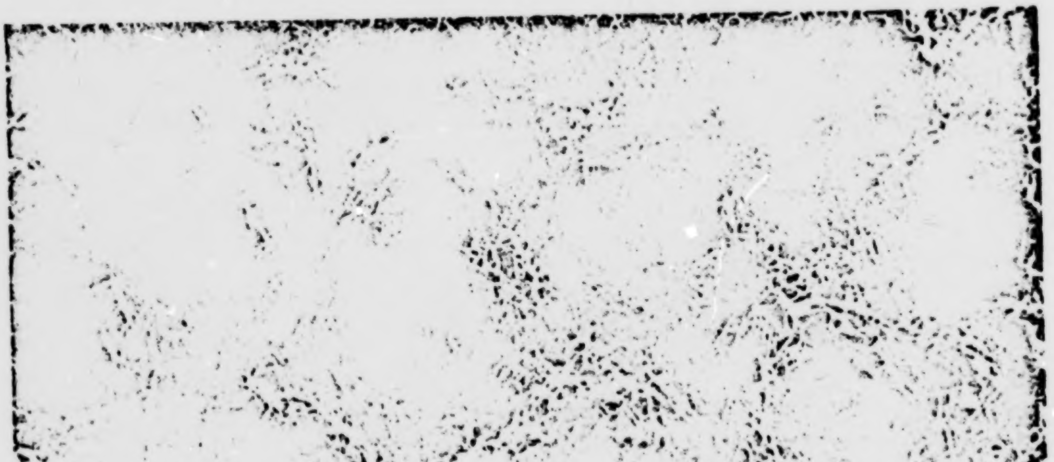

XBB 784-4578

50X

VI. CONCLUSIONS

1. The increase in erosion rate of a face centered cubic metal, 1100-0 aluminum at temperatures to 0.8 homologous temperature (471°C) does not exceed twice its room temperature rate at all angles of impingement in spite of the fact that the tensile strength decreases by a factor of 3.25. The flow stress term in the micro-machining model of low angle impingement erosion at room temperature must be reconsidered for elevated temperature erosion.

2. At low impingement angles and a velocity of 100 fps, the erosion rate decreases with increasing temperature to 0.6 HT. At 200 fps, the erosion rate increases with increasing temperature.

3. The effect of angle of impingement on erosion rate is markedly decreased at homologous temperatures near 0.8. At lower elevated temperatures the typical erosion rate Vs. angle of impingement curve with a peak rate around 15° occurs.

4. The slope of the curve of impingement angle Vs. erosion rate for 0.8 HT is approximately 1/2 that of the curves for lower temperatures, indicating that a different loss mechanism may be predominant at the highest temperature.

5. A pattern of ripples forms on the surface of the metal at the lower impingement angles (10°, 15°, 30°) and a pattern of moguls (alternating depressions and mounds) occurs at the high impingement angles (60°, 90°).

6. The surface of the eroded material is severely distorted as evidenced by particles of erodent material being embedded in the surface several microns below the final surface. Cracks or void areas leading in

from the final surface on the downstream side of the particle flow occur beneath some of the ripples indicating flow of the rippled material over the surface. Propagation of these cracks completely separating a segment of ripple could be a mechanism of material loss in addition to losses by a micro-machining mechanism.

REFERENCES

1. I. Finnie, Erosion by Solid Particles in a Fluid Stream, Symposium on Erosion and Cavitation, Special Technical Publication No. 307 for A.S.T.M. (1961) 70.
2. J. Bitter, A Study of Erosion Phenomena, Part One, Wear, 6 (1963) 5.
3. J. Bitter, A Study of Erosion Phenomena, Part Two, Wear, 6 (1963) 169.
4. J. Neilson, A. Gilchrist, Erosion by a Stream of Solid Particles, Wear, 11 (1968) 111.
5. G. Tilly and W. Sage, The Interaction of Particle and Material Behavior in Erosion Processes, Wear, 16 (1970) 447.
6. I. Hutchings and R. Winter, Particle Erosion of Ductile Metals: A Mechanism of Material Removal, Wear, 27 (1974) 121.
7. .A. W. Ruff and L. K. Ives, Measurement of Solid Particle Velocity in Erosive Wear, Wear received May 5, 1975 (to be published).
8. G. P. Tilly, Erosion Caused by Airborne Particles, Wear, 14 (1969)63-79.
9. C. E. Smeltzer, Mechanisms of Metal Removal by Impacting Dust Particles, Journal of Basic Engineering, Sept. 1970, 639-654.
10. J. A. Pettit, et al., On the Design of Materials for Use Under Erosion/Corrosion Conditions at High Temperatures in Coal Gasification and Coal Combustion Systems. Report #75-200-7107-4, Nov. 15, 1976.
11. J. A. Pettit et al., On the Design of Materials for Use Under Erosion/Corrosion Conditions at High Temperatures in Coal Gasification and Coal Combustion Systems. Report #75-200-7101-4, Feb. 15, 1977.
12. I. G. Wright and R. B. Herchenboede, Design of Materials for Use Under Erosion/Corrosion Conditions at High Temperatures in Coal Gasification and Coal Combustion Systems. Quarterly Letter Report No. 6. on Project No. RP 589-1, April 18, 1977.

TABLE I

Temperature Profile Recorded Inside Nozzle (°C)

Distance From Nozzle Exit (Inches)	Without Gas Flow	$\Delta P=0.9$psi	$\Delta P=3.6$psi
8	1100	1117	960
6	1000	1080	960
4	250	892	894
2	280	740	863
0	75	754	787

TABLE II

Temperature Profile of Gas Stream from Nozzle Exit to Sample Surface (°C)

(No sample or test chamber heating.)

Distance Below Nozzle Exit (Inches)	$\Delta P=0.9$psi	$\Delta P=3.6$psi
just below exit	600	675
1/4	510	621
1/2	422	473
3/4	333	358

TABLE III

Recorded Temperatures for Two Runs (°C)		
Particle Velocity (fps)	100	200
Desired Temperature (°C)	471	471
Impingement Angle	30°	30°
Tapes	195	165
Gas Heater	550	536
Particle Heater	498	515
Particle Heater Cold Zone	286	250
Mixing Chamber Inside	292	305
Mixing Chamber Outside	322	319
Nozzle Heater	473	471
Nozzle Heater Cold Zone	390	394
Tip of Nozzle	471	478
Test Specimen	466	485
Outside of Test Chamber	342	354

TABLE IV - EROSION TEST DATA

Particle Velocity: 100 fps
Test Duration: 30 min.
Eroding Particle: SiC
Particle Size: 250-350 μm

1100-0 Aluminum

Temperature Homo.	Temperature °C	Angle of Impingement (Degrees)	Velocity fps Before	Velocity fps After	Feed Rate gm/min Before	Feed Rate gm/min After	Aluminum Weight Loss mg	$\frac{\Delta Wt.\ Al}{\Delta Wt.\ SiC}$ $x10^{-5}$(gm/gm)
0.32	21	10	106.	104.	35.46	35.36	38.3	3.61
0.32	21	15	109.2	106.	35.33	35.46	38.0	3.58
0.32	21	30	104.	109.2	36.47	35.33	31.2	2.90
0.32	21	60	102.7	104.	36.23	36.47	18.7	7.71
0.32	21	90	106.0	102.7	36.1	36.23	13.5	1.24
0.39	94	10	101.95	106.8	35.36	37.4	33.4	3.06
0.39	92	15	97.5	101.95	35.8	35.36	37.4	3.50
0.40	95	30	97.8	97.5	35.3	35.8	26.3	2.47
0.40	100	60	92.6	97.8	35.76	35.3	16.3	1.53
0.40	103	90	103.8	92.6	36.16	35.76	13.3	1.23
0.59	277	10	101.25	93.1	38.3	35.53	28.0	2.53
0.59	280	15	92.2	101.25	35.63	38.36	33.2	3.00
0.58	270	30	101.2	92.2	35.83	35.63	22.5	2.10
0.60	289	60	89.33	101.2	35.8	35.83	9.5	0.88
0.60	285	90	89.82	89.33	40.73	35.8	15.1	1.32
0.80	471	10	96.2	96.2	38.53	38.1	29.0	2.52
0.80	473	15	96.2	96.1	38.1	36.5	34.1	3.05
0.79	466	30	91.6	115.4	36.5	36.6	31.4	2.86
0.81	476	60	115.4	96.2	36.6	36.77	25.3	2.30
0.80	468	90	96.2	105.0	36.77	36.4	21.4	1.95

TABLE V - EROSION TEST DATA

Particle Velocity: 200 fps
Test Duration: 10 min.

Eroding Particle: SiC
Particle Size: 250-350 μm

1100-0 Aluminum

Temperature		Angle of Impingement (Degrees)	Velocity fps		Feed Rate gm/min		Aluminum Weight Loss mg	$\frac{\Delta \text{Wt. Al}}{\Delta \text{Wt. SiC}}$ $\text{x}10^{-5}$(gm/gm)
Homo.	°C		Before	After	Before	After		
0.32	20	10	196.7	192.0	47.2	48.1	87.8	1.84
0.32	20	15	196.7	196.7	44.6	47.2	85.2	1.86
0.32	20	30	196.7	196.7	46.5	46.6	68.7	1.48
0.32	20	60	196.7	196.7	40.9	46.5	45.0	1.03
0.32	20	90	194.4	194.4	49.16	50.73	41.2	0.82
0.40	99	10	190.6	196.7	57.0	55.23	108.3	1.93
0.39	93	15	189.8	190.6	52.3	57.0	112.9	2.07
0.39	93	30	198.3	189.8	53.0	52.3	92.4	1.75
0.40	101	60	176.7	189.3	54.66	53.0	62.7	1.16
0.41	104	90	188.3	176.7	56.4	53.33	53.4	0.97
0.58	270	10	215.9	198.3	52.9	53.3	129.3	2.44
0.57	260	15	196.7	215.9	65.4	52.9	143.3	2.42
0.58	263	30	198.4	196.7	53.6	65.4	116.4	1.96
0.61	291	60	199.2	198.4	56.9	53.6	80.9	1.46
0.59	280	90	190.6	199.2	61.1	56.9	80.4	1.36
0.79	464	10	206.8	211.3	57.5	55.9	134.3	2.37
0.77	443	15	216.0	206.8	60.2	57.5	144.7	2.46
0.82	485	30	216.0	216.0	57.6	60.2	136.8	2.32
0.82	488	60	216.0	216.0	60.0	57.6	128.5	2.19
0.82	494	90	202.5	216.0	65.1	60.0	126.2	2.02

FIGURE CAPTIONS

1. High Temperature Erosion-Corrosion Test Device
2. Schematic of Test Device
3. Particle Velocity Measurement Device
4. Erosion Rate Vs. Angle of Impingement - 100 fps
5. Patterns of Erosion at 0.32 (RT) at 100 fps
6. Patterns of Erosion at 0.40 (99°C) at 100 fps
7. Patterns of Erosion at 0.6 (285°C) at 100 fps
8. Patterns of Erosion at 0.8 (471°C) at 100 fps
9. Erosion Rate Vs. Angle of Impingement - 200 fps
10. Patterns of Erosion at 0.32 (RT) at 200 fps
11. Patterns of Erosion at 0.40 (99°C) at 200 fps
12. Patterns of Erosion at 0.6 (285°C) at 200 fps
13. Patterns of Erosion at 0.8 (471°C) at 200 fps
14. Erosion Rate vs. Homologous Temperature at 100 fps
15. 15° Impingement Angle at Various Temperatures - 100 fps
16. 90° Impingement Angle at Various Temperatures - 100 fps
17. Erosion Rate vs. Homologous Temperature at 200 fps
18. 15° Impingement Angle at Various Temperatures - 200 fps
19. 90° Impingement Angle at Various Temperatures - 200 fps
20. Surface Condition at 30° Impingement Angle - 100 fps
21. Surface Condition at 60° Impingement Angle - 100 fps
22. Surface Condition at 90° Impingement Angle - 100 fps
23. SEM at Shallow Impingement Angle
24. SEM at Steep Impingement Angle

LBL-12015
Preprint

Lawrence Berkeley Laboratory
UNIVERSITY OF CALIFORNIA

Materials & Molecular Research Division

Submitted to Wear

EROSION OF ELEVATED TEMPERATURE CORROSION SCALES ON METALS

J.A. Maasberg and A.V. Levy

May 1981

Prepared for the U.S. Department of Energy under Contract W-7405-ENG-48

LBL-12015

EROSION OF ELEVATED TEMPERATURE CORROSION SCALES ON METALS

J. A. Maasberg and A. V. Levy

Materials and Molecular Research Division
Lawrence Berkeley Laboratory
University of California
Berkeley, CA 94720

May 1981

This work was supported by the Director, Office of Energy Research, Office of Basic Energy Sciences, Materials Sciences Division of the U.S. Department of Energy under Contract Number W-7405-ENG-48.

EROSION OF ELEVATED TEMPERATURE CORROSION SCALES ON METALS

J. A. Maasberg and A. V. Levy

Materials and Molecular Research Division
Lawrence Berkeley Laboratory
University of California
Berkeley, CA 94720

ABSTRACT

Combined erosion-corrosion poses a considerable problem to the design of long lifetime metallic components in energy conversion systems. To gain some insight into this problem, scales were formed on stainless steel at elevated temperature and subsequently were eroded at room temperature to determine the nature of the erosion rates and the mechanism of scale removal. Thin corrosion scales were formed on 310 stainless steel and an experimental Fe-18Cr-5Al-1Hf alloy at high temperatures (900^0 and 980^0C) in gas mixtures with various levels of oxygen and combined oxygen-sulfur. The corroded specimens were eroded at room temperature in an air-solid particle stream using 50μm SiC at 60 ms^{-1}. The conditions of the corrosive exposures, the rates of erosion of these scales and the microscopic appearance of the eroded surface were correlated to determine the mechanism of thin scale erosion.

INTRODUCTION

The high temperature environments in advanced energy conversion systems, in particular coal gasifiers, have caused the degradation of metallic components due to the combined actions of particle erosion with high temperature corrosion. Protective oxide layers which form at high temperatures are often damaged by rapidly moving particles, thus leaving metals susceptible to further corrosive damage. This investigation determined the dependence of erosion damage on the corrosion conditions, specimen surface conditions, and the structure of the corrosion product scale. In addition, microscopic examination was used to determine the mechanism of erosion of a thin oxide on a metal formed at an elevated temperature and subsequently eroded at room temperature.

Originally investigated by Finnie[1,2], the removal of material from ductile metals by the erosive action of small angular particles was attributed to a different mechanism than material removed from brittle materials. Brittle materials were determined to erode by a microfracturing of the ceramic, whereas ductile metals erode by a plastic deformation mechanism. Figure 1 shows the impingement angle dependence of the erosion rate for typically ductile and brittle materials and clearly differentiates the behavior of each. Erosion of brittle, thin oxide scales formed in-situ on metals which occurs in coal gasifier environments could be classified as occurring in either a ductile or brittle manner. It was necessary to determine which mechanism is active. An understanding of combined erosion-corrosion could be achieved by separating the formation of the scale from its erosive removal. In order to accomplish this, the scale was separately formed on the metal and then eroded.

Work by Zambelli[3] has shown that relatively thick (20-100μm) oxide scales on nickel behave in a brittle manner, undergoing hertzian cup-cone and radial fractures to break up the scale upon impact by particles. He reported that the thinner the scale, the more of a contribution the ductile metal substrate made to the erosion behavior. The thin scales that we investigated were expected to behave more like ductile than brittle materials because they were so thin that it was felt that the ductile substrate would be the governing factor. This work disproved that premise.

EXPERIMENTAL PROCEDURE

The high temperature corrosion of 310 stainless steel (310SS) makes it a much used material in highly corrosive areas of energy conversion systems. Because of this, it was selected for this project to study the combined effects of erosion and corrosion. For comparison, an alumina scale forming experimental Fe-18Cr-5Al-1Hf alloy was included in a few of the tests. Corroding gas mixtures were selected to be representative of conditions encountered in coal gasification systems.

The specimens were alloy coupons approximately 2.54 x 1.90 x 0.318 cm, with a small hole drilled toward one side in order to attach them to the support in the corrosion furnace. The specimens were suspended in various gas mixtures at temperatures of 900° and 980°C for a period of 100 hours in order to develop a continuous surface scale. The following corrodant mixtures were used:

air

$P_{O_2} = 10^{-15}$

$P_{O_2} = 10^{-16.5}$

$P_{O_2} = 10^{-15} + P_{S_2} = 10^{-6}$

$P_{O_2} = 10^{-15} + P_{S_2} = 10^{-8.5}$

$P_{O_2} = 10^{-16.9} + P_{S_2} = 10^{-6}$

$P_{O_2} = 10^{-17.4} + P_{S_2} = 10^{-7}$

They were made by mixing H_2, H_2S, H_2O and argon in the test furnace.

The gas compositions were selected to represent the wide range of conditions that could occur in coal gasifiers forming different types of scales. For example, oxidizing the 310SS in air results in an oxide scale whose morphology and, hence, erosion behavior should differ from an oxide scale formed at an oxygen partial pressure of 10^{-15} atmos. In the combined oxidation-sulfidation tests, partial pressure combinations were selected based on the thermodynamic equilibrium stability diagrams that would result in a protective oxide and no sulfide, mixtures near the oxide-sulfide formation dividing line and a mixture in the sulfide forming region of the stability diagram. In order to determine whether an oxide scale that had formed not in competition with sulfur could provide erosion protection after a subsequent exposure to combined oxygen and sulfur, some pre-oxidized specimens were prepared. Burnished and as-received specimen surface conditions were studied.

Erosion testing was performed at room temperature on previously formed corrosion scales. The air-blast erosion tester is illustrated in figure 2. 50μm size SiC particles carried by air at 60 ms^{-1} were used to erode away the scales on the test coupons without eroding the base metal. The weight loss of the specimens was measured intermittently during erosion and the resulting weight losses were compared to determine the erosion behavior. Generally, the weight loss after 0.3g of SiC indicated the steady state erosion rate of the scale. The metal substrate was reached after eroding with 0.3g to 1.0g of SiC. The threshold period of no erosion of the metal substrate was completed only after 3-5g of erodent was used. Since no weight loss due to erosion occurred on an unoxidized 310SS specimen after erosion by 1g of erodent, the weight loss on the corroded specimens is due entirely from the scale. Figure 3 shows a before-after cross section of an oxidized 310SS specimen eroded with 1.2g of SiC. Note that the scale was removed, yet the metal substrate was unaffected.

Microstructural examinations of the specimens were performed by cross sectioning with a diamond saw and mounting them in bakelite, using Klarmount about the face of the specimen in order to avoid rounding off the scale edge. Cross sections were ground on abrasive paper to 600 grit, polished with 5 and 1 m cerium oxide polishing compound. Analysis of the corrosion scale was performed by optical microscopy, scanning electron microscopy with x-ray fluorescence analysis, and x-ray powder diffraction.

Results

Figure 4 shows the 310SS specimens after the elevated temperature corrosion had occurred yet prior to erosion testing of the scales that had formed. The scales were generally continuous; only those exposed to the $P_{O_2} = 10^{-16.9} + P_{S_2} = 10^{-6}$ gas mixture formed a visible sulfide formation on the surface. No distinct areas of sulfide could be found, microscopically or analytically, on any of the other specimens that were exposed to sulfur bearing gases. The specimens with the visible sulfide formations were not erosion tested. Figure 5 shows a typical specimen after being eroded. The removal of the thin, 3-6 m, scale by the eroding particles impacting at 90° caused a circular lightened area to occur on the specimen. Weight losses measured were generally near a milligram.

Scales in Oxidizing Atmospheres

Table 1 presents the results of the erosion tests on the oxidized 310SS specimens. It can be seen that increasing the oxidation temperature from 900°C (1650°F) to 980°C (1800°F) increased the thickness of the scale formed in air from 2.5μm to 15μm. The thinner scale eroded at a lower rate, 0.003g/g erodent. This follows the trend found by Zambelli[3] where thinner scales on metal substrates erode at a lower rate than thicker scales.

The erosion that occurred on the scale formed at the low P_{O_2} was less than that formed in air. The erosion that occurred at a 90° impingement angle was more than that which occurred at a 30° impingement angle, indicating that the scale eroded like a brittle material even though it was very thin and was on a ductile metal substrate. No apparent difference in erosion behavior resulted from burnishing the specimens prior to oxidizing them. It is known that burnishing does extend the straight oxidation resistant life of specimens not subsequently exposed to an eroding environment.[4] No difference in erosion behavior was measured for specimens oxidized at the two different low oxygen partial pressures used.

The amount of erosion only approximately doubled after four times the amount of particles had been used, 0.3g compared to 1.2g of erodent. This indicates that the amount of erosion per unit of particles decreased with increasing erosion. Figure 6 shows this more clearly. The curve plots material loss for each subsequent 0.1gm of eroding SiC particles. The higher initial slope of the curves indicates a high rate of erosion; when the curves become straight, a steady state erosion condition has been reached where each 0.1g of particles causes the removal of the same weight of target scale. When the lower curves become flat, all of the scale has been removed.

Since the threshold period for the initiation of erosion in the ductile metal substrate is approximately 5g of material[3], no metal was observed to be removed in these tests. Figure 3 shows this; the internal oxidation just below the scale-metal interface is intact in the eroded specimen, indicating that only the Cr_2O_3 scale in the upper photo was removed in the erosion process.

Figure 6 compares the erosion behavior of air oxidized and low P_{O_2} oxidized 310SS and the erosion of an alumina scale which was formed on an experimental FeCrAlHf alloy. The low P_{O_2} atmosphere developed a much more erosion resistant scale that averaged 4μm thick. The air oxidized specimen lost more total weight than the low P_{O_2} formed scale because it had a thicker scale to start with. Comparing the early portions of the erosion of each scale, up to 0.4g of particles, shows a much higher rate of loss of the air oxidized scale. The difference in morphology that accounts for this behavior is still under investigation. There was no apparent difference in the erosion behavior of scales formed at two different, low P_{O_2} levels.

The erosion rate of the alumina scale was significantly less than that of the chromia scale, as shown in figure 6. Figure 7 shows the cross section of the chromia and alumina scales. The dark colored internal oxides below the chromia scale are SiO_2. They form a discontinuity at the scale-metal interface that reduces the erosion resistance of the scale by deteriorating the bond between the scale and the metal substrate. The alumina scale, by comparison, has no alternate oxide at the scale-metal interface. The alumina scale continues into the base metal in the form of pegs or fingers of alumina, markedly improving the bond between the scale and substrate. This structure is promoted by the presence of the hafnium in the alloy and is known to also enhance the corrosion resistance of the alloy.[5]

Scales in Oxidizing-Sulfidizing Atmospheres

The scales formed in the presence of both oxygen and sulfur that were erosion tested had no discernible sulfides in them as determined by energy dispersive x-ray analysis in the scanning electron microscope (SEM), and by powder x-ray diffraction. However, their formation in the presence of sulfur did reduce their erosion resistance to a level below that of straight oxidized scale. Figure 8 shows the effect of combined oxidation-sulfidation on the chromia scale and figure 9 shows the effect on the alumina scale. The attempt to form a more erosion resistant scale on the 310SS by first forming an oxide of Cr_2O_3 that was not in competition with sulfur and subsequently exposing the specimen to a combined oxidizing-sulfidizing atmosphere had some success, as can be seen by the pre-oxidized curve in figure 8.

The greater erosion resistance of the alumina scale formed in a straight oxidizing atmosphere compared to that formed in a combined oxidizing atmosphere, shown graphically in figure 9, can be related to the scales' microstructures in figure 10. The reduction in the amount of pegging shown in the lower photo, the oxidized-sulfidized specimen, reduces the bond between the scale and the substrate and the erosion increases. It was observed that no difference in erosion rate occurred as the result of differences in the particle impingement angle between 30^o and 90^o. A decided difference was measured in straight oxidized specimens (see Table 1).

The increased erosion rate of the 2.5-5μm thick chromia scale that was formed in the presence of sulfur compared to a straight oxidized chromia, as shown in figure 8, can be at least partially related to observed differences in their microstructure. The thickness of both of the scales was essentially the same and did not contribute to the difference observed in their erosion behavior. Figure 11 shows that an almost continuous SiO_2 scale formed along the scale-metal interface of the oxidized-sulfidized specimen while only near perpendicular fingers of SiO_2 formed in the straight oxidized 310SS. The resulting deterioration of the oxidized-sulfidized scale-metal interface increased the erosion role of the scale. Figure 12 is a sketch of how the morphology of the scale-metal interface affected the erosion behavior of the scales. The first picture represents the pegging type of structure found in the straight oxidized alumina scale. The second and third figures depict the straight oxidized chromia scale and the fourth figure represents the combined oxidized-sulfidized chromia scale.

The effect of pre-oxidizing the 310SS on the scale-metal interface morphology is shown in figure 13. The primary difference is the morphology of the SiO_2 internal oxides. By pre-oxidizing, the SiO_2 that forms essentially parallel to the scale-metal interface is almost eliminated, with a consequent improvement in the erosion resistance.

Mechanism of Erosion

In order to determine the mechanism by which the thin scales eroded, the technique of sequential erosion used in the investigation of the erosion of NiO scales formed on nickel[3] was used. After each few particles had impacted the surface, the specimen was removed from the erosion tester and the eroded surface observed in the SEM. Figure 14 shows the scale surface after a few particle impacts had occurred in the area under observation. The small crystallite surfaces have not yet been impacted. The darker appearing areas representing less than 50% of the total area shown have received at least one SiC particle impact. Figure 15 shows one of the impacted areas at a higher magnification. In the left center of the photo some smeared crystallites can be seen, indicating that plastic deformation of the immediate scale surface had occurred. The flat areas at different planes to one another indicate that cracks had formed at various angles but near parallel to the plane of the scale and pieces of scale had been chipped out. Even though the scale is only approximately 4μm thick, the cracks that resulted in chip removal occurred in the scale above the scale-metal interface. The remaining material in the chipped areas is Cr_2O_3 and not base metal.

DISCUSSION

The principal finding of this investigation is that both the chromia and alumina scales formed in-situ on aluminum and/or chromium containing alloys behave in a brittle manner when eroded, even though they were as thin as 2.5μm and were generally intimately bonded to the ductile metal substrate. They behaved as other ceramic materials do in gas-solid particle erosion environments, losing material in sequentially removed layers of scale by a cracking and chipping mechanism. While the scale-metal interface appeared to play an important role in determining the erosion rate with greater bonding resulting in lower erosion rates, the scale was not removed by separation at the scale-metal interface. Also, the scale of the straight oxidized specimen eroded at higher rates at an impingement angle of 90° than at 30°. This behavior is typical of brittle materials. The difference in the amount of erosion as a function of impact angle was not observed in the scales formed in oxidizing-sulfidizing atmospheres. This anomaly indicates that the weakened scale formed in the presence of sulfur may be eroding at such a high rate as to not provide effective crack resistance at shallow impingement angles where the crack formation stresses are not as great as those which occur nearer 90° impingement angles.

The behavior of the thin, brittle scale formed in-situ on the ductile substrate was much more independent of the substrate than had been expected. It was initially thought that the erosion behavior of the thin scale would be modified by the ductile nature of the substrate because of the trend of thinner scale having a lower erosion rate in the work of Zambelli.[3] The thicker (.015μm) chromia scale formed in air eroded at a rate 3 times faster than the thinner (2.5μm) chromia scale formed in a low P_{O_2} gas atmosphere. This indicates that some degree of transfer of the particle impact stresses into the substrate had occurred. The somewhat more porous morphology of the air oxidized specimens may also have contributed to the difference. However, both scales eroded at rates representative of brittle materials rather than ductile ones. This implies that chromia and alumina scales on alloys will undergo rapid erosion when they form in a combined erosion-corrosion environment.

The erosion resistance of the scales depended to a strong degree on the conditions under which the scales were formed. Oxides formed more slowly at low partial pressures of oxygen eroded much more slowly than those that were formed in air. While it was not possible to discern any significant difference in the morphology or composition of the scales to account for this difference, a recent work by Kofstad and Tillerad[6,7] may shed some light on the differences. They found that chromium oxide formed on pure chromium at 1000°C had fewer cracks when formed at low P_{O_2} than when formed in air. They also found that the low P_{O_2} formed oxide had large, sintered grains of higher integrity near the scale-metal interface and small, more porous grain structure at the gas-scale interface. The smaller, more porous grain structure that formed in air could be more susceptible to erosion, based on Zambelli's work on NiO.[3] In Zambelli's work, the porous scale formed below the higher integrity larger grains, but the higher erosion rate occurred in the small grain, more porous structure. Also the presence of more erosion resistant Cr_2O_3 grains near the scale-metal interface compared to the more porous grains further out in the scale could account for the curves of erosion vs. amount of particles showing a decreasing amount of erosion with increasing amounts of particles.

It was also determined by Kofstad that the ability of the scale to deform plastically goes up significantly as the P_{O_2} decreases. This could also have improved the erosion resistance of the scale formed at low P_{O_2}. While Kofstad's work was done with pure Cr and this work with 310SS, the physical behavior of the Cr_2O_3 appears to be similar. More work is necessary to verify this.

Kofstad also observed that the Cr_2O_3 scale buckled as it grew laterally as well as in the thickness direction, causing void areas to appear midway in the scale. These blisters would present a preferred target to the eroding particles, accounting for the initial areas of erosion. Also, increased Cr transfer across the void area could take place because of the high CrO vapor pressure that occurs near 1000°C. This could cause an enrichment in the iron content of the scale beneath each buckled blister which would account for the iron enriched areas observed in the areas beneath the initial eroded blisters in the sequential erosion of the scale on the 310SS.

The temperature at which the scale formed, 900°C and 980°C, also appeared to have a significant effect on the erosion behavior of the scale. Thus, the nucleation and growth mechanism as well as the scale growth rate affects the erosion rate of the scale.

The presence of sulfur in the corroding gas markedly decreased the erosion resistance of the resulting scale to below that of the straight oxygen produced scale even though no direct evidence of sulfur was found in the scale. This indicates that the morphology of the scale is subtley modified in combined erosion-corrosion.

In work by Yurek[8] on the combined oxidation-sulfidation of pure Cr he observed that at a $P_{O_2} = 10^{-10}$ atmos nucleii of chromium sulfide formed on the scale-metal interface while no sulfide formed in the scale. The reduction in the integrity of the scale-metal interface of the 310SS by the same or a similar mechanism may have increased the erosion rate of the oxidized-sulfidized specimens. Specimens from the corrosion conditions that produced visible sulfide scale nodules on the surface were not eroded because of the obvious loss of surface integrity.

The relation between the composition and morphology of the scale-metal interface and the erosion rate of the scales tested was unexpected. The degree and orientation of internally oxidized SiO_2 near the scale-metal interface most directly related to the erosion rate of the scale. It was not determined why the large amounts of parallel to the interface oriented SiO_2 occurred in the combined oxidized-sulfidized specimens compared to the lower quantity and perpendicular to the interface orientation of the SiO_2 formed in the straight oxidized specimens. However, the effect of the difference on the erosion behavior of the chromia scale was marked.

The SiO_2 became an interface contaminant that may have blocked effective transfer of particle impact deformation stresses from the scale to the substrate. Such an occurrence would increase the force effect of the particles on the scale, enhancing their ability to crack the scale. The SiO_2 did not appear to directly reduce the adherence of the scale which could result in the pieces of scale that were removed leaving from the scale-metal interface in full scale thickness pieces. The scale was removed by sequential removal of layered chips of scale.

The difference in the erosion rates of the chromia and alumina scales appears to be related to at least three factors. The basic strength of the alumina was greater than that of the chromia in erosion type loading. The absence of a contaminant like the SiO_2 in the chromia scale specimens and the pegs of alumina extending into the substrate are the other two factors involved; they improved the scale-metal interface. Figure 12 shows the relationship between scale-metal interface morphology and erosion behavior graphically. The reason why such a relationship exists when erosion did not take place from the interface can only be speculated at this time.

Preventing the formation of the parallel to the interface contaminant by pre-oxidizing the chromia specimens did improve the erosion resistance of the specimens; this reduces the tendency toward erosion depicted in figure 12. Reducing the pegging of the alumina scale by combined oxidation-sulfidation, compared to straight oxidation reduced the erosion resistance of the alumina scale, which also supports the trend shown in figure 12. In the case of the alumina, the pegging may increase the transfer of stress from the impacted scale to the substrate, thereby increasing the erosion resistance, compared to the chromia scale where parallel SiO_2 decreased the transfer of stress which decreased the erosion resistance.

CONCLUSIONS

1. The thin chromia and alumina scales that form, in-situ, on aluminum and/or chromium containing alloys erode in a brittle manner, losing material by a cracking and chipping mechanism that sequentially moves through the scale thickness. Scale removal did not occur by separation directly from the scale-metal interface.
2. Low P_{O_2} containing gases form more erosion resistant scales than those formed in air.
3. The presence of sulfur in the corroding gases markedly increases the erosion rate of the chromia and alumina scales even though the presence of sulfur in the scales was not measureable.
4. Alumina scales with pegging into the substrate had greater erosion resistance than chromia scales. Greater extent of pegging resulted in greater erosion resistance.
5. The presence of SiO_2 internal oxides at the scale-metal interface of the chromia scales increased the erosion rate of the scale as their quantity and orientation parallel to the scale-metal interface increased.
6. Thinner scales eroded at a lower rate than thicker scales formed in the same air atmosphere indicating that the ductile substrate does absorb some of the kinetic energy of the eroding particles.

ACKNOWLEDGEMENT

We wish to acknowledge and express our appreciation to Professor David Whittle for his valuable discussions and Larry Lapides for his experimental assistance.

This work was supported by the Director, Office of Energy Research, Office of Basic Energy Sciences, Materials Sciences Division of the U.S. Department of Energy under Contract Number W-7405-ENG-48.

References

1. I. Finnie, J. Wolak, Y. Kabil, "Erosion of Metals by Solid Particles", J. of Materials, 2 (3), September 1967.
2. I. Finnie, "Erosion of Surfaces by Solid Particles", Wear, 3 (1960).
3. G. Zambelli, A. Levy, "Particulate Erosion of NiO Scales", Wear, 68 No. 3, p. 305-331, 1981.
4. R. Perkins, "Development of Alloys for Use in Coal Derived Gases"; Proceedings NACE International Conference on High Temperature Corrosion, San Diego, California; March, 1981.
5. D. P. Whittle and J. Stringer, Phil. Transactions, Royal Society London; A295 309 (1979).
6. K. P. Tillerad and P. Kofstad, J. Electrochemical Society, 127 (1980) 2397.
7. P. Kofstad and K. P. Tillerad, ibid, 127 (1980) 2410.
8. M. Labranceh, M. Gomez, G. J. Yurek; "Early Stages of the Oxidation of Chromium in H_2-H_2O-H_2S Gas Mixture"; Proceedings NACE International Conference on High Temperature Corrosion; San Diego, California; March 1981.

TABLE 1

Air Oxidation of 310 S.S.

				90° weight loss after		30° weight loss after	
Surface	°C	Log P_{O_2}	Scale thickness (µm)	0.3g SiC	1.2g SiC	0.3g SiC	1.2g SiC
As Received	900	air	2.5	0.9	1.6	0.6	1.2
	980	air	15	2.7	4.5	2.1	3.9
Burnished	900	air		0.5	1.05		
	980	air		3.4	5.6		

Low P_{O_2} Oxidation of 310 S.S.

	900	-15		0.4	0.7		
As Received	900	-15	4	0.3	0.6	0.1	0.3
	900	-16.5		0.4	0.7		
	980	-16.5		0.4	0.7		

Figures

1. Erosion of ductile and brittle materials vs. impingement angle
2. Schematic of erosion test apparatus
3. Cross section of oxide scale on 310SS before and after erosion
4. Corrosion specimens prior to erosion testing
5. Appearance of eroded specimen
6. Erosion of oxide scales
7. Cross section of chromia and alumina scales
8. Effect of combined oxidation-sulfidation on erosion of chromia scale
9. Effect of combined oxidation-sulfidation on erosion of alumina scale
10. Oxidized and oxidized-sulfidized alumina scale cross sections
11. Oxidized and oxidized-sulfidized chromia scale cross sections
12. Effect of scale-metal interface morphology on erosion behavior
13. Effect of pre-oxidizing 310SS on the scale-metal interface morphology
14. Cr_2O_3 surface after initial particle impacts
15. Higher magnification photo of impacted chromia area

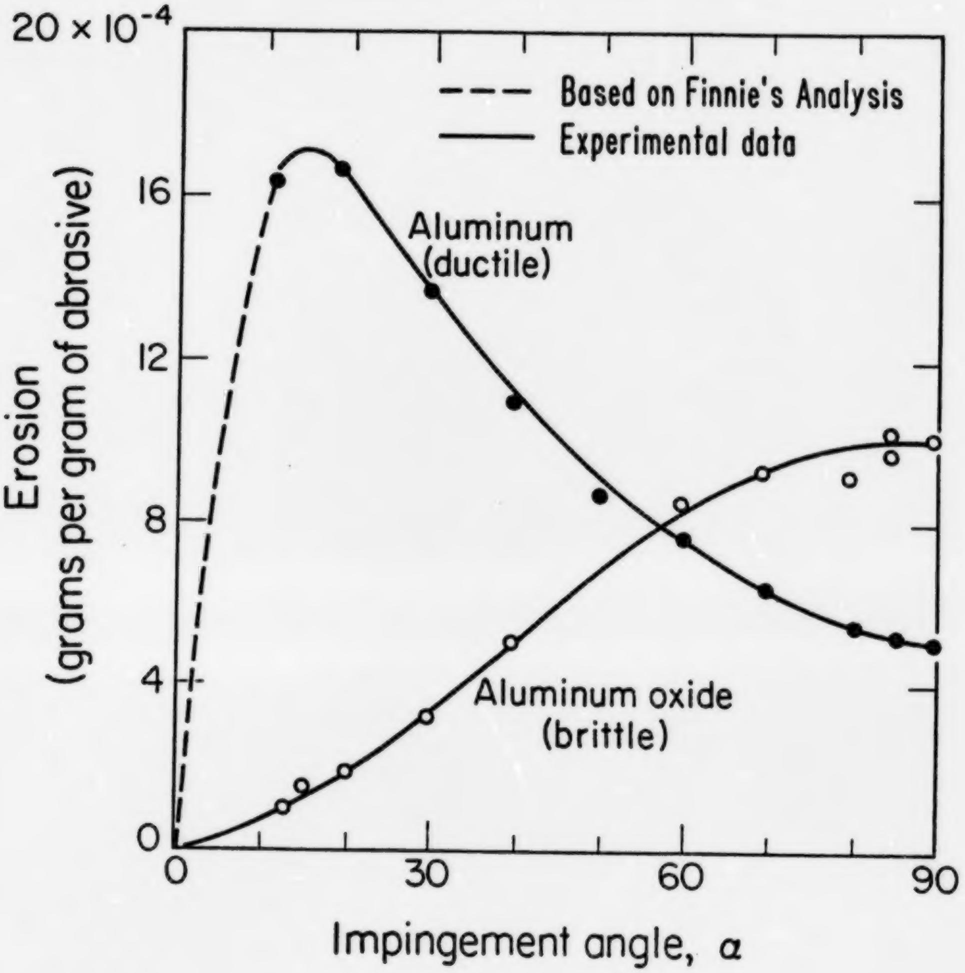

Fig. 1

XBL 793-974

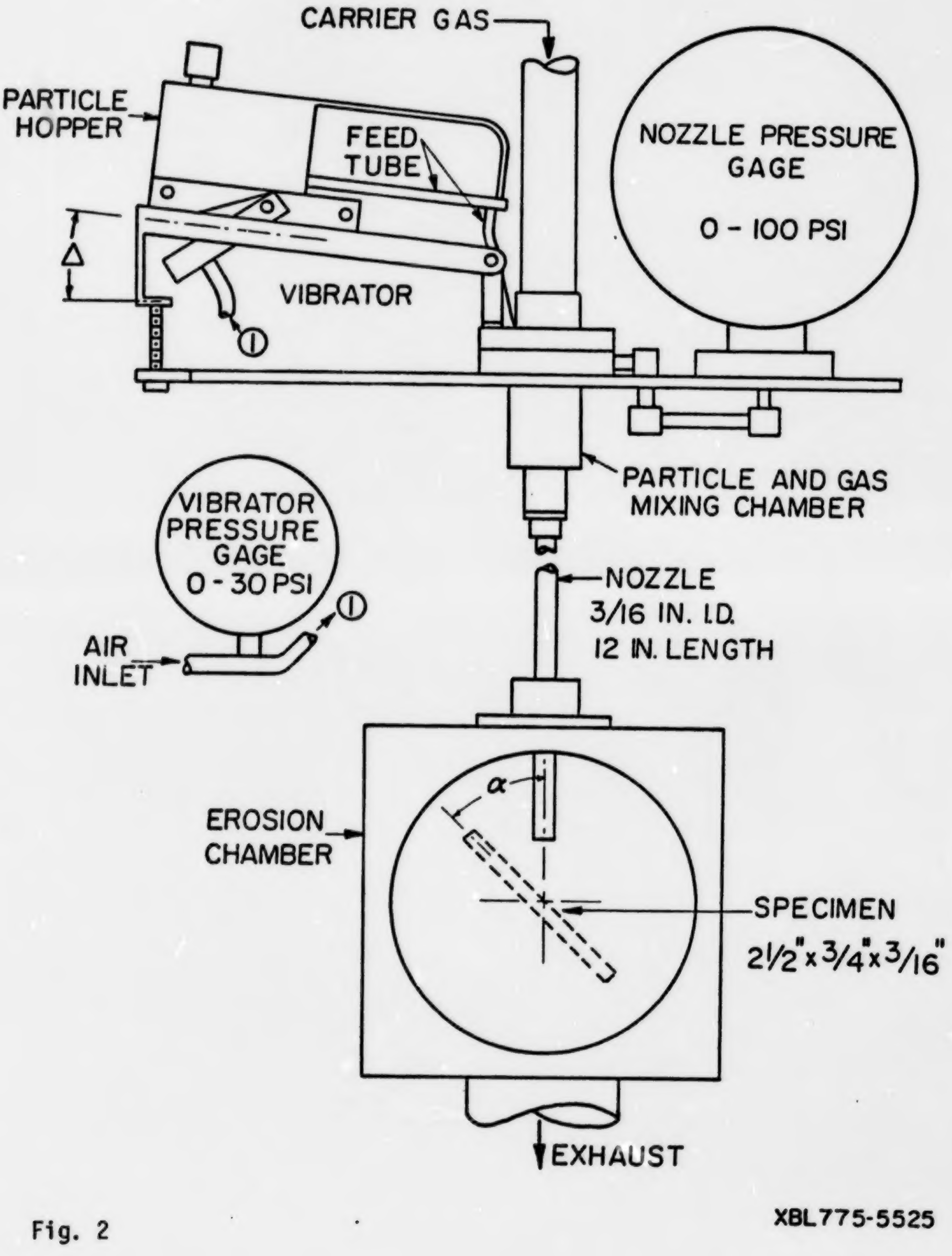
CARRIER GAS
PARTICLE HOPPER
FEED TUBE
NOZZLE PRESSURE GAGE
0 - 100 PSI
Δ
VIBRATOR
①
PARTICLE AND GAS MIXING CHAMBER
VIBRATOR PRESSURE GAGE
0 - 30 PSI
①
AIR INLET
NOZZLE
3/16 IN. I.D.
12 IN. LENGTH
α
EROSION CHAMBER
SPECIMEN
2½"x¾"x3/16"
EXHAUST

Fig. 2

XBL775-5525

Type 310 S.S. Oxidized: Log $P_{O_2} = -15$, 1650°F

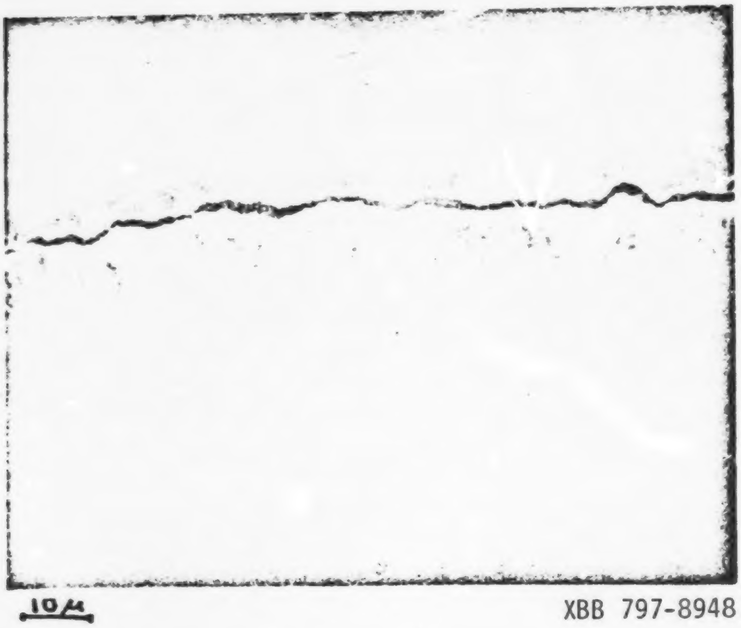

XBB 797-8948

Fig. 3 Type 310 S.S. Oxidized: Log $P_{O_2} = -15$, 1650°F
Eroded: 90° incidence angle

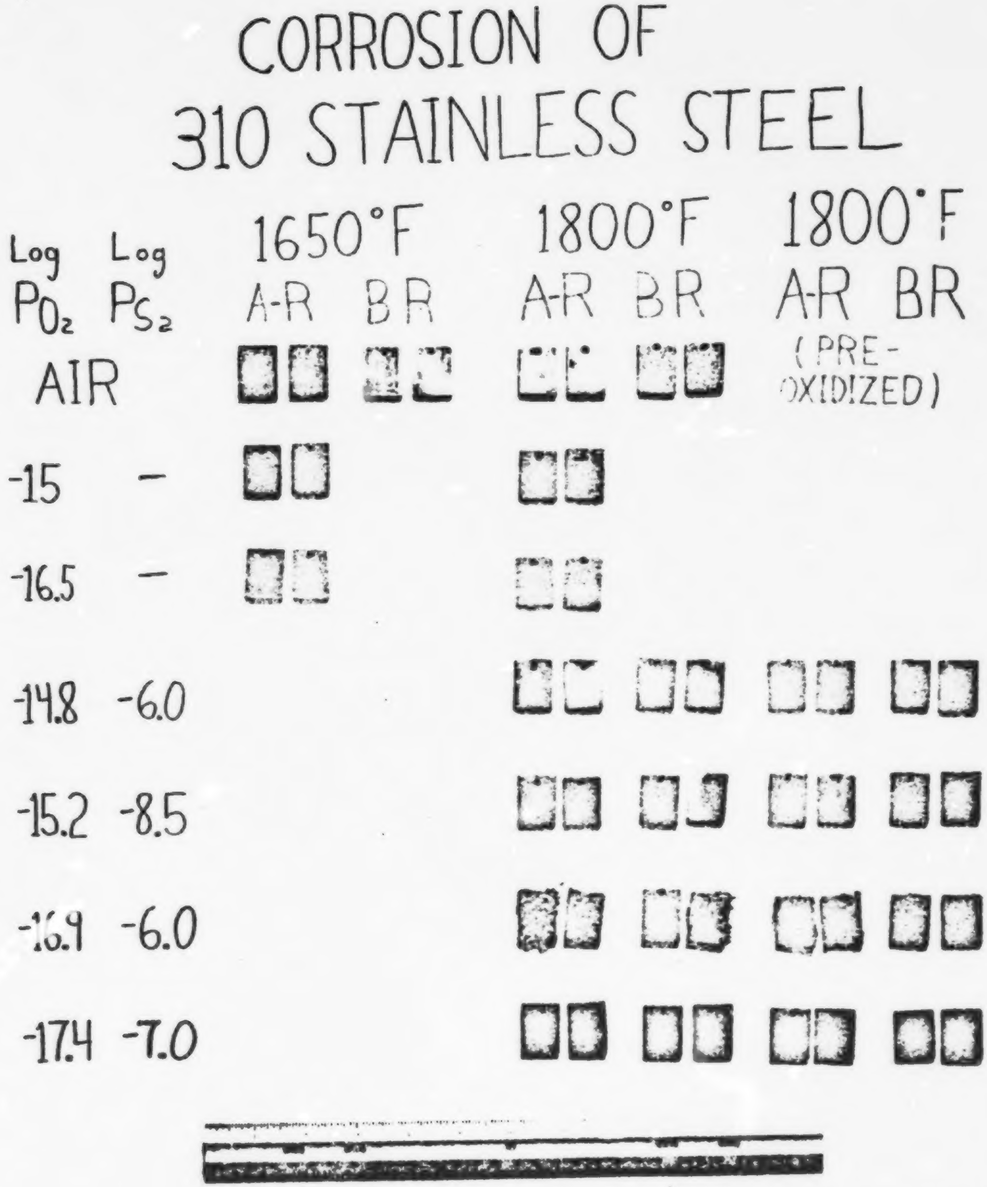
CORROSION OF
310 STAINLESS STEEL
Log P_{O_2}
Log P_{S_2}
1650°F
A-R
B R
1800°F
A-R
B R
1800°F
A-R
BR
(PRE-
OXIDIZED)
AIR
-15
-
-16.5
-
-14.8
-6.0
-15.2
-8.5
-16.9
-6.0
-17.4
-7.0

Fig. 4

CBB 791-349

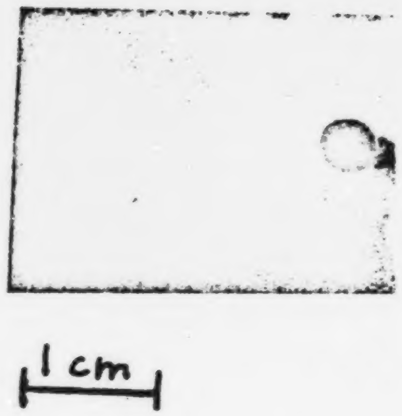

Erosion Specimen: Type 310 S.S.

Preoxidized: Log $P_{O_2} = -15$, 1800°F

Oxidized - Sulfidized: Log $P_{O_2} = -15$, Log $P_{S_2} = -9$, 1800°F

Fig. 5

CBB 797-8941

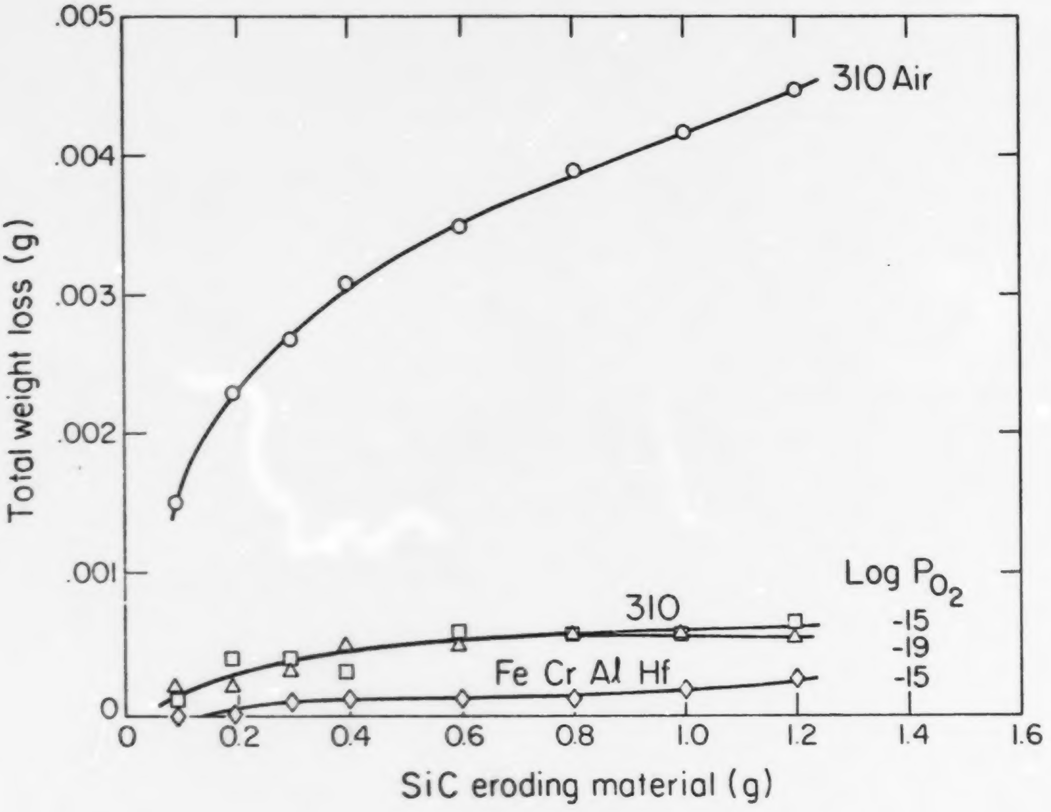

Fig. 6

XBL 793-803

Type 310 S.S. Oxidized: Log P_{O_2} = -15, 1650°F

XBB 797-8943

Fig. 7 Fe 18Cr 5Al 1Hf Oxidized: Log P_{O_2} = -15, 1800°F

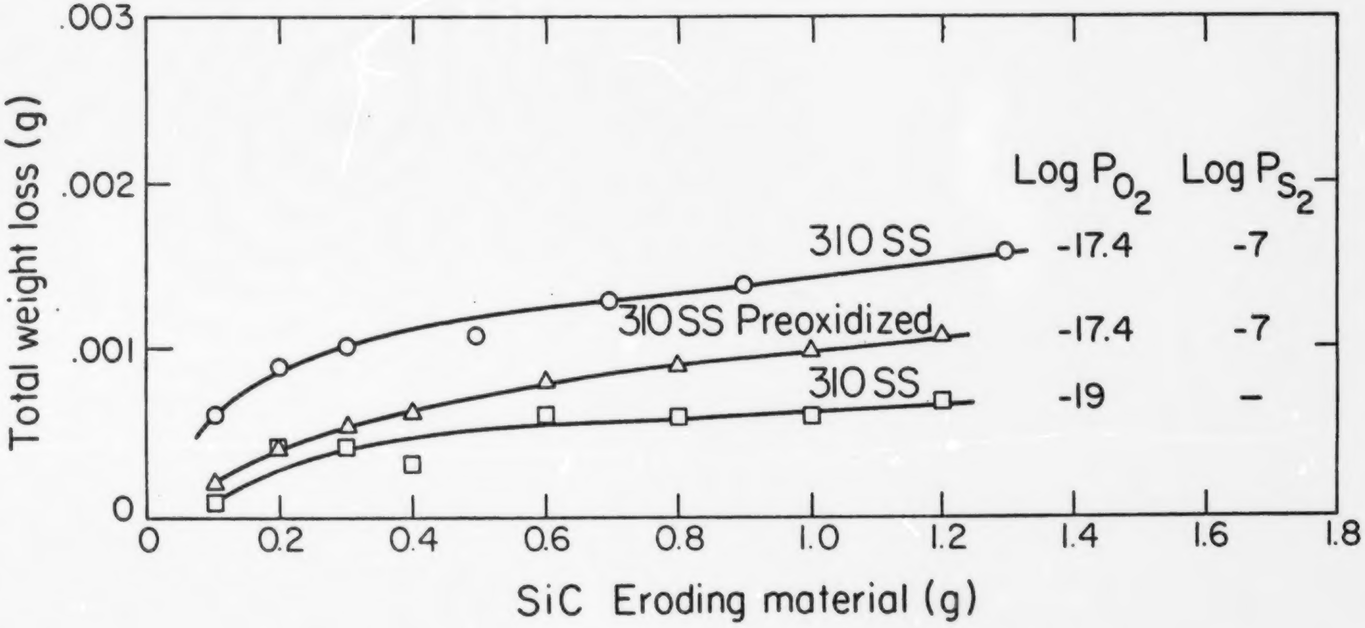

Fig. 8

XBL 793-805

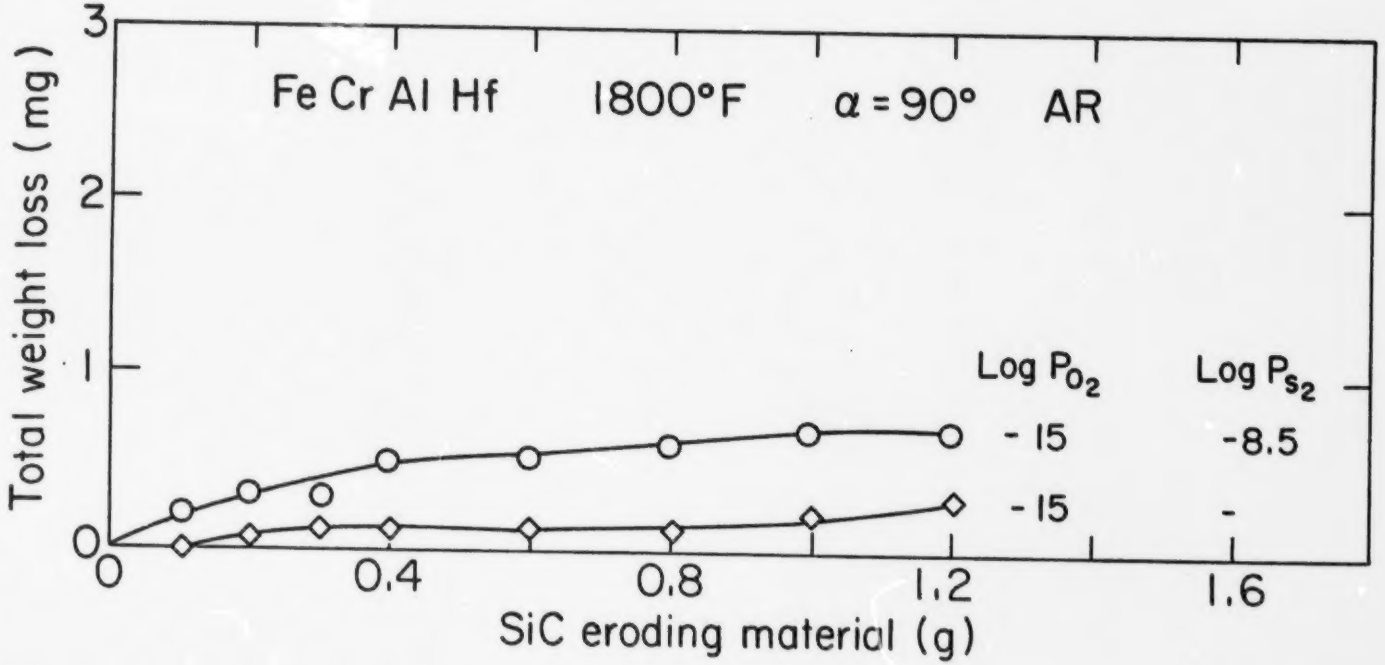

Fig. 9

XBL 801-95

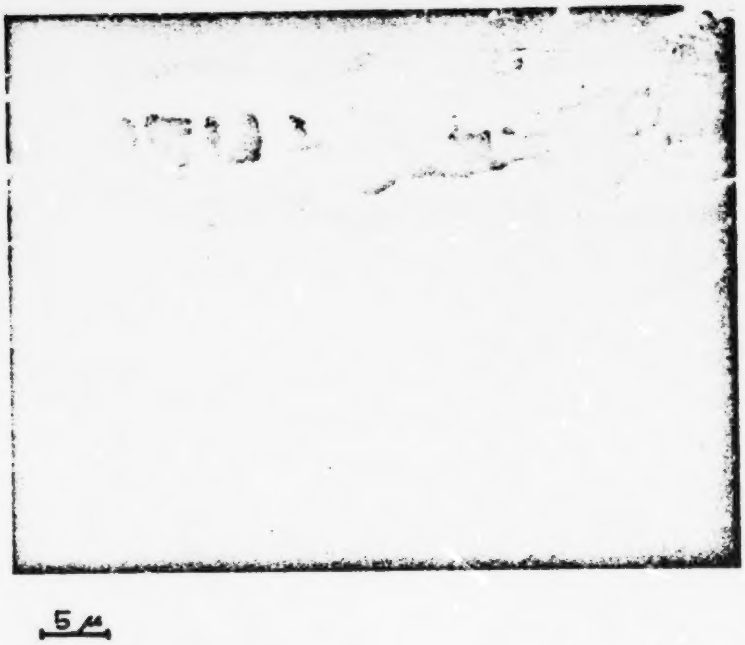

Fe 18Cr 5Al 1Hf Oxidized: Log $P_{O_2} = -15$, 1800°F

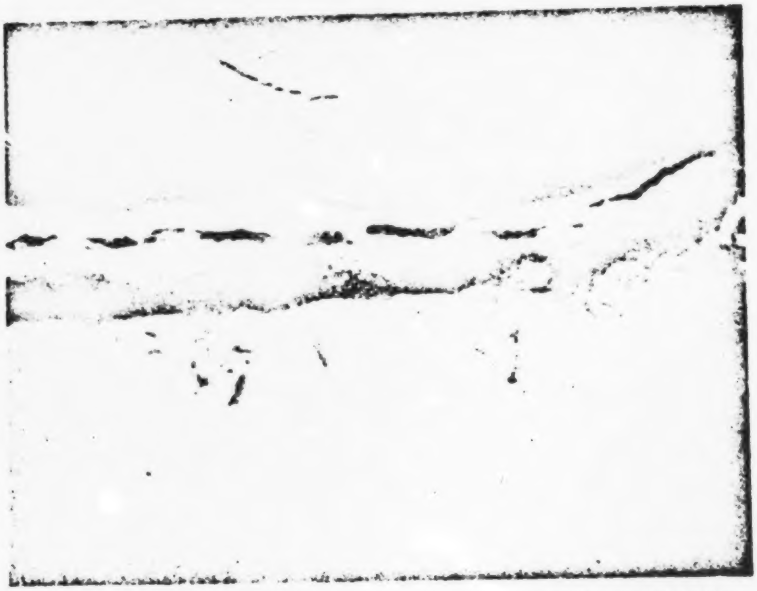

XBB 797-8946

Fig. 10 Fe 18Cr 5Al Hf

Oxidized - Sulfidized: Log $P_{O_2} = -15$, Log $P_{S_2} = -8.5$, 1800°F

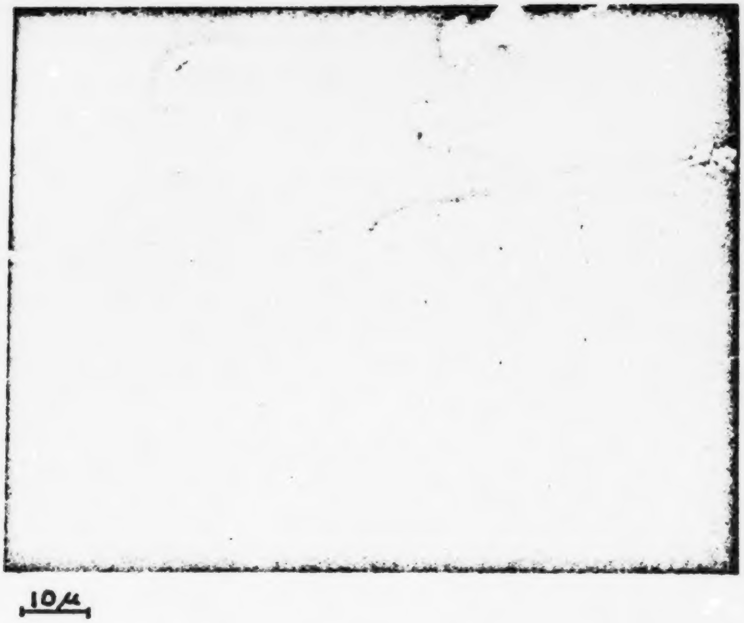

Type 310 S.S. Oxidized: Log P_{O_2} = -15, 1650°F

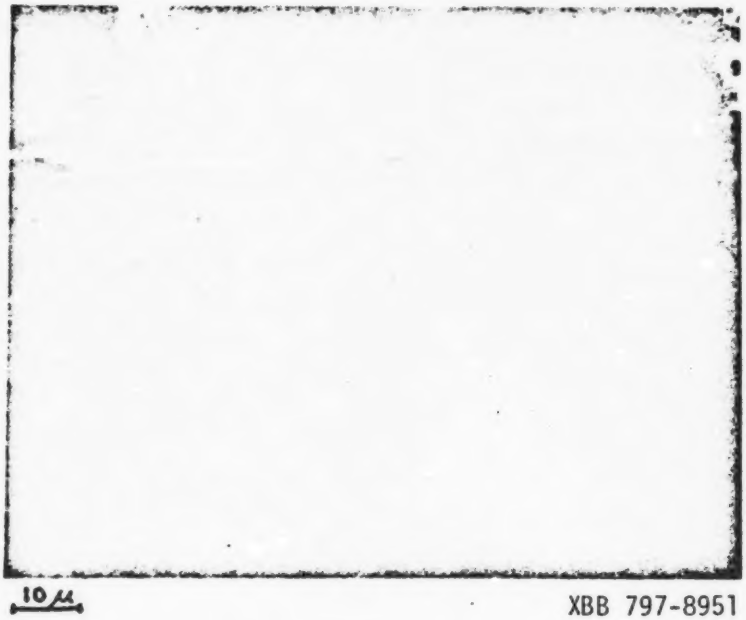

XBB 797-8951

Fig. 11 Type 310 S.S.

Oxidized - Sulfidized: Log P_{O_2} = -15, Log P_{S_2} = -6, 1800°F

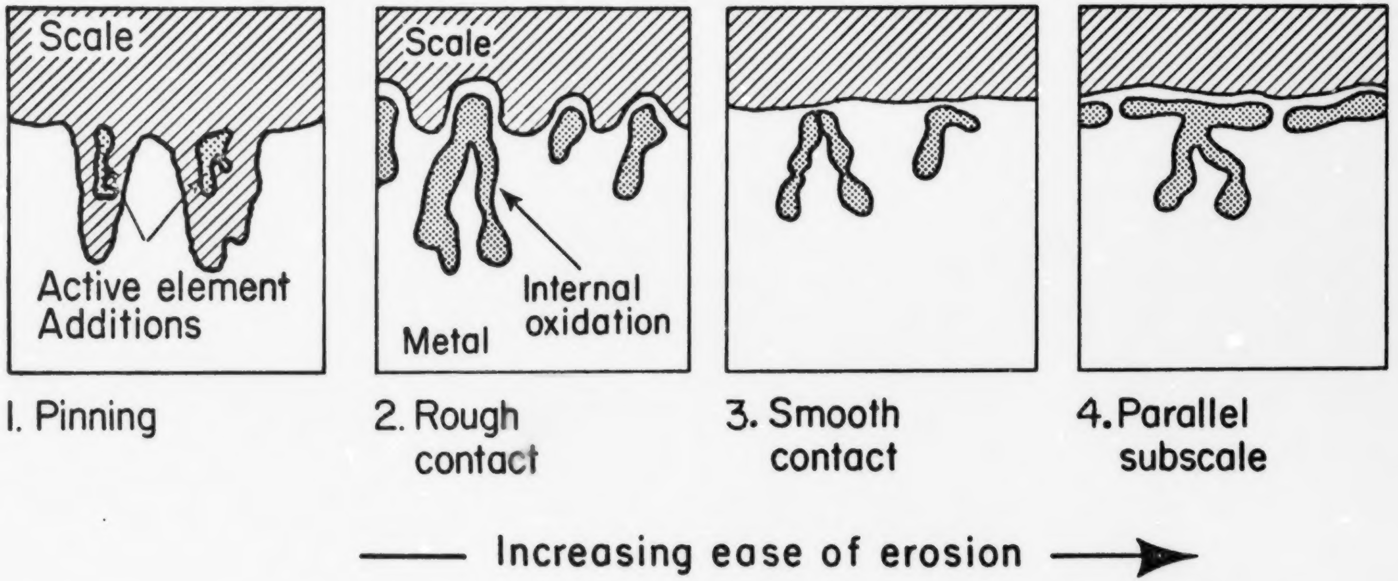
Scale
Active element
Additions
I. Pinning
Scale
Metal
Internal
oxidation
2. Rough
contact
3. Smooth
contact
4. Parallel
subscale
Increasing ease of erosion

XBL 7912-13356A

Fig. 12

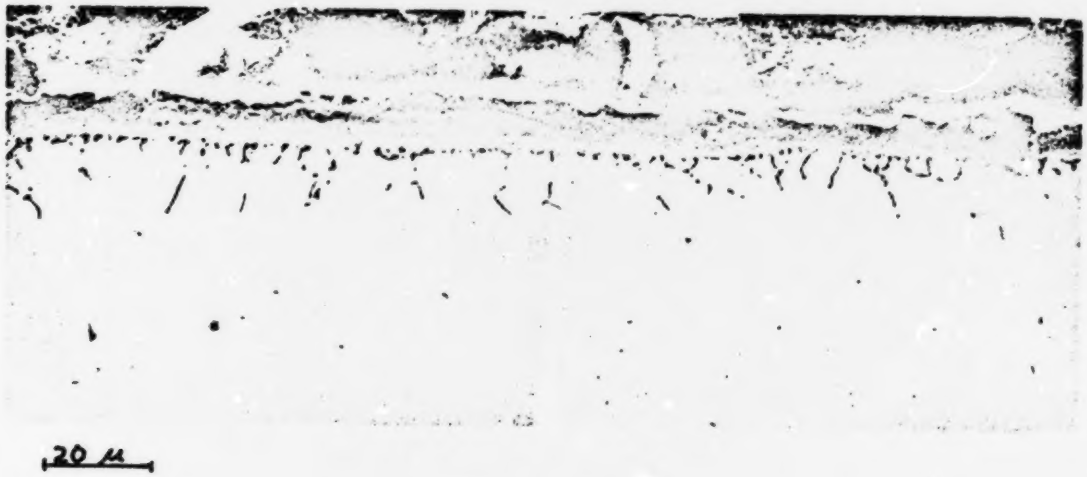

Type 310 S.S.

Oxidized - Sulfidized: Log P_{O_2} = -15, Log P_{S_2} = -6, 1800°F

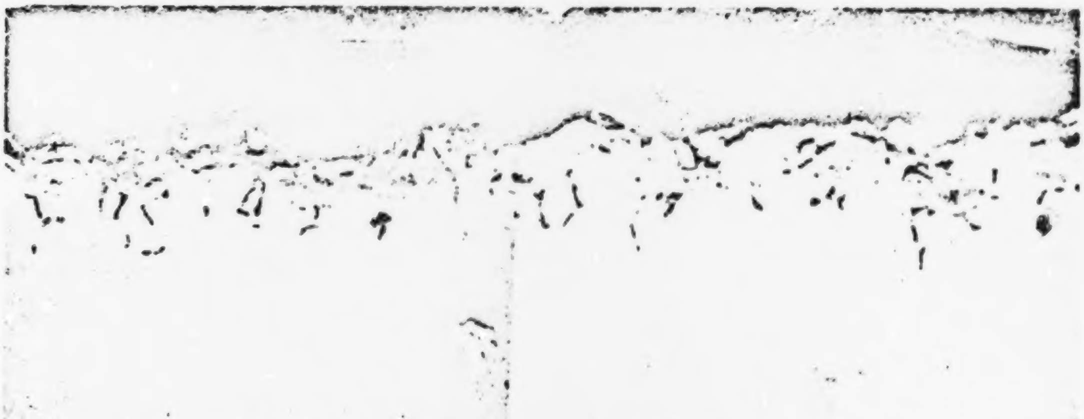

XBB 797-8945

Fig. 13

Type 310 S.S. Preoxidized: Log P_{O_2} = -15, 1800°F

Oxidized - Sulfidized: Log P_{O_2} = -15, Log P_{S_2} = -6, 1800°F

Fig. 14

XBB 808-10079

Fig. 15

XBB 808-10078

LBL-6279

EROSION OF DUCTILE METALS BY SOLID PARTICLES

David McFadden
(M. S. thesis)

June 1977

Prepared for the U. S. Energy Research and
Development Administration under Contract W-7405-ENG-48

LAWRENCE BERKELEY LABORATORY
UNIVERSITY OF CALIFORNIA

LBL-6279

LBL-6279

EROSION OF DUCTILE METALS BY SOLID PARTICLES

David McFadden

Materials and Molecular Research Division
Lawrence Berkeley Laboratory
and Department of Mechanical Engineering
University of California
Berkeley, California 94720

June 1977

ABSTRACT

The present work was undertaken to study the mechanism involved in the erosion of ductile metals by solid particles at grazing angles of incidence. To investigate the material removal process, a series of multiple and single particle tests was conducted on 1100-0 aluminum with silicon carbide particles. These results were correlated with existing analytical models. Departures of the experimental results from theoretical predictions were resolved by considering a more realistic model of the erosion process.

TABLE OF CONTENTS

Acknowledgement iv
I. Introduction 1
II. Experiments 10

III. Discussion and Results

A. Qualitative Interpretation of Single Particle Impacts . 13
B. Cutting Analysis 14
C. Modified Cutting Analysis 21
IV. Conclusion 30
References 32
Figure Captions 34
Figures 37

ACKNOWLEDGMENT

The author is grateful to Professor Iain Finnie for his guidance and help during the course of the investigation. Thanks are also due to Professors Shiro Kobayashi and Earl R. Parker for reviewing the manuscript.

The refurbishment and construction of the test apparatus by Mr. Walter Toutolmin is gratefully acknowledged.

This work was done under the auspices of the U. S. Energy Research and Development Administration.

I. INTRODUCTION

Through the years, erosion by solid particles in a fluid stream has been a problem in many industrial processes. Currently there is a great deal of interest in coal-hydrogenation. From pilot plant results and experience with similar operations, erosion appears to be an important, if not limiting, factor in the development of novel hydrogenation processes. The need for a better understanding of erosion in this connection is the motivation of the present work.

The study of erosion of ductile metals began in the 1930's. The first phase (1930~1960) of erosion research involved primarily the collection of erosion data for different materials and particles under varied conditions. This era defined the basic relationships involved in erosion and reported interesting observations on the erosion resistance of various metals and refractories. However, it was not until 1958 that the first analysis of erosion was performed. This study began the next phase of erosion work, that is, trying to develop an analysis to predict weight loss. An understanding of the basic mechanisms by which erosion occurs is necessary if predictions are to be made for new processes.

The first analysis of weight loss was given by Finnie,[1] who considered the erosion of an ideally ductile material by a hard angular particle as illustrated in Fig. 1. The basis of the analysis was the following assumptions:

(a) Material removal is the result of the cutting action of rigid particles.

(b) The plastic flow stress is constant.

(c) There is a constant ratio (k) between the horizontal and vertical forces acting on the particle during cutting.

(d) The volume removed is the product of the area swept out by the particle tip and the width (b) of the cutting face, $b\int_0^{t_c} Y_T dX_T$, where X_T and Y_T are the coordinates of the tip of the particle as shown in Fig. 1. The time at which cutting ceases is t_c.

(e) There are two conditions for which cutting may terminate. One possibility is that cutting ceases when the particle tip can no longer move forward ($\dot{X}_T(t_c) = 0$). The other case is when the particle leaves the surface while still cutting, that is, when the particle's tip has a horizontal velocity when $Y_T(t_c) = 0$.

(f) The area of contact is about twice the area given by the depth of cut ($L/Y_t \cong 2$).

The two dimensional case shown in Fig. 1 was used as the basis of Finnie's analysis.[2] By solving the equations of motion of the tip of the particle, the volume removed was determined. The resulting expression for volume removal was found to be[3]

$$\text{Vol} = \frac{CmV^2}{4p\left(1+\frac{mr^2}{I}\right)}\left(\cos^2\alpha - \left(\frac{\dot{X}_T}{V}\right)^2\right) \qquad (1)$$

where Vol = volume swept out

m = mass of eroding particle

I = moment of inertia of particle about its center of gravity

r = radius of particle

C = fraction of particles cutting in idealized manner

α = angle of attack

V = particle velocity

p = horizontal component of pressure on particle taken equal to Vicker's Hardness H_V

$\dot{X}_T(t_c)$ = horizontal velocity of particle tip when cutting ceases

This expression when evaluated for the two possibilities for the end of cutting reduces to

$$\mathrm{Vol} = \frac{CmV^2}{2p\left(1+\frac{mr^2}{I}\right)} \cos^2\alpha \quad ; \quad \dot{X}_T = 0 \qquad (2)$$

and

$$\mathrm{Vol} = \frac{CmV^2}{4p\left(1+\frac{mr^2}{I}\right)} \left(\frac{2}{P}\right)\left[\sin 2\alpha - \frac{2\sin^2\alpha}{P}\right] \qquad (3)$$

where

$$P = \frac{k}{\left(1+\frac{mr^2}{I}\right)}$$

Finnie, et al,[3] conducted experiments in which weight loss as a function of angle of incidence, particle velocity, and target hardness were determined and correlated with predictions from the analysis.

For hard angular particles, SiC and Al_2O_3, it was found that the velocity exponent, n, varied from 2.04 to 2.50 rather than n = 2 as predicted. It was found that the analysis predicted an angle of attack for maximum erosion which was similar to experimental results. The general shape of the predicted and experimental erosion curves were found to be similar. Weight loss in erosion was found to vary inversely with Vicker's hardness of the surface for annealed metals. This indication of erosion resistance was also predicted by the analysis ($Vol \propto \frac{1}{H_V}$). It was found that heat treating steels or cold working other metals had little effect on the materials' erosion resistance.

In 1962 Bitter[4] proposed a theory for solid particle erosion which was based on Hertzian contact theory and assorted energy balances. Bitter categorized the process as consisting of two distinct mechanisms, cutting wear and deformation wear. He asserted that for ductile metals at low angles of attack, the cutting mechanism was predominant with negligible deformation wear and at high angles of attack deformation wear caused the majority of the damage. It should be noted that Bitter's approach was developed for both brittle and ductile erosion and that the only differences in these erosion mechanisms was the amount to cutting or deformation wear present.

Neilson and Gilchrist[5] presented Bitter's erosion analysis in the simplified form:

$$W = \frac{MV^2\cos^2\alpha\sin\alpha}{2\phi} + \frac{MV^2\sin^2\alpha}{2\varepsilon} \quad ; \quad \alpha < \alpha_0$$

and

$$W = \frac{MV^2\cos^2\alpha}{2\phi} + \frac{MV^2\sin^2\alpha}{2\varepsilon} \quad ; \quad \alpha > \alpha_0$$

where W = weight loss

M = total mass of eroding particles

V = particle velocity

α = angle of attack

α_0 = angle at which the horizontal component of particle velocity is zero

ϕ = the cutting energy absorbed by the surface to release one unit of eroded material

ε = deformation energy absorbed by the surface to release one unit of material

It is interesting to note that the final expressions have little if any relationship to the basis of the analysis.

Bitter[4] found by adjusting certain parameters in his analysis that Finnie's experimental results for aluminum and steel could be predicted. Neilson and Gilchrist[6] were also able to fit Bitter's analysis to their experimental work with some accuracy. Bitter's final weight loss equations are essentially a "curve" fit method and his predictions are highly dependent on the two empirical energy constants, ϕ and ε.

Winters and Hutchings[7] conducted studies with individual angular particles striking lead and steel samples to determine the relationship between the particle's orientation at the point of impact and the subsequent material damage. It was found that two different regimes of deformation existed, ploughing and cutting. They found that ploughing occurred at large negative rake angles, that is, when the angle between the leading edge of the particle and the surface was small. Ploughing deformation was found to be reduced if the particle had some angular rotation while it was in contact with the surface. At more positive rake angles, cutting deformation occurred, but its effectiveness was reduced by any rolling of the particle. This rolling action resulted in the particle penetrating deeply into the surface rather than sweeping though the material. The authors also observed localized deformation, identified as adiabatic shear bands, in the lips raised during cutting deformation.[7,8] They suggested that materials susceptible to adiabatic shear may also have a lesser resistance to erosion.

Tilly[9] proposed a completely different two stage process for the erosion mechanism. This consisted of a primary and secondary process rather than two mechanisms which dominate under different conditions of rake angle and angle of attack. These two stages were identified as:

(a) Primary erosion starts with the indentation of the surface followed by a micromachining process for chip removal.

(b) The second stage consists of impacting particles fracturing and the resulting fragments producing additional removal. Tilly tried to support this mechanism by characterizing the particles size distribution and relating the size change to the observed erosion.

The studies by Goodwin, et al,[18] showed interesting variations in erosion parameters with particle size and base material. The velocity exponent was found, for small particles, to be 2 but for sizes above ~100 μm it was approximated as 2.3 for normal impacts. These tests were conducted on several ductile materials. Tilly and Sage[17] found a dependence of erosion rate on particle diameter for a given impact velocity. They found for a number of ductile materials that the results, weight loss as a function of particle diameter, could be divided into three regions. These areas consisted of a segment defined by a threshold diameter (d_{EL}) below which no erosion occurred, a region above d_{EL} where weight loss has a power law relationship to the diameter, and for still larger particles the erosion rate was constant.

Experiments relating the erosion characterists of single and multiple particle impacts were conducted by Sheldon and Kanhere.[11] These tests consisted of the erosion of 6061 aluminum (annealed and work hardened) by large diameter stell and glass shot (dia. ~2500 μm) at angles of incidence of 20 and 90 degrees. The velocity exponent (n) determined for single and multiple particle tests were similar. For work hardened aluminum at $\alpha = 20°$, the velocity exponent was approximately 2.8. The annealed specimen under similar conditions produced a velocity exponent which varied from 2.3 to 2.4.

Sheldon and Kanhere[11] developed an erosion model based on the materials' indentation hardness characteristics. The derivation, for normal impact only, consisted of a simple energy balance between the kinetic energy of the particle and the work expended during indentation. This approach produced a weight loss prediction of the form

$$W = \frac{D^3 V^3 (\rho)^{3/2}}{H_V^{3/2}} \qquad (4)$$

where D = particle diameter

V = particle velocity

ρ = particle density

H_V = Vicker's hardness

W = weight loss

The model assumed that the force necessary to indent the surface was proportional to the depth of penetration to a power m, somewhat like a "dynamic" hardness test, but it did not consider the strain harding of the surface or the inertia of the particle. Sheldon and Kanhere contend that the exponent for velocity ($n = 3$) is close to the actual experimental values. However, the prediction that the weight loss was proportional to $H_V^{-3/2}$ is in disagreement with experimental results.

Sheldon[12] maintained that the best material property for correlation with erosion wear is the hardness value of the target material in the fully work hardened condition as measured on the damaged surface. It was found, for a number of pure materials, that the hardness was as much as five times higher than that measured for the annealed material. Sheldon proposed that the fully work hardened value for hardness should be used in analyses which employ a particle cutting or material displacement mechanism for material removal.

Based on the preceding literature review it appears that different erosion mechanisms predominate at low and high angles of impingement.

Since low or grazing angles lead to the largest volume removal it was decided to concentrate on this aspect of erosion.

As a starting point we will investigate the model for solid particle erosion proposed by Finnie.[1,2] At the present time, this is the only theory which attempts to explain the erosion process. The theories proposed by Bitter or Neilson and Gilchrist seem to be little more than a curve fit, and those presented by Tilly, Sheldon, etc., are composed mostly of observations with very little modeling of the process.

The work that will be described involved experiments with both single and multiple impacts. These results are compared with those predicted analytically. Departures from the predicted behavior are considered and a modified analysis of erosion at grazing angles is developed.

II. EXPERIMENT

The tests were made with an erosion testing device originally developed by Sheldon.[13] The equipment was subsequently modified for velocity measurement and easier operation. In its final.form it is shown in Figs. 2 and 3.

The basic operation of the tester is simple and effective. The silicon carbide was fed into the air stream, mixed for uniform particle distribution, and then propelled down the tube by the air flow. By varying the pressure drop across the nozzle, the air and particle velocity could be controlled. It was found that the particle velocity was a function of the inner diameter of the tube, the loading factor (grams of particles/grams of air), the pressure drop across the nozzle, the surface roughness of the nozzle, and the size and shape of the particles. To ensure constant velocities during tests, the above parameters must be kept as constant as possible.

For multiple particle tests, the hopper feed arrangement shown in Fig. 3 was used. This arrangement provided a very satisfactory means of depositing the particles into the air stream at a constant rate. The mass of particles entering the air stream was a function of the hopper rake angle (Δ) and the air pressure applied to the hopper vibrator.

For the single particle tests, consisting of five particles impacting the target, the hopper was replaced by a glass and plastic tube device, and the larger particles were fed from the tube into the mixing chamber. A constant loading factor was not needed to ensure a constant velocity in that at such small loadings any small deviation of this value had negligible effect on the particle velocity.[14]

To determine the particle velocity, the rotating disc device shown in Fig. 4 was employed. This equipment was based on the design of Ruff and Ives.[15] To determine the particles' velocities, the parameters (R, S, L, V) shown in Fig. 4b were needed. The simple observation that the time it takes the particle to travel between the discs is equal to the time it takes the disc to rotate through the arc length was required.

There are several advantages of the rotating disc method when compared to a double flash photographic system. The strong points of the rotating disc are that it is less expensive to build and operate, it gives very accurate results, and less time is needed for particle velocity calibration. Its accuracy is due to the large number of particles which are used during a test and the resulting averaging of variations in operating conditions (particle orientation in the stream, particle loading, particle size). For several tests, at a given set of conditions, this method produced results which varied by less than 5%.

All but a few experiments used silicon carbide particles and 1100-0 aluminum targets. The choice of these materials was dictated by availability and the fact that an extensive amount of previous testing had been carried out with this combination. Specimens were prepared from sheared plates by polishing with silicon carbide abrasive papers starting at 240 grit and ending at 600 grit. For the multiple particle tests in which weight loss was determined as a function of velocity, angle of attack, and amount of abrasive, the silicon carbide particles had a size range between 48 and 62 mesh (250-300 μm). This size range corresponds to a weight equivalent spherical particle of 280 μm diameter. The purpose of the single particle experiments was to make observations on the craters formed during impact. To make the observations easier, larger, 12 to 16 mesh, silicon carbide particles were used. These particles had equivalent diameters of 1100 μm.

III. RESULTS

A. Qualitative Interpretation of Single Particle Impacts

A large number of single particle impacts were examined with the scanning electron microscope. It is not possible to present all of these so representative photographs are shown in Figs. 5-11. These stereo pairs (10° tilt) provide a graphic picture of the mechanisms involved in erosion. To supplement the photographs, a profile through the approximate centerline of the crater is also shown.

Figures 5 through 7 are craters that were formed by particles which had angles of incidence of 10, 11, and 15 degrees, respectively. These craters had similar characteristics in that each exhibits, to some degree, striation from the cutting edge of the particle, a lip at the end of the crater, and were shallow with an average length to depth ratio of about 10. At 10 degrees, the particle swept though the surface and removed the majority of the displaced material. The 11° and 15° impacts are similar in that the particles entered the surface in a cutting manner. However, in these cases the particles were unable to remove all of the displaced material and left a large lip of material at the end of the craters.

A transition in the removal mechanism appears to occur between 20 and 40 degrees. In this area, a change from a cutting mechanism of removal to one involving indentation appears to take place. The 20° and 30° impacts (Figs. 8 and 9) are typical of this region in that the particle entered the surface in a cutting manner and proceeded to plough the material forward. In this region, there is considerable displaced material and the craters are becoming shorter and deeper compared to the grazing impacts (10°-20°) with length to depth ratio of about 5.

At higher angles of incidence (40°-90°) the deformation mechanism is primarily one of indentation with very little cutting occurring. Figure 10 shows a crater formed at 60 degrees. The particle indents the surface as it moves across it with the resulting damage being the depression of the surface. The original surface can be seen on the floor of the crater. At 90°, Fig. 12, the damage is the result of surface indentation by the particle. As with the 60° crater, the 90° impact has only minor material displacement at the edges of the crater, and the crater floor has a remarkably constant slope.

B. Cutting Analysis

To determine the applicability of Finnie's cutting theory, a series of experiments were conducted. Since the single particle tests showed that a cutting type removal mechanism was appropriate over a range of $10 < \alpha < 30°$, the correlations between predictions and experimental results will be confined to this region. The theory and tests results were examined for the following cases:

(i) Multiple particle tests were compared to the predictions of Eq. 1.

(ii) Crater profiles obtained from the single particle experiments and profiles predicted from the analysis were compared. Also, an estimate of the material hardness (H_V) was obtained from single impacts and the analysis.

(iii) The assumptions made for several of the parameters (e.g. k) in the analysis were compared to the test results.

Erosion (expressed as g removed/g abrasive) as a function of the angle of incidence, for particle velocities of 77 m/s and 102 m/s, is shown in Fig. 12. By examining the normalized curves, it can be seen that the maximum amount of weight loss occurs at about 11° for the lower velocity and 12° for the higher, and that erosion curves have very similar shapes between 10 and 30 degrees but diverge after that point. (It is interesting to note that at 90°, for the lower velocity test, the erosion is 13% of the maximum, while at 107 m/s the erosion is about 22% of the peak value.) The velocity exponents for the expression erosion $\alpha\ V^n$, plotted on Fig. 12, range from 2.46 at 10 degrees to 3.12 for normal impacts.

A comparison of Finnie's analysis using Eq. 1 and the experimental results is shown in Fig. 13 (normalized about their peak weight loss values). Using Finnie's assumptions for the constants $k = 2$, $\frac{I}{mr^2} = \frac{1}{3}$, the results compare favorably for what we have termed the cutting region. For both velocities, the shape of the experimental curve and predicted curve are very similar in the region of $\alpha < 30°$, and the analysis predicts a peak erosion angle very similar to the test results. As would be expected, the cutting analysis and the experimental results diverge for higher angles.

There are several anomalies in the cutting analysis when compared to experimental results. The analysis predicts a constant velocity exponent of 2, whereas the experimental results show an exponent which is greater than 2 and increases with α. These aspects are discussed in detail in section C.

By plotting the erosion results in terms of erosion per particle for both experimental and analytical results (Fig. 14), it is possible to make an estimation of the cutting efficiency. Using the values of annealed hardness for the horizontal stress p, a cutting efficiency of one, and an average particle weight, the analysis underestimates the test results by about a factor of 10.5. This result is similar to Finnie's[1] assertion that the cutting efficiency for erosion should be similar to the efficiency found in abrasive wear studies, that is, 1 particle in 10 produces actual removal while the remainder displace and roughen the surface.

On the other hand, Sheldon[12] contends that eroding particles work harden a surface to about five times the annealed hardness. In this case the discrepancy between experimental and analysis is a factor of about two. In other words about half of the particles would then be cutting in the idealized manner. It is difficult to isolate the variables C and p in Eq. 1 but their quotient $\frac{C}{p}$ seems to be approximately $\frac{0.1}{H_V}$ when annealed metals are eroded by silicon carbide grains. We will later present some evidence to support the viewpoint that p should be taken as the Vickers hardness H_V.

The trajectory of the particle's tip, X_T and Y_T, as it cuts through the surface was predicted using Finnie's analysis. These results were compared to the profiles of typical single impacts.

Finnie[1] showed in his original paper that the motion of the particle's tip can be described as with reference to Fig. 1 as:

$$Y_T = Y \qquad (5)$$

$$X_T = X + r\phi \qquad (6)$$

where

$$Y = \frac{V\sin\alpha}{\beta}\sin\beta t$$

$$X = \frac{V\sin\alpha}{k\beta}\sin\beta t + V\cos\alpha(t) - \frac{V\sin\alpha}{k}(t)$$

$$\phi = \frac{mr\,V\sin\alpha}{kI\,\beta}\left[\sin\beta t - \beta t\right]$$

$$\beta = \left(\frac{pk\psi b}{m}\right)^{1/2}$$

Then expressing equations 5 and 6 in a dimensionless form, X^* and Y^*, the particle's trajectory is shown to be

$$X^* = \frac{\beta X_T}{V} = \sin\tau(2\sin\alpha) - \tau(2\sin\alpha) + \tau(\cos\alpha) \qquad (7)$$

$$Y^* = \frac{\beta Y}{V} = \sin\alpha\,\sin\tau \qquad (8)$$

where $\tau = \beta t$, $I = 1/3\ mr^2$ and $k \cong 2$.

A comparison of profiles predicted by Eqs. 7 and 8 and several typical single impacts are shown in Figs. 15 and 16. The curves are scaled such that the maximum depth of cut for the analysis and the test results are the same.

For an angle of 10 degrees the analysis predicts the general shape of the crater quite well, The positions of the maximum depth of cut (Y^*_{max} at $X^* = 1.2$) are similar as is the trajectory of the particle before it reaches Y^*_{max}. There is some dissimilarity near the end of the volume removal process in that, in two of the actual cases, the particle travels a bit further but raises a small lip. The analysis shows the particle covering a shorter horizontal distance but removing the entire volume.

Even at the limits of the cutting region ($\alpha \cong 30°$), the analysis is able to describe many of the features of the actual impact. The trajectory of the particle's motion for the predicted and experimental cases is similar up to the maximum depth of cut. After Y^*_{max} the comparison of the analysis and impact results is no longer valid. The analysis assumes that the particle removes all of the material up to Y^*_{max} and is then ejected from the surface. In reality, the particle displaces extra material past Y^*_{max} to create a large lip on the leading edge of the crater.

There is, of course, variability from one impact to another with angular particles so one should not expect precise predictions from an idealized model.

It was also of interest to determine whether the cutting theory could predict the plastic flow stress which a single particle would "see" during the removal process. By using the non-dimensional parameter Y^* and several dimensions from the single particle experiments, a "flow pressure" could be estimated and compared to the material hardness H_V.

From the cutting theory it is shown that

$$Y^* = \frac{\beta Y}{V}$$

or for the maximum depth, Y_{max},

$$\frac{\beta_{max} Y_{T_{max}}}{V} = \sin\alpha \tag{9}$$

Solving the above relationship for β_{max} yields

$$\beta_{max} = \left(\frac{pk\psi b}{m}\right)^{1/2} = \frac{V}{Y_T} \sin\alpha \tag{10}$$

where m = mass of particle

k = force ratio = 2

p = flow pressure

$\psi = L/Y_T \cong 2$

b = width of impact

The maximum flow pressure is then expressed as

$$p_{max} = \frac{mV^2\sin^2\alpha}{Y^2_{T_{max}} 4b} \tag{11}$$

By taking measurements for $Y_{T_{max}}$ and b and knowing the velocity, mass, and angle α, the flow stress for the single particle impacts at 10, 15, 30, and 60 degrees (Figs. 5, 7, 9, 10) could be determined. The results of this prediction are presented in Fig. 17 and are comparable to the actual hardness which the single particles "saw" on impact, that is, the hardness of the fresh aluminum surface ($H_V \cong 28$ kg/mm^2). It is interesting, although perhaps coincidental, to note that by extrapolating the results of Fig. 17 to $\alpha = 0°$, the hardness obtained is approximately equal to the value for the annealed specimen.

The average ratio of horizontal to vertical forces, k, was determined experimentally to be 2.12 (k = 2 in analysis). This experiment consisted of several angular particles (1400 μ dia. SiC) being mounted on styluses and the recording of the horizontal and vertical forces which the particles generated as they scratch the 1100-0 aluminum specimen.

Some of the assumptions of the cutting analysis can be verified by the experimental results already presented. It was assumed that the particle entered the surface at the angle of incidence of the air stream to the specimen. By measuring the initial slope of the particle's trajectory for single particle tests, it was found that for $\alpha < 40°$ the average slope deviates from the assumed angle of incidence by less than 7%. For the cutting region, only two modes of cutting are observed, that is, the particle was able to leave the surface in a cutting manner ($Y_T(t_c) = 0$) or the forward motion of the particle was stopped by the base material ($\dot{X}_T(t_c) = 0$). The lack of secondary damage in single particle tests indicates that the particle is rigid and did not fracture upon impact as was assumed in the analysis.

By using Figs. 18 and 19, the assumption that for multiple impacts the flow pressure each particle "sees" is the annealed hardness (H_v) of the base metal is shown to be reasonable. The results, represented as two linear regions with positive increasing slopes, indicate that the particle "sees" a constant hardness in the steady state region. This pressure must be similar to the annealed hardness observed in the incubation portion of the results in that the erosion rate had increased somewhat when compared to the initial rate. If it is assumed the particles see a progressively work hardened surface, then the erosion rate should decrease with the amount of abrasive and not increase as the results indicate. It is noted that the transition from the incubation portion of the curve to the steady state region (e.g. 180 gm at 27 $\frac{m}{s}$) is characterized by the onset of rippling.

C. Modification of the Cutting Analysis

In view of the success of the cutting analysis in explaining many features of erosion at low angle of impingement, it is disturbing that it underestimates the velocity exponent. As pointed out earlier the theoretical value of 2 in the relation volume $\sim V^n$ is rarely observed with experimental values ranging from 2.4 to 2.6 or greater. Other than the Sheldon and Kanhere[11] model based on indentation (Eq. 4) which predicts volume $\sim V^3$ and Tilly's suggestion[9] that shattering and secondary erosion occur at higher velocities. there has been little attention paid to this discrepancy. Both of these approaches are lacking in generality and clearly do not apply to the experiments we have reported.

One consideration is that the thermal properties of the eroded surface may be involved in the mechanism of erosion. This was disposed of by testing titanium. Its thermal diffusivity (.0282 cm^2/sec) differs greatly from that for aluminum (.712 cm^2/sec). However, the values for the exponent n were essentially the same as for aluminum (n_{Al} = 2.42, n_{Ti} = 2.47 at α = 10° and velocities of 39 and 97 $\frac{m}{s}$).

In searching for another explanation, Finnie[16] examined the assumptions of his original analysis. He suggested that the equation for angular rotation be modified to locate the resultant force at the correct distance from the C.G. of the particle. Originally this was taken to act at the tip of the particle since this simplified the analysis. However, as shown in Fig. 20 it is more realistic to locate the resultant force in the center of the material having contact with the particle. The symmetrical picture of two-dimensional cutting shown in the figure could be considered as an average condition for grains which are "tilted" in either direction as they strike the surface.

The equations of motion for the X and Y ($Y_T \equiv Y$) directions are unchanged by this modification and are

$$m\ddot{X} + pY\psi b = 0 \tag{12}$$

$$m\ddot{Y} + kpY\psi b = 0 \tag{13}$$

The equation for angular rotation now becomes:

$$I\ddot{\phi} + p\psi b(r-Y)Y - 2p\psi (Y)^2 bk = 0 \tag{14}$$

where $p\psi bY$ = horizontal force

$p\psi Yok$ = vertical force

The assumptions used in the above equations are identical to those used in the original analysis.

Solving Eq. 13, the vertical motion of the particle can be expressed as

$$Y(t) = c_1 \sin\beta t + c_2 \cos\beta t \tag{15}$$

where

$$\beta = \left(\frac{pk\psi b}{m}\right)^{1/2} \tag{15}$$

using the initial conditions that at $Y(0) = 0$ and $\dot{Y}(0) = V\sin\alpha$ the expression for $Y(t)$ reduces to

$$Y(t) = \frac{V}{\beta}\sin\alpha \sin\beta t \tag{16}$$

Substituting $Y(t)$ into Eq. (12), the horizontal motion of the particle is found to be

$$X(t) = \frac{V\sin\alpha}{k\beta} \sin\beta t + c_1 t + c_2 \tag{17}$$

For the boundary conditions $X(0) = V\cos\alpha$ and $X(0) = 0$, $X(t)$ may be expressed as:

$$X(t) = \frac{V\sin\alpha}{\beta k} \sin\beta t + \left\{V\cos\alpha - \frac{V\sin\alpha}{k}\right\} t \tag{18}$$

The rotation of the particle is found to be of the form

$$\phi(t) = \left\{\frac{P\psi b}{I}\right\}\left[\left\{\frac{dV^2\sin\alpha^2}{\beta^2}\right\}\left(\frac{1}{4}t^2 + \frac{1}{8\beta^2}\cos 2\beta t\right) + \frac{rV\sin\alpha}{\beta^3}\sin\beta t - \frac{trV\sin\alpha}{\beta^2} - \frac{d^2V^2\sin^2\alpha}{8\beta^4}\right] \tag{19}$$

where $d = 2k + 1$ and the other constants are as defined previously. It is assumed that for many impacts the initial particle rotation and angular velocity would, on the average, be zero ($\phi(0) = \dot{\phi}(0) = 0$). If it is assumed that $I = \frac{1}{3}mr^2$ and $k = 2$ for angular particles, then

$$\phi(t) = \frac{15}{16}\frac{V^2\sin^2\alpha}{\beta^2 r^2}\left[2(\beta t)^2 + \cos 2\beta t - 1\right] + \frac{3}{2}\frac{V\sin\alpha}{r\beta}(\sin\beta t - \beta t) \tag{20}$$

As in the original analysis, the motion of the particle's tip can be expressed as

$$Y_T \cong Y$$

and

$$X_T \cong X + r\phi$$

Again, this assumption implies an average condition exists for many impacts. Since the motion of the particle's tip is known, then the volume removed is

$$\text{Vol} = b \int_0^{t_c} Y_T \dot{X}_T \, dt \qquad (21)$$

where t_c = time at which cutting ceases

b = a unit width of the cutting face

Combining Eqs. 16, 18 and 20, the volume expression reduces to

$$\frac{\text{Vol}}{b} = \frac{V\sin\alpha}{\beta} \int_0^{t_c} (\sin\beta t) \left[(A_2 - A_3 - A_7) + (A_1 + A_6)\cos\beta t - A_5 \sin 2\beta t + A_4 t\right] dt$$

where $A_1 = \frac{V}{2}\sin\alpha$

$A_2 = V\cos\alpha$

$A_3 = \frac{1}{2} V\sin\alpha$

$A_4 = \frac{15}{4} \frac{V^2}{r} \sin^2\alpha$

$A_5 = \frac{15}{8} \frac{1}{r\beta} V^2 \sin^2\alpha$

$A_6 = \frac{3}{2} V\sin\alpha$

$A_7 = A_6$

Evaluating the integral from 0 to t_c, the volume expression is

$$\frac{Vol}{b} = \frac{V^2\sin^2\alpha}{\beta^2}\left[\cos\beta t_c(2 - \cot\alpha) + \cot\alpha - \frac{3}{2} - \frac{1}{2}\cos 2\beta t_c\right] +$$

$$\frac{V\sin\alpha}{\beta}\left[\frac{A_5}{\beta}\left(-\frac{1}{2}\sin\beta t_c + \frac{1}{6}\sin 3\beta t_c\right) + A_4\left(\frac{1}{\beta^2}\sin\beta t_c - \frac{1}{\beta}t_c\cos\beta t_c\right)\right] \tag{22}$$

This expression is composed essentially of Finnie's original solution (the first parentheses) and a correction term.

To determine the volume removal for the case when the tip of the particle is still moving horizontally as it leaves the surface, the condition on t_c is that $Y(t_c) = 0$ when $\dot{X}_T$ exists or $\beta t_c = \pi$. Using this condition, the expression is given as

$$\frac{Vol}{b} = \frac{V^2}{\beta^2}(\sin 2\alpha - 4\sin^2\alpha) + \frac{15}{4}\pi\frac{V^3\sin^3\alpha}{r\beta^3} \tag{23}$$

The other possibility for the manner in which the particle ceases to remove material is when it is prevented from moving through the surface, that is, when $\dot{X}_T(\beta t_c) = 0$. This condition for cutting termination can be expressed as

$$V\cos\alpha - 2V\sin\alpha + 2V\sin\alpha\cos\beta t_c - A_5\sin(2\beta t_c) + \frac{A_4}{\beta}(\beta t_c) = 0 \tag{24}$$

By combining this expression and Eq. 22, the volume removed for this region is given as

$$\frac{Vol}{b} = \frac{V\sin\alpha}{\beta}\left[\frac{V\cos\alpha}{\beta} - \frac{V\sin\alpha}{\beta}\sin^2\beta t_c + \frac{V^2\sin^2\alpha}{8\beta^2 r}(15\sin\beta t_c - 5\sin 3\beta t_c)\right] \tag{25}$$

It is noted that t_c, as determined from Eq. 24, is a function of the angle α and must be determined for each angle of impingement.

Since maximum erosion occurs when the particle leaves the surface while still cutting, the implications of Eq. 23 will be considered first.

If we assume that for two velocities V_2 and V_1 the volume removal can be expressed as Volume α V^n, then a value n may be estimated from Eq. 23. Recalling that $\beta^2 = pk\psi b/m$, then

$$\frac{Vol_{V_2}}{Vol_{V_1}} = \left(\frac{V_2}{V_1}\right)^n = \left(\frac{V_2}{V_1}\right)^2 \frac{\left(\sin 2\alpha - 4\sin^2\alpha + \frac{15}{4}\pi \frac{V_2\sin^3\alpha}{\beta r}\right)}{\left(\sin 2\alpha - 4\sin^2\alpha + \frac{15}{4}\pi \frac{V_1\sin^3\alpha}{\beta r}\right)}$$

Since $Y_{max} = \frac{V\sin\alpha}{\beta}$ the last term in parentheses becomes $\frac{15}{4}\pi\frac{Y_{max}}{r}$. If an estimate can be made for $\frac{Y_{max}}{r} = \lambda$ for V_1, then $\left(\frac{Y_{max}}{r}\right)$ for $V = V_2$ is merely $\left(\frac{V_2}{V_1}\right)\lambda$. The preceding equation becomes

$$\left(\frac{V_2}{V_1}\right)^{n-2} = \frac{\sin 2\alpha - 4\sin^2\alpha + \frac{15}{4}\pi\frac{V_2}{V_1}\lambda\sin^2\alpha}{\sin 2\alpha - 4\sin^2\alpha + \frac{15\pi}{4}\lambda\sin^2\alpha} \qquad (26)$$

Typically in erosion tests at two velocities used to determine the exponent n the value of λ is about 0.1. The following table shows n values calculated from the preceding equation for three velocity ratios as well as values for λ = .075 and .125.

Table 1. Velocity exponents as determined from Eq. 26 for several angles, velocity ratios, and $\lambda = .125$, .100 and .075.

		Velocity Exponent n		
λ	$\frac{V_2}{V_1}$	$\alpha = 11°$	$\alpha = 15°$	$\alpha = 18°$
.125	2	2.250	2.377	2.492
	1.75	2.237	2.261	2.457
	1.5	2.224	2.343	2.436
.100	2	2.212	2.326	2.420
	1.75	2.198	2.311	2.402
	1.5	2.186	2.294	2.368
.075	2.	2.168	2.267	2.358
	1.75	2.158	2.253	2.358
	1.50	2.148	2.239	2.333

While these values are somewhat smaller than the experimental results presented previously, they are in the range reported by Finnie[1] and Tilly.[9] The results also indicate that the exponent n increases with the angle α, as do the experimental results of Fig. 12 and those of Sheldon.[11] Varying λ and V_2/V_1 has little effect on the velocity exponent at a given angle with a maximum change of n of less than 6%.

Up to this point we have discussed only the effective velocity exponent for the situation of the particle leaving the surface while still cutting, but it is of interest to determine n for the case when the particle is prevented from moving through the surface. For the case of $\lambda = 0.1$, the transition between the two conditions occurs at 21°, a higher value than given by the simple analysis. The end of the cutting region ($\alpha \cong 30°$) will be considered. Solving Eq. 24 for the time at which cutting ceases (βt_c) and then evaluating Eq. 22, the effective veolcity exponent n for $\alpha = 30°$, $V_2/V_1 = 2$, and $\lambda = .1$ was found to be 2.76 which is very similar to experimental results.

The modified analysis does predict a shift in the peak angle of erosion with velocity. Differentiating Eq. 23 with respect to α, the relationship for the peak erosion is found to be

$$\tan 2\alpha = \frac{1}{2 - \frac{30}{16}\pi\left(\frac{V_2}{V_1}\right)\lambda} \qquad (27)$$

Evaluating Eq. 27 for velocities V_1 and $1.4V_1$, and assuming for typical impacts that $\lambda = .1$, then the peak erosion angles are

$\alpha_1 = 17.76°; \qquad V = V_1$

$\alpha_2 = 20.21°; \qquad V = 1.4V_1$

Determining the exact angle for peak erosion is very difficult, and trying to find such slight shifts in the peak value would require extensive experiments.

One of the features of the original analysis is its ability to predict the shape of single particle impacts, and it is necessary to determine if the new analysis predicts similar profiles. As before the non-dimensional parameters X^* and Y^* are used for profile determination and take the form of

$$X^* = 2\sin\alpha\sin\beta t + (\cos\alpha - 2\sin\alpha)\beta t + \frac{1.5}{16} V\sin\alpha\,(2(\beta t)^2 - \cos 2\beta t - 1) \tag{28}$$

$$Y^* = \sin\alpha\sin\beta t \tag{29}$$

where $\lambda = .1$. A comparison between the experimental profiles, those obtained from the original analysis, and those of the modified analysis are presented in Fig. 21. The new analysis predicts the crater profile somewhat more accurately than the original theory at 10°, but there is little difference in the results at 30°.

IV. CONCLUSION

The assumption in solid particle erosion that the particle removes material in a cutting manner was found to be valid for an angle of incidence of less than 30°. The basic model proposed by Finnie[1] was found, to a large extent, to describe the erosion process for this region. By making this model more realistic, some of the erosion characteristic were more precisely described.

Single particle experiments indicate the erosion process for $\alpha < 30°$ was primarily one of cutting, and for $\alpha > 40°$ the erosion process was predominately one of indentation. At angles between 20° and 40° degrees (a transition region) the mechanism for removal was a combination of cutting and indentation deformation.

Finnie's original analysis was able to predict many of the erosion characteristics of multiple and single particle damage. It was found to be very effective for multiple particle tests for $\alpha < 30°$, but for larger angles of incidence the experimental and predicted results diverged. Also, the cutting analysis was able to predict some of the features, crater profiles and the flow stress, of single particle impacts at $\alpha < 30°$. Both single and multiple impacts were used to confirm assumptions used in the analysis. It was shown that the assumptions for the force ratio k, the geometric parameters, and for treating the particle as rigid were valid. The proposal was made that the Vicker's hardness of the annealed specimen best described the surface that both multiple and single particles "see" on impact. Using this assumption for the flow stress, then the cutting efficiency was shown to be about .1 for multiple particle tests.

By modifying the original analysis, the discrepancy in predicting the role of velocity could now be explained. The modified cutting analysis produced an effective velocity exponent ranging from $\sim$2.2 at 10° to $\sim$2.7 at 30°. These results are similar to reported experimental results, that is, the exponent n is in the range of 2.2 to 2.8 and n increases with the angle of impingement α. A small shift in the peak angle of erosion with velocity is also predicted, but it was not distinguishable in the experiments. Also, the profiles for single impacts were predicted more accurately than before for $\alpha < 30°$

REFERENCES

1. I. Finnie, "The Mechanism of Erosion of Ductile Metals", Proc. 3rd U.S. Natl. Congr. Appl. Mech., (1958).

2. I Finnie, "Some Observations on the Erosion of Ductile Metals", Wear 19, 81-90 (1972).

3. I. Finnie, J. Wolak, Y. Kabil, "Erosion of Metals by Solid Particles", Journal of Materials 2, No. 3, 682-700 (1967).

4. J. G. A. Bitter, "A Study of the Erosion Phenomena", Parts 1 and 2, Wear 6, 5, 1969 (1963).

5. J. H. Neilson and A. Gilchrist, "Erosion by a Stream of Solid Particles", Wear 11, 111-122 (1968).

6. J. H. Neilson and A. Gilchrist, "An Experimental Investigation into Aspects of Erosion in Rocket Motor Tail Nozzles", Wear 11, 123-143 (1968).

7. I. M. Hutchings and R. E. Winter, "Particle Erosion of Ductile Metals: A Mechanism of Material Removal", Wear 27, 121-128 (1974).

8. R. E. Winter and I. M. Hutchings, "The Role of Adiabatic Shear in Solid Particle Erosion", Wear 34, 141-148 (1975).

9. G. P. Tilly, "A Two Stage Mechanism of Ductile Metals", Wear 23, 87-96 (1973).

10. G. P. Tilly, "Sand Erosion of Metals and Plastics: A Brief Review", Wear 14, 241-248 (1969).

11. G. L. Sheldon and A. Kanhere, "An Investigation of Impingement Erosion Using Single Particles", Wear 21, 195-209 (1972).

12. G. L Sheldon, "Effects of Surface Hardness and Other Material Properties on the Erosion Wear of Metals by Solid Particles", Trans. A.S.M.E. 99H, 133-137 (1977).

13. G. Sheldon, "Erosion of Brittle Materials", Ph.D. Thesis, University of California, Berkeley, Ca.

14. D. Kleist, "One Dimensional – Two Phase Flow", M.S. Thesis, University of California, Berkeley, Ca.

15. A. W. Ruff and L. K. Ives, "Measurement of Solid Particle Velocity in Erosive Wear", Wear 35, 195 (1977).

16. I. Finnie, Personal Correspondence.

17. G. P. Tilly and Wendy Sage, "The Interaction of Particle and Material Behavior in Erosion Process", Wear 16, 447-465 (1970).

18. J. E. Goodwin, W. Sage, C. P. Tilly, "Study of Erosion by Solid Particles", Proc. Inst. Mech. Engrs. 184 (15), 279-292 (1969).

FIGURE CAPTIONS

Fig. 1. (A) Two-dimensional picture of an angular particle surface material. (B) The forces acting on a particle during the removal process.

Fig. 2. A photograph of the test apparatus used for the erosion experiments.

Fig. 3. Schematic drawing of the erosion tester.

Fig. 4. (A) A drawing of the velocity calibration equipment and the modified test apparatus. (B) Parameters measured for determining particle velocity.

Fig. 5. (A) Single particle damage caused by 1100 μm diameter SiC at 10° angle of impingement with initial velocity of 67 m/s on 1100-0 aluminum. (B) Profile of impact through approximate centerline of crater. (C) Stereo photographs of impact (use stereo viewer provided in Metals Handbook, Vol. 9).

Fig. 6. (A) Silicon carbide particle (1100 μm diameter) struck the 1100-0 aluminum specimen at 67 m/s at $\alpha = 11°$ causing the crater shown. (B) Profile of impact taken along section line X-X. (C) Stereo pair of damage (use viewer provided in Metals Handbook, Vol. 9).

Fig. 7. (A) Impact damage on 1100-0 aluminum the result of a single 1100 μm diameter. SiC particle with initial velocity of 67 m/s and at angle of incidence of 15°. (B) Crater profile along section X-X. (C) Stereo photographs (use viewer provided in Metals Handbook, Vol.9).

Fig. 8. (A) Damage of 1100-0 aluminum specimen due to 1100 μm diameter. SiC particle at $\alpha = 20°$ and initial velocity of 67 m/s. (B) Stereo photographs of damage (use viewer provided in Metals Handbook, Vol. 9).

Fig. 9. (A) Photograph of 1100-0 aluminum specimen damaged by SiC particle with 1100 μm diameter at $\alpha = 30°$ and with initial velocity of 67 m/s.

(B) Crater profile along section X-X. (C) Stereo view of impact crater (use viewer provided in Metals Handbook, Vol. 9).

Fig. 10. (A) Single impact crater in 1100-0 aluminum the results of SiC particle (1100 μm diameter) striking the surface at α = 60° and at 67 m/s. (B) Profile of crater through approximate centerline. (C) Stereo pairs of damage (use viewer found in Metals Handbook, Vol. 9).

Fig. 11. (A) Damage to 1100-0 aluminum specimen due to 1100 μm diameter SiC particle with angle of impingement of 90° and initial velocity of 67 m/s. (B) Profile of crater through section X-X. (C) Stereo photographs of crater (use viewer provided in Metals Handbook, Vol. 9).

Fig. 12. Plot of normalized erosion as a function of the angle of incidence, and also shown is velocity exponent n for several angles.

Fig. 13. Normalized experimental and predicted erosion (g/g) results as a function of the angle α.

Fig. 14. Plot of erosion per particle (gm/part) as a function of angle of incidence (α) for experimental and predicted results.

Fig. 15. Single particle crater profiles found experimentally and predicted for α = 10°.

Fig. 16. Plot of crater profiles found experimentally and predicted by the analysis for α = 30°.

Fig. 17. For single impacts, a plot of the predicted plastic flow stress as a function of the angle α.

Fig. 18. Weight loss (gms) plotted as a function of the amount of SiC abrasive.

Fig. 19. Plot of erosion (gms) as a function of the amount of silicon carbide abrasive.

Fig. 20. (A) Two-dimensional picture of angular particle removing material. (B) Forces acting on particle during material removal process as used in the modified analysis. (C) Location of forces acting on particle assuming an included angle of about 120°.

Fig. 21. Single particle crater profiles for representative experimental results and profiles predicted by original and modified analysis at (A) $\alpha = 10$ and (B) $\alpha = 30°$. Results are scaled such that the maximum depth of cut for experimental and predicted results are equal for a given α. Experimental curves correspond to the dash-dot curves in Fig. 15 and 16.

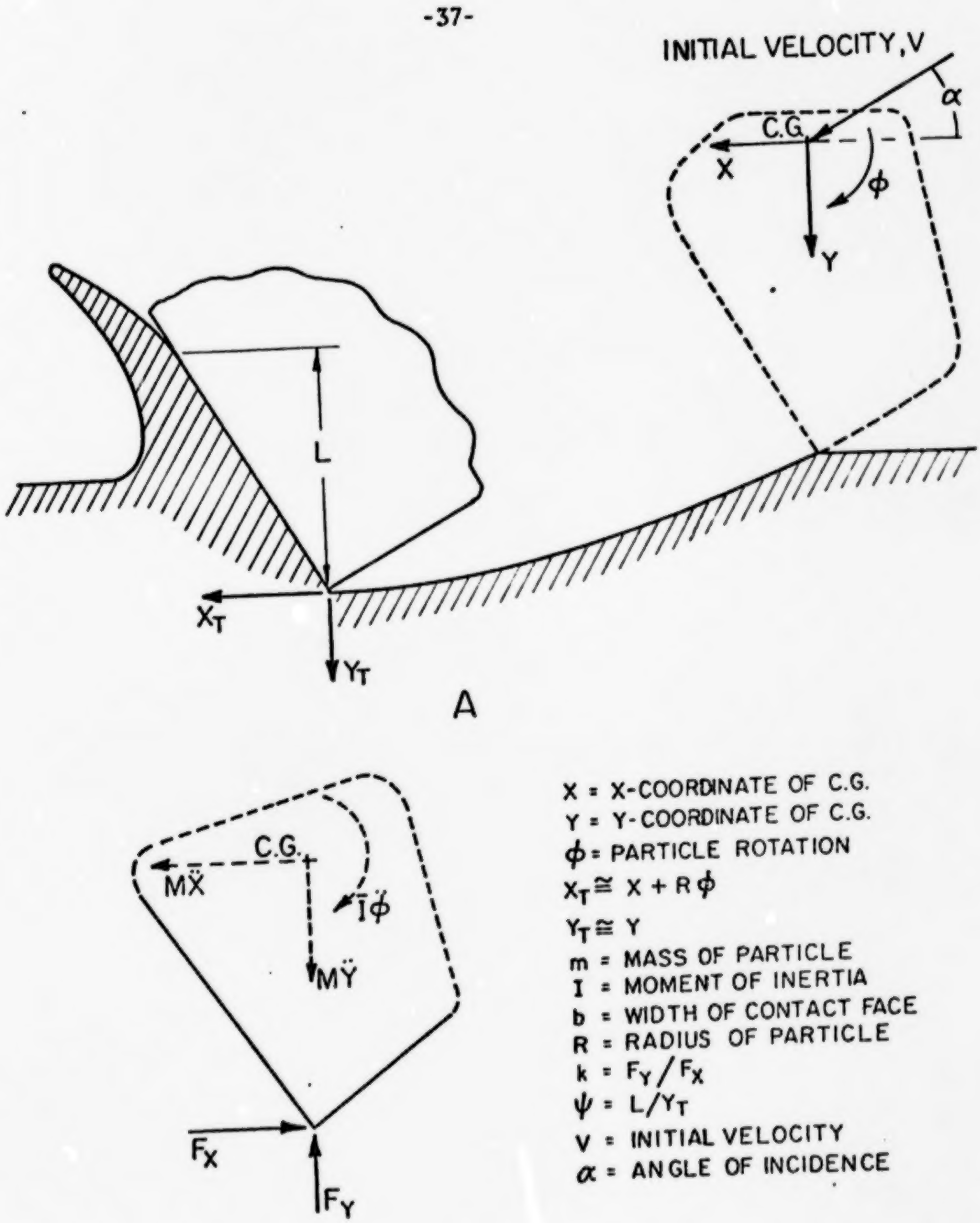
INITIAL VELOCITY, V
α
C.G.
X
φ
Y
L
X_T
Y_T
A
C.G.
$M\ddot{X}$
$\bar{I}\ddot{\phi}$
$M\ddot{Y}$
F_X
F_Y
B
X = X-COORDINATE OF C.G.
Y = Y-COORDINATE OF C.G.
φ = PARTICLE ROTATION
$X_T \cong X + R\phi$
$Y_T \cong Y$
m = MASS OF PARTICLE
I = MOMENT OF INERTIA
b = WIDTH OF CONTACT FACE
R = RADIUS OF PARTICLE
$k = F_Y / F_X$
$\psi = L / Y_T$
V = INITIAL VELOCITY
α = ANGLE OF INCIDENCE

XBL775-5526

Fig. 1

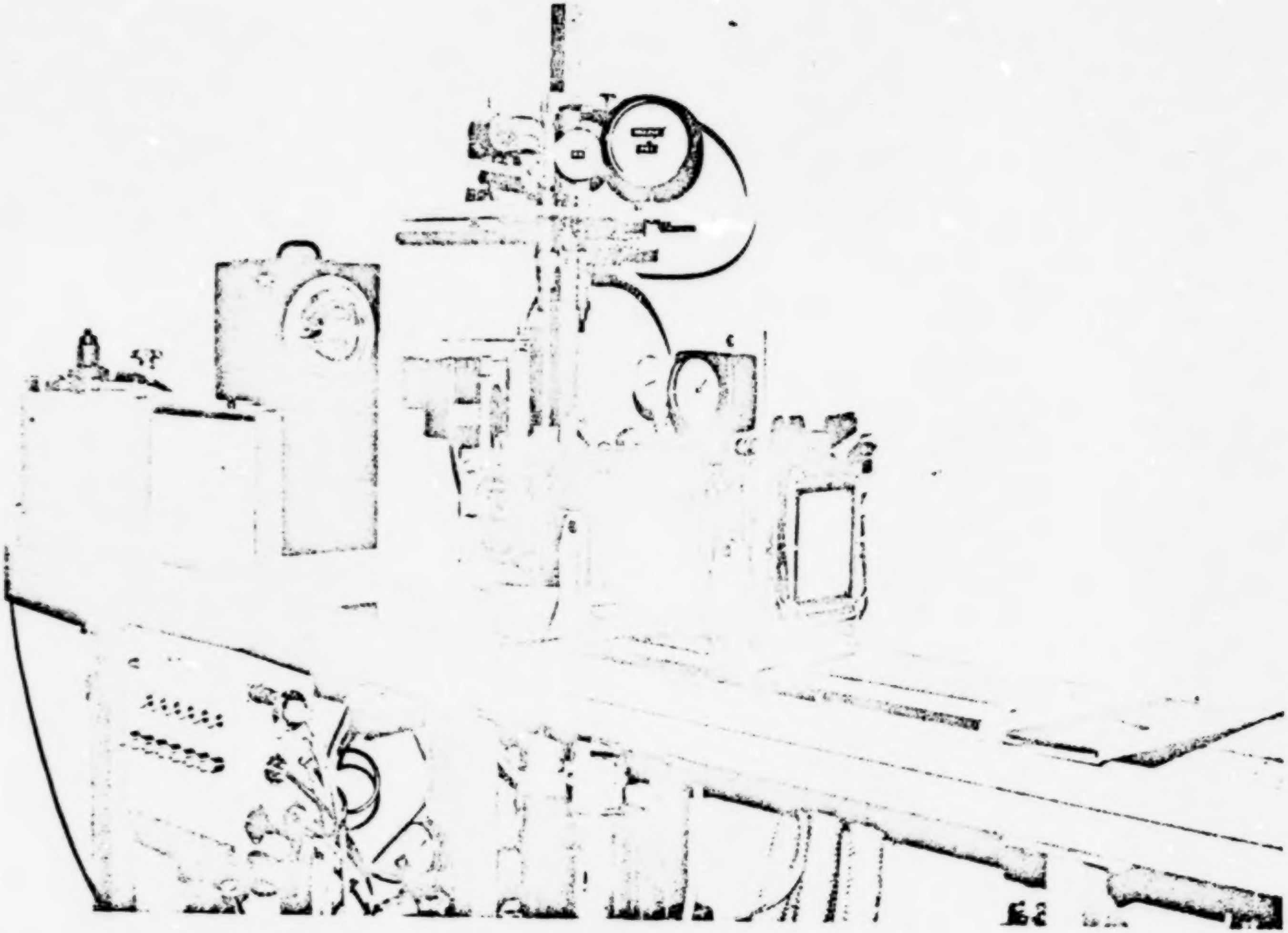

Fig. 2

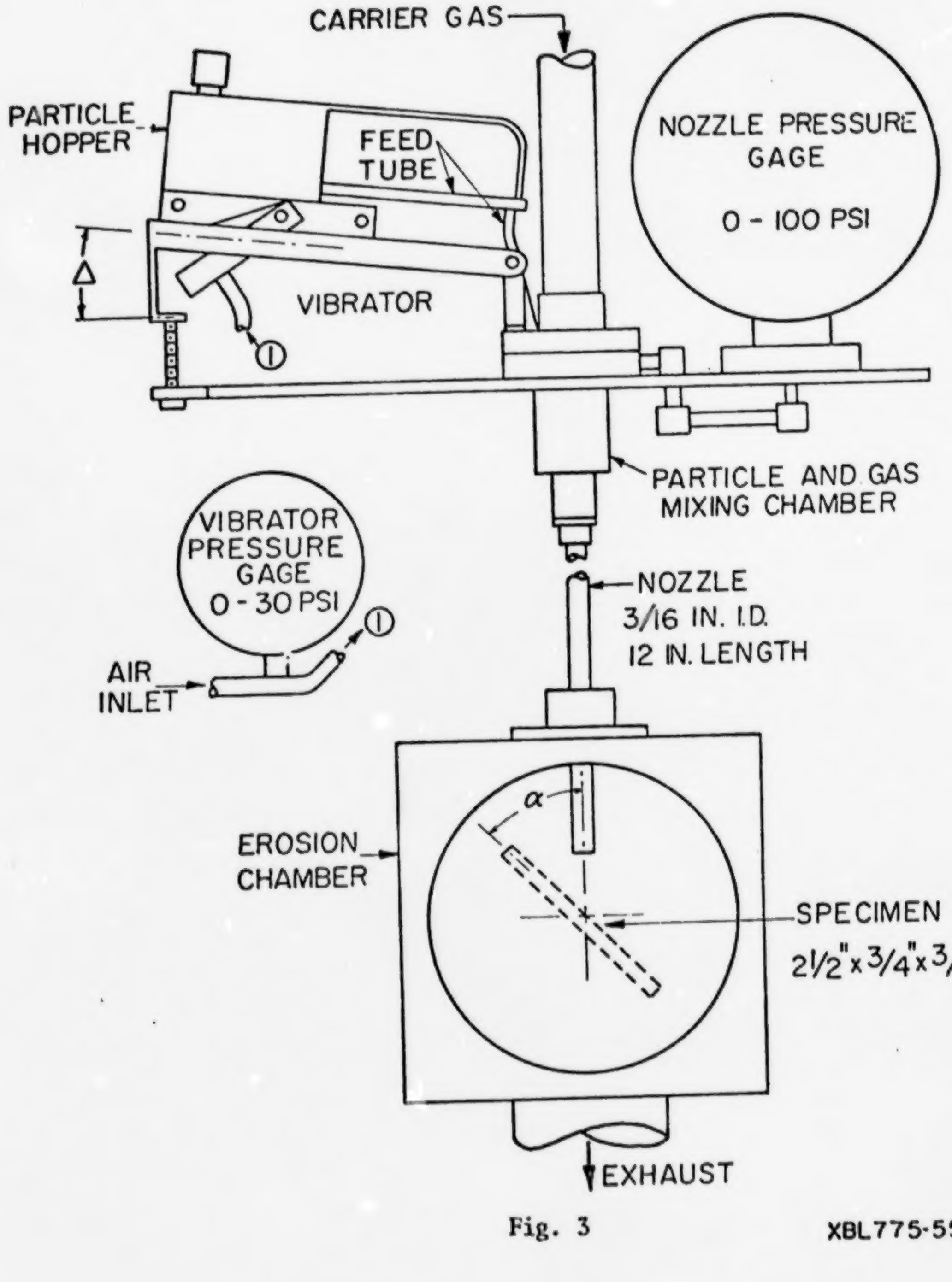
CARRIER GAS
PARTICLE HOPPER
FEED TUBE
NOZZLE PRESSURE GAGE
0 - 100 PSI
Δ
VIBRATOR
①
PARTICLE AND GAS MIXING CHAMBER
VIBRATOR PRESSURE GAGE
0 - 30 PSI
①
AIR INLET
NOZZLE
3/16 IN. I.D.
12 IN. LENGTH
α
EROSION CHAMBER
SPECIMEN
2½"x¾"x3/16"
EXHAUST

Fig. 3

XBL775-5525

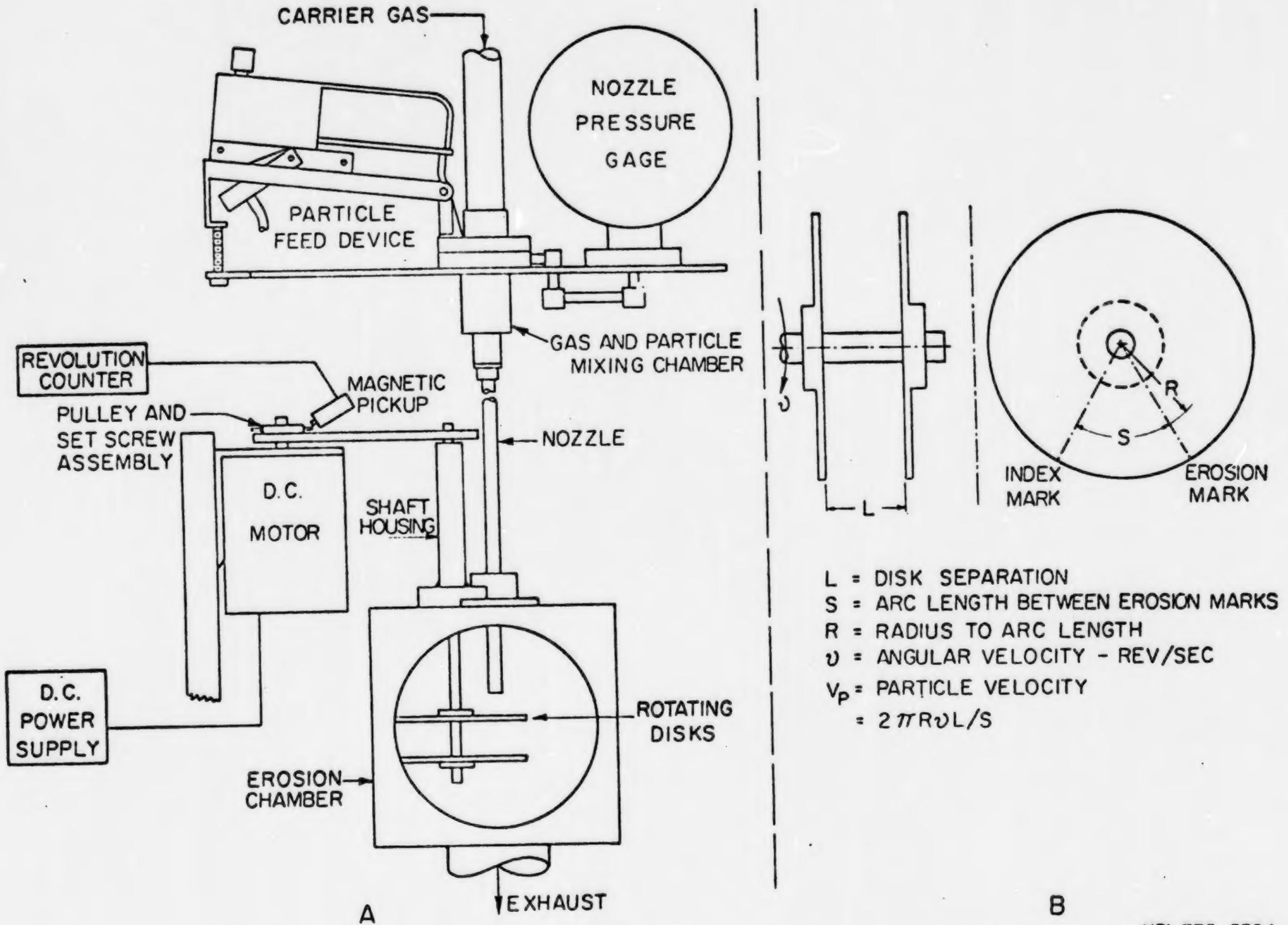
CARRIER GAS
NOZZLE PRESSURE GAGE
PARTICLE FEED DEVICE
GAS AND PARTICLE MIXING CHAMBER
REVOLUTION COUNTER
MAGNETIC PICKUP
PULLEY AND SET SCREW ASSEMBLY
NOZZLE
D.C. MOTOR
SHAFT HOUSING
D.C. POWER SUPPLY
ROTATING DISKS
EROSION CHAMBER
EXHAUST
A
υ
L
R
S
INDEX MARK
EROSION MARK
L = DISK SEPARATION
S = ARC LENGTH BETWEEN EROSION MARKS
R = RADIUS TO ARC LENGTH
υ = ANGULAR VELOCITY - REV/SEC
V_P = PARTICLE VELOCITY
= 2πRυL/S
B

Fig. 4

XBL 775-5524

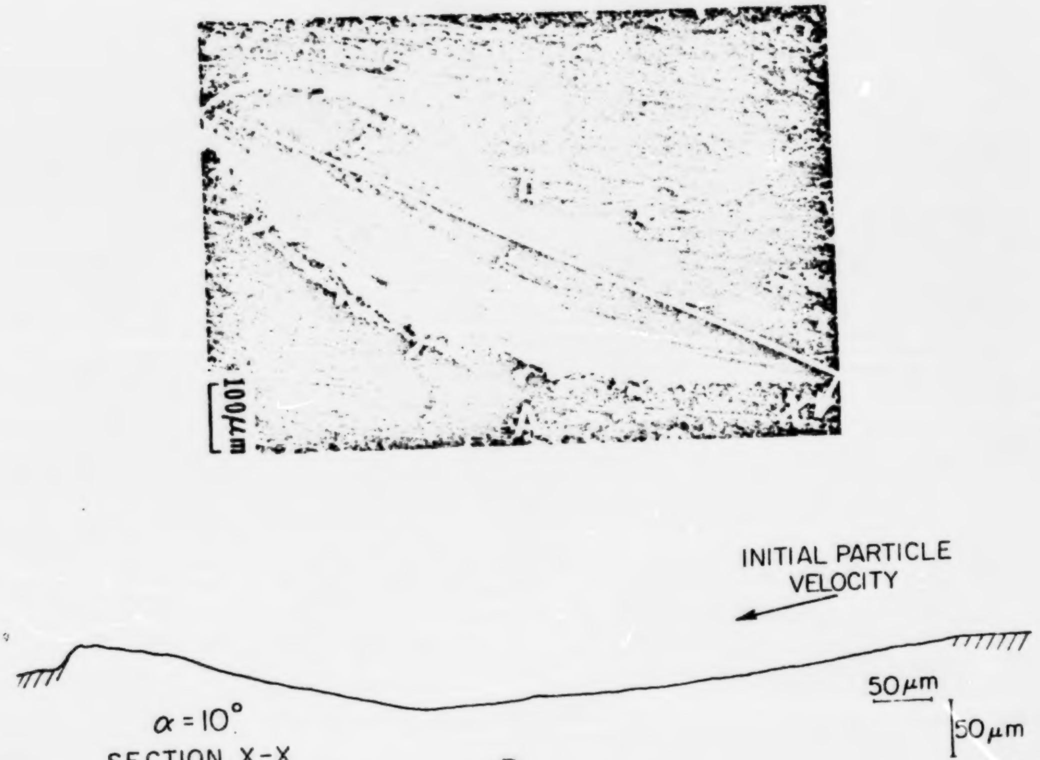
100μm
INITIAL PARTICLE VELOCITY
50μm
50μm
α = 10°
SECTION X-X
B
100μm
100μm

Fig. 5

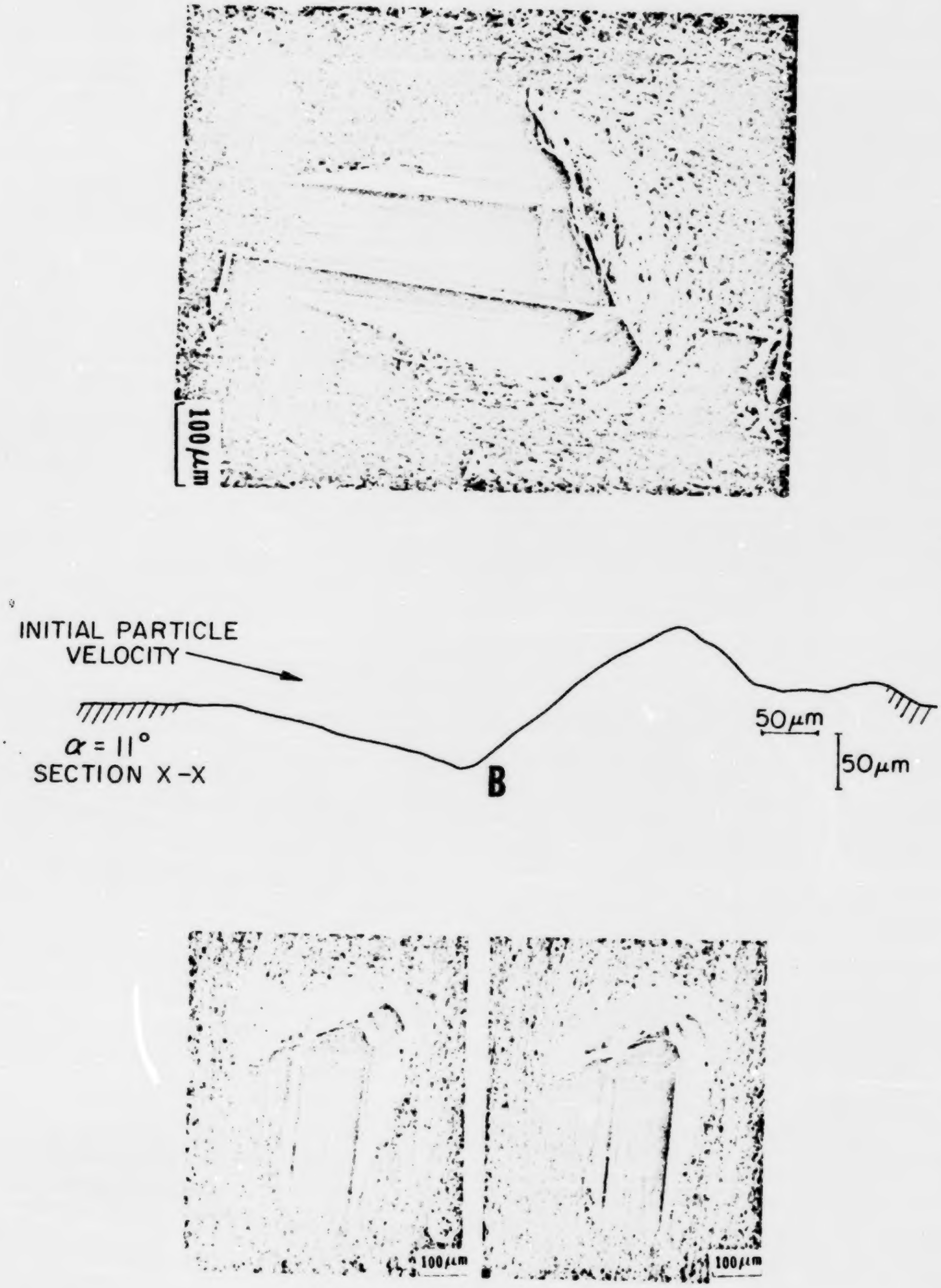
100µm
INITIAL PARTICLE VELOCITY
α = 11°
SECTION X-X
B
50µm
50µm
100µm
100µm

Fig. 6

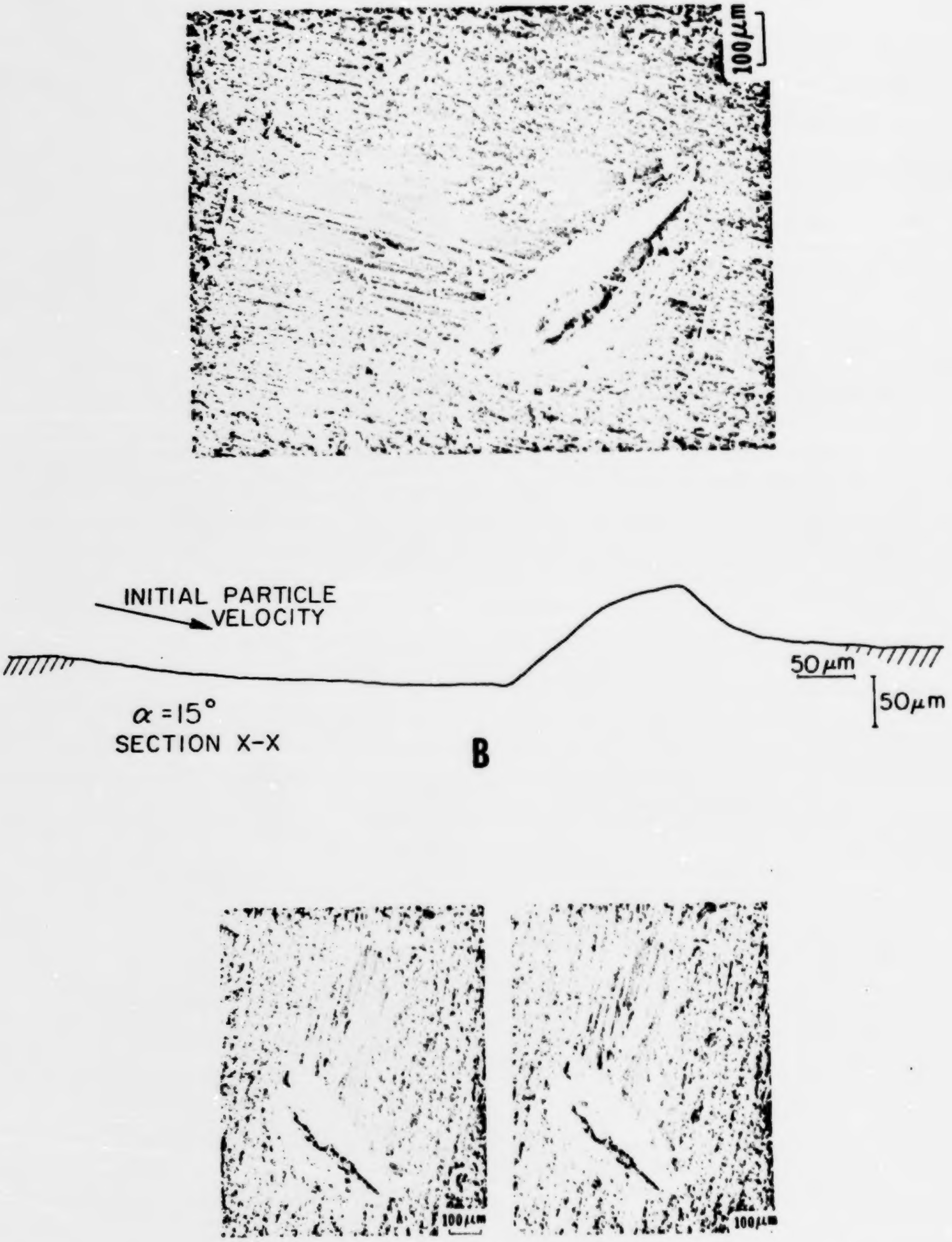
100μm
INITIAL PARTICLE
VELOCITY
50μm
50μm
α =15°
SECTION X-X
B
100μm
100μm

Fig. 7

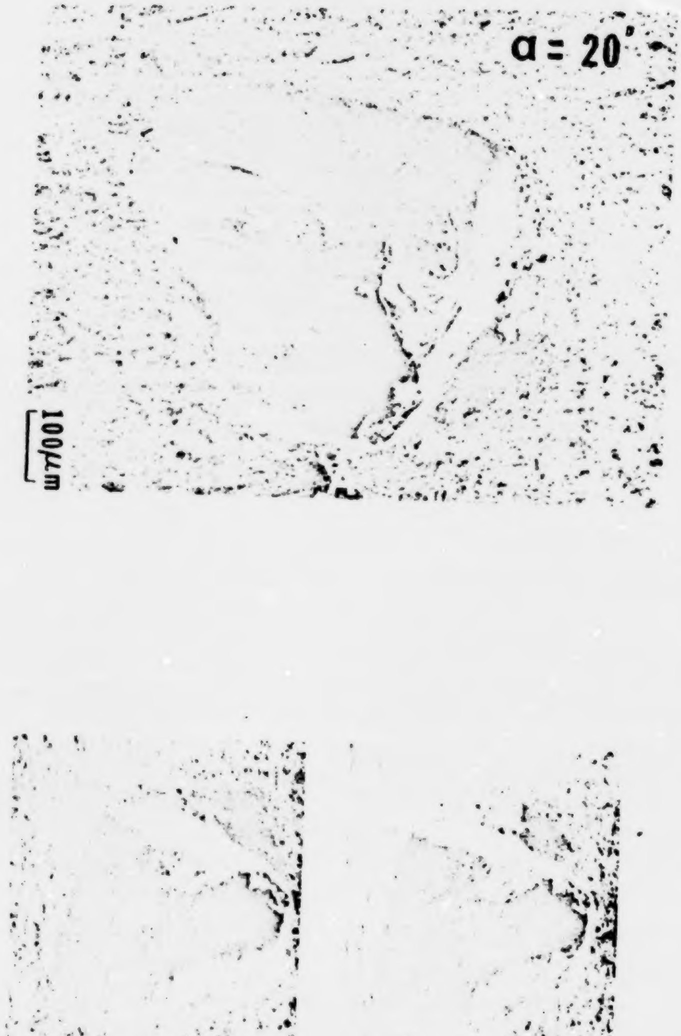
α = 20°
100μm
100μm
100μm

Fig. 8

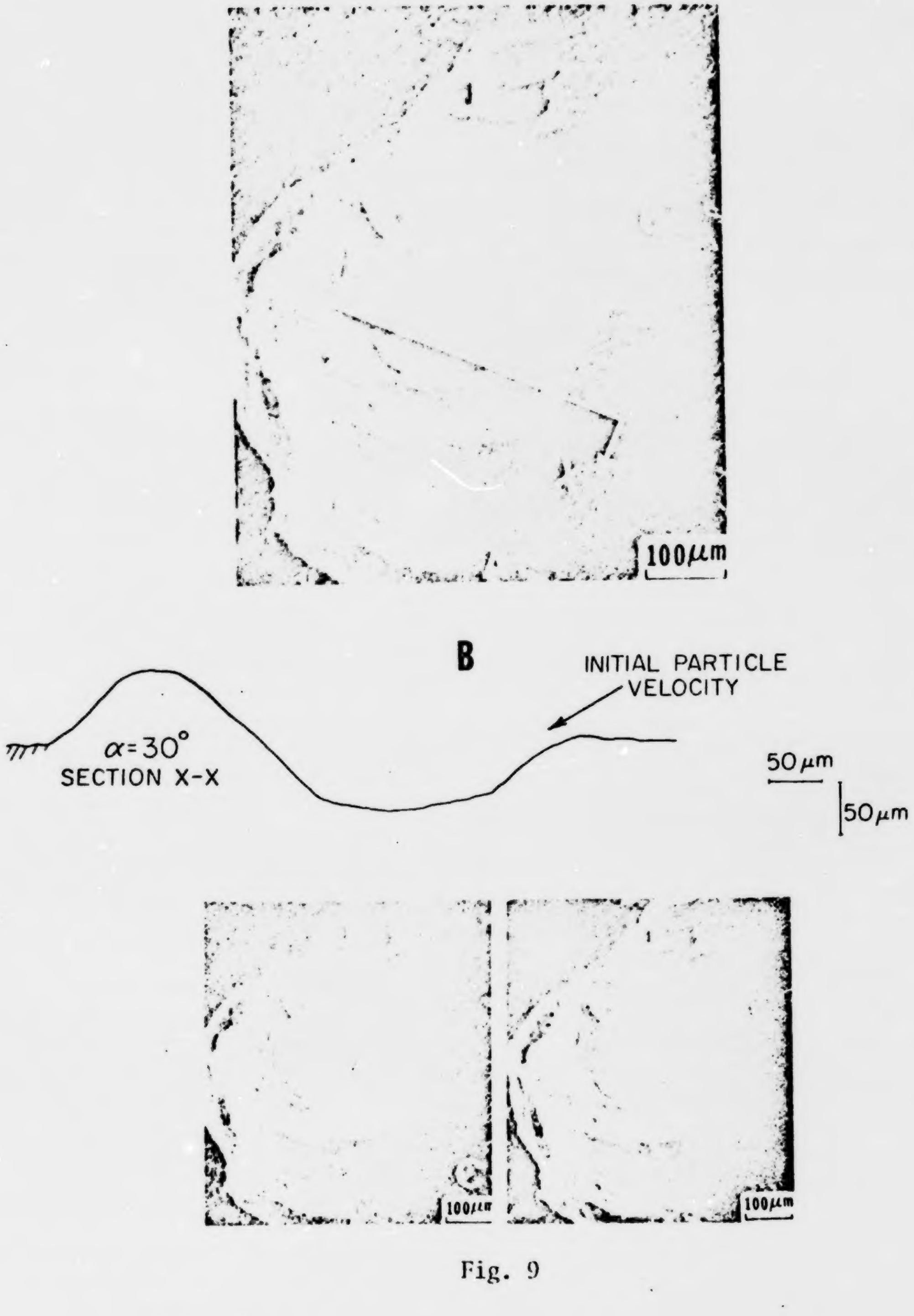
100μm
B
INITIAL PARTICLE VELOCITY
α=30°
SECTION X-X
50μm
50μm
100μm
100μm

Fig. 9

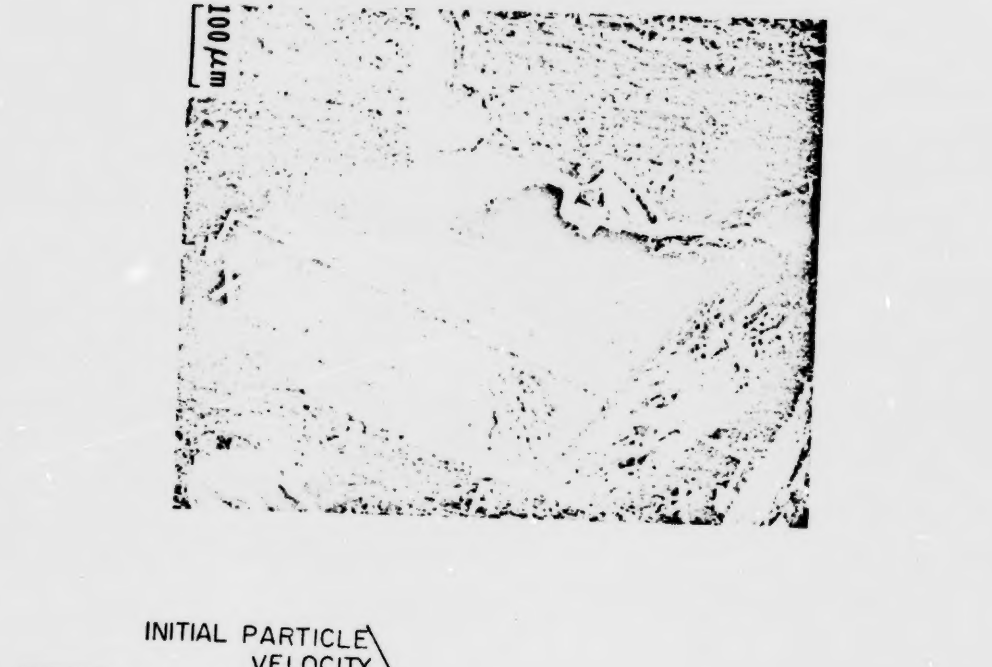
100 µm
INITIAL PARTICLE VELOCITY
α = 60°
SECTION X-X
B
50 µm
50 µm
100µm
100µm

Fig. 10

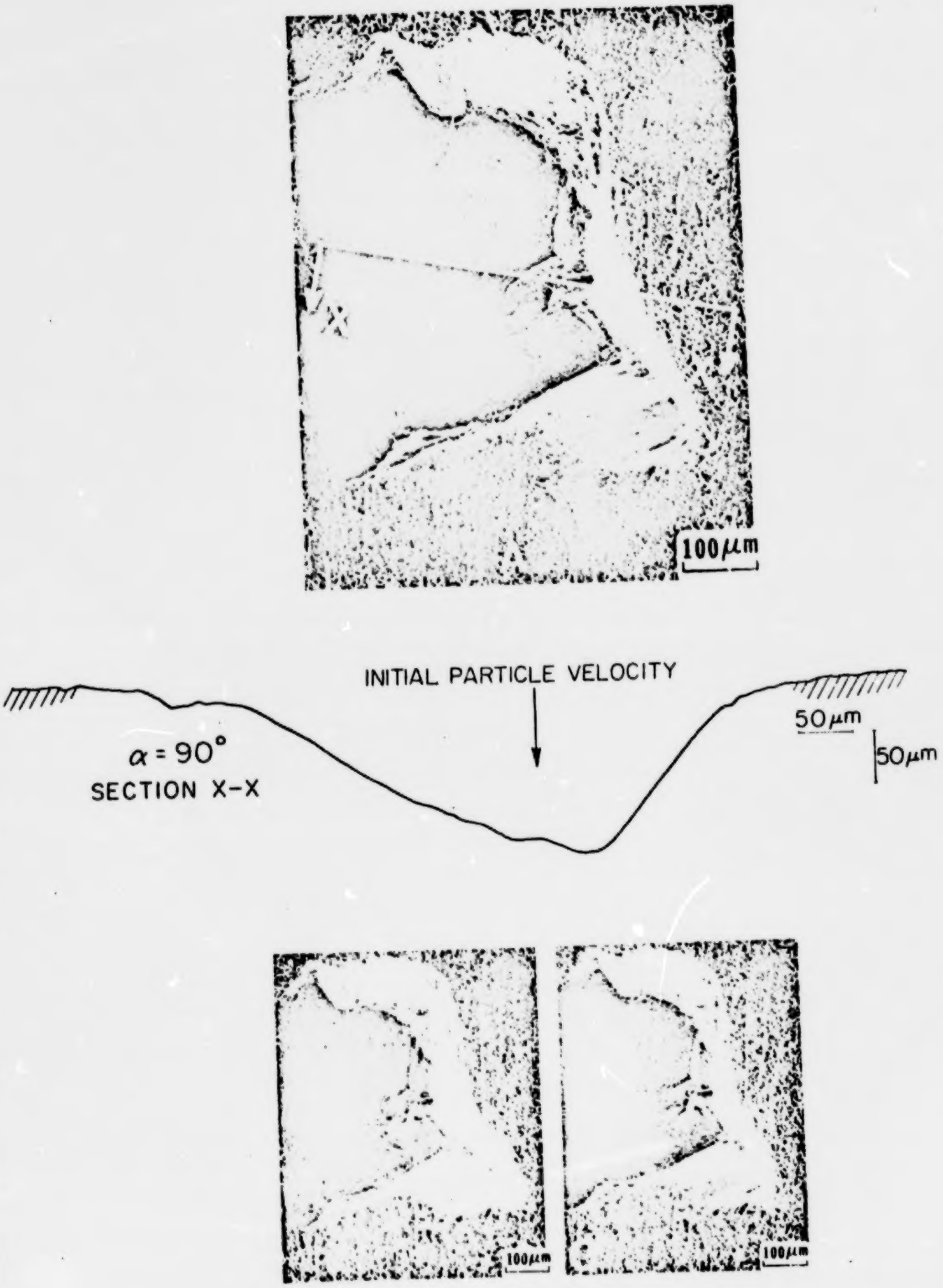
X
100μm
INITIAL PARTICLE VELOCITY
α = 90°
SECTION X-X
50μm
50μm
100μm
100μm

Fig. 11

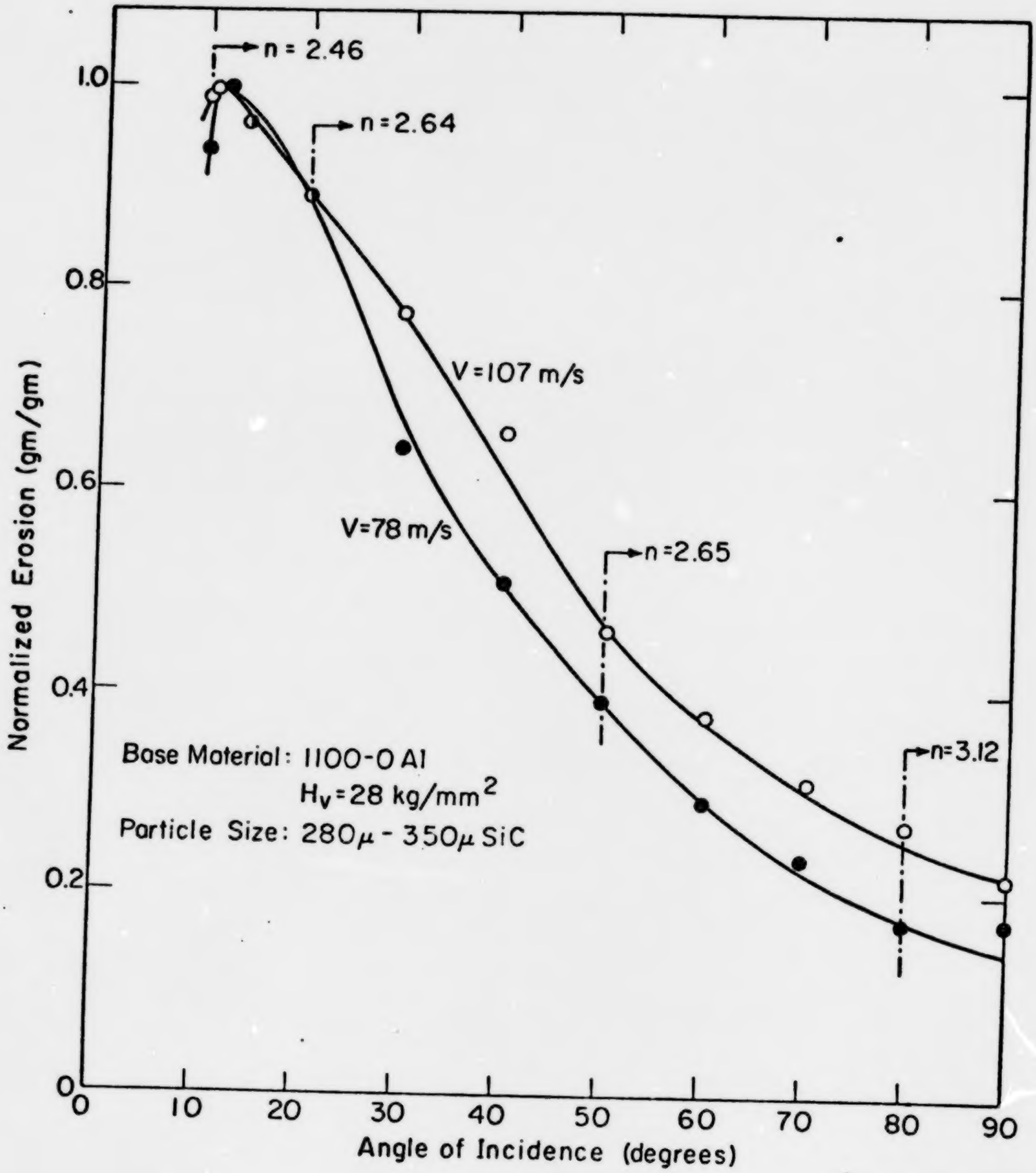

Fig. 12

XBL775-5522

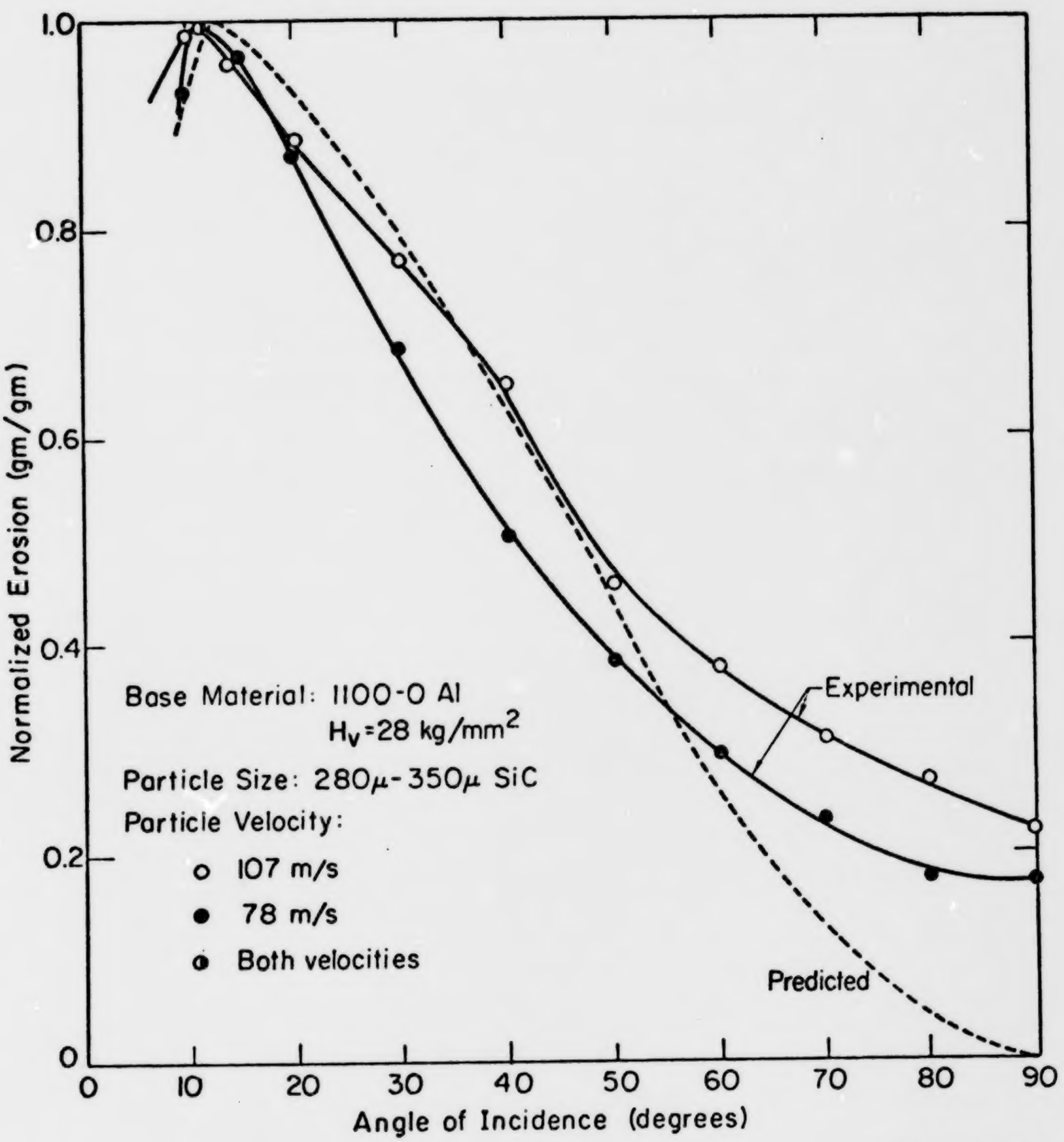

XBL775-5521

Fig. 13

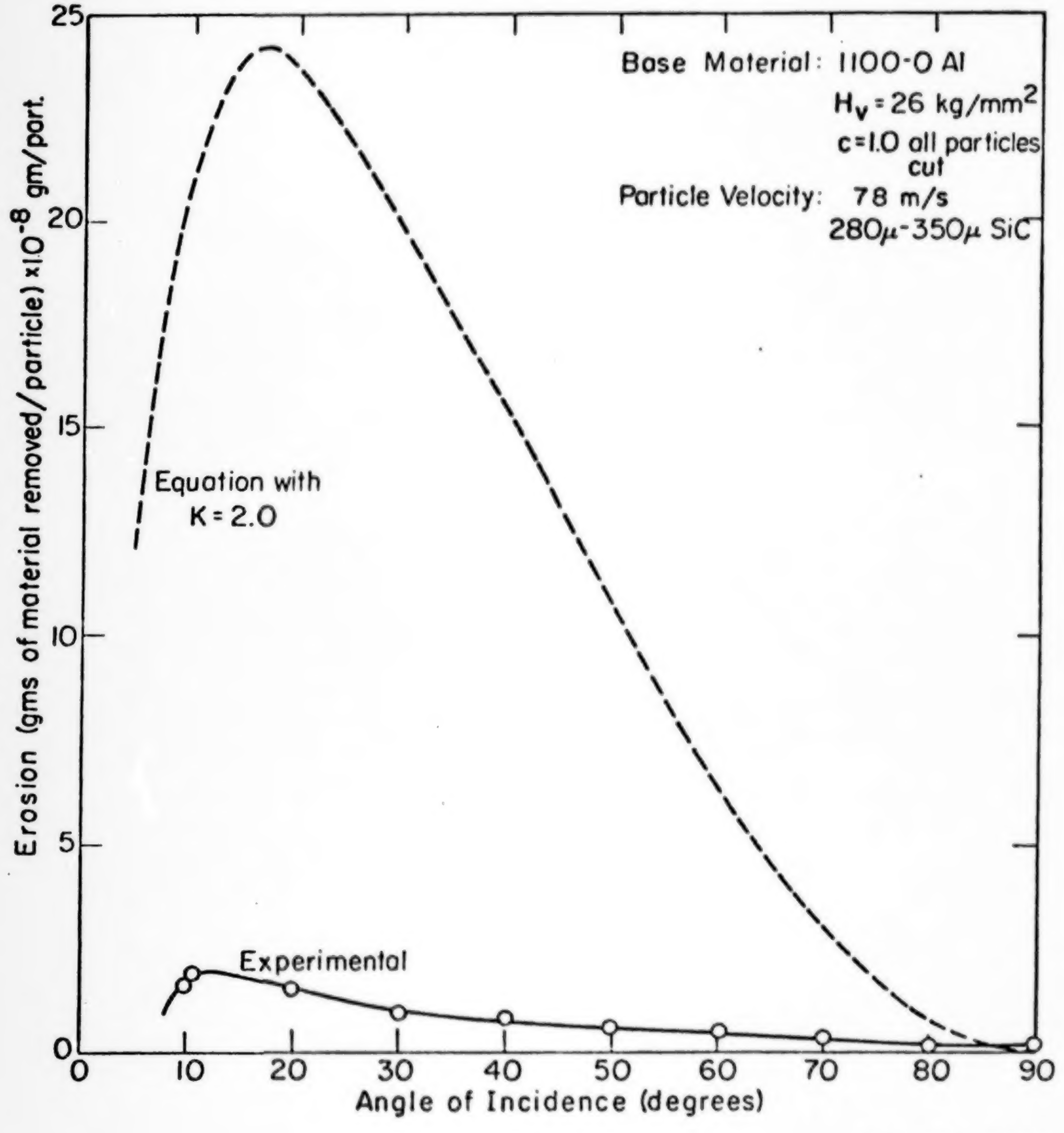

Fig. 14

XBL 775-5523

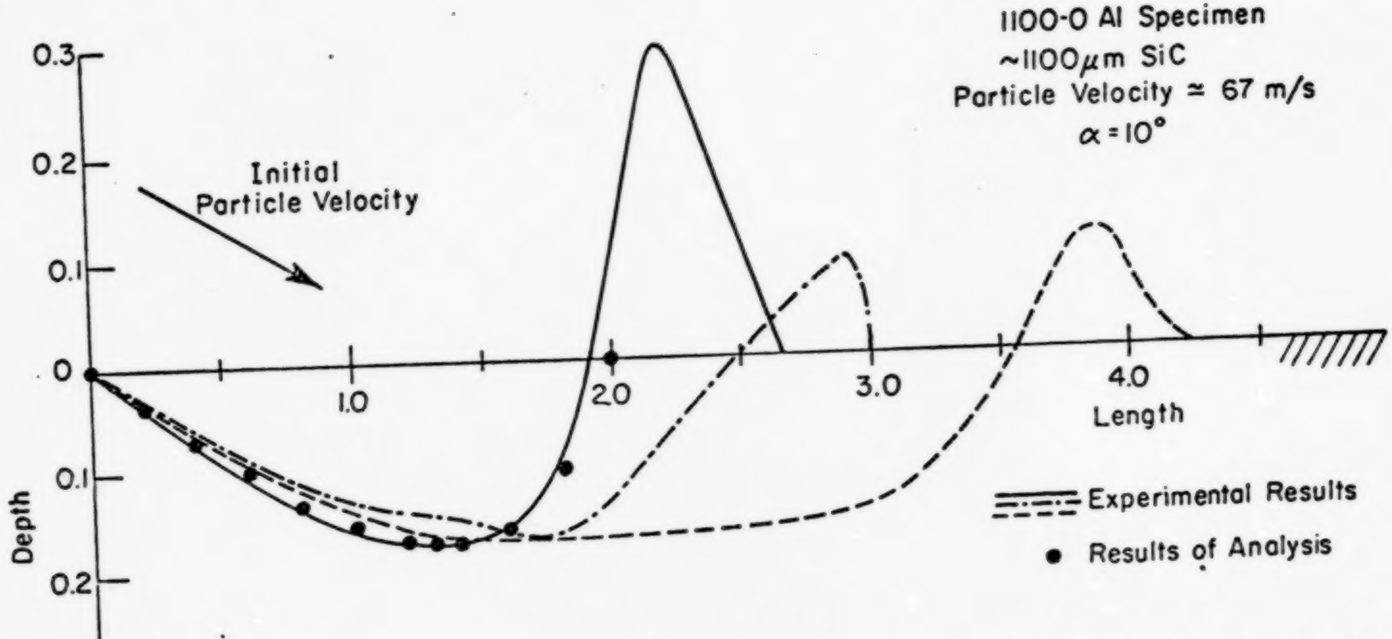

XBL 775-5528

Fig. 15

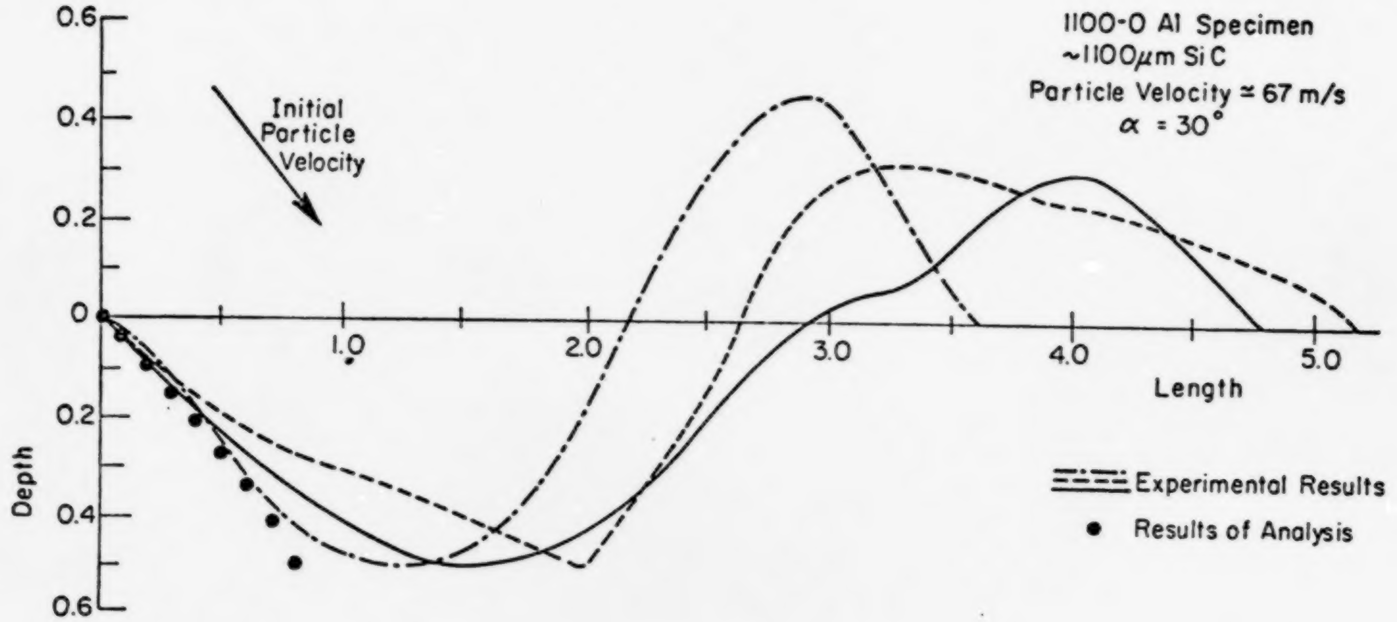

Fig. 16

XBL 775-5529

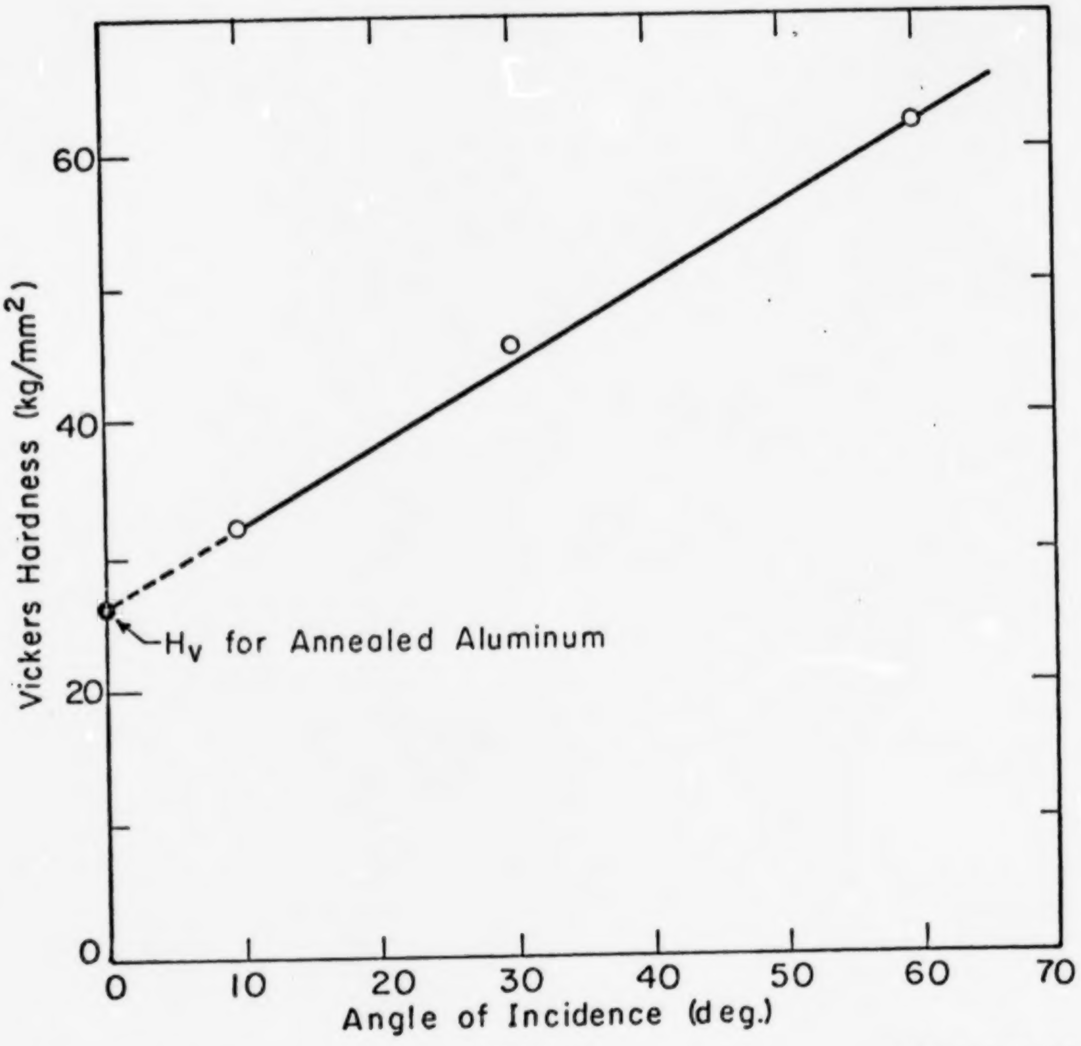

Fig. 17

XBL775-5519

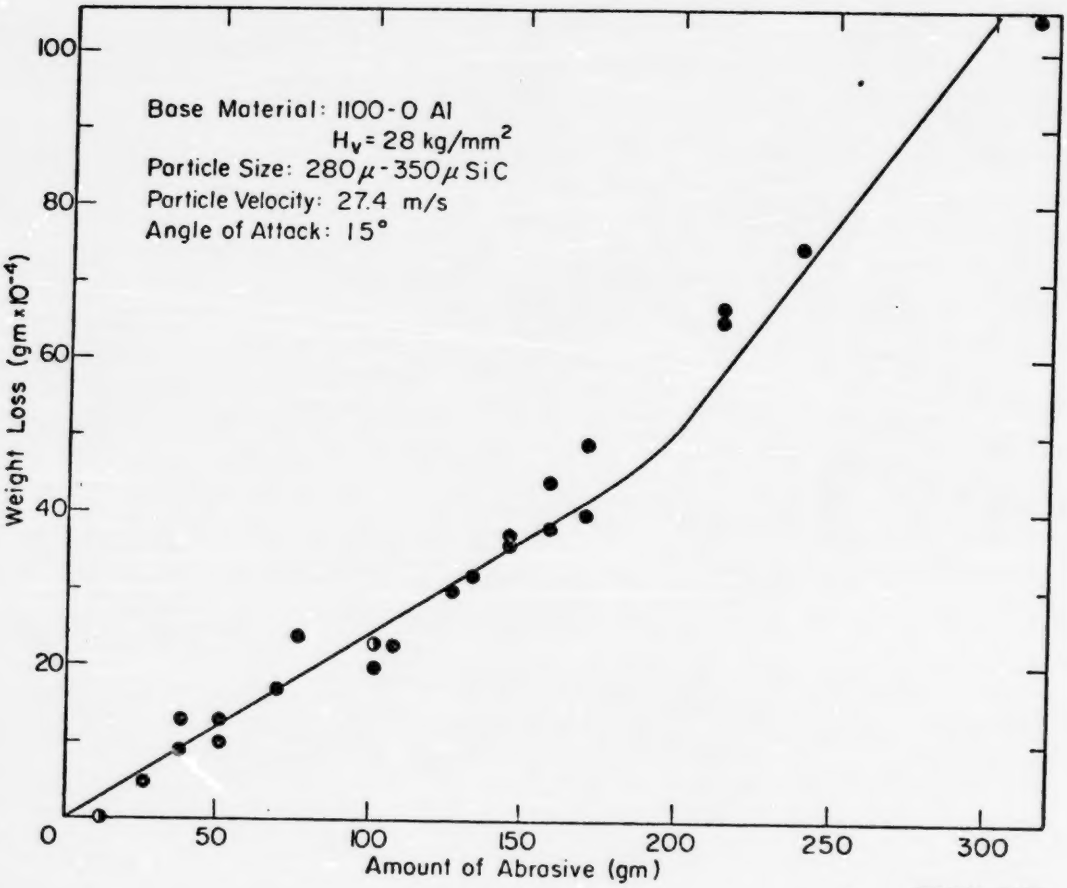

XBL775-5520

Fig. 18

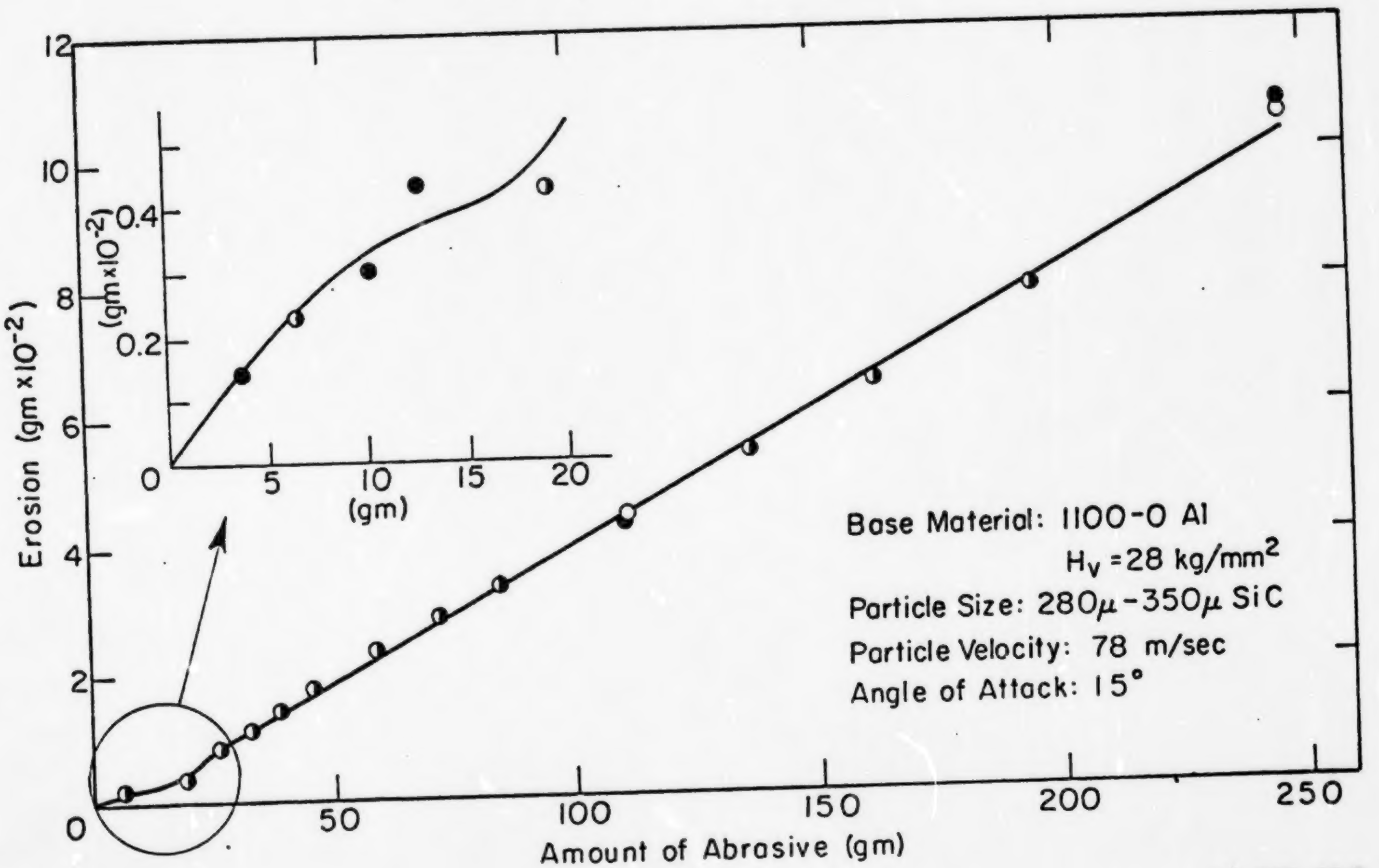

XBL775-5518

Fig. 19

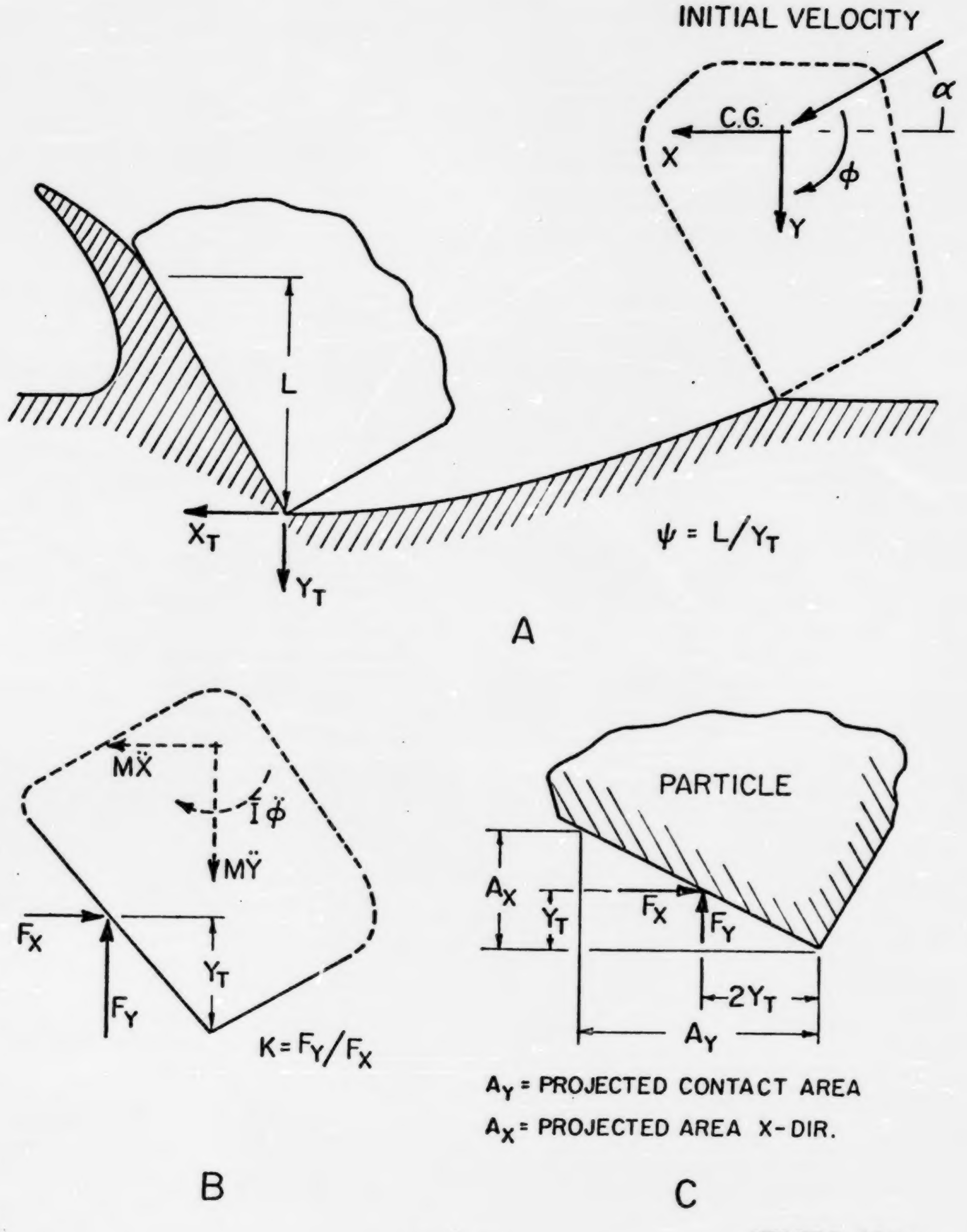
INITIAL VELOCITY
α
C.G.
X
φ
Y
L
X_T
Y_T
$\psi = L/Y_T$
A
$M\ddot{X}$
$I\ddot{\phi}$
$M\ddot{Y}$
F_X
F_Y
Y_T
$K = F_Y/F_X$
B
PARTICLE
A_X
Y_T
F_X
F_Y
$2Y_T$
A_Y
A_Y = PROJECTED CONTACT AREA
A_X = PROJECTED AREA X-DIR.
C

Fig. 20

XBL775-5527

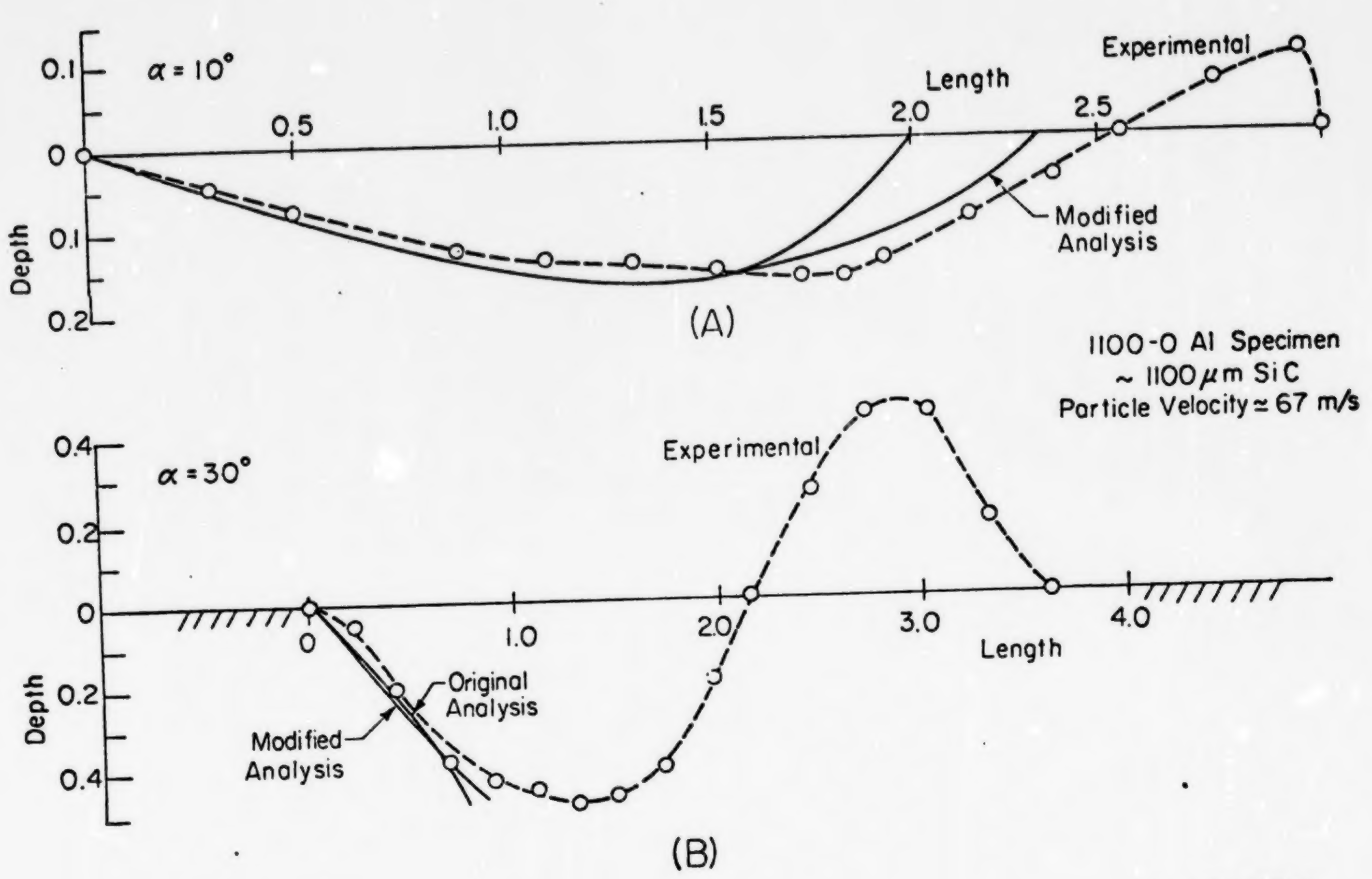

XBL775-5530

Fig. 21

Reprinted from ENGINEERING FOR POWER, *Vol. 102, No. 1, January 1980*

Study of Metals Erosion in High Temperature Coal Gas Streams

W. Tabakoff
Professor.
Mem. ASME

A. Hamed
Associate Professor.
Mem. ASME

J. Ramachandran
Graduate Research
Assistant.

Department of Aerospace Engineering,
University of Cincinnati,
Cincinnati, OH 45221

In order to provide the basis for alloy selection in future turbines using pulverized coal, an investigation is undertaken to obtain a basic understanding of the mechanisms of erosion at high temperatures. The test equipment has been designed to simulate the aerodynamic and thermodynamic conditions in the turbine. This facility has the capability of providing between ambient and a 1093°C (2000°F) environment temperature for erosion testing of various materials. The effects of high temperature on the erosion rate was determined and the test results from 304 stainless steel alloy are presented.

Introduction

The use of pulverized coal as fuel in many power plants and industrial establishments is inevitable both in the present and in the future. The products of combustion will contain solid particles, whose presence cause erosion of the engine components and in a very short time possible deterioration of the power output. Filtration cannot accomplish a 100 percent removal of the particles and results in performance reduction. In coal gasification both the coal and the catalyst contribute to the resulting particulate flow. While larger particles can be removed by cyclones, a quantity of particles ranging in size between 5 and 25 μm dia still pass through the cyclones and enter the turbine resulting in a very limited life of this component.

The design and development of high performance turbomachinery operating in an ambient with coal particles or coal ash therefore requires a thorough knowledge of the fundamental erosion phenomena. The future of advanced turbomachinery for use in the coal industry, gasification, mining, pipelines' gas transport, powder coal burning, coal-oil gas refinery, and many others is dependent upon this understanding. If erosion could be incorporated as an engine design parameter, perhaps an erosion tolerant engine could be produced.

Two problems are involved in erosion prediction. First the velocity, direction, and number of particles striking the surface must be determined. These are naturally affected by the general and local flow conditions. The second part involves the calculation of the surface material removed using the information obtained from the first part. The problem of predicting erosion in rotating machinery is particularly complexed by tracing trajectories through the flow field after multiple impacts [1].

Present State of the Art

The theoretical studies concerning erosion are predominantly empirical. They involve basic assumptions as to the process governing material removal. Finnie [2] and Smeltzer, et al. [3] have conducted theoretical analyses of the erosion of ductile materials. In more recent investigations [1, 4, 5], further insight into the actual mechanism of erosion has been obtained by examining the target surface at high magnification using metallographic techniques and electron microscopy. The work reported in [2-5] has been conducted using the sand-blasting erosion test facility described in [5] or modifications of it. This facility utilizes a small jet of particle-laden air impacting on a stationary specimen, and therefore does not simulate the aerodynamic effect of the flow field over the erosion specimen. This effect can be a very important factor in turbomachine erosion, where the flow is constantly turned by rotating and stationary cascades. Two cold gas particle erosion test facilities have been built at the University of Cincinnati's Propulsion Laboratory. The first was designed to obtain basic erosion data, particle impact, and rebound characteristics for particulate flow over a stationary specimen. Another test facility was then designed to simulate and measure the erosion of stationary and rotating turbomachine blades. A detailed description of these test facilities can be found in [1] and [6].

In many turbomachinery applications, however, erosion takes place at elevated temperatures near the strength limiting temperatures of the materials used. For example, even in the case of turbojet engine compressors, titanium used in the early stages and the INCO 718 used in the aft stages are operated at metal temperatures in excess of 316°C and 593°C (600°F and 1100°F), respectively. In both cases, these temperatures are very close to the maximum operating temperatures used for these materials. The erosion characteristics can significantly change under elevated temperatures as evidenced in the data presented by Tabakoff and Hamed [6]. These data were obtained in the facility used by [1], with the sample heated to temperatures up to 204°C (400°F). Although this temperature falls far short of those experienced in turbine engines, it still indicates the significant effect of temperature on erosion and probably on the rebound characteristics.

High Temperature Erosion Rig

An erosion test facility was designed to provide erosion and rebound data in the range of operating temperatures experienced in compressors and turbines. For that purpose, this facility has been designated to operate at a test section temperature in the range of ambient to 1093°C (2000°F). In addition to high temperatures, the facility

---

Contributed by the Gas Turbine Division and presented at the Gas Turbine Conference and Exhibit and Solar Energy Conference, San Diego, California, March 12-15, 1979 of THE AMERICAN SOCIETY OF MECHANICAL ENGINEERS. Manuscript received as ASME Headquarters December 18, 1978. Paper No. 79-GT-88.

properly simulates all erosion parameters which were found to be important from previous testing at ambient temperatures. These parameters include particle velocity, angle of impact, particle size, particle concentration and sample size.

As with the cold flow erosion test facility, close attention was given to aerodynamic effects to insure that important parameters such as angle of attack are not masked or altered. To insure the correlation of data from the high and low temperature erosion tunnels, flowpath and acceleration tunnel length were kept almost identical with those of the facility described in [6]. The cross section was increased, however, from 76.2 mm × 25.5 mm to 88.9 mm × 25.4 mm (3 in. × 1 in. to 3½ 1n. × 1 in.) in order to reduce the tunnel blockage by the test sample.

General Description of the Erosion Rig. The schematic of the test apparatus is shown in Fig. 1. It consists of the following components: particle feeder (A), main air supply pipe (B), combustor (C), particle preheater (D), particle injector (E), acceleration tunnel (F), test section (G), and exhaust tank (H).

The equipment functions as follows: a measured amount of abrasive grit of a given constituency is placed into the particle feeder. The particles are fed into a secondary air source and blown up to the particle preheater, and then to the injector, where it mixes with the main air supply (B), which is heated by the combustor. The particles are accelerated by the high velocity air in a constant area duct, which is steam cooled, before impacting the specimen in the test section. Past the test section, the particulate flow is mixed with the coolant, and dumped in the exhaust tank. The expected range of testing parameters are listed in Table 1, but they are not necessarily restricted to the tabulated values.

The individual components of the high temperature erosion facility are described below. Each component was designed with cost, maintainability, availability and functionality as prime considerations.

Particle Feeder Assembly (A). The particles from the feeder are blown up to the particle injector area. The feeder (Fig. 2) is designed as a pressure vessel to operate at high air pressures. However, this pressure is equalized above and below the plunger by a by-pass line. This allows the system to be calibrated under gravity feed conditions. Further, an electric eye records the plunger rpm such that the operating conditions are maintained. The metering orifice is designed to be replaceable for greater versatility through using variable size orifices, along with corresponding rod diameter.

Main Air Supply (B). This air is drawn from air tank storages to allow continuous testing.

Combustor (C). High temperature combustion products are supplied by a modified General Electric J93 can combustor. The J93 can is encased in a 228.6 mm (9 in.) ID stainless steel pipe with provisions for the fuel nozzle and igniter. A system consisting primarily of a propane fired torch containing a spark plug was used for the fuel ignition. Due to heat loss in the acceleration tunnel, a combustor exit temperature of 1204.4°C (2200°F) is required in order to maintain the maximum test section temperature at 1093°C (2000°F). The J93 can combustor was modified to obtain this exit temperature. The modifications include using a large fuel nozzle and blanking off most of the downstream dilution air ports. A smaller fuel nozzle is used for tests involving low combustion temperatures in the range of 93°C (200°F) through 260°C (500°F).

Particle Preheater (D) and Injector (E). The preheater consists of a coil contained in a 203.2 mm (8 in.) ID pipe section with a distributor/injector to provide a well distributed preheated particle supply. The particles are blown up to the accelerating section of the tunnel by secondary air which flows from the particle feeder and passes through the preheater coils. As the particulate air mixture passes through the coils, it is heated by the combustion products to a temperature of 538°C (1000°F) before being injected into the tunnel. The particles are distributed in the main air stream through their impingements on a specially contoured ball. The particle gas mixture is accelerating through an elliptical nozzle to the acceleration section.

Acceleration Section (F). The acceleration tunnel has a rectangular cross section of 89 mm × 25.4 mm (3½ in. × 1 in.) which is

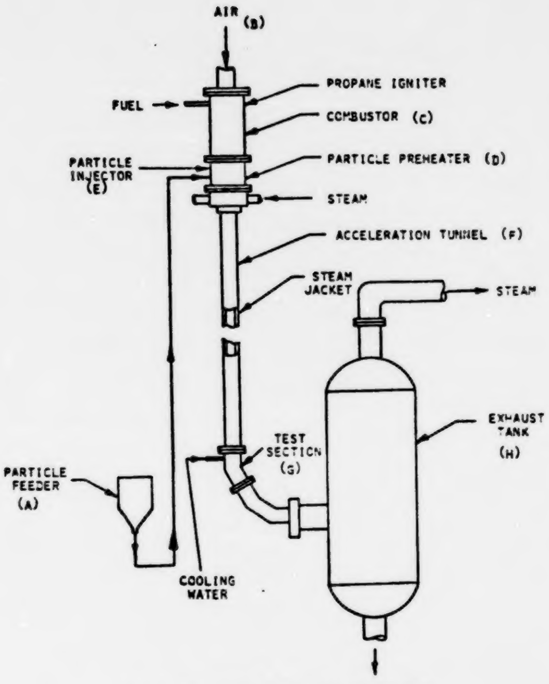

Fig. 1 Schematic of erosion test facility

Table 1 Erosion parameters

Parameters	
Temperature	10-1093°C (50-2000°F)
Particle Angle of Attack	0-90°
Particle Velocity	60-450 m/s (200-1500 ft/s)
Particle Concentration	0-5 percent
Particle Size	1μ-2000μ
Particle Type and Material	Silica Sand, Alumina, Ash and Others
Sample Size	6.35 mm-25.4 mm (¼ in.-1 in.)
Sample Material	Various Engine Materials

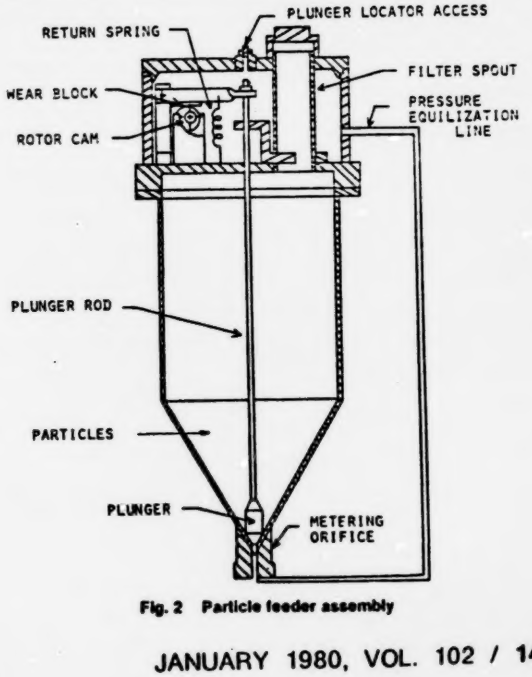

Fig. 2 Particle feeder assembly

3.66 m (12 ft) long. This section is steam cooled to minimize the heat losses. With this type of cooling, the 316 stainless steel liner operates at a maximum of 760°C (1400°F). This results in a drop in the gas stream temperature of about 93°C (200°F). The use of water as a coolant would have resulted in at least three times the heat loss and an unacceptable gas stream temperature drop in this section.

The particle velocities attained in this acceleration section were predicted analytically and verified by experimental methods. Pressure measurements at the inlet, mid-section, and exhaust were used to account for the tunnel friction when calculating the fluid velocity variation in this section. These velocities were used in calculating the particle velocities due to their acceleration by the gas stream. The calculated particle velocities are shown in Fig. 3 in the case of low fluid velocity of 122 m/s (400 ft/s) at 1093°C (2000°F) and at ambient temperature. From this figure it can be seen that the particle velocity is an exponential function of tunnel length. The law of diminishing returns would dictate that a tunnel length of 0.6 m to 0.92 m (2 to 3 ft) would be sufficient for both relatively large and small particles (200 μ and 20 μ). A tunnel length of 3.66 m (12 ft) was chosen however for several theoretical and practical reasons.

Test Section (G). The test section is designed such that the particle laden air is channeled over the specimen and the aerodynamics of the fluid surrounding the test sample are preserved. The test specimen can be oriented at different angles to the gas stream by rotating the specimen holder. The test section flowpath turns 30 deg at the plane of the test section to help turn the flow when the test specimen is oriented at an angle. The test section is water cooled, but this does not result in significant reduction in the primary gas stream temperature because of its relatively small size. The coolant water is discharged into the particulate gas stream at the downstream end of the test section.

Several interchangeable inserts can be used in this section such that the fluid profile can be determined using conventional instrumentation, and the particle impact and rebound characteristics can be recorded. A special test section with a glass window is constructed for the purpose of using photographic and L.D.V. means to measure the speeds and the angles of the impinging and rebounding particles.

Exhaust System (H). The flow leaving the test section, mixed with the cooling water, is exhausted into a settling tank. In this tank,

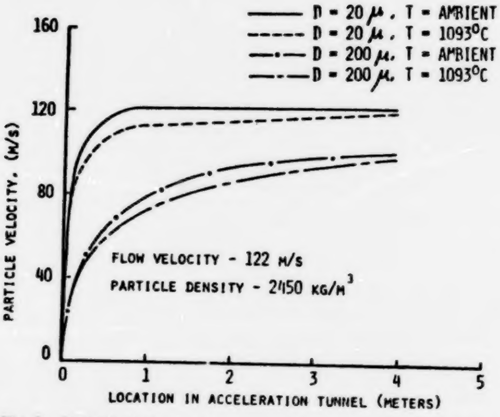

Fig. 3 Particle dynamics in a constant area acceleration tube

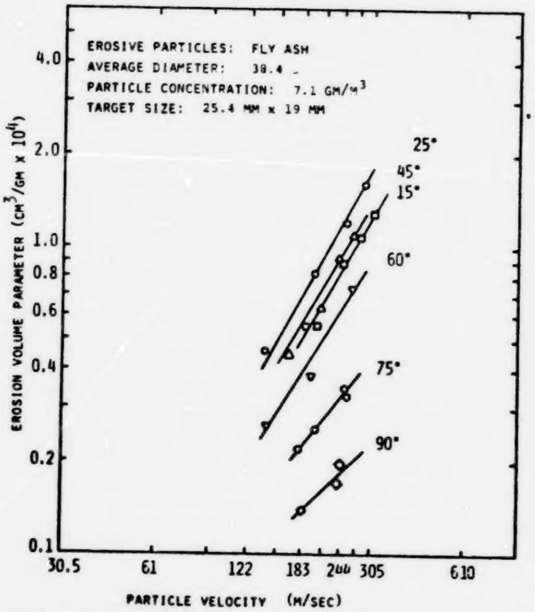

Fig. 4 Effect of velocity on erosion of 304 stainless steel at 316°C

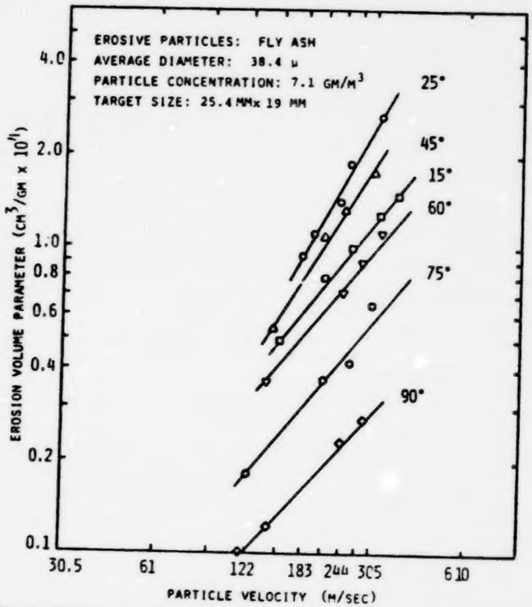

Fig. 5 Effect of velocity on erosion of 304 stainless steel at 482°C

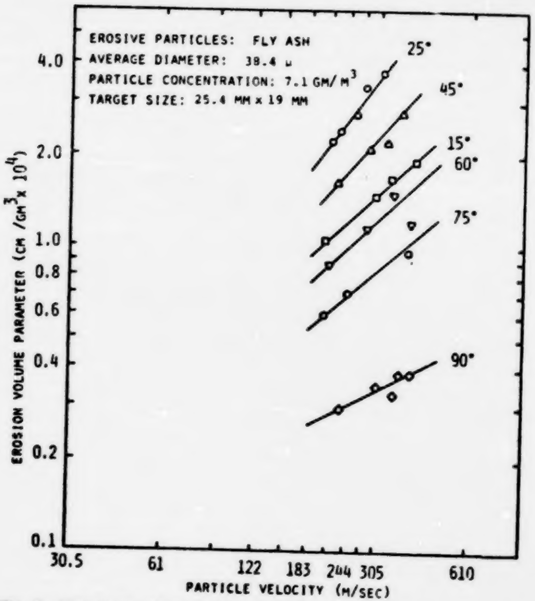

Fig. 6 Effect of velocity on erosion of 304 stainless steel at 649°C

the water is removed from the air, taking with it most of the erosion particles. The particle laden water is drained from the bottom of the tank through a 101.6 mm (4 in.) line, while the air leaves the top of the tank through a 152.4 mm (6 in.) line which discharges the air outside the building. The steam used for cooling the acceleration tunnel is also discharged through the same exit line (152.4 mm). A more detailed description of these test facilities may be found in [7].

Experimental Results and Discussion

The previously described erosion test facility was used to obtain basic erosion data for 304 stainless steel. The material erosion was determined from the weight of the 19.0 × 25.4 mm specimen before and after the testing. The abrasive particles used, consisted of fly ash supplied by the Cincinnati Gas and Electric Company with mean particle diameter of 38.4 μm. The experimental measurements were obtained for coal particle velocities varying from 120 to 350 m/s and target temperatures varying from ambient to 649°C (1200°F).

Figs. 4, 5 and 6 show plots of erosion rate versus particle velocity for various incidence angles. These figures represent the erosion data obtained for the 304 stainless steel specimen at target temperatures of 316, 482 and 649°C (600, 900 and 1200°F). An examination of these plots indicates that the maximum erosion takes place at the 25 deg incidence angle, while the minimum erosion occurs at 90 deg. The erosion rate is also shown for the intermediate incidence angles of 45, 60 and 75 deg, between these two extremes as well as at 15 deg incidence. In all the cases, the erosion rate was always found to increase with increased incidence velocities under the varying temperatures and particle incidence angles. The dependence of the erosion rate on incidence velocities is greater, at the impingement angles associated with the larger erosion rates as can be seen from these figures.

The dependence of the erosion rate on the incidence angles and velocities of the impinging particles can be seen more clearly in Figs. 7, 8 and 9. The experimental data presented in these figures are for three particle velocities, namely 305, 244 and 183 m/s (1000, 800 and 600 ft/s). From the inspection of these figures it may be seen that as the angle of attack increases beyond 25 deg, the erosion rate decreases up to a residual value at 90 deg. The effect of the angle of attack on the erosion rate is shown to persist, independent of the magnitude of the particle velocities. The definition of the point of maximum erosion becomes much more explicit, however, with increasing velocity. A comparison of the curves in Figs. 7, 8 and 9 shows that the rate of erosion increases with increased test material temperatures for all angles of attack. This can be seen more clearly in Figs. 10, 11 and 12. The maximum increase in erosion rate with increased specimen target temperatures can be observed around the 25 deg incidence which corresponds to the highest erosion rate.

Fig. 13 illustrates the effect of the temperature on erosion. In this figure the variation of the erosion rate with temperature is shown for two different velocities at the critical impingement angle of 25 deg. Two length scales are given on the horizontal axis of the same figure, one giving the ratio of the target temperature to the melting temperature, and the other, the ratio of the target temperature to the annealing temperature. For the 304 stainless steel, the melting temperature is between 1400–1455°C (2550–2650°F) and the annealing temperature between 1000–1120°C (1850–2025°F). From the two curves of Fig. 13, it can be seen that for both velocities the erosion rate decreases very slightly for increased temperatures between ambient and about 150°C (300°F). The predominant influence of the temperature on erosion is observed however at temperatures above 150°C (300°F). With increased temperature, the erosion rate is found to increase initially at a lower rate up to about 316°C (600°F) and then increases at an even higher rate.

Presently we are investigating other alloys which will be used in future gas turbine operating with coal. After the experimental work is completed, the data obtained will be used in developing empirical equations for predicting the erosion rates of ductile alloys at different temperatures. The empirical equations which were developed by Tabakoff, et al. [8] are applicable only at ambient temperatures. These relations will be used as a base for modifications to include the measured effects of higher temperatures on erosion. These modifications will incorporate the dependency of the erosion rate on the target

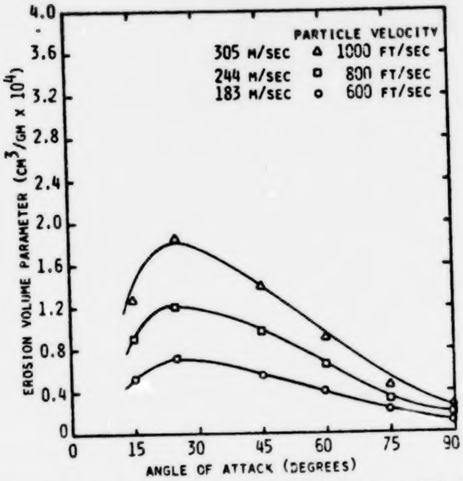

Fig. 7 Effect of angle of attack on erosion of 304 stainless steel at 316°C

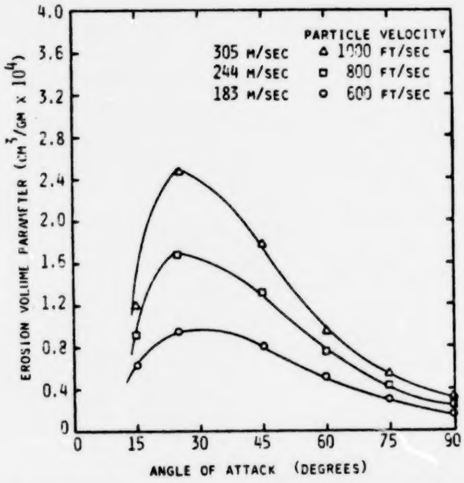

Fig. 8 Effect of angle of attack on erosion of 304 stainless steel at 482°C

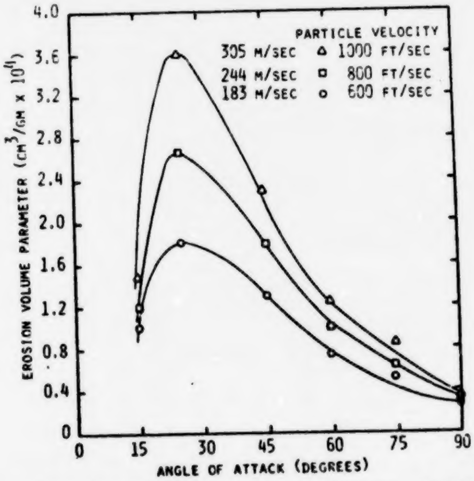

Fig. 9 Effect of angle of attack on erosion of 304 stainless steel at 649°C

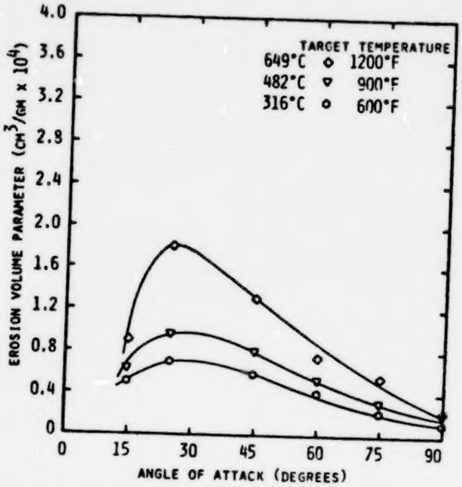

Fig. 10 Effect of angle of attack on erosion of 304 stainless steel at particle velocity of 183 m/s

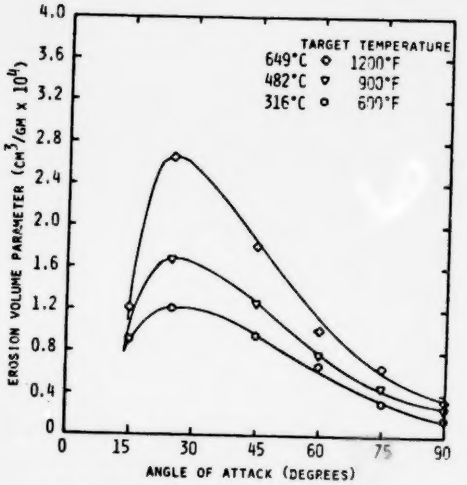

Fig. 11 Effect of angle of attack on erosion of 304 stainless steel at particle velocity of 244 m/s

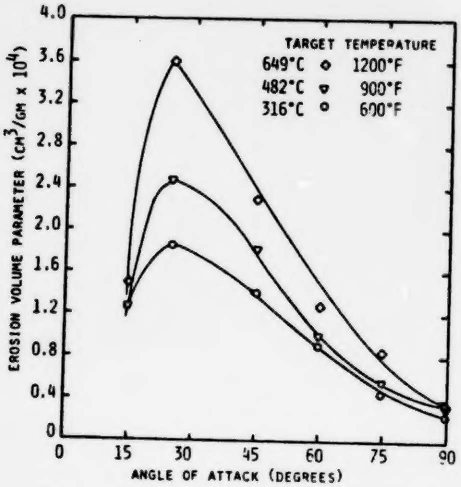

Fig. 12. Effect of angle of attack on erosion of 304 stainless steel at particle velocity of 305 m/s

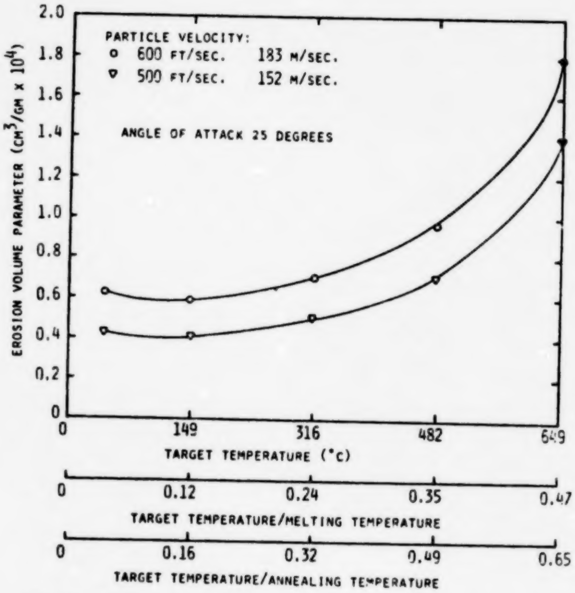

Fig. 13 Effect of temperature on erosion of 304 stainless steel

temperature, as well as, on the properties of the target material itself.

Acknowledgment

This research work was sponsored by ERDA Contract No. E(49-18)-2465.

References

1 Grant, G. and Tabakoff, W., "Erosion Prediction in Turbomachinery Resulting From Environmental Solid Particles," *Journal of Aircraft*, Vol. 12, No. 5, May 1975, pp. 471-478.

2 Finnie, I., Wolak, J., and Kabil, Y., "Erosion of Metals by Solid Particles," *Journal of Materials*, Vol. 2, No. 3, Sept. 1967, pp. 682-700.

3 Smeltzer, C. E., et al., "Mechanisms of Sand and Dust Erosion in Gas Turbine Engines," USAAVLABS Technical Report, Aug. 1970.

4 Fraas, A. P., "Survey of Turbine Bucket Erosion, Deposits, and Corrosion," ASME Paper No. 75-GT-123, presented at the Gas Turbine Conference, Houston, Texas, March 2-6, 1975.

5 Finnie, I., "An Experimental Study on Erosion," *Proceedings of the Society for Experimental Stress Analysis*, Vol. 17, No. 2, pp. 65-70.

6 Tabakoff, W. and Hamed, A., "Aerodynamic Effects on Erosion in Turbomachinery," JSME and ASME Paper No. 70, 1977 Joint Gas Turbine Congress, Tokyo, Japan, May 22-27, 1977.

7 Tabakoff, W. and Wakeman, T., "Test Facility for Material Erosion at High Temperatures," ASTM Publication, *Erosion: Prevention and Useful Applications*, STP 664, 1978.

8 Tabakoff, W., Kotwal, R. and Hamed, A., "Erosion Study in Turbomachinery Affected by Coal Ash Particles," ASME Paper No. 78-GT-136, 23rd International Gas Turbine Conference, April 9-13, 1978, London.

W. Tabakoff and T. Wakeman

Test Facility for Material Erosion at High Temperature

Authorized Reprint from
Special Technical Publication 664

Copyright American Society for Testing and Materials
1916 Race Street, Philadelphia, Pa. 19103
1979

W. Tabakoff[1] *and T. Wakeman*[1]

Test Facility for Material Erosion at High Temperature

REFERENCE: Tabakoff, W. and Wakeman, T., "**Test Facility for Material Erosion at High Temperature,**" *Erosion: Prevention and Useful Applications, ASTM STP 664,* W. F. Adler, Ed., American Society for Testing and Materials, 1979, pp. 123-135.

ABSTRACT: One of the next steps in experimental material erosion investigation is the testing at high temperatures comparable to those found inside a jet engine. Described in this paper is the design of the high-temperature erosion facility at the University of Cincinnati. This facility has the capability of providing between ambient and a 1093°C (2000°F) environment temperature for erosion testing of various materials. In addition, this facility has the capability for varying material, specimen size, angle to the flow, particle concentration, particle size, and velocity. This facility is expected to provide basic material erosion data which will be used in predicting erosion in jet engines and other devices.

KEY WORDS: erosion test facility, high temperatures, high-speed particles, particle feeder assembly, wind tunnel, gas turbines, erosion

In many industrial and military applications the erosive action of high-speed particles results in serious problems. Erosion has been pointed out as as problem in as diverse areas as aero gas turbines [*1,2*],[2] rocket nozzles [*3*], coal-fired boiler systems [*4*], and others. Recent interest in this old problem coincides with increased usage of gas turbines in dusty terrains. The cost of maintaining such engines in dusty environments is great. Air filtration has alleviated the problem somewhat, but filtration reduces both payload and engine performance. If erosion can be incorporated as an engine design parameter, perhaps an erosion-tolerant engine can be produced.

A description of a sand-blasting erosion test facility, in which a small jet of particle-laden air was impacted on a stationary specimen, was provided by Finnie [*5*]. Extensive erosion research has been conducted using this facility or modifications of it. Other testing methods used an apparatus where particles dropped through a vacuum impact a stationary specimen, or a specimen attached to the end of a rotating arm [*6, 7*]. A common characteristic among all these test facilities is that the fluid profile over the specimen is completely or partially eradicated.

---

[1] Professor and graduate research assistant, respectively, Department of Aerospace Engineering and Applied Mechanics, University of Cincinnati, Cincinnati, Ohio 45221.

[2] The italic numbers in brackets refer to the list of references appended to this paper.

Experimental Equipment

From the literature reviewed, it was concluded that the design of the test facility can affect the resulting erosion rate. Further, the test facilities designed thus far do not investigate the influence of a flow field on erosion. This factor is especially important in rotating machinery, where the fluid is abruptly turned by the rotating or stationary blades. The test facilities reported herein have been designed to investigate these problems.

Stationary Specimen Test Facility

Previously, a wind tunnel was constructed at the University of Cincinnati to obtain the basic erosion data and to photograph the particle impacts on the specimen. Controlling the primary variables of fluid velocity, particle velocity, particle flow rate, and particle sizes in a representative aerodynamic environment were main considerations in designing this tunnel. A detailed description of this test facility can be found in Ref *8*. A significant amount of research has been carried out using this facility, which provided basic erosion data and particle rebound characteristics for various test materials [*9*]. These data have been used in analytical models to predict turbomachinery erosion. This was accomplished by following a sufficiently large number of particles through the turbomachine and determining these individual contributions to arrive at a general erosion pattern for the machine.

In many applications, however, erosion takes place at elevated temperatures near the strength-limiting temperatures of the materials used. As an example, titanium used in early stages of jet engine compressors and INCO 718 used in aft stages are operated at metal temperatures in excess of 316 and 593°C (600 and 1100°F), respectively. In both cases, these temperatures are near the maximum operating temperatures used for these materials. Such elevated temperatures can have a significant effect on erosion characteristics as evidenced in data presented by Tabakoff and Hamed [*10*]. These data were obtained in the same facility as the Ref *8* data, except that the specimen was heated to a maximum of 204°C (400°F). Although this temperature falls far short of those experienced in jet engines, the data indicate the significance of the effect of temperature on erosion and probably on the rebound characteristics.

The erosion test facility described herein is designed to provide erosion and rebound data in the range of operating temperatures experienced in jet engine compressors and low-temperature turbines. For that purpose, the facility has been designed to operate at a test section temperature in the range of ambient to 1093°C (2000°F). The facility properly stimulates, in addition to high temperatures, all erosion parameters found to be important from previous testing at ambient temperatures. These parameters include velocity, angle of impact, particle size, particle concentration, and specimen size.

In designing the high-temperature erosion facility, close attention was given to aerodynamic effects to insure that important parameters such as angle of attack are not masked or altered. To insure the correlation of data from the high-temperature facility with those of Ref *8*, the facility flowpath and acceleration tunnel length are almost identical with those of the facility described in that reference. The flowpath cross section was increased, however, from 76.2 by 25.4 mm to 88.9 by 25.4 mm (3 by 1 in. to 3½ by 1 in.). This change was instituted to decrease tunnel blockage by the test specimen.

The particle rebound characteristic velocities will be obtained photographically and with the laser velocimeter. Presently, we do not have any data at the maximum temperature of 1093°C, but we do not anticipate any difficulties. The velocities of the particles in the range of 20 μm and smaller are measured strictly with the laser velocimeter.

General Description of High-Temperature Erosion Rig

A schematic of the test apparatus is shown in Fig. 1; it consists of the following components: particle feeder (A), main air supply pipe (B), combustor (C), particle preheater (D), particle injector (E), acceleration tunnel (F), test section (G), and exhaust tank (H).

The equipment functions as follows. A measured amount of abrasive grit of a given constituency is placed into the particle feeder (A). The particles are fed into a secondary air source and blown up to the particle preheater (D), and then to the injector (E), where they mix with the main air supply (B), which is heated by the combustor (C). The particles are then accelerated by the high-velocity air in a constant-area steam-cooled duct (F) and impact the specimen in the test section (G). The particulate flow is then mixed with the coolant and dumped in the exhaust tank. This facility is capable of supplying erosion data at temperatures in the range of ambient to 1093°C (2000°F). The expected range of testing parameters is given in Table 1, but is not necessarily restricted to the tabulated values.

The individual components which make up the high-temperature erosion facility are described in the following. Each component was designed with cost, maintainability, availability, and functionality as prime considerations.

Particle Feeder Assembly (*A*)—The particles from the feeder (Fig. 2) are blown up to the particle injector area. The feeder is designed as a pressure

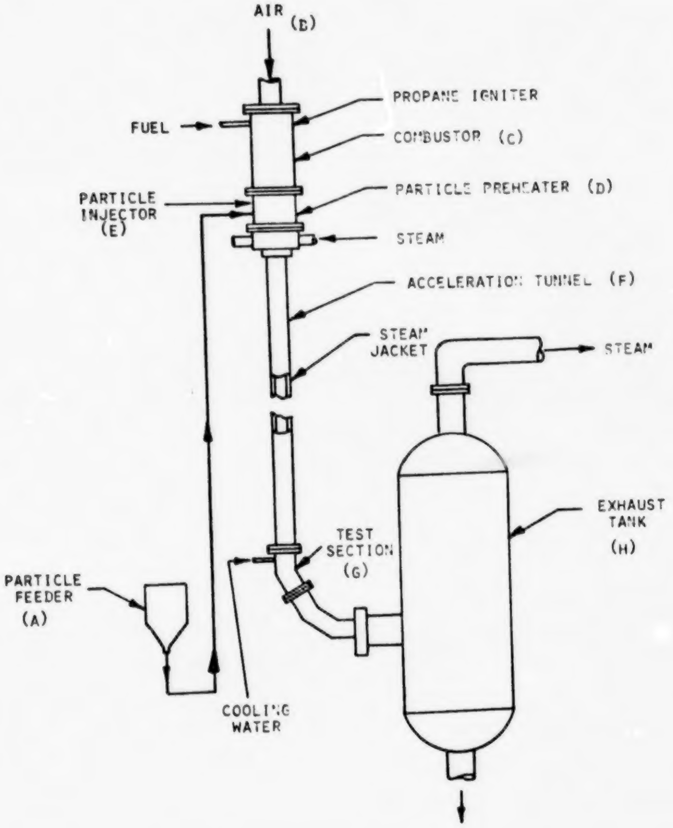
AIR (B)
PROPANE IGNITER
FUEL
COMBUSTOR (C)
PARTICLE PREHEATER (D)
PARTICLE INJECTOR (E)
STEAM
ACCELERATION TUNNEL (F)
STEAM JACKET
STEAM
EXHAUST TANK (H)
TEST SECTION (G)
PARTICLE FEEDER (A)
COOLING WATER

FIG. 1—*Schematic of erosion test facility.*

TABLE 1—*Erosion parameters.*

Parameters	
Temperature	10 to 1093°C (50 to 2000°F)
Particle angle of attack	0 to 90 deg
Particle velocity	60 to 450 m/s (200 to 1500 ft/s)
Particle concentration	0 to 5 percent
Particle size	1 to 2000 μm
Particle type and material	silica sand, alumina, ash
Specimen size	6.35 to 25.4 mm (¼ to 1 in.)
Specimen material	various jet engine materials

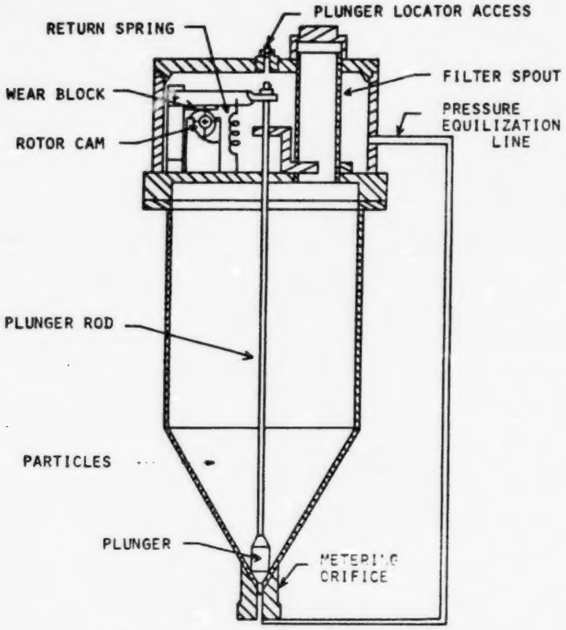
PLUNGER LOCATOR ACCESS
RETURN SPRING
FILTER SPOUT
WEAR BLOCK
PRESSURE EQUILIZATION LINE
ROTOR CAM
PLUNGER ROD
PARTICLES
PLUNGER
METERING ORIFICE

FIG. 2—*Particle feeder assembly.*

vessel to operate at high air pressures. However, this pressure is equalized above and below the plunger by a bypass line. This allows the system to be calibrated under gravity feed conditions. Further, an electric eye records the plunger rpm such that the operating conditions are maintained. The metering orifice is designed to be replaceable. In this manner, a larger (or smaller) orifice may be used, along with corresponding rod diameter, to allow versatility of the feeder.

Main Air Supply (*B*)—This air is drawn from air tank storages, which allow continuous testing.

Combustor (*C*)—High-temperature combustion products are supplied by a modified General Electric J93 can combustor as shown in Fig. 3. The J93 can is encased in a 228.6-mm (9 in.) inside-diameter stainless steel pipe with provisions for the fuel nozzle and igniter. Due to heat loss in the acceleration tunnel, achieving the maximum test section temperature of 1093°C (2000°F) requires a combustor exit temperature of 1204.4°C (2200° F). To obtain this temperature from a J93 can combustor, certain modifications were required, including use of a large fuel nozzle and blanking off most of the downstream dilution air ports. In order to obtain low com-

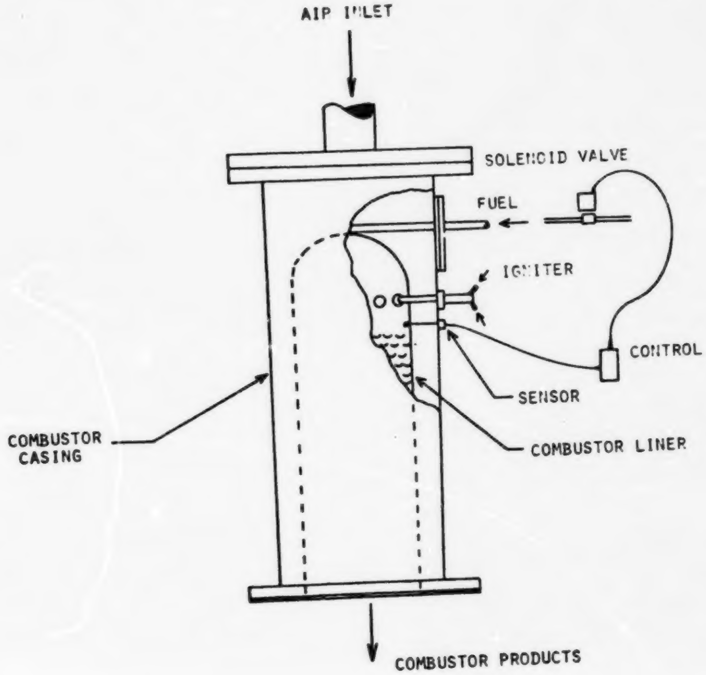

FIG. 3—*Combustion chamber schematic.*

bustion temperatures in the range of 93 through 260°C (200 through 500°F), a smaller fuel nozzle is used. The fuel is ignited by a system consisting primarily of a propane-fired torch containing a spark plug.

Particle Preheater (*D*) *and Injector* (*E*)—The preheater consists of a coil contained in a 203.2-mm (8 in.) inside-diameter pipe section with a distributor/injector to provide a well-distributed preheated particle supply (Fig. 1). The particles are blown up to the accelerating section of the tunnel by secondary air which flows from the particle feeder and passes through the preheater coils. As the particulate air mixture passes through the coils, it is heated by the combustion products to a temperature of 538°C (1000°F) before being injected into the tunnel. The spread-out of the particles in the main airstream is accomplished by impinging them on a specially contoured ball, and then accelerating them through an elliptical nozzle to the acceleration duct section.

Acceleration Section (*F*)—Figure 4 shows the acceleration section, which is 3.66 m (12 ft) long with a rectangular cross section [89 by 25.4 mm (3½ by 1 in.)]. The acceleration tunnel is steam cooled to minimize heat loss.

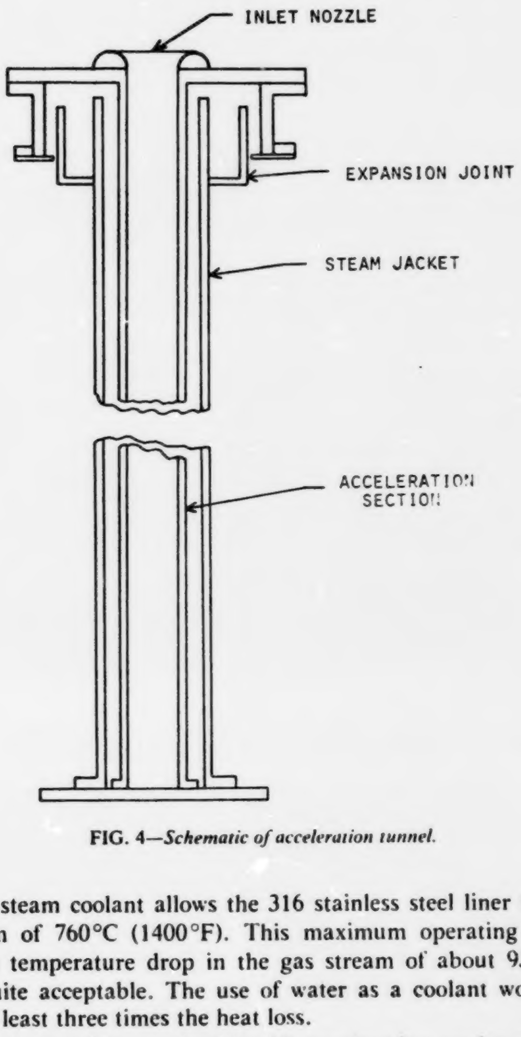

FIG. 4—*Schematic of acceleration tunnel.*

The use of steam coolant allows the 316 stainless steel liner to operate at a maximum of 760°C (1400°F). This maximum operating temperature results in a temperature drop in the gas stream of about 93°C (200°F), which is quite acceptable. The use of water as a coolant would have resulted in at least three times the heat loss.

The particle velocities attained in this acceleration section are predicted analytically and verified by experimental methods. Since the particles are accelerated by aerodynamic drag forces imparted by the high-velocity air, it is necessary to know the air velocity at all locations in the tunnel. For this reason, the tunnel pressure is measured at the inlet, midsection, and exhaust. Using these data, the tunnel friction is accounted for when calculating the fluid velocity. The dynamics of relatively large and small particles (200 and 20 μm) for ambient and 1093°C (2000°F) temperatures for low-speed fluid velocity [122 m/s (400 ft/s)] are shown in Fig. 5. From this figure it can be seen that the particle velocity is an exponential function of tunnel length. The law of diminishing returns would indicate that a tunnel length of 0.61 to 0.92 m (2 to 3 ft) would be sufficient; however, a tunnel length of 3.66 m (12 ft) was chosen, for several theoretical and practical reasons. An additional plot of the ratio between particle and fluid velocity at the end of the acceleration section (starting test section) for various particle sizes is given in Fig. 6. This figure illustrates the obvious fact that a longer tunnel will result in higher particle velocities, but that the rate of change of particle velocity with particle size is smaller for a longer tunnel.

Test Section (*G*)—The test section (Fig. 1) is designed such that the particle-laden air is channeled over the specimen and the aerodynamics of the fluid surrounding the test specimen are preserved. This section contains several interchangeable inserts such that the fluid profile can be determined using conventional instrumentation, and the particle trajectories can be recorded using high-speed photographic methods.

The test specimen can be oriented at different angles to the gas stream by rotating the specimen holder. The test section flow path turns 30 deg at the plane of the test section to help turn the flow when the test specimen is oriented at an angle. The test section is water-cooled. This does not significantly cool the primary gas stream due to the section's small size. The

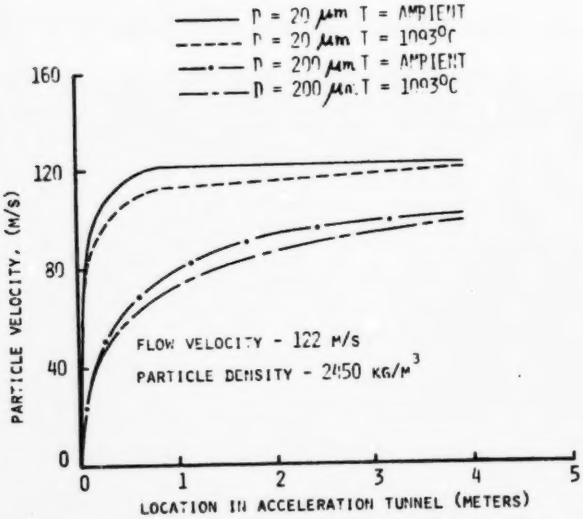

FIG. 5—*Particle dynamics in a constant-area acceleration tube.*

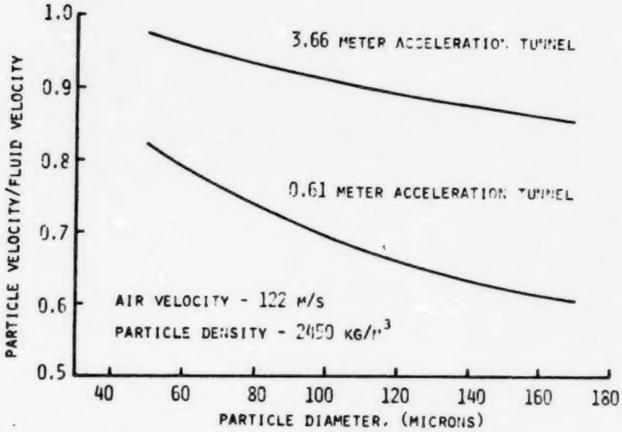

FIG. 6—*Effect of acceleration tunnel length on particle dynamics.*

coolant water is discharged into the particulate gas stream at the downstream end of the test section.

Testing of particle rebound characteristics is also planned, using photographic means to measure the speed and angle of the impinging and rebounding particles. For this purpose, a special test section with a glass window has been constructed.

Exhaust System (*H*)—The erosion rig exhaust system consists primarily of a settling tank (Fig. 1). The exhaust from the erosion test section is loaded with cooling water. In the settling tank, the water is removed from the air, taking with it most of the erosion particles. The particle-laden water is drained from the bottom of the tank through a 101.6-mm (4 in.) line. The air leaves the top of the tank through a 152.4-mm (6 in.) line which discharges the air outside the building. The steam used in cooling the 3.66-m (12 ft) acceleration tunnel is also discharged through the same exit line.

Analysis of Photographic Data

In the previous tunnel [*8*], two techniques of analyses were used in reducing the photographic data. The same techniques may be used in the high-temperature erosion tunnel. These techniques are complimentary in that one was used to check the other. Both of these methods relied on a reference distance which was marked on the test section background. The particle velocities were obtained by comparing the distance traveled by the particle in two successive frames to this reference distance.

The first method of analysis is essentially one of streak photography. The velocity is determined by dividing the distance traveled by the particle during the exposure for one frame.

The velocity is calculated using

$$V = \left(L\,\frac{r}{R}\right)\Big/ t_r \qquad (1)$$

where

V = particle velocity, m/s,
L = length of particle streak on screen, m,
r = actual length of reference line, m,
R = reference line projected on screen, m, and
t_r = exposure time of frame observed, s.

The second method of analysis was based on the distance a particle travels in successive frames. The basic concept is the same as the first method; however, it was found to give more accurate results. The particle velocity is determined using

$$V = n\,\frac{r}{R}\,S \qquad (2)$$

where

n = length traveled by particle between two successive frames, m,
S = film speed (local quantity), m/s, and
r, R = same as in Eq 1.

In practice, a combination of the two methods was used and checked against each other.

Test Results

To date, erosion data have been accumulated for three target materials (2024 aluminum, Ti-6Al-4V and INCO 718) varying particle velocity, impingement angle, and target temperature. Figure 7 shows preliminary results for Ti-6Al-4V. These data indicate that for Ti-6Al-4V target material with impingement angle of 25 deg, the erosion rate increases with increasing target temperature. Additionally, the slope of the data appears to be decreasing with increasing temperature; however, more data are required to substantiate this trend.

The accuracy of the erosion rates presented depends on the errors accrued in measuring the amount of erosion and in the independent parameters influencing the erosion. At present the most significant error results from

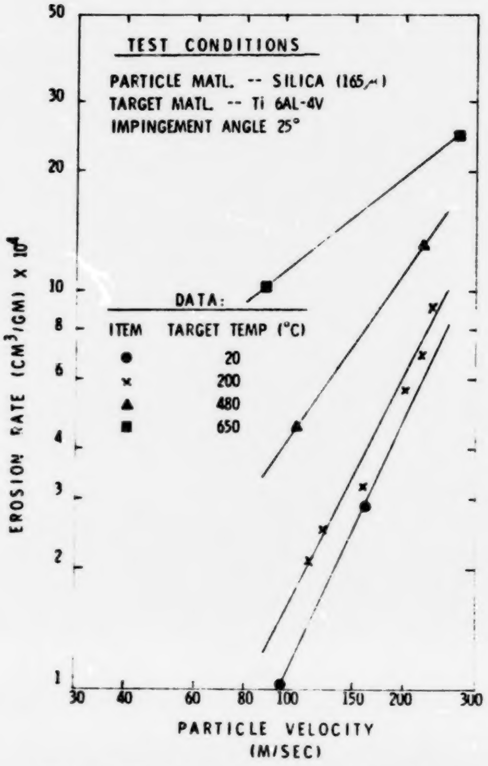

FIG. 7—*Effect of erosion versus particle velocity.*

the calculation of the particle velocity from air pressure, temperature, and flow plus the flow path metal temperature. An estimated maximum error of ±5 percent in particle velocity results in a ±8 percent error in erosion rate due to the strong dependence of erosion on particle velocity. Smaller errors of the order of ±1 percent result from the measurement of impact angle, specimen weight, specimen temperature, and particle weight. The mean square error of all these errors is ±8.2 percent maximum. This maximum error will be substantially reduced by calibrating the calculated particle velocity with measured values. The measured velocities will be obtained using both photographic techniques and a laser velocimeter.

Acknowledgment

This work was sponsored under Grant No. DAAG-29-76-G-0229, U.S. Army Research Office, Research Triangle Park, N.C.

References

[1] Montgomery, J. E. and Clark, J. M., Jr., "Dust Erosion Parameters for a Gas Turbine," SAE Summer Meeting Preprint No. 538A, Society of Automotive Engineers, New York, 1962.

[2] Hibbert, W. A., *Journal of the Royal Aeronautical Society*, Vol. 69, Nov. 1965, pp. 769-776.

[3] Neilson, J. H. and Gilchrist, A., *Wear*, Vol. 11, 1968, pp. 301-315.

[4] Raask, E., *Wear*, Vol. 13, 1969, pp. 301-315.

[5] Finnie, I. in *Proceedings*, Society for Experimental Stress Analysis, Vol. 17, No. 2, 1960, pp. 65-70.

[6] Kleis, I., *Wear*, Vol. 13, 1969, pp. 199-215.

[7] Tilly, G. P. and Sage, W., *Wear*, Vol. 16, 1970, pp. 447-465.

[8] Grant, G. and Tabakoff, W., *Journal of Aircraft*, Vol. 12, No. 5, May 1975, pp. 471-478.

[9] Ball, R. and Tabakoff, W., "An Experimental Investigation of the Particle Dynamics of Quartz Sand Impacting 6Al-4V Titanium in an Erosive Environment," Technical Report No. 74-43, University of Cincinnati, Cincinnati, Ohio, Oct. 1974.

[10] Tabakoff, W. and Hamed, A., "Aerodynamic Effects on Erosion in Turbomachinery," JSME and ASME Paper No. 70, Japan Society of Marine Engineers and American Society of Mechanical Engineers Joint Gas Turbine Congress, Tokyo, Japan, May 22-27, 1977.

DISCUSSION

G. Mayer[1] (*written discussion*)—In the schematic of your apparatus a fairly sharp angle was shown in the flow system as it enters the test section. Was the flow in the test section laminar?

W. Tabakoff and T. Wakeman (*authors' closure*)—The flow in the wind tunnel test section is turbulent. The size of the particles which we used in this investigation are large—this means over 50 μm. Despite the high turbulence in the flow, these particles follow very much established particle streamwise paths which to the outside observer look like laminar paths (this depends strongly on the particle sizes). This observation was made by high-speed film camera, approximately 40 000 frames per second. The turbulence of the main flow core is measured with optical devices.

A. Levy[2] (*written discussion*)—What was the particle velocity profile across the containment pipe into test section and what was the size of the specimen? Was there a velocity variation across the specimen?

W. Tabakoff and T. Wakeman (*authors' closure*)—The particle velocity profile across the test section was uniform. The specimen sizes were 6.35, 12.70, 19.05, 25.4, and 31.75 mm (0.25, 0.50, 0.75, 1.0, and 1.25 in.). The approach velocity to the specimen was uniform.

I. Finnie[3] (*written discussion*)—Do the velocity fluctuations in turbulent boundary layers formed around turbine blades have a strong effect on the particle trajectories and on the resulting erosion damage?

---

[1] Army Research Center, Research Triangle Park, N.C. 27709.

[2] University of California, Berkeley, Calif.

[3] University of California, Berkeley, Calif.

M. Menguturk[4] (*written discussion*)—Since the main flow turbulence level is quite high in gas turbines, the boundary layers developing around the blades are predominantly turbulent. The turbulent velocity fluctuations inside the boundary layer are small in magnitude compared with the local root-mean-square velocity of the fluid, and they occur very rapidly. Particles which possess considerable inertia to impact blade surface with sufficient velocity to effectively remove blade material will not even feel the presence of these fluctuations. Only extremely fine particles can adjust to the turbulent velocity fluctuations owing to their negligible inertia. However, these particles will cause virtually no erosion. By the time they reach the surface, they will nearly assume the surface gas velocity, which is zero. The result is deposition. Deposition rates of such small particles can be calculated by considering their diffusion due to Brownian motions, turbulent fluctuations, and temperature gradients in the case of cooled blades. Professor Tabakoff is justified in neglecting the flow turbulence in his erosion measurements.

W. Tabakoff and T. Wakeman (*authors' closure*)—Professor Finnie's question is well answered by the comment of Dr. Menguturk.

---

[4] Westinghouse Electric Corp., Research and Development Center, Pittsburgh, Pa. 15235.